ON THE VARIABILITY OF COMPOSITE LAMINATE PROPERTIES: PREDICTION AND MINIMIZATION

by

Bari M. Southard

B.S. in Aerospace Engineering, The University of Michigan, Ann Arbor
(1996)

Submitted to the Department of Aeronautics and Astronautics
in partial fulfillment of
the requirements for the degree of

Master of Science
in Aeronautics and Astronautics

at the
Massachusetts Institute of Technology

August 1996

Signature of Author _____
Department of Aeronautics and Astronautics
August 26, 1996

Certified by _____
Professor Hugh L. McManus
Thesis Supervisor

Accepted by _____
Professor Jaime Peraire
Chairman, Departmental Graduate Committee

ON THE VARIABILITY OF COMPOSITE LAMINATE PROPERTIES: PREDICTION AND MINIMIZATION

by

Bari M. Southard

Submitted to the Department of Aeronautics and Astronautics on August 26, 1996 in partial fulfillment of the requirements for the Degree of Master of Science in Aeronautics and Astronautics

ABSTRACT

A general methodology is developed to (i) determine the mean and standard deviation of laminate properties given models for them, (ii) tailor mean laminate properties to specified goals (if possible) while also minimizing the standard deviation of the laminate properties, and (iii) quantify the sensitivity of a laminate property to variations in the constituent properties that appear in the model for the laminate property. New probabilistic methods, including an extended Monte Carlo technique that provides for the definition of sensitivity metrics, are developed to predict the means, standard deviations, and sensitivity metrics of laminate properties. Here, laminate stiffness, hygroelastic, thermoelastic, and strength properties are predicted. A new global optimization method, dubbed the Stochastic Simplex Method (SSM), is developed to tailor mean laminate properties and also minimize their standard deviations. The probabilistic and optimization methods provide a means to design composite laminates to have specified thermo/hygro elastic and/or stiffness properties with minimal variability about the specified values. Favorable comparisons with experimental data for the elastic, thermoelastic, and strength properties are shown to verify the analysis methods. Extensive parametric studies are presented which demonstrate the strong dependence of the amount of variability of a laminate property on laminate design (e.g. layup angles). Contour plots of the predicted mean, standard deviation, and coefficient of variation (when applicable) of all the predicted laminate properties are presented for the $[\pm\theta/\pm\beta]_s$ (where θ and β are variables) laminate family. Sensitivity studies are presented showing the relative importance of variations in different constituent properties to variations in laminate properties. Optimal layups for maximal dimensional stability and stiffness (often the desired characteristics for space structures) are presented.

Thesis Supervisor: Hugh L. McManus
Title: Class of 1943 Assistant Professor,
Department of Aeronautics and Astronautics,
Massachusetts Institute of Technology

This thesis is dedicated
to my
Grandmother

ACKNOWLEDGMENTS

Thanks Mom and Dad. I would have never gotten this far without you.

Thanks Hugh. Thanks for giving me the opportunity to finish this work. I know you took a "risk" given my thesis topic (optimization stuff), and I very much appreciate your trust in me to produce something useful.

All family and friends have been great. Thanks for your advice, encouragement, and all your support in general. Special thanks to Ron for giving me a place to stay when I needed it, ..., !*&%*&% (you figure it out), ..., and interesting conversations while pacing around the backyard (quantum mechanical economics!?). I must mention George and Kim; if it wasn't for you guys I wouldn't have a B.S.

Much thanks to the TELAC professors: Prof. Dugundji, Hugh, Mark, and Paul. Thanks for all the helpful questions, "technical challenges" (i.e. Paul's questions), and criticisms during presentations. I am a far better presenter than when I first got here, thank you all for the valuable skill. Lots of thanks to Deb and Ping for everything.

Everyone in TELAC is great. I will (believe it or not) miss this place. It was a privilege to learn, work, and drink lots of beer with a group of very talented people. I will miss you all:

Bethany "eat your beans" Foch
Brian "Director, National Bureau of Masters Thesis Standards" Wardle
Chris "SSABMUD" Dunn
Hary "where is the house?" Budiman
Lauren "West Virginia mountain climbing expert" Kucner Crews
Mark "oatmeal cream puff cookie" Tudela
Ronan "crash the computer two days before the thesis deadline" Cunningham
Sharath "drank too many scorpion bowls" Shetty
Steve "Ya, I did Rutherford's oil drop experiment in high school" Czepiela

Last, but not least, the TELAC wanna be:
Greg "lets take the Harvard bridge boys" Giffen

FOREWARD

This research was completed at the Technology Laboratory for Advanced Composites (TELAC) at the Massachusetts Institute of Technology.

TABLE OF CONTENTS

LIST OF FIGURES

add one page

LIST OF TABLES

NOMENCLATURE

$\mathbf{a}^*$	Part of inverse laminate stiffness matrix
A	Laminate extensional stiffness matrix
A_i	Secondary weight factor on i^{th} laminate property goal portion of cost function
ASA	Adaptive Simulated Annealing
A1	Refers to linear probabilistic method (approach of McManus)
A2	Refers to extended linear probabilistic method
A3	Refers to Monte Carlo approach
A4	Refers to general approach to determine sensitivity metrics
$\mathbf{b}^*$	Part of inverse laminate stiffness matrix
B	Laminate coupling stiffness matrix
B_i	Secondary weight factor on standard deviation of i^{th} laminate property portion of cost function
CMB	Coefficient of Moisture Bending
CME	Coefficient of Moisture Expansion
CTB	Coefficient of Thermal Bending
CTE	Coefficient of Thermal Expansion
c_{jk}	Correlation coefficient
c_i	Parameter in annealing schedule for i^{th} parameter temperature
$\hat{c}$	Parameter in annealing schedule for acceptance temperature
$\mathbf{d}^*$	Part of inverse laminate stiffness matrix

D	Dimension of design space
$\mathbf{D}$	Laminate bending stiffness matrix
${}^{A2}d_{ij}$	Sensitivity of i^{th} laminate property to j^{th} ply property or geometric parameter variations, from approach A2
${}^{A4}d_{ij}$	Sensitivity of i^{th} laminate property to j^{th} ply property or geometric parameter variations, from approach A4
${}^{A2}d_{i\,[...]}$	Combined (over all plies in laminate) sensitivity of i^{th} laminate property to [specified ply property], from approach A2
${}^{A4}d_{i\,[...]}$	Combined (over all plies in laminate) sensitivity of i^{th} laminate property to [specified ply property], from approach A4
E	Cost function value (or "Energy") of a new point
E_o	Cost function value (or "Energy") of the most recent accepted (i.e. that passed the Boltzmann test) point
E_x	Laminate longitudinal stiffness
E_{lk}	Longitudinal stiffness of k^{th} ply
E_y	Laminate transverse stiffness
E_{tk}	Transverse stiffness of k^{th} ply
$\widetilde{E}_x$	Laminate longitudinal stiffness goal
$\widetilde{E}_y$	Laminate longitudinal stiffness goal
f_{Yi}	Function for laminate property Y_i
GA	Genetic Algorithm
G_{xy}	Laminate shear stiffness
G_{ltk}	Shear stiffness of k^{th} ply

$\tilde{G}_{xy}$	Laminate shear stiffness goal
h	Laminate thickness
K	Boltzmann's constant
k	Annealing time steps
k_i	Annealing time steps for i^{th} parameter temperature
k_{fi}	Number of annealing time steps, for the i^{th} parameter, to reach temperature T_{fi}
k_i'	Rescaled annealing time for i^{th} parameter temperature
$k_{\text{acceptance}}$	Number of acceptance (pass Boltzmann test) events
k_{rescale}	Number of annealing time steps between rescaling (reannealing) the parameter temperatures
k_{restart}	Number of annealing time steps between replacing the worst point in the simplex with the best point found so far
L_i	Lower bound of i^{th} parameter
m_i	Parameter in annealing schedule for parameter temperatures
$\mathbf{M}$	Vector of running-moments
$\mathbf{M}^{\mathrm{H}}$	Vector of hygral running-moments
$\mathbf{M}^{\mathrm{T}}$	Vector of thermal running-moments
n	Number of plies in laminate
n_i	Parameter in annealing schedule for parameter temperatures
N	Number of samples
$\mathbf{N}$	Load case
$\mathbf{N}$	Vector of running-loads
$\mathbf{N}^{\mathrm{H}}$	Vector of hygral running-loads

$\mathbf{N}^T$	Vector of thermal running-loads
O1,...,O6	Refer to optimization runs one through six that each correspond to a different set of primary weight factors
P_o	Probability that a system (e.g. a molecule) has some minimum energy
PMC	Polymer Matrix Composite
q	Quenching parameter in annealing schedules
$\mathbf{Q}$	Reduced ply stiffness matrix in ply coordinates
$\overline{\mathbf{Q}}$	Reduced ply stiffness matrix in laminate coordinates
$r^{(j)}$	j^{th} uniformly distributed random deviate between 0 and 1
R	Load factor
R_{FPF}	First ply failure load factor
R_{LPF}	Last ply failure load factor
s_i	Sensitivity at of i^{th} parameter at the best point found so far, used for rescaling parameter temperatures
s_{max}	Maximum sensitivity of the parameters at the best point found so far, used for rescaling parameter temperatures
S_k	Shear strength of k^{th} ply
SD[*]	Standard Deviation of *
SSM	Stochastic Simplex Method
t_k	Thickness of k^{th} ply
$\mathbf{T}$	Transformation matrix
$T_i^{(k)}$	Parameter temperature of i^{th} parameter at annealing time step k
T_{oi}	Initial parameter temperature of i^{th} parameter

$T_i^{(k)}$	Parameter temperature of i^{th} parameter at annealing time step k
$T_i^{(k_{acceptance})}$	Acceptance temperature at $k_{acceptance}$ acceptance events
${}^{o}T_{acceptance}$	Initial acceptance temperature
T_{fi}	Parameter temperature of i^{th} parameter reached in k_{fi} annealing time steps
U_i	Upper bound of i^{th} parameter
$\mathbf{W}^{H}$	Vector of hygral bending coefficients
$\mathbf{W}^{T}$	Vector of thermal bending coefficients
$\widetilde{W}_x^H$	Minimum standard deviation of longitudinal hygral bending coefficient
$\widetilde{W}_x^T$	Minimum standard deviation of longitudinal thermal bending coefficient
x_i	i^{th} parameter
$\mathbf{x}$	Vector of parameters
$\mathbf{x_o}$	Vector of parameters from previous iteration
X_j	Constituent (ply) material property or geometric parameter
$\bar{X}_j$	Mean constituent (ply) material property or geometric parameter
${}^{C}X_k$	Longitudinal compressive strength of k^{th} ply
${}^{T}X_k$	Longitudinal tensile strength of k^{th} ply
${}^{C}Y_k$	Transverse compressive strength of k^{th} ply
${}^{T}Y_k$	Transverse tensile strength of k^{th} ply
Y_i	i^{th} laminate property

$Y_i^{(k)}$	k^{th} value in a data set of i^{th} laminate property values
α	Vector of ply in-plane coefficients of thermal expansion in ply coordinates
$\bar{\alpha}$	Vector of ply in-plane coefficients of thermal expansion in laminate coordinates
${}^{l}\bar{\alpha}$	Vector of laminate in-plane coefficients of thermal expansion
α_{lk}	Longitudinal coefficient of thermal expansion of k^{th} ply in ply coordinates
α_x	Laminate longitudinal coefficient of thermal expansion
$\tilde{\alpha}_x$	Laminate longitudinal coefficient of thermal expansion goal
${}^{l}\bar{\beta}$	Vector of laminate in-plane coefficients of thermal expansion
β_{lk}	Longitudinal coefficient of moisture expansion of k^{th} ply in ply coordinates
β_x	Laminate longitudinal coefficient of moisture expansion
$\tilde{\beta}_x$	Laminate longitudinal coefficient of moisture expansion goal
ΔH	Difference between laminate moisture content (percent fraction of dry weight) and stress free moisture content
ΔT	Difference between laminate temperature and stress free temperature
ε	Perturbation parameter used in approach A4
ε	Vector of laminate strains in ply coordinates
$\bar{\varepsilon}$	Vector of laminate strains in laminate coordinates
ε°	Vector of laminate midplane strains
γ_{ij}	Constants in general expression for laminate property standard deviations (approach A4)

η	Parameter in annealing schedule for acceptance temperature
$\boldsymbol{\kappa}$	Vector of laminate curvatures
$\boldsymbol{\kappa}^{\mathbf{H}}$	Vector of laminate curvatures induced by a uniform moisture content change
$\boldsymbol{\kappa}^{\mathbf{T}}$	Vector of laminate curvatures induced by a uniform temperature change
λ	Numerical differentiation parameter used in approach A2
ν_{ltk}	Major Poisson's ratio of k^{th} ply
ν_x	Major Poisson's ratio of laminate
$\tilde{\nu}_{xy}$	Laminate major Poisson's ratio goal
$\boldsymbol{\theta}$	Vector of layup angles
θ_k	Layup angle of k^{th} ply
$\boldsymbol{\theta}^*$	Vector of optimal layup angles
$\boldsymbol{\sigma}$	Vector of stresses in a ply in ply coordinates
$\overline{\boldsymbol{\sigma}}$	Vector of stresses in a ply in laminate coordinates
σ_l	Longitudinal stress in a ply in ply coordinates
σ_t	Transverse stress in a ply in ply coordinates
σ_{lt}	Shear stress in a ply in ply coordinates
$\hat{\sigma}_{Xj}$	Standard deviation of ply property X_j
$\hat{\sigma}_{Yi}$	Standard deviation of laminate property Y_i
${}^{\varepsilon}\hat{\sigma}^2_{Yij}$	Standard deviation of the i^{th} laminate property with the j^{th} ply standard deviation perturbed
ω_f	Fundamental frequency of optical support structure

ξ_i Primary weight factor in cost function

CHAPTER 1

INTRODUCTION

Space structures often have strict performance requirements on thermal and hygral deformation, strength, stiffness, and weight. Composite materials, particularly polymer matrix composites (PMCs), are strong candidates for such applications because of their high specific strength and stiffness, and the flexibility they give the designer to tailor properties. For example, it is possible to tailor composite laminates to have very low coefficients of thermal expansion (CTEs). This makes them attractive for dimensionally critical space structures such as antennae and waveguide supports, optical platforms, solar reflectors, truss tubes, and instrument support panels. A high level of dimensional stability may be a requirement for such structures; for example, a recently proposed microsatellite design for a space based telescope requires that the optical support structure have a near-zero CTE [1].

Composites used in space structures are often exposed to humid air (e.g. prior to launch), extremes in temperature (e.g. in orbit), and mechanical loads (e.g. during launch). Many matrix materials used in PMCs absorb moisture causing the matrix to swell. Also, without some form of

temperature control, exposed objects in low earth orbit experience approximately ±65 ^{o}C (±150 ^{o}F) temperature swings; exposed objects in geosynchronous orbit can experience ±120 ^{o}C (±250 ^{o}F) temperature swings. Deformation due to these large temperature swings and swelling due to moisture absorption may result in a failure to meet mission objectives. Thus, there is a large demand for dimensionally stable materials, i.e. materials that do not deform with changes in temperature and/or moisture environment.

The advantages of the tailorability of PMCs are not limited to dimensional stability. There are numerous applications where particular laminate stiffness and/or elastic properties are desired. For example, it may be desired to match the CTE of a laminate to that of another material bonded to it (e.g. solar cells) to help prevent delamination. Particular stiffness properties which result in favorable dynamic or aeroelastic behavior are often desired. The strength of composite laminates, which can also be tailored, is of concern since large loads are often encountered during launch. For example, a payload on the Pegasus launch vehicle experiences up to 13g axial and 9.5g lateral loading [2].

1.1 MOTIVATION

Methods exist for calculating composite laminate properties based on the known ply properties. However, material and manufacturing uncertainties, such as variations in ply material properties, layup angles,

fiber volume fractions, and cured thicknesses, result in variations of laminate properties. When dimensional stability is required it is critical to take into account the variability of laminate properties. For example, in theoretically-zero CTE laminates, the performance metric becomes the magnitude of the variation of the CTE, since the mean CTE is zero (or nearly so).

Over the past decade there has been an increasing trend to include the effects of the variability of loads, geometry, material properties, etc., when analyzing structures. This trend is in large part driven by the drawbacks of using a "traditional" knockdown (safety) factor approach to deal with uncertainty. The use of a safety factor approach in the design of composite structures is particularly restrictive.

The magnitude of the variation of composite laminate properties is a function of design variables (e.g. layup angles). This makes it difficult to define a safety factor based on "engineering judgment" and accumulated experience that blankets the infinite possible laminate designs. Furthermore, to do so would negate an important advantage of composites: the ability to tailor the magnitude of variation of the laminate properties themselves. This is a particularly important point with regard to the design for dimensional stability. There are often many candidate designs for dimensionally stable structures based on deterministic analyses, but many of these designs are found to be poor when the effects of uncertainty are included.

The use of safety factors (for strength, thermal deformation, etc.) can significantly alter design allowables, often resulting in a substantial increase in weight in order to meet mission objectives. This is of particular importance for aerospace structures since a substantial increase in weight corresponds to a substantial increase in cost. There is no general measure of the reliability of these safety factors; they are established by "engineering judgment" and accumulated experience. An alternate approach that accounts for the variability of laminate properties being a function of laminate design is of practical importance from both engineering and economic perspectives.

1.2 PRESENT WORK

The goal of the present work is to develop a general methodology to (i) determine the mean and standard deviation of laminate properties given models for them, (ii) tailor mean laminate properties to specified goals (if possible) while also minimizing the standard deviation of the laminate properties, and (iii) quantify the sensitivity of a laminate property to variations in the constituent properties that appear in the model for the laminate property. This methodology can be used by designers of composite structures to anticipate and minimize the magnitude of variability in laminate properties and to identify the critical properties and/or geometric variables that must be controlled during manufacture to assure laminate performance.

New probabilistic methods to determine the means, standard deviations, and sensitivities of laminate properties are developed. The probabilistic methods are coupled with models for the laminate stiffness, hygroelastic, thermoelastic, and strength properties. Also, some recently defined laminate properties are modeled: the coefficients of thermal and moisture bending (CTB and CMB respectively) [3]. The CTB and CMB are the out-of-plane analogs to the in-plane CTEs which characterize the bending or warping of a laminate due to changes in temperature and moisture content. A new global optimization method, here dubbed the Stochastic Simplex Method (SSM), is developed for tailoring mean laminate properties to specified goals while also minimizing their standard deviations. The probabilistic and optimization analysis methods are implemented in an easy-to-use menu-driven computer code.

The probabilistic and optimization methods, developed here, form a tool for the analysis and design of composite laminates. The methods provide a means to design composite laminates to have specified thermo/hygro elastic and/or stiffness properties with minimal variability about the specified values. Comparisons with experimental data for the elastic, thermoelastic, and strength properties are shown to verify the analysis methods and demonstrate where there is a need for more accurate modeling. Extensive parametric studies were performed to examine predicted trends; contour plots of the predicted mean, standard deviation, and coefficient of variation (when applicable) of all the predicted laminate properties are presented for

the $[\pm\theta/\pm\beta]_s$ family of laminates (where θ and β are variables). The probabilistic methods were used to carry out sensitivity studies to examine the relative importance of variations in the different ply material properties and geometric parameters to the variations in laminate properties. Optimal layups were determined for maximizing dimensional stability and stiffness, which are often the desired characteristics for space structures.

1.3 OVERVIEW

In Chapter 2 the previous work relevant to the problem is reviewed. This includes relevant examples of both analytical and experimental studies of laminate elastic, thermoelastic, hygroelastic, and strength properties. Relevant optimization methods and works where optimization methods are used in the design of composite laminates are also reviewed. A problem statement summarizing the present work is presented in Chapter 3. The analytical methodology and optimization method are developed in Chapter 4. In Chapter 5 the analysis is verified against existing experimental data; extensive parametric analyses and optimal layups for maximum dimensional stability and stiffness are presented; and the present approach is used to design a satellite structure for maximal dimensional stability with complex constraints imposed by the satellite mission objectives. Chapter 6 is a discussion of the results presented in Chapter 5 and the overall lessons

learned from this work. Finally, conclusions and recommendations for future work are presented in Chapter 7.

CHAPTER 2

BACKGROUND

It is well known that composite materials can be tailored to achieve a high level of dimensional stability [4-9]. However, the variability of constituent material properties, geometric parameters, etc., have placed limits on the achievable level of dimensional stability. This variability also limits the ability to precisely predict stiffness and strength properties. Consequently, much research has recently been devoted to probabilistic analysis methods that are capable of predicting the effects of this variability. Considerable work has been done on probabilistic methods for calculating the reliability of structures [10-12], including composite structures [13-17], and for calculating the functional performance of space systems [18, 19]. The aim of the present work is more modest than these efforts at global structural analysis, although it is not removed from them. The present work concentrates on the design of composite laminates to have specified properties, and the minimization of the variability expected in these properties.

One of the most important advantages of composites is the freedom they give a designer to tailor their properties. Much work has been done on optimization methods to determine how to tailor composites for specific problems. However, very little work has been done on optimization methods that account for effects due to the inherent variability of geometric parameters and material properties. Specifically, no work known to the author has been done on optimization methods to tailor composite laminates to have specified stiffness and/or elastic properties with minimal variability about the specified values.

In this chapter, works for the deterministic and probabilistic prediction of laminate properties, and relevant optimization methods, are reviewed. This review, as with any, is not complete. In areas of particular relevance, such as optimization and the prediction of CTE variations, an attempt was made to be thorough. Otherwise, only works used in the development and verification of the present analysis methods are reviewed.

2.1 LAMINATE STIFFNESS, THERMO/HYGRO ELASTIC, AND STRENGTH PROPERTIES

The accuracy of predicted themoelastic and hygroelastic properties is critical when designing dimensionally stable composite structures. Considerable work has been done on micromechanical models to predict ply and laminate properties based on properties of the fiber and matrix [20-27]. Bowles and Tompkins [20] compared ply longitudinal and transverse CTE

predictions from several micromechanics models with finite element models and experimental data from 0° unidirectional laminates. They found the models predicted the longitudinal CTE well, but the predicted transverse CTE did not compare well with the experimental data. They also carried out a sensitivity study and concluded that the longitudinal CTE was most sensitive to the longitudinal fiber CTE, and that the transverse CTE was most sensitive to the matrix CTE. Their approach was based on micromechanics and did not model variations in geometry or material properties that vary from ply to ply in a laminate.

Rogers *et al.* [28, 29] measured the CTEs of several different laminates at various temperatures. They noted that specimens with the same layup had different CTEs, but offered no explanation for the differences. Jones *et al.* [30] and Romeo and Frulla [31] also presented data showing differences in the CTEs of nominally identical laminates, neither addressed the differences. Experiments carried out by Abernathy [3] showed significant differences between the CTBs of nominally identical laminates. These differences were shown to be significantly larger than the uncertainty inherent in the test methods, and was attributed to variations in ply material properties and geometric parameters.

Experimental data for the coefficient of moisture expansion (CME) also show differences in nominally identical laminates [32, 33]. Stiffness and strength properties exhibit this behavior as well, e.g. [34, 35].

2.2 PROBABILISTIC METHODS FOR THE PREDICTION OF LAMINATE PROPERTIES

The variability of laminate properties, particularly the thermoelastic and hygroelastic properties, impose a practical limit on the level of dimensionally stability that can be achieved. This variability also limits the ability to tailor laminate properties to precise goals. Consequently, much research has centered on the development of probabilistic methods to predict the amount of variability to expect in laminate properties.

Tompkins and Funk [36] studied the effects of changing the ply stiffness and thermoelastic properties by 10% of their mean values. They considered several different layups and material systems and used CLPT to calculate the laminate CTEs. They found that variations in the ply CTEs and longitudinal stiffness had the most influence on the laminate CTE.

Wanthal and Petter [33] determined the statistical distributions of the fiber and matrix elastic and strength properties using extensive databases built from quality control tests from two manufacturers. They found that, by using probabilistic micromechanics models developed by Chamis *et al.* [15, 25, 37], that statistical distributions of the laminate stiffness properties can be predicted well, but that the same cannot be said for the strength properties. They supposed that the full strength of the fibers (as measured in individual fiber tests) is not realized in the laminate due to damage induced during the prepregging process. They proposed that the effective statistical

properties of the fibers should be back-calculated from unidirectional laminate tests to account for the damage. Yamada and Sun [38] determined the statistical distribution of the ultimate strength of four different laminates by doing a Monte Carlo simulation assuming that the ply strengths are random variables with a two parameter Weibull distribution. They demonstrated excellent correlation with experiment using fitted parameters in the Weibull distribution and a quadratic ply failure criteria (which they proposed). However, the sources of the variability of the ply strengths was not addressed.

McManus [39] developed a method for calculating the mean and standard deviations of the stiffness and elastic properties of composite laminates. The laminate properties were considered dependent random variables that are functions of ply material properties and geometric parameters, which were assumed to be independent random variables. The functions for the laminate properties were linearized about the mean ply material properties and geometric parameters. The linearization greatly simplified the mathematics and, via basic probability theory and CLPT, a simple and efficient method capable of determining the means and standard deviations of the laminate properties was achieved. However, this approach is limited to cases where the laminate properties can locally (in the vicinity of the mean ply material properties and geometric parameters) be approximated as a linear function of the ply properties. Also, the stiffness and elastic properties were assumed to be constant from ply to ply and only

vary from laminate to laminate. Sable [40] used the method developed by McManus and various other analysis tools to determine performance metrics for an antenna. This work demonstrated how probabilistic methods could be used as practical tools in the analysis of larger space structures. Abernathy and McManus [41] extended the method of McManus to include the effects of volume fraction variations and to predict variations in the CTBs and CMBs.

2.3 OPTIMIZATION

Given that one of the major advantages of composites is that they can be tailored, it is important that methods are available to determine how to tailor composites for particular problems. Numerous investigators have proposed techniques for optimizing composite laminates and structures. A good general review of optimization methods applied to composite laminates (e.g. for buckling, strength, frequency, etc.) can be found in [42].

The present review concentrates on optimization methods that have been used to optimize laminate stiffness and/or elastic properties. The reason for this greatly abridged review is that for purposes of optimization this work is primarily concerned with two problems: (i) design for maximal dimensional stability, and (ii) the tailoring of thermo/hygro elastic and stiffness properties to precise goals. All of the optimization methods reviewed maximize/minimize some function that is a metric of "goodness/badness" of, for example, the design of a composite laminate for a particular problem. This function is often referred to as the cost function and

is generally problem specific. (The "cost function" is also often referred to as the "objective function." The name "cost function" is used here.)

Analytical methods using closed form and/or graphical solution methods have been used to optimize laminates for stiffness [43-47]. Most of these methods are limited to optimization with respect to only a few parameters, or to consideration of only symmetric and balanced laminates. Nonlinear programming methods, which use techniques from multivariate calculus to find the extrema of continuous functions, have been extensively used to optimize composite laminates [47-54]. All of these optimization techniques are based on deterministic cost functions that do not include the effects of the variability of material properties and geometric parameters. To this end, Murotsu and Shao [55] present an optimization method that is capable of including the effects of the variability of material properties and geometric parameters. They use a reliability index (see reference [10] for a good introduction to reliability theory) as a measure of the variability of the laminate properties. However, none of these methods account for the multimodal cost functions that can arise for composite laminate properties (e.g. minimizing laminate CTEs). These optimization methods have no guaranteed of finding the global (as opposed to local) optima of a multimodal cost function; they converge to the first minima they encounter.

Given the difficulties of applying the previously discussed optimization methods to composite laminates, some investigators have used so-called Genetic Algorithms (GA). GAs are optimization algorithms based

on Darwinian models of natural selection and evolution. The original concepts of GAs were developed by Holland [56]. Many empirical simulations have demonstrated the efficiency and robustness of GAs on different optimization tasks [57-59]. GAs have only recently been used to optimize composite laminates, with much success [60-65]. A GA has recently been incorporated into the PANDA2 [66] laminated composite panel analysis program, demonstrating the usefulness of optimization in the design of composite panels [64].

Although GAs have been used successfully for the optimization of composite laminates, the rate of convergence is excessively slow [64, 67]. GAs typically converge to better solutions than the previously discussed methods when applied to multimodal cost functions. However, GAs are not guaranteed to find the global optima for two reasons: (i) the algorithms introduce precision limits that can substantially reduce solution accuracy, and (ii) the search process does not ergodically cover and search the design space [67]. The first deficiency has partly been addressed using methods such as dynamic parameter encoding [101]. However, the second deficiency has been largely unresolved.

None of the optimization methods discussed have been applied to the problem of designing composite laminates for maximum dimensional stability. This is probably in part due to the complex multimodal nature of the problem, which most optimization methods cannot handle, and the fact

that efficient probabilistic analysis methods suited to optimization have only recently been developed [3, 39, 68].

In the present work a new optimization method is developed that is a hybrid of a modified version of the downhill simplex method and a modified version of the simulated annealing algorithm. The downhill simplex method was first developed by Spendley *et al.* [69] and later revised by Nelder and Mead [70]. In its original form the downhill simplex method is a relatively simple optimization method which cannot handle multimodal cost functions.

The simulated annealing algorithm was first introduced as a Monte Carlo importance-sampling technique for doing large dimensional path integrals arising in statistical physics [71]. The name of the algorithm was coined from an intuitively satisfying analogy with thermodynamics, specifically the way that liquids freeze and crystallize, or metals cool and anneal [72]. For a theoretical treatment of the algorithm the reader is referred to Romeijn [73] as a good starting point. The algorithm has been used to solve a variety of problems, e.g., finding the optimal wiring for a densely wired computer chip [74]. More recently, the algorithm was modified by Ingber [75], significantly improving convergence speed and renamed Very Fast Simulated Re-Annealing (VFSR). VFSR was later renamed Adaptive Simulated Annealing (ASA) by Ingber [76]. The algorithm has been applied to several systems, ranging from combat analysis [77, 78], to finance [79, 80],

to neuroscience [81, 82]. The algorithm is now used world-wide across many disciplines [83].

The SSM is a combination of modified versions of the Downhill Simplex Method and the ASA algorithm that is capable of handling multimodal cost functions. In this thesis, the convergence speed of the SSM is compared with that of a GA and the ASA algorithm on a set of test cost functions typically used for GA and ASA benchmarking [67]. The SSM lends itself to a simple statistical proof of convergence to the global optima by drawing on results derived by Ingber [75].

CHAPTER 3

APPROACH

This chapter presents a concise statement of the problem addressed in this thesis and a very brief summary of the modeling and optimization approach used to solve the problem. The full development of the modeling and optimization methods is presented in Chapter 4.

3.1 PROBLEM STATEMENT

The goal of the present work is to develop a general methodology to (i) determine the mean and standard deviation of laminate properties given models for them, (ii) tailor mean laminate properties to specified goals (if possible) while also minimizing the standard deviation of the laminate properties, and (iii) quantify the sensitivity of a laminate property to variations in the constituent properties that appear in the model for the laminate property.

The laminate properties of interest are the laminate longitudinal stiffnesses E_x and E_y, major Poisson's ratio ν_{xy}, shear stiffness G_{xy}, coefficients of thermal expansion α, coefficients of moisture expansion β, coefficients of

thermal bending $\mathbf{W}^T$, coefficients of moisture bending $\mathbf{W}^H$, and the First and Last Ply Failure (FPF and LPF respectively) load factors of the laminate, R_{FPF} and R_{LPF}. The "starting" lengthscale of the present models for the laminate properties is at the scale of a ply. The ply material properties that appear in the models are: the longitudinal and transverse stiffnesses E_l and E_t, major Poisson's ratio ν_{lt}, shear stiffness G_{lt}, longitudinal and transverse CTEs α_l and α_t, and longitudinal and transverse coefficients of moisture expansion (CME) β_l and β_t. The ply geometric parameters are the thicknesses t and layup angles θ.

In order to use an optimization method to tailor laminate properties to specific goals an appropriate measure of cost must be defined. The optimization problem statement is as follows:

$$f_c(\theta) \equiv \sum_i \left[A_i \left| P_i - P_{gi} \right| + B_i \hat{\sigma}_{Pi} \right]$$

$$f_c(\theta^*) = \min_{\theta} \{ f_c(\theta) \} \qquad (3.1,a,b)$$

$$\text{subject to: } -\frac{\pi}{2} \le \theta \le \frac{\pi}{2}$$

Where $f_c(\theta)$ is the cost function, θ is a vector of the ply layup angles, and θ^* is a vector of the optimal layup angles. The A_i and B_i are weight factors that have the inverse units of their respective laminate properties (some may be zero). The P_i are the mean laminate properties (which are functions of the ply geometric parameters and material properties), the P_{gi} are the goals for

the mean laminate properties (which are specified), and the $\hat{\sigma}_{P_i}$ are the standard deviations of the laminate properties.

3.2 MODELING AND OPTIMIZATION APPROACH

The probabilistic analysis makes use of Classical Laminate Plate Theory (CLPT) and a stress based failure criterion. The laminate properties are assumed to be dependent random variables that are deterministic functions (via CLPT and failure criteria) of ply geometric parameters and material properties, which are considered to be independent random variables. Two new probabilistic methods are developed: a Monte Carlo method for the laminate failure properties, and a novel extension of the method originally developed by McManus for the laminate stiffness and elastic properties. Both probabilistic methods provide for the definition of sensitivity metrics. The sensitivity metric quantifies the contribution of the variation of a particular ply property to the variation of a particular laminate property.

For optimization a new global optimization method is developed. The method may be briefly described as an adaptive importance sampling technique (see Chapter 4 for the full development). The optimization method is used to determine the global minimum of the cost function defined in Eq. 3.1.

The probabilistic and optimization methods are implemented in an easy-to-use menu-driven computer program. Predicted results are compared with those from a general Monte Carlo method (which operates on the full nonlinear problem, but is very computationally expensive and does not provide for the definition of sensitivity metrics) and experimental data. The computer program is used to carry out extensive parametric analyses on general laminate families for all the laminate properties.

CHAPTER 4

ANALYSIS AND OPTIMIZATION METHODS

In this chapter the modeling and optimization methods are developed. In section 4.1 Classical Laminated Plate Theory is briefly reviewed and the laminate stiffness and elastic properties are defined. The failure models are described in Section 4.2. The probabilistic methods are developed in Section 4.3. The optimization method is described in Section 4.4. Last, the implementation scheme is described in Section 4.5.

4.1 CLASSICAL LAMINATED PLATE THEORY

Classical Laminated Plate Theory (CLPT) allows for the prediction of laminate elastic, thermoelastic, and hygroelastic properties from ply geometric parameters and material properties. Here, CLPT is only briefly reviewed since the intent is more to define notation rather than present the theory. For a more thorough introduction to CLPT the reader is referred to [84]. There are three basic assumptions made in the development of CLPT: (i) the thickness of the laminate is small compared to the other dimensions, (ii) strain varies linearly through the laminate thickness, and (iii) plane sections of the laminate remain plane and perpendicular to the midplane.

Assumptions ii and iii are collectively known as the Kirchoff-Love hypothesis. A global coordinate system, *xyz*, is considered to be aligned with the laminate. This coordinate system is referred to as the laminate coordinate system. The laminate is made up of n unidirectional plies. Ply properties for each individual ply are designated by the subscript k, where k=1,2,...,n. The material axes of the plies, *ltz*, are rotated an angle θ_k relative to the laminate axes. This rotated coordinate system is referred to as the ply coordinate system. Each ply has the following known material properties: longitudinal and transverse stiffness E_{lk} and E_{tk}, major Poisson's ratio ν_{ltk}, shear stiffness G_{ltk}, longitudinal and transverse CTEs α_{lk} and α_{tk}, and longitudinal and transverse CMEs β_{lk} and β_{tk}. The subscripts l and t designate longitudinal and transverse ply properties respectively.

4.1.1 Constitutive Relations

For each ply, in ply coordinates, the constitutive equations are

$$\sigma = \mathbf{Q}(\varepsilon - \alpha\Delta T - \beta\Delta H) \tag{4.1}$$

where σ is the in-plane stress vector, $\mathbf{Q}$ is the reduced ply stiffness matrix, ε is the in-plane engineering strain vector, α is the in-plane CTE vector, β is the in-plane CME vector, ΔT is the difference in temperature from the stress-free temperature, and ΔH is the difference, in percent weight change, from the stress-free moisture content.

The reduced ply stiffness matrix for the k^{th} ply is a symmetric 3x3 matrix. Using the usual notation [84] the indices of the rows and columns take the values of 1, 2, and 6. The elements of the reduced ply stiffness matrix (in ply coordinates) are as follows:

$$\begin{aligned} Q_{11(k)} &= \frac{E_{lk}}{D_k} \qquad Q_{12(k)} = \frac{\nu_{ltk} E_{tk}}{D_k} \\ Q_{22(k)} &= \frac{E_{tk}}{D_k} \qquad Q_{66(k)} = G_{ltk} \\ Q_{16(k)} &= Q_{26(k)} = 0 \\ D_k &= 1 - \nu_{ltk}^2 \frac{E_{tk}}{E_{lk}} \end{aligned} \tag{4.2}$$

The vectors of CTEs and CMEs for each ply in ply coordinates are:

$$\alpha_k = \begin{Bmatrix} \alpha_{lk} \\ \alpha_{tk} \\ 0 \end{Bmatrix} \qquad \beta_k = \begin{Bmatrix} \beta_{lk} \\ \beta_{tk} \\ 0 \end{Bmatrix} \tag{4.3 a,b}$$

To determine laminate properties, the ply material properties must be transformed from the ply coordinate systems (which are different for each ply) to the single laminate coordinate system. Material properties for each ply are transformed with the transformation matrix $\mathbf{T}_k$:

$$\mathbf{T}_k = \begin{bmatrix} \cos^2\theta_k & \sin^2\theta_k & 2\sin\theta_k\cos\theta_k \\ \sin^2\theta_k & \cos^2\theta_k & -2\sin\theta_k\cos\theta_k \\ -\sin\theta_k\cos\theta_k & \sin\theta_k\cos\theta_k & \cos^2\theta_k - \sin^2\theta_k \end{bmatrix} \tag{4.4}$$

where θ_k is the layup angle of ply k. The ply reduced stiffness in laminate coordinates is found from $\mathbf{Q}_k$ by a simple transformation of coordinates [84]:

$$\overline{\mathbf{Q}}_k = \mathbf{T}_k^{-1}\mathbf{Q}_k\mathbf{T}_k^{-\mathrm{T}} \tag{4.5}$$

Vectors and matrices in laminate coordinates are denoted by an over-bar. The superscript -T denotes first taking the inverse and then the transpose of the matrix. The transformations for the vectors of stress, strain, CTEs and CMEs are:

$$\overline{\boldsymbol{\sigma}} = \mathbf{T}_k^{-1}\boldsymbol{\sigma} \tag{4.6}$$

$$\overline{\boldsymbol{\varepsilon}} = \mathbf{T}_k^{\mathrm{T}}\boldsymbol{\varepsilon} \tag{4.7}$$

$$\overline{\boldsymbol{\alpha}}_k = \mathbf{T}_k^{\mathrm{T}}\boldsymbol{\alpha}_k \tag{4.8}$$

$$\overline{\boldsymbol{\beta}}_k = \mathbf{T}_k^{\mathrm{T}}\boldsymbol{\beta}_k \tag{4.9}$$

Transforming the ply constitutive relation, Eq. 4.1, to the laminate coordinate system yields:

$$\overline{\boldsymbol{\sigma}} = \overline{\mathbf{Q}}\left(\overline{\boldsymbol{\varepsilon}} - \overline{\boldsymbol{\alpha}}\Delta T - \overline{\boldsymbol{\beta}}\Delta H\right) \tag{4.10}$$

The Kirchoff-Love hypothesis assumes a linear variation of strain through the thickness of the laminate:

$$\overline{\boldsymbol{\varepsilon}} = \boldsymbol{\varepsilon}^{\circ} + \boldsymbol{\kappa} z \tag{4.11}$$

where the strain $\overline{\boldsymbol{\varepsilon}}$ includes contributions from the laminate midplane strain $\boldsymbol{\varepsilon}^{\circ}$ and the laminate curvature $\boldsymbol{\kappa}$.

The total thickness of the laminate is h, and the origin of the z axis is assumed at the laminate midplane. Substituting Eq. 4.11 into 4.10 and integrating through the thickness of the laminate:

$$\int_{-h/2}^{h/2} \bar{\sigma} dz = \int_{-h/2}^{h/2} \bar{\mathbf{Q}} \varepsilon^{\circ} dz + \int_{-h/2}^{h/2} \bar{\mathbf{Q}} \kappa z dz - \int_{-h/2}^{h/2} \bar{\mathbf{Q}} \bar{\alpha} \Delta T dz - \int_{-h/2}^{h/2} \bar{\mathbf{Q}} \bar{\beta} \Delta H dz \tag{4.12}$$

The running loads **N**, extensional stiffness matrix **A**, coupling stiffnesses **B**, bending stiffnesses **D**, running thermal "loads" $\mathbf{N}^{T}$, and running hygral "loads" $\mathbf{N}^{H}$ are defined as:

$$\mathbf{N} = \int_{-h/2}^{h/2} \bar{\sigma} dz \tag{4.13}$$

$$\mathbf{A} = \int_{-h/2}^{h/2} \bar{\mathbf{Q}} dz \tag{4.14}$$

$$\mathbf{B} = \int_{-h/2}^{h/2} \bar{\mathbf{Q}} z dz \tag{4.15}$$

$$\mathbf{D} = \int_{-h/2}^{h/2} \bar{\mathbf{Q}} z^2 dz \tag{4.16}$$

$$\mathbf{N}^{T} = \int_{-h/2}^{h/2} \bar{\mathbf{Q}} \bar{\alpha} \Delta T dz \tag{4.17}$$

$$\mathbf{N}^{H} = \int_{-h/2}^{h/2} \bar{\mathbf{Q}} \bar{\beta} \Delta H dz \tag{4.18}$$

Using the symbols for the vectors and matrices defined in Eqs. 4.13–4.18, Eq. 4.12 can be rewritten as:

$$\mathbf{N} = \mathbf{A}\boldsymbol{\varepsilon}^{\circ} + \mathbf{B}\boldsymbol{\kappa} - \mathbf{N}^{\mathrm{T}} - \mathbf{N}^{\mathrm{H}} \tag{4.19}$$

Rearranging gives:

$$\mathbf{N} + \mathbf{N}^{\mathrm{T}} + \mathbf{N}^{\mathrm{H}} = \mathbf{A}\boldsymbol{\varepsilon}^{\circ} + \mathbf{B}\boldsymbol{\kappa} \tag{4.20}$$

Similarly, moments are calculated by multiplying Eq. 4.10 by the out-of-plane coordinate z and integrating through the thickness:

$$\int_{-h/2}^{h/2} \bar{\sigma} z dz = \int_{-h/2}^{h/2} \bar{\mathbf{Q}}\boldsymbol{\varepsilon}^{\circ} z dz + \int_{-h/2}^{h/2} \bar{\mathbf{Q}}\boldsymbol{\kappa} z^2 dz - \int_{-h/2}^{h/2} \bar{\mathbf{Q}}\bar{\boldsymbol{\alpha}}\Delta T z dz - \int_{-h/2}^{h/2} \bar{\mathbf{Q}}\bar{\boldsymbol{\beta}}\Delta H z dz \tag{4.21}$$

The running moments **M**, running thermal "moments" $\mathbf{M}^{\mathrm{T}}$, and running hygral "moments" $\mathbf{M}^{\mathrm{H}}$ are defined as:

$$\mathbf{M} = \int_{-h/2}^{h/2} \bar{\sigma} z dz \tag{4.22}$$

$$\mathbf{M}^{\mathrm{T}} = \int_{-h/2}^{h/2} \bar{\mathbf{Q}}\bar{\boldsymbol{\alpha}}\Delta T z dz \tag{4.23}$$

$$\mathbf{M}^{\mathrm{H}} = \int_{-h/2}^{h/2} \bar{\mathbf{Q}}\bar{\boldsymbol{\beta}}\Delta H z dz \tag{4.24}$$

Using the symbols for the vectors and matrices defined in Eqs. 4.15, 4.16, and 4.22-4.24, Eq. 4.21 can be rewritten as:

$$\mathbf{M} = \mathbf{B}\boldsymbol{\varepsilon}^{\circ} + \mathbf{D}\boldsymbol{\kappa} - \mathbf{M}^{\mathrm{T}} - \mathbf{M}^{\mathrm{H}} \tag{4.25}$$

or

$$\mathbf{M} + \mathbf{M}^{\mathrm{T}} + \mathbf{M}^{\mathrm{H}} = \mathbf{B}\boldsymbol{\varepsilon}^{\circ} + \mathbf{D}\boldsymbol{\kappa} \tag{4.26}$$

Combining Eqs. 4.20 and 4.26 in matrix form:

$$\begin{Bmatrix} \mathbf{N} + \mathbf{N}^T + \mathbf{N}^H \\ \mathbf{M} + \mathbf{M}^T + \mathbf{M}^H \end{Bmatrix} = \begin{bmatrix} \mathbf{A} & \mathbf{B} \\ \mathbf{B} & \mathbf{D} \end{bmatrix} \begin{Bmatrix} \varepsilon^o \\ \kappa \end{Bmatrix} \tag{4.27}$$

Inverting Eq. 4.27:

$$\begin{Bmatrix} \varepsilon^\circ \\ \kappa \end{Bmatrix} = \begin{bmatrix} \mathbf{A} & \mathbf{B} \\ \mathbf{B} & \mathbf{D} \end{bmatrix}^{-1} \begin{Bmatrix} \mathbf{N} + \mathbf{N}^T + \mathbf{N}^H \\ \mathbf{M} + \mathbf{M}^T + \mathbf{M}^H \end{Bmatrix} \tag{4.28}$$

For convenience another notation for the inverse laminate stiffness matrix in Eq. 4.28 is introduced:

$$\begin{bmatrix} \mathbf{a}^* & \mathbf{b}^* \\ \mathbf{b}^{*T} & \mathbf{d}^* \end{bmatrix} = \begin{bmatrix} \mathbf{A} & \mathbf{B} \\ \mathbf{B} & \mathbf{D} \end{bmatrix}^{-1} \tag{4.29}$$

Using this notation, Eq. 4.28 becomes:

$$\begin{Bmatrix} \varepsilon^\circ \\ \kappa \end{Bmatrix} = \begin{bmatrix} \mathbf{a}^* & \mathbf{b}^* \\ \mathbf{b}^{*T} & \mathbf{d}^* \end{bmatrix} \begin{Bmatrix} \mathbf{N} + \mathbf{N}^T + \mathbf{N}^H \\ \mathbf{M} + \mathbf{M}^T + \mathbf{M}^H \end{Bmatrix} \tag{4.30}$$

where $\mathbf{a}^*$, $\mathbf{b}^*$, and $\mathbf{d}^*$ are 3x3 matrices whose indices follow the previously mentioned convention (subscripts with values of 1, 2, and 6). The stresses in ply coordinates, for each ply, may be determined by substituting Eq. 4.30 into Eq. 4.11 and using the transformation Eq. 4.7 and ply constitutive relation Eq. 4.1.

4.1.2 Laminate Engineering Constants

The total laminate thickness h is the sum of the individual ply thicknesses t_k:

$$h = \sum_{k=1}^{n} t_k \tag{4.31}$$

The laminate stiffnesses are calculated using elements of the inverted reduced laminate stiffness matrix and the total thickness of the laminate. E_x is the longitudinal laminate stiffness, E_y is the transverse laminate stiffness, ν_{xy} is the laminate major Poisson's ratio, and G_{xy} is the laminate shear stiffness.

$$E_x = \frac{1}{a_{11}^* h} \tag{4.32}$$

$$E_y = \frac{1}{a_{22}^* h} \tag{4.33}$$

$$\nu_{xy} = -\frac{a_{12}^*}{a_{11}^*} \tag{4.34}$$

$$G_{xy} = \frac{1}{a_{66}^* h} \tag{4.35}$$

Laminate CTEs and CMEs are found as follows: for a uniform temperature change, setting **N**, **M**, $\mathbf{N}^H$ and $\mathbf{M}^H$ to zero, substituting the definition of $\mathbf{N}^T$ and $\mathbf{M}^T$ from Eqs. 4.17 and 4.23 into Eq. 4.30 and replacing the integral through the thickness with an equivalent summation on the plies shows the thermally induced deformation to be a constant vector multiplied by ΔT. This constant vector consists of the laminate CTEs, which are:

$$^{l}\overline{\alpha} = \mathbf{a}^{*}\sum_{k=1}^{n}\overline{\mathbf{Q}}_{k}\overline{\alpha}_{k}t_{k} + \mathbf{b}^{*}\sum_{k=1}^{n}\overline{\mathbf{Q}}_{k}\overline{\alpha}_{k}t_{k}\bar{z}_{k} \tag{4.36}$$

Similarly, the laminate CMEs are:

$$^{l}\overline{\beta} = \mathbf{a}^{*}\sum_{k=1}^{n}\overline{\mathbf{Q}}_{k}\overline{\beta}_{k}t_{k} + \mathbf{b}^{*}\sum_{k=1}^{n}\overline{\mathbf{Q}}_{k}\overline{\beta}_{k}t_{k}\bar{z}_{k} \tag{4.37}$$

CLPT provides a means for calculating the in-plane laminate properties. In the following section it is shown that CLPT may also be used to determine the recently defined coefficients of thermal and moisture bending [3, 41], which are the out-of-plan analogs of the in-plane CTEs and CMEs.

4.1.3 Coefficients of Thermal and Moisture Bending

Following the development of Abernathy [3], this section presents a derivation of the coefficients of thermal and moisture bending, $\mathbf{W}^{T}$ and $\mathbf{W}^{H}$ respectively. The derivation begins with Eq. 4.30 in Section 4.1.1. For the case of no mechanical or moisture loading, $\mathbf{N}$, $\mathbf{M}$, $\mathbf{N}^{H}$ and $\mathbf{M}^{H}$, are all zero. Deformation is then caused only by a temperature change. For a uniform temperature change in the laminate, substituting the definition of $\mathbf{N}^{T}$ and $\mathbf{M}^{T}$ from Eqs. 4.17 and 4.23 into Eq. 4.30 and replacing the integral through the thickness with an equivalent summation on the plies shows the thermally induced curvature to be:

$$\boldsymbol{\kappa}^{T} = \left[\mathbf{b}^{*T}\sum\overline{\mathbf{Q}}_{k}\overline{\alpha}_{k}t_{k} + \mathbf{d}^{*}\sum\overline{\mathbf{Q}}_{k}\overline{\alpha}_{k}t_{k}\bar{z}_{k}\right]\Delta T \tag{4.38}$$

where $\bar{z}_k$ is the z coordinate of the midplane of the kth ply. The terms inside the brackets are only dependent on material properties and geometry, so a laminate property can be defined as:

$$\mathbf{W}^{\mathrm{T}} \equiv \mathbf{b}^{*\mathrm{T}} \sum \bar{\mathbf{Q}}_k \bar{\boldsymbol{\alpha}}_k t_k + \mathbf{d}^{*} \sum \bar{\mathbf{Q}}_k \bar{\boldsymbol{\alpha}}_k t_k \bar{z}_k \tag{4.39}$$

where $\mathbf{W}^{\mathrm{T}}$ is the coefficient of thermal bending vector. In a case where there is no mechanical or temperature loading and a uniform moisture distribution, the induced curvature due to a change of moisture content is:

$$\boldsymbol{\kappa}^{\mathrm{H}} = \left[\mathbf{b}^{*\mathrm{T}} \sum \bar{\mathbf{Q}}_k \bar{\boldsymbol{\beta}}_k t_k + \mathbf{d}^{*} \sum \bar{\mathbf{Q}}_k \bar{\boldsymbol{\beta}}_k t_k \bar{z}_k \right] \Delta H \tag{4.40}$$

hence

$$\mathbf{W}^{\mathrm{H}} \equiv \mathbf{b}^{*\mathrm{T}} \sum \bar{\mathbf{Q}}_k \bar{\boldsymbol{\beta}}_k t_k + \mathbf{d}^{*} \sum \bar{\mathbf{Q}}_k \bar{\boldsymbol{\beta}}_k t_k \bar{z}_k \tag{4.41}$$

where $\mathbf{W}^{\mathrm{H}}$ is the coefficient of moisture bending vector. $\mathbf{W}^{\mathrm{T}}$ and $\mathbf{W}^{\mathrm{H}}$ are the out-of-plane analogs to the in-plane vectors of the CTEs and CMEs α and β, respectively.

The laminate engineering constants, as defined in Section 4.1.2, are strictly valid only for symmetric laminates. In contrast, in a symmetric laminate, $\mathbf{W}^{\mathrm{T}}$ and $\mathbf{W}^{\mathrm{H}}$ are both zero. These properties are only meaningful for unsymmetric laminates. The different types of thermal and hygral deformation (for a laminate with free boundary conditions) is shown in Figure 4.1.

Longitudinal Expansion (α_x, β_x)

Longitudinal Bending (W_x^T, W_x^H)

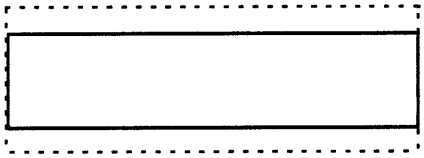

Transverse Expansion (α_y, β_y)

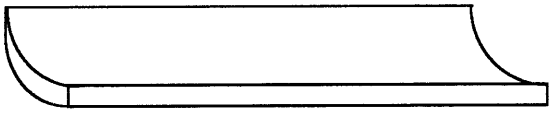

Transverse Bending (W_y^T, W_y^H)

Shearing (α_{xy}, β_{xy})

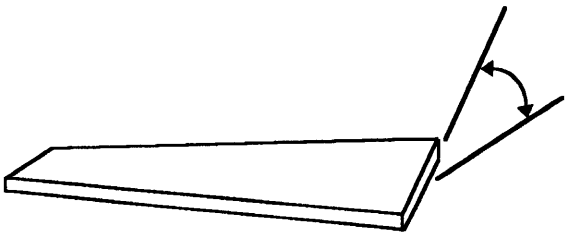

Twisting (W_{xy}^T, W_{xy}^H)

Figure 4.1 Types of thermal and hygral deformation of a free laminate

4.2 FAILURE MODELS

For the present work there are two desired outputs of the failure models: (i) the load at which damage initiates, and (ii) the load at which global failure occurs. The physics of failure in composites is very complex. Presently no quantitatively accurate mechanistic based models of the failure of composite laminates that can handle arbitrary laminate designs (e.g. different layup angles, ply thicknesses, etc.) exist [92]. Consequently, the simplest existing models that are known to capture some of the interesting and relevant phenomena are adopted here. It is assumed that only in-plane failure modes occur, and that damage occurs at the lengthscale of a ply (as opposed to, e.g., the lengthscale of a fiber). More complex models exist that include the possibility of out-of-plane failure modes, e.g. edge delamination [85], or that model the progressive microcracking of plies [93]. The failure models used here are admittedly simplistic, however. The simple failure models capture a significant amount of interesting and relevant phenomena. Also, it is believed that the simple failure models capture sufficient detail to determine if the probabilistic methods (developed in Section 4.3) are applicable to other, perhaps more complex, failure models.

The maximum stress failure theory is assumed [84]. The maximum stress theory assumes that damage occurs in a ply if any one of the stresses in the ply (in ply coordinates) exceeds its respective ply strength, that is, for tensile stresses:

$$\begin{aligned} \text{Longitudinal tensile failure} \quad & \sigma_l > {}^{T}X \\ \text{Transverse tensile failure} \quad & \sigma_t > {}^{T}Y \\ \text{Shear failure} \quad & \sigma_{lt} > S \end{aligned} \tag{4.42a}$$

and for compressive stresses:

$$\begin{aligned} \text{Longitudinal compresive failure} \quad & -\sigma_l > {}^{C}X \\ \text{Transverse compresive failure} \quad & -\sigma_t > {}^{C}Y \end{aligned} \tag{4.42b}$$

Where ${}^{T}X$, ${}^{T}Y$, S, ${}^{C}X$, and ${}^{C}Y$ are the ply strengths and are assumed to be constants. The stresses in Eqs. 4.42 are determined using CLPT (Section 4.1) with a constant ΔT and ΔH and the curvatures set to zero in Eq. 4.27. This is representative of what actually occurs in a typical test coupon.

For the failure analysis the mechanical loads are scaled as follows:

$$\mathbf{N} \rightarrow R\{\mathbf{N}'\} \tag{4.43}$$

Where N is the running load vector (defined in Eq. 4.13), R is a dimensionless scaling factor referred to as the *load factor*, and $\mathbf{N}'$ is a load case (typically with elements of order one). R controls the magnitude of $\mathbf{N}$; $\mathbf{N}'$ controls the relative magnitude of the different components of $\mathbf{N}$. For example, $\mathbf{N}' = \{1 \quad 0 \quad 0\}^{T}$ is a load case for uniaxial tension; $\mathbf{N}' = \{-1 \quad -1 \quad 0\}^{T}$ is a load case for biaxial compression.

The lowest load factor at which any of Eqs. 4.42 hold for any ply is assumed to be the load at which damage initiates, and is referred to as the first ply failure (FPF) load factor, R_{FPF}. To determine the load factor at which global failure occurs a *progressive failure analysis* is carried out since all the plies may not satisfy Eqs. 4.42 at the FPF load factor.

The first step in the progressive failure analysis is to determine the load factor at which the stress(es) in one or more of the plies just reaches the ply strength (i.e. the FPF load factor). This load factor is equal to the smallest (in magnitude) ratio of the stresses in each ply (in ply coordinates) to their corresponding ply strengths since stress scales linearly with applied load. The ply or plies with stresses exceeding any one of their respective strengths at this load factor are assumed to be damaged. The effect of damage is modeled as a reduction in ply material properties. For shear or transverse tensile or compressive ply failure (Eqs. 4.42a,b) the ply shear and transverse stiffnesses (G_{ltk} and E_{tk} respectively) in Eq. 4.3, for the ply that failed, are reduced by being multiplied by a *knockdown* factor of 0.5; for longitudinal tensile or compressive ply failure all the ply material properties in Eq. 4.3 (E_{lk}, E_{tk}, G_{ltk}, and ν_{ltk}), for the ply that failed, are multiplied by a knockdown factor that is very small, but greater than zero to prevent computational problems. Plies that initially fail in shear or transverse tension or compression may later fail, at a higher load factor, in the longitudinal tension or compression modes. This procedure, as summarized in Figure 4.2, is repeated until a load factor is reached for which all the plies are *completely* failed, at which point global failure is assumed. A ply is considered completely failed when it has failed in a longitudinal mode, with one exception. If the magnitude of the layup angle of a ply is greater than a

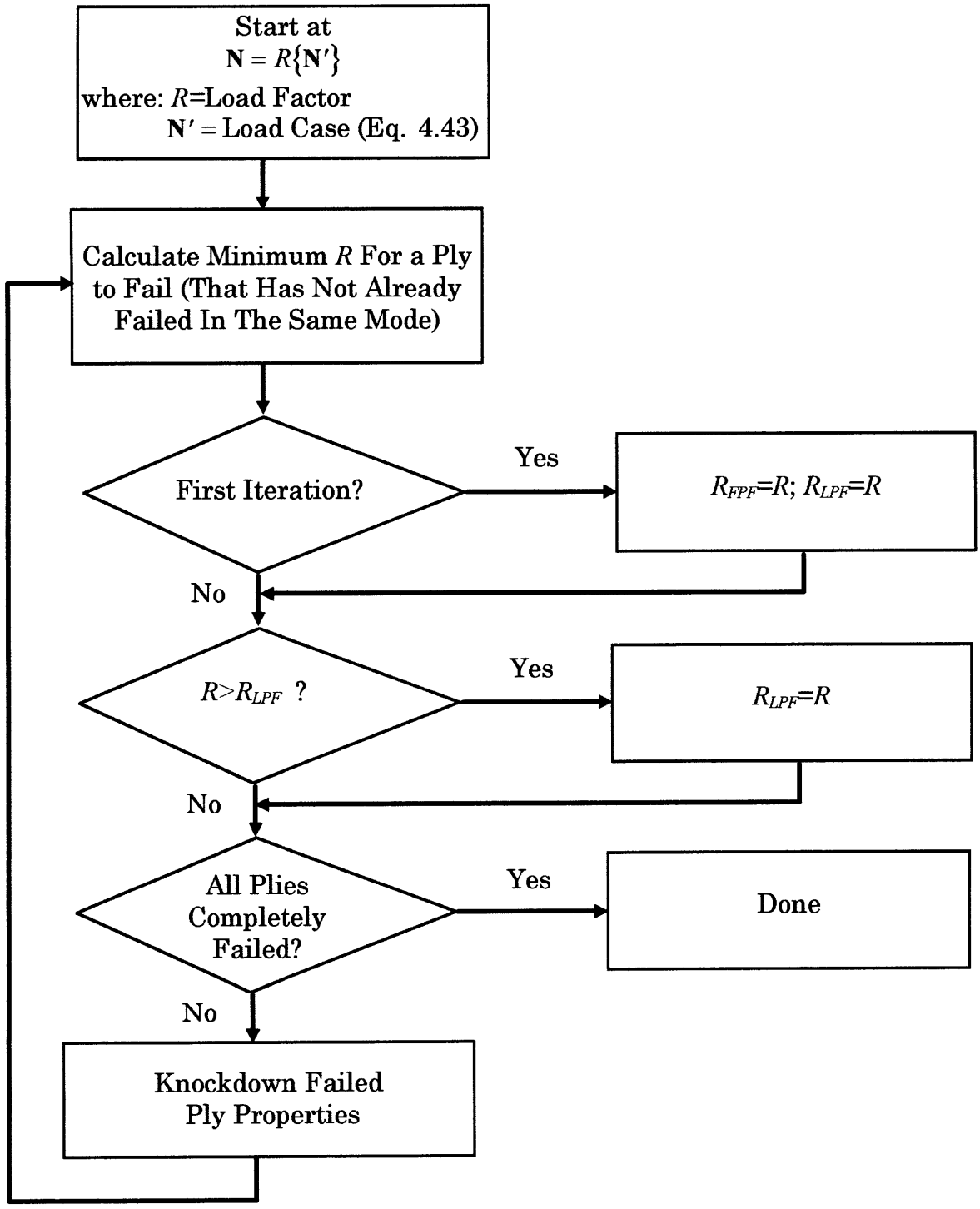

Figure 4.2 Flowchart of Progressive Failure Algorithm

specified *critical angle* the ply is considered completely failed when it has failed in a transverse and/or longitudinal mode. The maximum load factor that is reached during the progressive failure is referred to as the last ply failure (LPF) load factor, R_{LPF}. Note that in some cases it is possible that the first and last ply failure load factors are equal.

Later in this thesis it is convenient to define the laminate longitudinal strength as the average of the longitudinal stress (in laminate coordinates) in each of the plies at the LPF load (with a load case of $\mathbf{N}' = \{1 \quad 0 \quad 0\}^T$). That is, laminate longitudinal strength equals the LPF load factor, R_{LPF}, divided by the laminate thickness, h. This definition of strength reduces to the usual one if the laminate were isotropic.

The maximum stress failure criterion coupled with the progressive failure analysis and CLPT allows for the prediction of the FPF and LPF loads given the ply geometric parameters, material properties, and strengths. An important attribute of this simple procedure is that it can easily be extended to incorporate other failure theories. For example, a microcracking model can easily be implemented since knockdown factors may be defined that are a function of the load factor [93]; the dependence of the ply strengths on ply thickness and adjacent ply layup angles can also easily be modeled [99, 100].

4.3 PROBABILISTIC METHODS

The desired outputs of the probabilistic methods are the mean and standard deviations of all of the laminate properties, which are summarized in Table 4.1. Also, a sensitivity metric that quantifies the contribution of the variability of a ply material property or geometric parameter to the variability of the laminate properties is desired. Four probabilistic methods are considered to achieve this goal, here referred to as A1-A4 for convenience.

The first approach, A1, is that of McManus [39], which may be used to determine the mean and standard deviation of the laminate stiffness, thermoelastic, and hygroelastic properties. The second approach, A2, is a generalization of the method of McManus that can handle a higher level of nonlinearity. The third approach, A3, is a Monte Carlo method that is capable of determining the mean and standard deviations of the FPF and LPF loads, as well as the laminate stiffness and elastic properties. The fourth approach, A4, is an extension of the Monte Carlo method that allows for the definition of a sensitivity metric.

4.3.1 Approach A1

Following McManus [39], the laminate properties in Table 4.1 are considered dependent random variables Y_i. They are known deterministic functions of the ply properties and geometric parameters summarized in Table 4.2, which are assumed to be independent random variables X_j, hence:

Table 4.1 Predicted Laminate Properties

Variable	Symbol	Laminate Property Name
Y_1	E_x	longitudinal stiffness
Y_2	E_y	transverse stiffness
Y_3	G_{xy}	shear stiffness
Y_4	ν_{xy}	major Poisson's ratio
Y_5	α_x	longitudinal CTE
Y_6	α_y	transverse CTE
Y_7	α_{xy}	shear CTE
Y_8	W_x^T	longitudinal CTB
Y_9	W_y^T	transverse CTB
Y_{10}	W_{xy}^T	twist CTB
Y_{11}	β_x	longitudinal CME
Y_{12}	β_y	transverse CME
Y_{13}	β_{xy}	shear CME
Y_{14}	W_x^H	longitudinal CMB
Y_{15}	W_y^H	transverse CMB
Y_{16}	W_{xy}^H	twist CMB
Y_{17}	R_{FPF}	FPF load factor
Y_{18}	R_{LPF}	LPF load factor

Table 4.2 Independent Variables

Variable	Symbol	Ply Property/Parameter
$X_1,..,\ X_n$	$t_1,..,\ t_n$	thickness of ply 1,..,n
$X_{n+1},..,\ X_{2n}$	$\theta_1,..,\ \theta_n$	layup angle of ply 1,.., n
$X_{2n+1},..,\ X_{3n}$	$E_{l1},..,E_{ln}$	longitudinal stiffness of ply 1,.., n
$X_{3n+1},..,\ X_{4n}$	$E_{t1},..,\ E_{tn}$	transverse stiffness of ply 1,.., n
$X_{4n+1},..,\ X_{5n}$	$G_{lt1},..,\ G_{ltn}$	shear stiffness of ply 1,.., n
$X_{5n+1},..,\ X_{6n}$	$\nu_{lt1},..,\ \nu_{ltn}$	major Poisson's ratio of ply 1,.., n
$X_{6n+1},..,\ X_{7n}$	$\alpha_{l1},..,\ \alpha_{ln}$	longitudinal CTE of ply 1,.., n
$X_{7n+1},..,\ X_{8n}$	$\alpha_{t1},..,\ \alpha_{tn}$	transverse CTE of ply 1,.., n
$X_{8n+1},..,\ X_{9n}$	$\beta_{l1},..,\ \beta_{ln}$	longitudinal CME of ply 1,.., n
$X_{9n+1},..,\ X_{10n}$	$\beta_{t1},..,\ \beta_{tn}$	transverse CME of ply 1,.., n
$X_{10n+1},..,\ X_{11n}$	${}^{T}X_1,..,\ {}^{T}X_n$	longitudinal tensile strength of ply 1,.., n
$X_{11n+1},..,\ X_{12n}$	${}^{C}X_1,..,\ {}^{C}X_n$	longitudinal compressive strength of ply 1,.., n
$X_{12n+1},..,\ X_{13n}$	${}^{T}Y_1,..,\ {}^{T}Y_n$	transverse tensile strength of ply 1,.., n
$X_{13n+1},..,\ X_{14n}$	${}^{C}Y_1,..,\ {}^{C}Y_n$	transverse compressive strength of ply 1,.., n
$X_{14n+1},..,\ X_{15n}$	$S_1,..,\ S_n$	shear strength of ply 1,.., n

$$Y_i = f_{Yi}(X_1, X_2, \ldots, X_{15n}) \tag{4.44}$$

The functions f_{Yi} are determined from CLPT coupled with the progressive failure analysis for determining the FPF and LPF load factors. The functions f_{Yi} are in general highly nonlinear, particularly for the FPF and LPF load factors.

In this approach the functions for the laminate properties, f_{Yi}, are linearized about the mean values of the independent variables. Expanding f_{Yi} in a Taylor series:

$$f_{Yi}(X_1, X_2, \ldots, X_{15n}) = f_{Yi}(\overline{X}_1, \overline{X}_2, \ldots, \overline{X}_{15n}) + \sum_{j=1}^{15n} \left.\frac{\partial f_{Yi}}{\partial X_j}\right|_{\overline{X}_1, \overline{X}_2, \ldots, \overline{X}_{15n}} (X_j - \overline{X}_j) + H.O.T. \tag{4.45}$$

Neglecting the higher order terms in Eq. 4.45, f_{Yi} is expressed as a linear function of the X_j. It will later prove useful to visualize this linear function as a hyperplane that is tangent at the point defined by the mean values of the X_j. Using the linear approximation for f_{Yi}, the mean and standard deviation of the laminate properties can be approximated by [86]:

$$\overline{Y}_i \approx f_{Yi}(\overline{X}_1, \overline{X}_2, \ldots, \overline{X}_{15n}) \tag{4.46}$$

$$\hat{\sigma}_{Yi}^2 \approx \sum_{j=1}^{15n} \sum_{k=1}^{15n} \left\{ c_{jk} \left[\frac{\partial f_{Yi}}{\partial X_j} \frac{\partial f_{Yi}}{\partial X_k} \right]_{\overline{X}_1, \overline{X}_2, \ldots, \overline{X}_{15n}} \hat{\sigma}_{Xj} \hat{\sigma}_{Xk} \right\} \tag{4.47}$$

Where $\hat{\sigma}_{Xj}$ is the standard deviation of the ply property or geometric parameter X_j, and c_{jk} is the correlation coefficient between X_j and X_k. Noting

the assumption that the X_j are independent, and therefore uncorrelated, Eq. 4.47 can be simplified to:

$$\hat{\sigma}_{Y_1}^2 \approx \sum_{j=1}^{15n} \left(\left. \frac{\partial f_{Y_1}}{\partial X_j} \right|_{\bar{X}_1, \bar{X}_2, \ldots, \bar{X}_{15n}} \hat{\sigma}_{Xj} \right)^2 \tag{4.48}$$

since $c_{jk}=\delta_{jk}$, where δ_{jk} is the Kronecker delta ($\delta_{jk}=0$ if $j \neq k$ and $\delta_{jk}=1$ if $j=k$).

This approach has the advantage of being computationally efficient for laminates with a low number of plies n. This follows since Eq. 4.44 only need be evaluated once for Eq. 4.46 and $30n$ times for equation 4.48 (using a central difference approximation in place of the derivatives). Another advantage is that detailed information about the distribution functions of the X_j, aside from the mean and standard deviation, is not necessary.

This approach has the disadvantage that it only results in a good approximation for functions that do not deviate much from the linear approximation in a region (typically a $15n$-dimensional rectangle with sides a few standard deviations, $\hat{\sigma}_{Xj}$, in length) about the point of linearization. Another disadvantage is that in order for this approach to make sense f_{Yi} must be smooth. The functions for the FPF and LPF loads are in general nonsmooth since corners and/or discontinuities exist. Corners may exist at changes of failure mode for the FPF load; corners or discontinuities may exist where there is a change in the path to failure for the LPF load. This approach is obviously not applicable at a corner or a discontinuity; in the

context of approach A1 the derivative is undefined at corners and discontinuities.

4.3.2 Approach A2

The second approach consists of a slight modification of Eq. 4.48 (or Eq. 4.47 in the general case). Rather than attempting to approximate the function f_{Yi}, as in A1, we seek to find a function that results in a good approximation of $\hat{\sigma}_{Xj}$. Specifically, we again consider a hyperplane, although, as opposed to A1, it is not required that the hyperplane be tangent at the point defined by the mean values of the X_j.

Eq. 4.46 is again considered as an approximation for the mean of Y_i. To approximate the standard deviation of Y_i the derivatives of f_{Yi} in Eq. 4.48 are "redefined" as:

$$\frac{\partial f_{Y_i}}{\partial X_j} \equiv \frac{\left[\begin{array}{r} f_{Y_i}\left(\overline{X}_1, \overline{X}_2, \ldots, \overline{X}_j + \lambda\hat{\sigma}_{Xj}, \ldots, \overline{X}_{15n}\right) - \\ f_{Y_i}\left(\overline{X}_1, \overline{X}_2, \ldots, \overline{X}_j - \lambda\hat{\sigma}_{Xj}, \ldots, \overline{X}_{15n}\right) \end{array}\right]}{2\lambda\hat{\sigma}_{Xj}} \tag{4.49}$$

Here, λ is a dimensionless constant that is carefully chosen to give a good approximation for $\hat{\sigma}_{Y_i}$. A graphical representation of this "redefined" derivative is shown in Figure 4.3. The original formulation of McManus [39] may be recovered by setting λ to unity and interpreting Eq. 4.49 as an approximation for the derivatives in Eq. 4.48. For small λ Eq. 4.49 is simply a central difference approximation for the derivatives in Eq. 4.48. Here, a

value of 2 is used for λ since it results in very good correlation with Monte Carlo simulations for the laminate stiffness and elastic properties listed in Table 4.1 (as shown in Chapter 5). A key difference between this approach and A1 is that the finite value of λ allows for the collection of information over a range as opposed to a point (as in A1). The advantage of a finite λ can be seen in figure 4.3 where if λ where very small (i.e. approach A2 becomes A1) the effects of the "cliff" would not be taken into account resulting in a poor approximation for the standard deviation. In Appendix A it is shown that $\lambda \approx 2$ is an optimal choice for a class of nonlinear functions that exhibit the typical types of nonlinearities of the f_{Yi}.

This simple approach was shown by Southard and McManus [68] to be able to handle highly nonlinear/nonsmooth f_{Yi} for determining the variability of the FPF and LPF loads due to variations of layup angles and ply thicknesses and batch to batch variations of stiffness and elastic properties (i.e. the stiffness and elastic properties are assumed constant from ply to ply within a particular laminate, but vary from laminate to laminate). This simple approach is particularly useful when the f_{Yi} is highly nonlinear/nonsmooth in a single variable and relatively well behaved in the other variables, as was the case in reference [68]. However, when variations of the stiffness and elastic properties from ply to ply are considered this approach is not applicable for predicting the standard deviation of the FPF and LPF loads. The primary reason that this approach is no longer

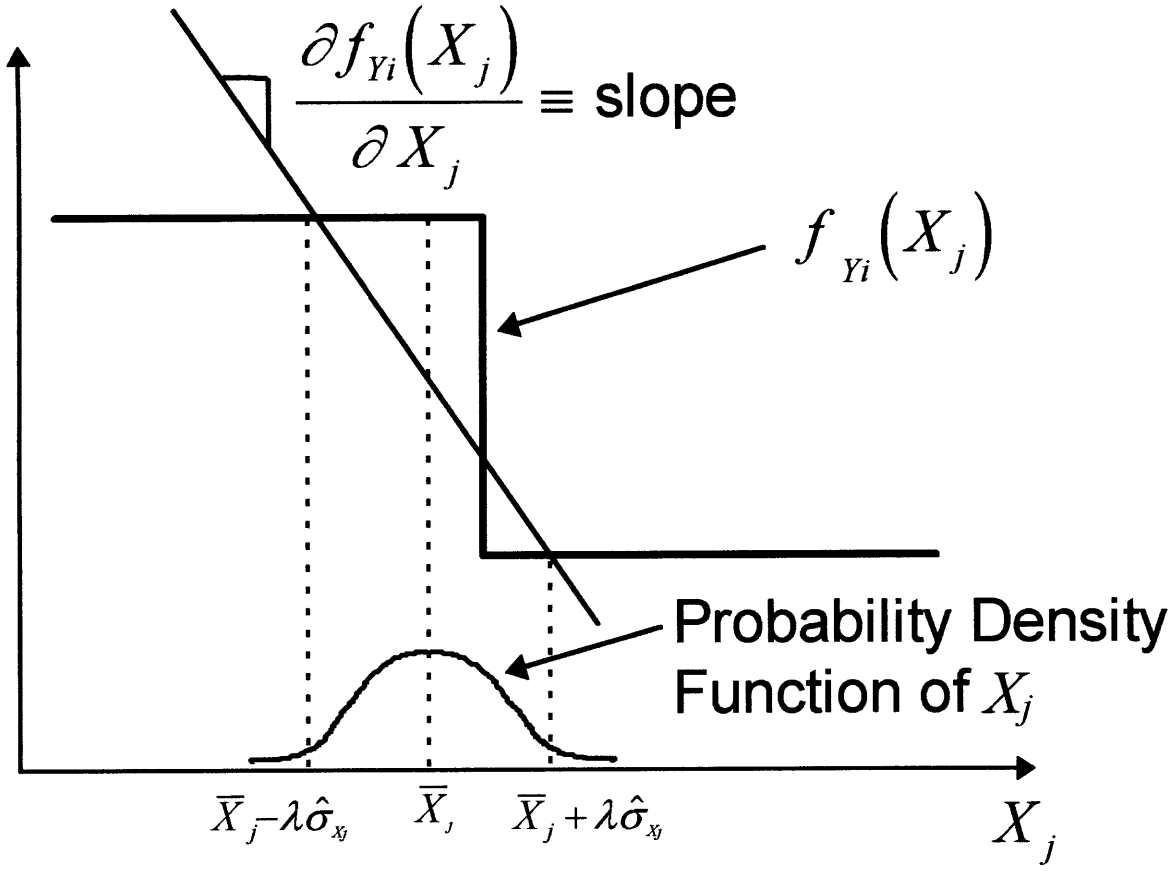

Figure 4.3 Graphical representation of redefined derivative

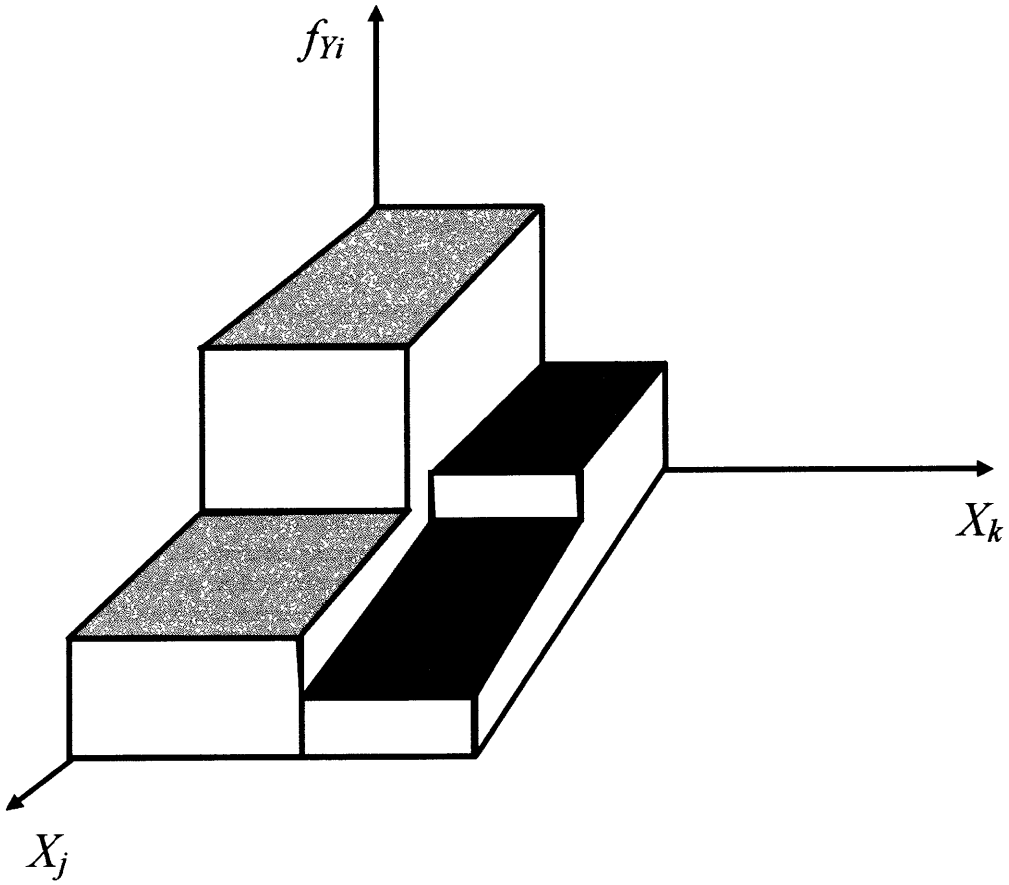

Figure 4.4 Example of nonsmooth function in multiple variables

applicable is that the FPF and LPF loads are highly nonlinear and discontinuous in *multiple* variables. As a result, as can be seen in figure 4.4, the derivative of f_{Yi} with respect to X_j (defined in Eq. 4.49) can suddenly change magnitude with a small change in X_k. The derivatives are very different in the light and dark gray regions of Figure 4.4 (since the height of the cliffs are different). Hence, the predicted standard deviation suddenly changes with a slight change in X_k. This approach is not appropriate for this multiply discontinuous problem since it is only capable of gathering information over a range in one direction; it is not capable of "seeing" nearby cliffs in other *directions*. Another reason that this approach is not applicable is due to an *interaction* phenomenon discussed in Appendix B.

4.3.3 Sensitivity Metrics From A1 and A2

Both A1 and A2 provide for a natural definition of a sensitivity metric. The contribution of the variation of independent variable X_j to the variation of dependent variable Y_i is the absolute value of the term inside the brackets in Eq. 4.48 (for A1). For A2 the derivative is again replaced by Eq. 4.49, resulting in the following sensitivity metric:

$$ {}^{A2}d_{ij} = \left| \frac{\left[f_{Yi}\left(\overline{X}_1, \overline{X}_2, \ldots, \overline{X}_j + \lambda\hat{\sigma}_{Xj}, \ldots, \overline{X}_M\right) - f_{Yi}\left(\overline{X}_1, \overline{X}_2, \ldots, \overline{X}_j - \lambda\hat{\sigma}_{Xj}, \ldots, \overline{X}_M\right) \right]}{2\lambda} \right| \tag{4.50} $$

This sensitivity metric can be thought of as the slope of the hyperplane (with respect to the j^{th} independent variable) weighted by the standard deviation of the j^{th} independent variable. Taking the Euclidean norm of the sensitivities results in the standard deviation of the i^{th} laminate property.

It is not practical to present sensitivity metrics for each ply (especially for laminates with a large number of plies). So, rather than present data for each ply the sensitivities are combined in the following way:

$$
\begin{aligned}
{}^{A2}d_{i\ ply\ thickness} &= \sqrt{\sum_{j=1}^{n} {}^{A2}d_{ij}^{2}} \\
{}^{A2}d_{i\ layup\ angle} &= \sqrt{\sum_{j=n+1}^{2n} {}^{A2}d_{ij}^{2}} \\
&\vdots \\
&\vdots \\
{}^{A2}d_{i\ shear\ strength} &= \sqrt{\sum_{j=14n+1}^{15n} {}^{A2}d_{ij}^{2}}
\end{aligned}
\tag{4.51}
$$

These combined sensitivity metrics are the Euclidean norm, over all the plies, of the sensitivities for a particular ply property. Taking the Euclidean norm of these combined sensitivities again results in the standard deviation of the i^{th} laminate property. These metrics provide a measure of the overall effect of the variability of a particular ply property on the variability of the laminate properties. The sensitivity metrics allow for the identification of critical ply properties that most contribute to the amount of variability in the laminate properties.

4.3.4 Approach A3

In the Monte Carlo approach, synthetic data sets are produced for the X_j using their (assumed known) probability distributions:

$$\left\{X_j^{(1)}, X_j^{(2)}, \ldots, X_j^{(k)}, \ldots, X_j^{(N-1)}, X_j^{(N)}\right\} \quad j = 1,..,15n \tag{4.52}$$

where N is a large number. These data sets are then run through the deterministic functions for the laminate properties, f_{Yi}, resulting in synthetic data sets for the laminate properties, Y_i:

$$\left\{Y_i^{(1)}, Y_i^{(2)}, \ldots, Y_i^{(k)}, \ldots, Y_i^{(N-1)}, Y_i^{(N)}\right\} \quad i = 1,..,18 \tag{4.53}$$

The mean and standard deviation of the Y_i are then approximated using the well known formulas (e.g. [88]):

$$\overline{Y}_i \approx \frac{1}{N}\sum_{k=1}^{N} Y_i^{(k)} \tag{4.54}$$

$$\hat{\sigma}_{Yi}^2 \approx \frac{1}{N-1}\left\{\sum_{k=1}^{N}\left(Y_i^{(k)} - \overline{Y}_i\right)^2\right\} \tag{4.55}$$

In the present work, for A3 and A4, the X_j are assumed to be normally distributed random variables. The Box-Muller method is used to generate the normally distributed $X_j^{(k)}$ [87]:

$$X_j^{(k)} = \overline{X}_j + \hat{\sigma}_{Xj}\cos\left(2\pi r^{(k)}\right)\sqrt{-2\ln\left(r^{(k)}\right)} \tag{4.56}$$

where $r^{(k)}$ is a uniform random deviate between 0 and 1. The random number generator of Park and Miller, with Bays-Durham shuffle, is used to generate the $r^{(k)}$ [88]. The $Y_i^{(k)}$ are then determined using Eq. 4.44:

$$Y_i^{(k)} = f_{Y_i}\left(X_1^{(k)}, X_2^{(k)}, \ldots, X_{15n}^{(k)}\right) \tag{4.57}$$

This approach has the advantage of generality in that it makes minimal assumptions on the functions for the laminate properties f_{Y_i} (e.g. smoothness). The approach has the disadvantage of being computationally expensive for large N, since N corresponds to the number of evaluations of Eq. 4.57. This is a significant drawback when the procedure must be repeated many times, e.g. for making high resolution plots (some details concerning this point are discussed in Appendix C). The approach, as described here, also has the disadvantage that there is no sensitivity metric. In the following section this approach is extended in a way that allows for the definition of a sensitivity metric.

4.3.5 Approach A4

In this approach it is assumed that the square of the standard deviation of a laminate property can be represented as a linear sum of the squares of the standard deviations of the ply properties and geometric parameters:

$$\hat{\sigma}_{Y_i}^2 = \sum_{j=1}^{15n}\left(\gamma_{ij}\hat{\sigma}_{X_j}\right)^2 \tag{4.58}$$

The γ_{ij} are constants that are to be determined. This functional form is consistent with those derived in A1 and A2 (it is possible to choose other functional forms, however). In A1 the γ_{ij} are the derivatives in Eq. 4.48; for

A2 the γ_{ij} are the "redefined" derivatives in Eq. 4.49. To determine the γ_{ij} in the present approach a perturbation on $\hat{\sigma}_{Xj}$ in Eq. 4.58 is considered:

$$ {}^{\varepsilon}\hat{\sigma}^2_{Yij} = \gamma^2_{i1}\hat{\sigma}^2_{X1} + \ldots + \gamma^2_{i(j-1)}\hat{\sigma}^2_{X(j-1)} + \gamma^2_{ij}\left(\hat{\sigma}_{Xj} + \varepsilon\hat{\sigma}_{Xj}\right)^2 + \ldots + \gamma^2_{i(15n)}\hat{\sigma}^2_{X(15n)} \tag{4.59} $$

Here, ${}^{\varepsilon}\hat{\sigma}^2_{Yij}$ is the standard deviation of the i^{th} laminate property with the j^{th} ply material property or geometric parameter standard deviation, $\hat{\sigma}_{Xj}$, perturbed by the amount $\varepsilon\hat{\sigma}_{Xj}$. It is possible that the γ_{ij} are dependent on all the $\hat{\sigma}_{Xj}$ (in Appendix B this is shown to be the case); here, it is assumed that the j^{th} γ_{ij} is dependent on the j^{th} $\hat{\sigma}_{Xj}$ to a lower order than the other $\hat{\sigma}_{Xj}$. Hence, for small ε, subtracting Eq. 4.58 from 4.59 yields:

$$ {}^{\varepsilon}\hat{\sigma}^2_{Yij} - \hat{\sigma}^2_{Yi} = \gamma^2_{ij}\left(\hat{\sigma}_{Xj} + \varepsilon\hat{\sigma}_{Xj}\right)^2 + H.O.T. \tag{4.60} $$

Neglecting the higher order terms, and solving for $\gamma^2_{ij}\hat{\sigma}^2_{Xj}$:

$$ \gamma^2_{ij}\hat{\sigma}^2_{Xj} = \frac{{}^{\varepsilon}\hat{\sigma}^2_{Yij} - \hat{\sigma}^2_{Yi}}{\varepsilon(\varepsilon+2)} \approx \frac{{}^{\varepsilon}\hat{\sigma}^2_{Yij} - \hat{\sigma}^2_{Yi}}{2\varepsilon} \tag{4.61} $$

The choice of ε is arbitrary (as long as it is not too large). Here ε is set to 0.01 (1% change), so Eq. 4.61 becomes:

$$ \gamma^2_{ij}\hat{\sigma}^2_{Xj} \approx 50\left({}^{\varepsilon}\hat{\sigma}^2_{Yij} - \hat{\sigma}^2_{Yi}\right) \quad \text{when: } \varepsilon = 0.01 \tag{4.62} $$

In analogy with the sensitivity metric defined in Section 4.3.3, Eq. 4.62 is used as a sensitivity metric:

$$ {}^{A4}d_{ij} = \sqrt{50\left({}^{\varepsilon}\hat{\sigma}^2_{Yij} - \hat{\sigma}^2_{Yi}\right)} \tag{4.63} $$

Taking the Euclidean norm of the sensitivities, as before, results in the standard deviation of the i^{th} laminate property. As before, these sensitivity metrics are combined by taking the Euclidean norm over all the plies of each of their ply properties and geometric parameters (see Section 4.3.3):

$$\begin{aligned} {}^{A4}d_{i\ ply\ thickness} &= \sqrt{\sum_{j=1}^{n} {}^{A4}d_{ij}^2} \\ {}^{A4}d_{i\ layup\ angle} &= \sqrt{\sum_{j=n+1}^{2n} {}^{A4}d_{ij}^2} \\ &\vdots \\ &\vdots \\ {}^{A4}d_{i\ shear\ strength} &= \sqrt{\sum_{j=14n+1}^{15n} {}^{A4}d_{ij}^2} \end{aligned} \tag{4.64}$$

In this work A3 is used to determine $\hat{\sigma}_{Y_i}$ in Eq. 4.63, in general any approach may be used. To determine the ${}^{\varepsilon}\hat{\sigma}_{Yij}$ A3 is again used with the j^{th} ply property standard deviation perturbed:

$$\hat{\sigma}_{Xj} \rightarrow \hat{\sigma}_{Xj} + 0.01\hat{\sigma}_{Xj} \tag{4.65}$$

This approach takes into account the possibility that the γ_{ij} may be a function of all of the $\hat{\sigma}_{Xj}$. This *interaction* behavior can play an important role for the FPF and LPF loads (as a result of their high nonlinearity), as explained in detail in Appendix B. Chapter 5 contains comparisons of standard deviations recovered by taking the Euclidean norm of the sensitivity metrics using A4 with direct predictions from A3. Correlation is

shown to be excellent indicating that the assumptions and functional form (Eq. 4.58) used are appropriate.

4.4 OPTIMIZATION METHODS

In this section an optimization method is developed that is capable of tailoring mean laminate properties to specified goals, while also minimizing the standard deviation of the laminate properties. In order to use an optimization method to tailor laminate properties, an appropriate measure of cost that is to be minimized must be defined. The optimization problem statement is as follows:

$$f_c(\theta) \equiv \sum_i \left[A_i \left| P_i - P_{gi} \right| + B_i \hat{\sigma}_{P_i} \right]$$

$$f_c(\theta^*) = \min_{\theta} \{ f_c(\theta) \} \qquad (4.66,a,b)$$

$$\text{subject to: } -\frac{\pi}{2} \le \theta \le \frac{\pi}{2}$$

$f_c(\theta)$ is the cost function, where θ is a vector of the ply layup angles and θ^* is a vector of the optimal layup angles that correspond to the global minima of $f_c(\theta)$. The A_i and B_i are weight factors that have the inverse units of their respective ply properties (some may be zero). The P_i are the mean laminate properties (which are functions of the ply geometric parameters and material properties), the P_{gi} are the goals for the laminate properties (which are specified), and the $\hat{\sigma}_{P_i}$ are the standard deviations of the laminate properties (which are also functions of the ply geometric parameters and material

properties). This cost function is designed to match laminate properties to specified goals and minimize the variability of the laminate properties about these goals. If the goals are not obtainable the layup angles that result in the laminate properties being "closest" (in an average sense) to the goals is found; the variability of the "closest" properties is also minimized.

In general, $f_c(\theta)$ contains local minima. For example, a simple cost function for minimizing the mean and standard deviation of the longitudinal CTE (with weights A and B equal to one °F/με) contains local minima, as can be seen in Figure 4.5 (the SD[ ] operator shown in the plot reads as: Standard Deviation of). As a result of the existence of local minima a global optimization technique must be used to determine the θ^*.

Here, a new optimization method is developed that is a hybrid of a modified version of the downhill simplex method and a modified version of the simulated annealing algorithm called Adaptive Simulated Annealing (ASA) [76]. The downhill simplex method was first developed by Spendley *et al.* [69] and later revised by Nelder and Mead [70]. In its original form the downhill simplex method is a relatively simple optimization method that cannot handle multimodal cost functions. The hybrid method, here dubbed the Stochastic Simplex Method (SSM), is capable of handling the complex multimodal cost functions that arise when optimizing composite laminates (e.g. for minimal thermal distortion). Despite the simple reasoning used in

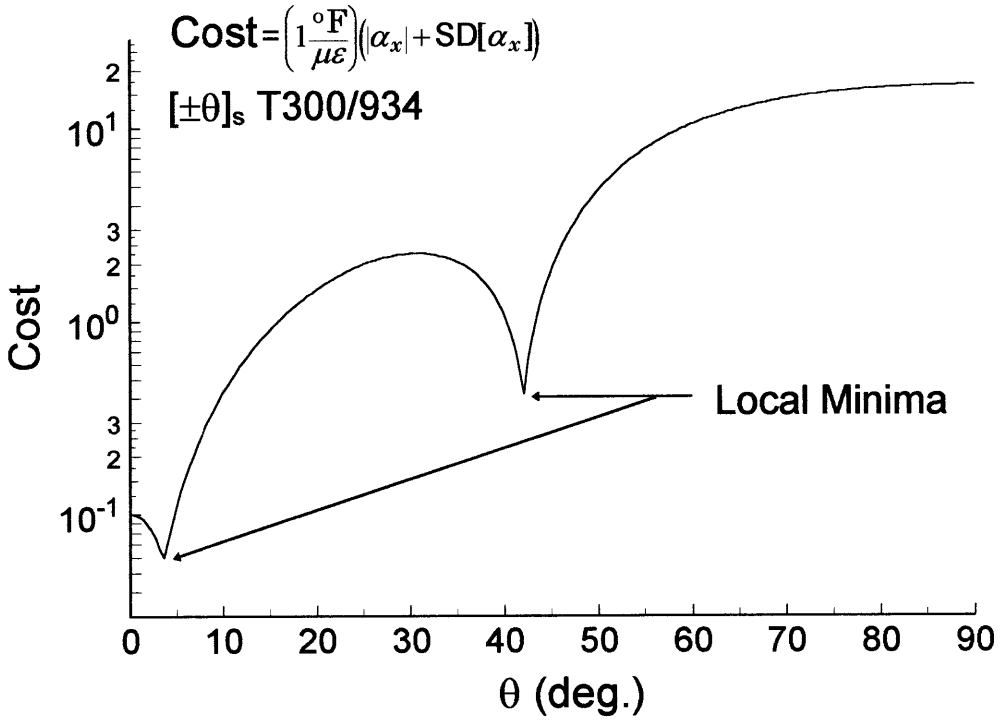

Figure 4.5 Plot demonstrating existence of local minima

the development of the SSM, it is on average two orders of magnitude faster than a Genetic Algorithm and one order of magnitude faster than the ASA algorithm (as shown in Appendix E), based on the convergence speed for a set of test cost functions typically used for GA and ASA benchmarking [67]. The SSM also lends itself to a simple statistical proof of convergence to the global optima by drawing on results derived by Ingber [75].

The ASA algorithm is described in Section 4.4.1. The downhill simplex method and the SSM are described in Section 4.4.2. Last, termination criteria are described in Section 4.4.3.

4.4.1 The Adaptive Simulated Annealing (ASA) Algorithm

This section closely follows discussions from [67] and [88]. The author has filled in many gaps and added a number of his own explanations. This has been done in the hopes of creating a clearer and more concise presentation of the ASA algorithm.

Simulated annealing was first introduced as a Monte Carlo importance-sampling technique for doing large dimensional path integrals arising in statistical physics problems [71]. The method has an intuitively satisfying analogy with thermodynamics, specifically the way that liquids freeze and crystallize, or metals cool and anneal.

At high temperatures, the molecules of a liquid move freely with respect to one another. If the liquid is cooled slowly, thermal mobility is lost. The molecules are often able to line themselves up and form a pure crystal

that is completely ordered over a distance up to billions of times the size of an individual atom in all directions. The crystal is the state of minimum energy for this system. The amazing fact is that for slowly cooled systems, nature is able to find this minimum energy state. In fact, if a liquid metal is cooled quickly, or "quenched," it does not reach this state but rather ends up in a polycrystalline or amorphous state having somewhat higher energy.

So the essence of the processes is in the cooling schedule. Ample time must be allowed for the redistribution of the atoms as they lose mobility. This is the definition of annealing, and it is essential for ensuring that a low energy state will be achieved.

Natures minimization algorithm (in this context) is "based" on the so-called Boltzmann probability distribution: $Prob(E)=P_o exp(-(E-E_o)/KT)$, which expresses the idea that a system of, e.g., molecules, in thermal equilibrium at temperature T has its energy probablisticly distributed among all different energy states E. The quantity K (Boltzmann's constant) is a constant of nature that relates temperature to energy; P_o is the probability that a molecule has some minimum energy E_o. Even at a low temperature, there is a chance, albeit very small, of a particular molecule being in a high energy state. Therefore, there is a corresponding chance for the molecules to get out of a local energy minimum in favor of finding a better, more global, one. Put simply, the system sometimes goes "uphill" as well as "downhill"; but the lower the temperature, the less likely is any significant uphill excursion.

In order to make use of the simulated annealing algorithm for other than thermodynamic systems three functional relationships are required:

- $g(\mathbf{x})$: Probability density of state-space of D parameters $\mathbf{x}=\{x_i;\ i=1,...,D\}$ (used for generating new states, $\mathbf{x}$)
- $h(\mathbf{x})$: Probability for acceptance of a new state, $\mathbf{x}$, given the previous state, $\mathbf{x}_o$ ($\mathbf{x}_o$ is typically the mean of $g(\mathbf{x})$).
- $T(k)$: Schedule of "annealing" the "temperature" T in annealing-time steps k. T can loosely be thought of as a standard deviation of g and h.

The basic idea is to generate a new point using the probability density $g(\mathbf{x})$ about an initial guess to the function minimum, say $\mathbf{x}_o$. Then, use a so called *Boltzmann test* to see if the new point is accepted. That is, the point is accepted with probability $h(\mathbf{x})$, which is often skewed to accept points that correspond to downhill moves. If the point is accepted the initial guess $\mathbf{x}_o$ is replaced with it. Every time a point is generated (not necessarily accepted) the *annealing time k* is increased. That is, k=0 on the first call of $g(\mathbf{x})$, 1 on the second call, 2 on the ... etc. Each time k is increased the temperature is decreased from its original value T_o according to some annealing schedule $T^{(k)}=T_o[f_a(k)]$. This continues until $\mathbf{x}_o$ converges to a minimum.

The problem is to find an annealing schedule, $f_a(k)$, that reduces the temperature as fast as possible while still allowing ample time to search the

space so as to avoid getting caught in a local minima. The reason a fast annealing schedule is desired is because as the temperature decreases the points generated using $g(\mathbf{x})$ deviate less from $\mathbf{x}_o$, and the ratio of points accepted that correspond to uphill moves to the points that correspond to downhill moves decreases. This results in the convergence to a minimum at low temperatures. If the space was sampled sufficiently this minima is likely to be the global one. So, the faster the annealing schedule, the faster the convergence. This all boils down to less function evaluations and a faster algorithm.

Originally there were sound physical principles underlying the choices of $g(\mathbf{x})$ and $h(\mathbf{x})$. However, this method of finding the global minimum is not limited to physics examples requiring *bona fide* "temperatures" and "energies." Rather, this methodology can be readily extended to any problem for which a reasonable probability density can be formulated. In particular, if $g(\mathbf{x})$ is defined such that:

$$\hat{g}(\mathbf{y}) = \prod_{i=1}^{D} \frac{1}{2\left(|y_i| + T_i^{(k)}\right) ln\left(1 + \frac{1}{T_i^{(k)}}\right)} \qquad y_i \in [-1,1] \tag{4.67}$$

$$x_i = x_{oi} + y_i (U_i - L_i)$$

Where:

D is the number of parameters

x_i is the i^{th} parameter of the point $\mathbf{x}$ generated at annealing time k

L_i is the lower bound of the i^{th} parameter

U_i is the upper bound of the i^{th} parameter

$T_i^{(k)}$ is the temperature associated with the i^{th} parameter, at annealing time k

y_i is the i^{th} random variable associated with the i^{th} parameter, x_i, distributed according to $\hat{g}(\mathbf{y})$

it can be shown [67] that a sufficient condition for finding the global minimum is an annealing schedule not faster than:

$$T_i^{(k)} = T_{oi}\, exp\left(-c_i k^{1/D}\right) \tag{4.68}$$

The c_i are arbitrary constants that may be used to tune the algorithm to specific problems.

There are three important advantages for this choice of $g(\mathbf{x})$:

- The search space can be bounded, as is usually required in many physical situations.
- Each individual parameter has a "temperature" associated with it, making it possible to adaptivly adjust individual temperatures for more or less sensitive parameters.
- The annealing schedule is exponentially fast, usually resulting in faster convergence to the global minimum. This is due to the fat tail of this distribution, making it easier to test for surrounding local minima.

It is sensible to choose control over the c_i, such that

$$T_{fi} = T_{oi}\, exp(-m_i)$$

$$k_{fi} = exp(n_i) \qquad (4.69,\text{a-c})$$

$$c_i = m_i\, exp\left(-\frac{n_i}{D}\right)$$

Here, T_{fi} is the parameter temperature that is reached in annealing time k_{fi}, in accordance with the annealing schedule defined in Eq. 4.68. The expression for c_i (Eq. 4.69c) can be found by substituting the expressions for T_{fi} and k_{fi} (Eqs. 4.69a and 4.69b respectively) into Eq. 4.68 and solving for c_i. The m_i and n_i can be solved for, after the T_{fi} and k_{fi} are chosen, and used to determine the corresponding c_i. It has empirically been found that T_{fi}=0.1 and k_{fi}=100 $\forall i$ (i.e. all the c_i are the same) works well for the present cost function. Only the initial parameter temperatures, T_{oi}, still need be chosen to completely determine the annealing schedule defined in Eq. 4.68. In general, T_{oi}=1 is a good choice for the initial parameter temperatures that results in sufficient coverage from the lower to upper bounds of the parameters.

In many situations it has proven useful to define a quenching parameter q, which speeds up the annealing schedule in the following way:

$$T_i^{(k)} = T_{oi}\, exp\left(-c_i k^{q/D}\right) \qquad (4.70)$$

If q is equal to one the annealing schedule defined in Eq. 4.68 is recovered; if q is greater than one the parameter temperatures are decreased faster. A

value of q greater than one (e.g. two or three) often greatly increases the rate of convergence to the global optima, however. When q is greater than one the proof of convergence is void. Nevertheless, the quenching parameter is very useful for speeding convergence (to perhaps no longer the global optima) when faced with a real world problem [76], especially when D becomes large (the dramatic decrease in convergence speed as D increases, which is apparent in Eq. 4.68, is often referred to as the "curse of dimensionality"). The optimization results presented in this thesis were generated with q equal to one.

The deviates $y_i^{(j)}$ in Eq. 4.67, distributed according to $\hat{g}(\mathbf{y})$, may be generated from uniform random deviates, $r^{(j)}$, between 0 and 1. First, the Cumulative Distribution Function (CDF) of $\hat{g}(\mathbf{y})$ is determined:

$$G(\mathbf{y}) = \int_{-1}^{y_1} \cdots \int_{-1}^{y_D} \hat{g}(\mathbf{y}')dy_1' \cdots dy_D' = \prod_{i=1}^{D} G_i(y_i)$$

$$G_i(y_i) = \frac{1}{2} + \frac{sgn(y_i)}{2} \frac{ln\left(1 + \frac{|y_i|}{T_i^{(k)}}\right)}{ln\left(1 + \frac{1}{T_i^{(k)}}\right)} \tag{4.71}$$

The $y_i^{(j)}$ can be solved for in terms of the $r^{(j)}$ by setting the $G_i(y_i)$ to a $r^{(j)}$ and solving for the $y_i^{(j)}$ (this can be done since the y_i are independent by definition):

$$r^{(j)} = \frac{1}{2} + \frac{sgn\left(y_i^{(j)}\right)}{2} \frac{ln\left(1 + \frac{\left|y_i^{(j)}\right|}{T_i^{(k)}}\right)}{ln\left(1 + \frac{1}{T_i^{(k)}}\right)} \tag{4.72}$$

Solving for the $y_i^{(j)}$:

$$y_i^{(j)} = T_i^{(k)}\, sgn\left(r^{(j)} - \frac{1}{2}\right)\left[\left(1 + \frac{1}{T_i^{(k)}}\right)^{\left|2r^{(j)}-1\right|} - 1\right] \tag{4.73}$$

If a generated $y_i^{(j)}$ results in a x_i that is outside of the specified lower and upper bounds (see Eq. 4.67) another $y_i^{(j)}$ is generated until a x_i is generated within the bounds. This approach may be used to generate an admissible x_i given arbitrary constraints on the x_i (other than the simple upper and lower bounds). That is, if a x_i is generated that violates some arbitrary constraint(s) another x_i is generated until the constraint(s) are satisfied.

In line with the physical analogy $h(\mathbf{x})$ is defined as:

$$h(\mathbf{x}) = exp\left(\frac{-\left(E - E_o\right)}{T_{\text{acceptance}}^{(k)}}\right) \tag{4.74}$$

Here, E-E_o = $f_c(\mathbf{x})$-$f_c(\mathbf{x}_o)$ (where f_c is the cost function to be minimized) represents the energy difference. The new point $\mathbf{x}$ is accepted with probability $h(\mathbf{x})$, where $\mathbf{x}_o$ is the previously accepted point. This acceptance test is known as the *Boltzmann test*. Note that if $E<E_o$ this probability is greater than unity; in such cases the change is arbitrarily assigned probability $h(\mathbf{x})$=1, i.e., the algorithm always takes such an option (downhill step). In the limit as $T_{\text{acceptance}} \rightarrow 0$ only downhill moves are accepted. Points

corresponding to uphill moves that are approximately as high as the temperature $T_{\text{acceptance}}$ are commonly accepted (with probability 1/e~0.3679). This is the heart of the simulated annealing algorithm: it wanders freely among local minima of depth less than about $T_{\text{acceptance}}$ during the search for the global minimum.

The rate that $T_{\text{acceptance}}$ is decreased has no bearing on the proof of convergence. Usually the annealing schedule used for the parameter temperatures, T_i, is also used for $T_{\text{acceptance}}$, with the exception that the number of acceptance events, $k_{\text{acceptance}}$, is used instead of the annealing time k. In the present implementation the following annealing schedule is used for the acceptance temperature:

$$T_i^{(k_{\text{acceptance}})} = {}^{\circ}T_{\text{acceptance}} \exp\left(-\eta \hat{c} k_{\text{acceptance}}^{\,q/D}\right) \tag{4.76}$$

The initial acceptance temperature, ${}^{\circ}T_{\text{acceptance}}$, is set to a value that is much greater than the depth of local minima (or the depth that one might guess or bound if this information cannot be obtained). It has empirically been found that η equal to 1.5 and $\hat{c}$ equal to c_i (all the c_i are the same) works well for the present cost function.

The clever choice of $g(\mathbf{x})$ which allows the use of a very (exponentially) fast annealing schedule is the essence of the ASA algorithm. However, reannealing, which is explained next, significantly improves performance.

Reannealing is the name that has been given [67] for adaptivly adjusting the temperatures associated with each individual parameter. If a

parameter x_i has a high temperature T_i the search is "stretched out" over the bounds for that parameter (from L_i to U_i); if it has a low temperature the search is more localized. Whenever doing a multi-dimensional search in the course of a real-world nonlinear physical problem, inevitably one must deal with different changing sensitivities of the x_i throughout the search. At any given annealing time k, it seems sensible to "stretch out" the range over which the relatively insensitive parameters are being searched, relative to the ranges of the more sensitive parameters. This is accomplished by periodically rescaling the annealing time k, say every time a hundred or so points are accepted, in terms of the sensitivities s_i (not the same as the sensitivity metrics discussed in previous sections) calculated at the most current minimum value $\mathbf{x}_{min}$ encountered so far:

$$s_i = \left.\frac{\partial f(\mathbf{x})}{\partial x_i}\right|_{\mathbf{x}_{min}} \tag{4.77}$$

$$s_{max} = max\{s_i; i = 1,\ldots,D\}$$

The annealing time for each parameter, k_i (which are now different for each parameter, hence the subscript i), is rescaled in the following way:

$$\begin{aligned} &k_i \rightarrow k_i' \\ &T_i^{(k_i')} = \begin{cases} T_i^{(k_i)}\left(\frac{s_{max}}{s_i}\right) & if\ T_i^{(k_i')} > T_{oi} \\ T_i^{(k_i')} = T_{oi} & otherwise \end{cases} \\ &k_i' = \left(\frac{ln(T_{oi} / T_i^{(k_i')})}{c_i}\right)^D \end{aligned} \tag{4.76}$$

The annealing schedule for each parameter now becomes:

$$T_i^{(k)} = T_{oi}\, exp\left(-c_i k_i^{q/D}\right) \tag{4.77}$$

The annealing time for each parameter, k_i, can only decrease or remain the same as a result of a rescaling. This results in the temperatures for relatively insensitive parameters being increased (reannealing) thereby "stretching out" the search for these parameters. The temperature used for the Boltzmann test, $T_{\text{acceptance}}$, is similarly rescaled, except that it is set to the lowest value of the cost function so far encountered.

4.4.2 The Stochastic Simplex Method (SSM)

SSM is essentially ASA combined with a carefully chosen multidimensional optimization method called the downhill simplex method, originally due to Spendley *et al.* [69] and later revised by Nelder and Mead [70].

The search space of physical problems almost always has some sort of direction(s) towards the minimum associated with it. All efficient optimization methods make use of this information. Deterministic optimization methods, at the price of being easily fooled and converging to a local minima, make better use of information from these directions than the ASA method. This usually results in much faster convergence to a minimum. The basic idea of the SSM is to incorporate the speed of a deterministic optimization algorithm with the robustness of the ASA algorithm.

First a brief review of the Downhill Simplex Method is given. The following description has been adopted from [88]: "A *simplex* is a geometrical figure consisting, in D dimensions, of D+1 points (or vertices) and all their interconnecting line segments, polygonal faces, etc. In two dimensions, a simplex is a triangle. In three dimensions it is a tetrahedron, not necessarily the regular tetrahedron. In general we are only interested in simplexes that are nondegenerate, i.e., that enclose a finite inner D-dimensional volume. If any point of a nondegenerate simplex is taken as the origin, then the D other points define vector directions that span the D-dimensional vector space.

The Downhill Simplex Method takes a series of steps, most steps just moving the point of the simplex where the function is largest (highest point) through the face of the simplex to a lower point. These steps are called reflections, and they are constructed to conserve the volume of the simplex (hence maintain its nondegeneracy). When it can do so, the method expands the simplex in one or another direction to take larger steps. When it reaches a "valley floor," the method contracts itself in the transverse direction and tries to ooze down the valley. If there is a situation where the simplex is trying to "pass through the eye of a needle," it contracts itself in all directions, pulling itself in around its lowest (best) point" [88].

Figure 4.6 shows the possible outcomes for a step in the downhill simplex method. "The simplex at the beginning of the step, here a tetrahedron, is shown, top (of Figure 4.6). The simplex at the end of the step

can be any one of (a) a reflection away from the high point, (b) a reflection and expansion away from the high point, (c) a contraction along one dimension from the high point, or (d) a contraction along all dimensions towards the low point. An appropriate sequence of such steps will always converge to a minimum of the function" [88].

The present implementation of the downhill simplex method is similar to that of [88]. The downhill simplex method first tries a reflection (a). If the reflected point is lower than the low point then an expansion is done (b). If the reflected point is higher than the second-highest point a contraction is done (c). If the contraction results in a point that is higher than the highest point a multiple contraction is done (d). If this sequence of steps is repeated the simplex will eventually shrink into a minimum (see [88] for details).

The downhill simplex method is not guaranteed to find the global minimum when multiple minima exist; it is also not very efficient in comparison to other methods (e.g. the Broyden-Fletcher-Goldfarb-Shanno method [88]) on convex cost functions. The important property of the downhill simplex method that makes it a prime candidate for combining with ASA is that each iteration is, in a sense, independent of previous iterations.

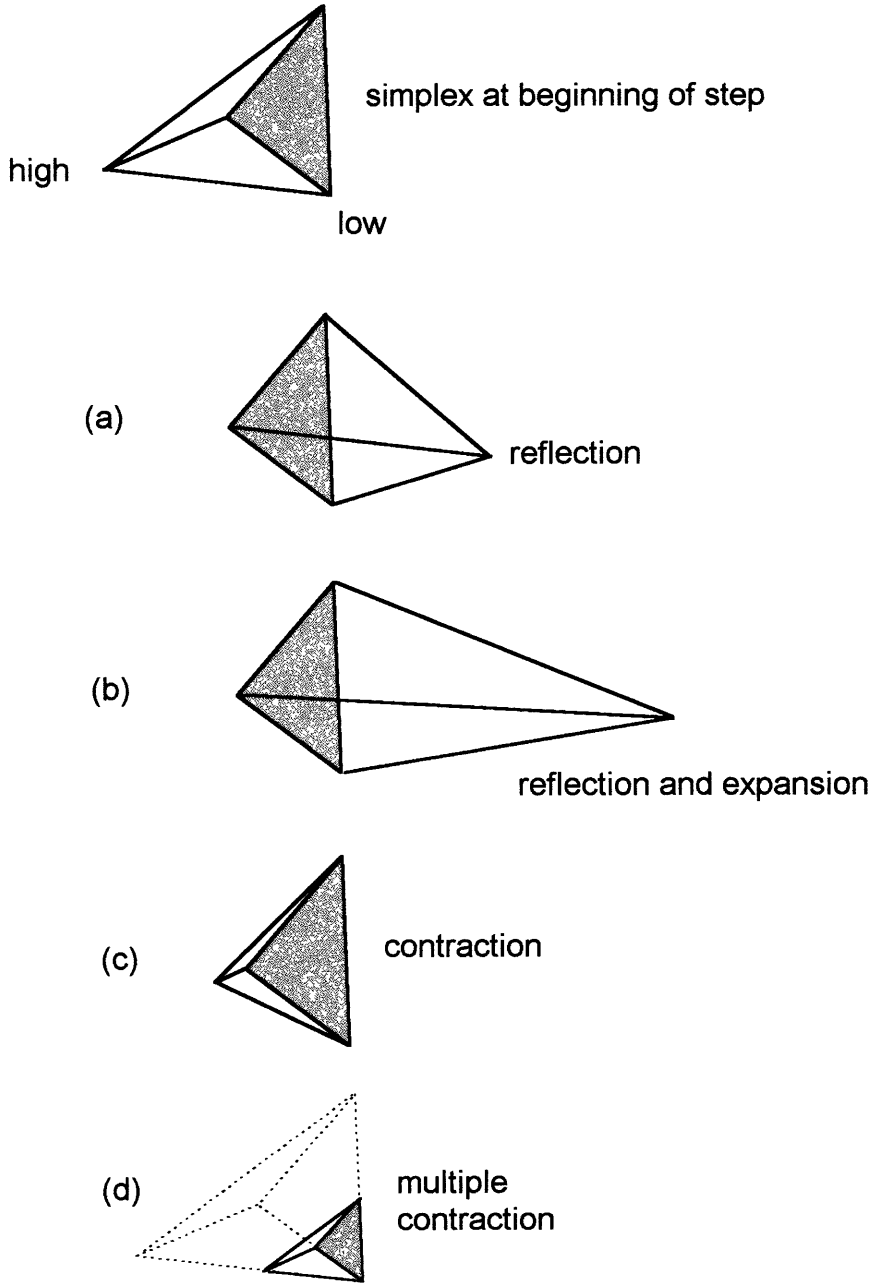

Figure 4.6 Possible outcomes for a step in the downhill simplex method [88]

It is possible to arbitrarily change the location of the vertices of the simplex without destroying the algorithm on the next iteration.

ASA is combined with the downhill simplex method to create the SSM in the following way:

1. Given an initial simplex that contains D+1 points, choose the point that corresponds to the lowest value of the cost function and call it $\mathbf{x}_o$.
2. Iterate through the remaining D points until a point passes the Boltzmann Test. Let $\mathbf{x}_o$ now refer to the point that passed the Boltzmann Test (as opposed to the lowest point).
3. Generate a new point, about $\mathbf{x}_o$, as in the ASA algorithm. If the new point does not satisfy all specified constraints continue generating new points until the constraints are satisfied.
4. Use the Boltzmann test to see if the point is accepted. If the point is accepted replace $\mathbf{x}_o$ with it (a point in the simplex is replaced).
5. If the point was accepted in step 4 do an iteration using the downhill simplex method. If this results in a x_i that is outside of its bounds (or any other constraint) multiple contractions (Figure 4.6d) are done until the constraints are satisfied.
6. If the point was accepted in step 4, decrease the acceptance temperature according the annealing schedule and increase the acceptance events counter by one.

7. If $k_{rescale}$ points have been accepted, rescale (reanneal) the acceptance and parameter temperatures and reset the counter of acceptance events. Here, $k_{rescale}$ is set to 100.
8. If $k_{restart}$ points have been accepted replace the current highest point in the simplex with the lowest point encountered so far (if the lowest point is not already in the simplex)*. Here, $k_{restart}$ is set to 100.
9. Decrease the parameter temperatures according to the annealing schedule
10. Test for termination
11. Goto step 1

The only difference between the SSM and ASA are steps 1, 2, 5, and 8. These steps have no bearing on the proof that assures that the global minimum is found using ASA, so the proof also applies to the SSM. At higher parameter temperatures, steps 3 and 4 tend to keep the simplex large. As a result, the simplex is not allowed to shrink into a local minima. The simplex often "steps over" local minima at the higher parameter temperatures due to its relatively large size in comparison with the radius of convergence of local minima. As the parameter temperatures get small the algorithm becomes the downhill simplex method, which converges orders of

* In step 4 it is possible that the lowest point is replace with a point that is higher, so the lowest point encountered during optimization may not always be in the simplex. If the lowest point encountered is in the simplex the worst point cannot be replaced with it since this would result in a degenerate simplex (i.e. a simplex enclosing zero volume).

magnitude faster than ASA. In Appendix E it is shown that the SSM often converges one to two orders of magnitude faster than ASA on a set of test cost functions typically used for benchmarking global optimization codes.

4.4.3 Termination Criteria

In the present implementation a shunt temperature is defined such that when any parameter temperature goes below it the SSM is completely shunted over to the downhill simplex method. The shunt temperature used here is 0.001, which has been empirically found to be a good choice for the present cost function. The downhill simplex method is assumed to have converged when the distance (Euclidean) between the highest and lowest point is below a specified tolerance. The tolerance used here is 0.0001.

4.5 IMPLEMENTATION

A1-A4 and the SSM were implemented in a easy-to-use menu-driven computer program. It was written in C to the ANSI standard to ensure compatibility across platforms.

The λ and ε factors defined in Sections 4.3.2 and 4.3.5 respectively are user inputs. The mean and standard deviations of the ply material properties and geometric parameters, temperature and moisture content (and their respective "stress-free" values), and knockdown factors (for the progressive failure model) are input on a ply-by-ply basis. All of the optimization parameters discussed in Section 4.4 are also user inputs.

When first running the code all of the inputs are set to reasonable defaults to give inexperienced users a starting point. The default layup is $[\pm 0/\pm 90]_s$. The default λ and ε factors are 2 and 0.01 respectively (which is consistent with the values discussed in Sections 4.3.2 and 4.3.5). The default values for the optimization parameters are summarized in Table 4.3 (which are consistent with the values discussed in Sections 4.4.1 and 4.4.2). The default ply material properties and geometric parameters are for the AS4/3501-6 material system, which are defined in Chapter 5 in Table 5.1. The defaults for the weight factors, A_l and B_l, in the cost function (Eq. 4.66a) are zero. If the user changes the defaults (via easy to use menus) the session may be saved under a specified file name which may be opened for later use.

The code allows for a considerable amount of freedom when generating files for plots. It is capable of producing files for both one parameter and two parameter plots (e.g. contour or surface plots) of all of the laminate properties, including their means, standard deviations, and respective sensitivity metrics. The synthetic data sets for the laminate properties (used for A3) may also be saved to files, which may be used for making plots of distribution functions etc. Information about an optimization run may also be saved to files; the lowest cost function value found, number of cost function evaluations, and the coordinates of accepted points may be saved to files every time a specified number of iterations are completed.

The manual, source code, and executables for the code are available by request from the author or the TELAC laboratory.

Table 4.3 Default Optimization Parameter Values

Symbol	Value
T_{oi}	1
${}^{o}T_{\text{acceptance}}$	100
T_{fi}	0.1
k_{fi}	100
q	1
L_i	0
U_i	$\pi/2$
η	1.5
k_{rescale}	100
k_{restart}	100

CHAPTER 5

RESULTS

Experimental and predicted results are presented in this chapter. Since the purpose of this chapter is to present results, rather than give detailed interpretations of them, the discussion of the results is kept to a minimum. Detailed discussions of the results are in Chapter 6.

In Section 5.1 the predictions from the probabilistic analysis methods are compared with experimental data. Comparisons of predictions from approaches A2 and A4 with A3 are shown in Section 5.2. Sensitivity and parametric studies are presented in Section 5.3. Optimization results, including optimal laminates for maximum stiffness and dimensional stability are presented in Section 5.4. An example of how the present probabilistic and optimization methods may be used to design a satellite structure for maximal dimensional stability with arbitrary constraints is presented in Section 5.5.

5.1 COMPARISON WITH EXPERIMENTAL DATA

In this section experimental and predicted results are compared. The experimental data is used to verify that the present analysis methods correctly predict the trends and magnitudes of the variability of the longitudinal stiffness, tensile strength, and CTB for various laminates. When there is sufficient data experimental and predicted Cumulative Distribution Functions (CDF) are compared. When there is not enough data to compare CDFs the data is plotted along with a predicted standard deviation band (mean ± standard deviation), allowing for a loose comparison of trends predicted and in the experimental data.

5.1.1 Experimental Data

The experimental data is from two sources. The stiffness and strength data is from the US Army Materials Technology Laboratory [91]. The test specimens used in [91] were manufactured from 12 inch wide AS4/3501-6 carbon fiber/epoxy resin prepreg tape (bleed cure material), purchased from Hercules, Inc. Details of the manufacturing and experimental procedures are discussed in [91].

The data for the CTBs is from the Technology Laboratory for Advanced Composites (TELAC) [3]. The test specimens used in [3] were manufactured from 12 inch wide AS4/3501-6 carbon fiber/epoxy resin prepreg tape (net cure

material) purchased from Hercules, Inc. Details of the manufacturing and experimental procedures are discussed in [3].

The mean ply material properties and geometric parameters, and their respective standard deviations, used for the predicted results are shown in Table 5.1. One exception to the table is that a moisture content of 0% was used for the CTB predictions since the test specimens were "baked out" before testing.

5.1.2 Comparison of Experimental and Predicted CDFs

In this section experimental and predicted CDFs are compared. The predicted CDFs are determined from synthetic data sets generated using approach A3 (Section 4.3.4). The synthetic data sets for the laminate properties are:

$$\left\{Y_i^{(1)}, Y_i^{(2)}, \ldots, Y_i^{(k)}, \ldots, Y_i^{(N-1)}, Y_i^{(N)}\right\} \quad i = 1,..,18 \tag{5.1}$$

The $Y_i^{(k)}$ are arranged in ascending order with k=1,...,N. The CDFs are generated by using the simple relation:

$$P_i^{(k)} = \frac{k}{N} \quad k = 1,\ldots,N \tag{5.2}$$

A plot of a predicted CDF is obtained by plotting $P_i^{(k)}$ verse $Y_i^{(k)}$, for k=1,...,N. The k^{th} $P_i^{(k)}$ is the probability that a laminate property will be less than the k^{th} $Y_i^{(k)}$. An experimental CDF is obtained by using a real data set in place of

the synthetic one (Eq. 5.1). For the predicted CDFs N is set to 5000; for the experimental CDFs N is 20.

Figure 5.1 and 5.2 are plots of predicted and experimental CDFs for longitudinal stiffness and tensile strength, respectively.

5.1.3 Comparison of Experimental Data With Predicted Standard Deviation Bands

In this section experimental data is plotted along with a corresponding predicted standard deviation band. Although there is not enough data to claim statistical significance, these plots do allow for a loose comparison of trends predicted and in the experimental data.

Figures 5.3 and 5.4 are plots of experimental data and the corresponding predicted 3-standard-deviation band for longitudinal stiffness for the $[\pm\theta]_s$ and $[\pm\theta]_{2s}$ laminate families. Figures 5.5 and 5.6 are the same types of plots for longitudinal tensile strength. Note that the strength of the $[\pm 15^\circ]_s$ and $[\pm 15^\circ]_{2s}$ is significantly over-predicted. This is most likely due to a delamination failure mode. The $[\pm 15^\circ]_s$ and $[\pm 15^\circ]_{2s}$ laminates are known to often fail in a delamination mode [85] which is not presently modeled. Figure 5.7 is a plot of experimental data and predicted 1-standard-deviation bands for the longitudinal tensile strength of $[0^\circ]_n$ laminates for various numbers of plies, n. Figure 5.8 is a plot of experimental data and the corresponding predicted 1-standard-deviation band for the longitudinal CTB for the $[\pm\theta]_s$ laminate family. Figure 5.9 is a plot of experimental data and

the predicted 1-standard deviation bands for the laminates $[\pm 30^{o}]_{ns}$ with n=1,2,4.

5.2 COMPARISON OF APPROACHES A2 AND A4 WITH A3

To determine if approaches A2 and A4 are accurate (within the context of the mathematical models) results from them were compared to results from A3, which operates on the full nonlinear problem. The $[\pm\theta]_s$ laminate family was considered. Predicted standard deviations from A2 for the longitudinal stiffness, CTE, and CTB where compared with predictions from A3. Predicted standard deviations calculated by taking the Euclidean norm of the sensitivity metrics from A4 were compared with direct predictions from A3 for longitudinal tensile strength. In general, the correlation between the different approaches is excellent, giving some confidence that the assumptions made in A2 and A4 are appropriate.

Figures 5.10, 5.11, and 5.12 are comparisons of the predicted standard deviations for the longitudinal stiffness, CTE, and CTB, respectively, using approaches A2 and A3. Figure 5.13 is a comparison of the predicted standard deviations for longitudinal strength using approaches A3 and A4.

5.3 SENSITIVITY AND PARAMETRIC STUDIES

5.3.1 Sensitivity Study

A sensitivity study for the $[\pm\theta]_s$ laminate family is presented in Figures 5.14-5.25. Longitudinal stiffness, CTE, and longitudinal tensile strength are

considered. For the longitudinal stiffness and CTE the sensitivity metrics defined in Eq. 4.51 are used. For the longitudinal strength the sensitivity metrics defined in Eq. 4.64 are used.

Figure 5.14 is a plot of the sensitivity of the laminate longitudinal stiffness, E_x, to layup angle and ply thickness variations. Note that the sensitivity to ply thickness variations is very small relative to layup angle variations. Figure 5.15 is a plot of the sensitivity of E_x to ply stiffness (E_l, E_t, G_{lt}) and Poisson's ratio (ν_{lt}) variations.

Figure 5.16 is a plot of the sensitivity of the laminate longitudinal CTE, α_x, to ply layup angle and ply thickness variations. Note that the sensitivity to ply thickness variations is very small relative to layup angle variations. Figure 5.17 is a plot of the sensitivity of α_x to ply stiffness (E_l, E_t, G_{lt}) and Poisson's ratio (ν_{lt}) variations. Figure 5.18 is a plot of the sensitivity of α_x to ply thermoelastic properties, α_l and α_t.

Figure 5.19 is a plot of the sensitivity of the laminate longitudinal CTB, W_x^T, to ply layup angle and ply thickness variations. Figure 5.20 is a plot of the sensitivity of W_x^T to ply stiffness (E_l, E_t, G_{lt}) and Poisson's ratio (ν_{lt}) variations. Figure 5.21 is a plot of the sensitivity of α_x to ply thermoelastic properties, α_l and α_t.

Figure 5.22 is a plot of the sensitivity of the laminate longitudinal tensile strength to ply layup angle and ply thickness variations. Figure 5.23 is a plot of the sensitivity of the LPF load to ply strength (^TX, ^TY, S)

variations (the compressive ply strengths do not figure into this example problem). Figure 5.24 is a plot of the sensitivity of the longitudinal tensile strength to ply stiffness (E_l, E_t, G_{lt}) and Poisson's ratio (ν_{lt}) variations. Figure 5.25 is a plot of the sensitivity of the LPF load to ply thermo and hygro elastic properties (α_l, α_t, β_l, β_t).

5.3.2 Parametric Study

A parametric study for the $[\pm\theta/\pm\beta]_s$ laminate family is presented in Figures 5.26-5.32; contour plots of the longitudinal stiffness, CTE, and strength properties are presented. Appendix D contains contour plots of all the laminate properties for the $[\pm\theta/\pm\beta]_s$ laminate family.

Figures 5.26 and 5.27 are contour plots of the mean and Coefficient of Variation (COV) of the laminate longitudinal stiffness, E_x, respectively. Figures 5.28 and 5.29 are contour plots of the mean and standard deviation of the laminate longitudinal CTE, α_x, respectively. Figure 5.30 is a contour plot of the standard deviation of the longitudinal CTB, W_x^T. Figures 5.31 and 5.32 are contour plots of the mean and COV of the longitudinal tensile strength, respectively.

Table 5.1 Means and Standard Deviations of Ply Properties And Parameters For AS4/3501-6

Symbol	Ply Property/Parameter	Mean	Standard Deviation
$t_1,..,\ t_n$	thickness of ply 1,..,n	$5.2(10)^{-3}$ in.	$5.2(10)^{-4}$ in.
$\theta_1,..,\ \theta_n$	layup angle of ply 1,.., n	-	2^o
$E_{l1},..,E_{ln}$	longitudinal stiffness of ply 1,.., n	20 Msi	2 Msi
$E_{t1},..,\ E_{tn}$	transverse stiffness of ply 1,.., n	1.9 Msi	0.19 Msi
$G_{lt1},..,\ G_{ltn}$	shear stiffness of ply 1,.., n	0.8 Msi	0.08 Msi
$\nu_{lt1},..,\ \nu_{ltn}$	major Poisson's ratio of ply 1,.., n	0.3	0.03
$\alpha_{l1},..,\ \alpha_{ln}$	longitudinal CTE of ply 1,.., n	-0.2 με/°F	0.1 με/°F
$\alpha_{t1},..,\ \alpha_{tn}$	transverse CTE of ply 1,.., n	16 με/°F	1 με/°F
$\beta_{l1},..,\ \beta_{ln}$	longitudinal CME of ply 1,.., n	45 με/%	30 με/%
$\beta_{t1},..,\ \beta_{tn}$	transverse CME of ply 1,.., n	5500 με/%	300 με/%
${}^{T}X_1,..,\ {}^{T}X_n$	longitudinal tensile strength of ply 1,.., n	330 Ksi	33 Ksi
${}^{C}X_1,..,\ {}^{C}X_n$	longitudinal compressive strength of ply 1,.., n	180 Ksi	18 Ksi
${}^{T}Y_1,..,\ {}^{T}Y_n$	transverse tensile strength of ply 1,.., n	7.5 Ksi	0.75 Ksi
${}^{C}Y_1,..,\ {}^{C}Y_n$	transverse compressive strength of ply 1,.., n	35 Ksi	3.5 Ksi
$S_1,..,\ S_n$	shear strength of ply 1,.., n	14 Ksi	1.4 Ksi
-	Temperature (Stress Free Temperature)	70 °F (350 °F)	0 °F
-	Moisture content (Stress free moisture content)	1% (0%)	0 %

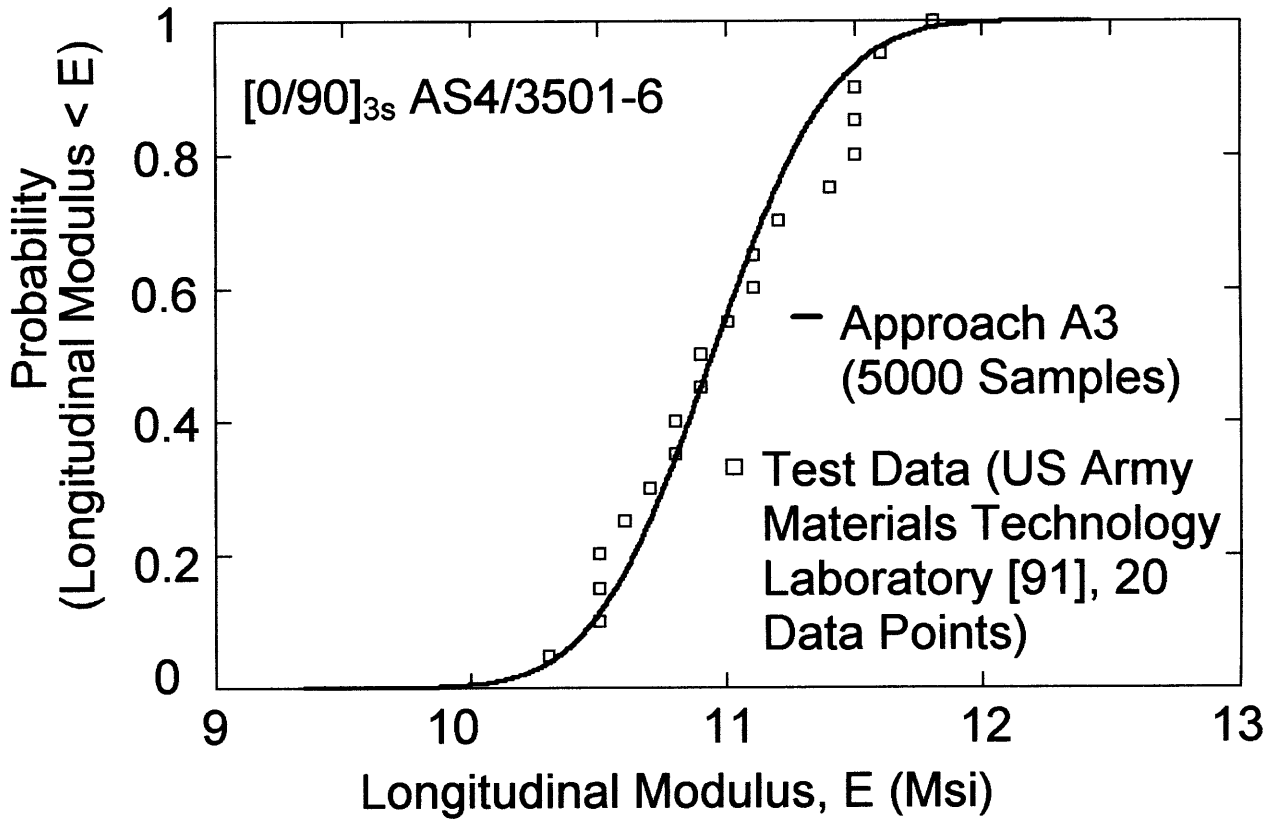

Figure 5.1 Experimental and predicted CDFs for longitudinal stiffness

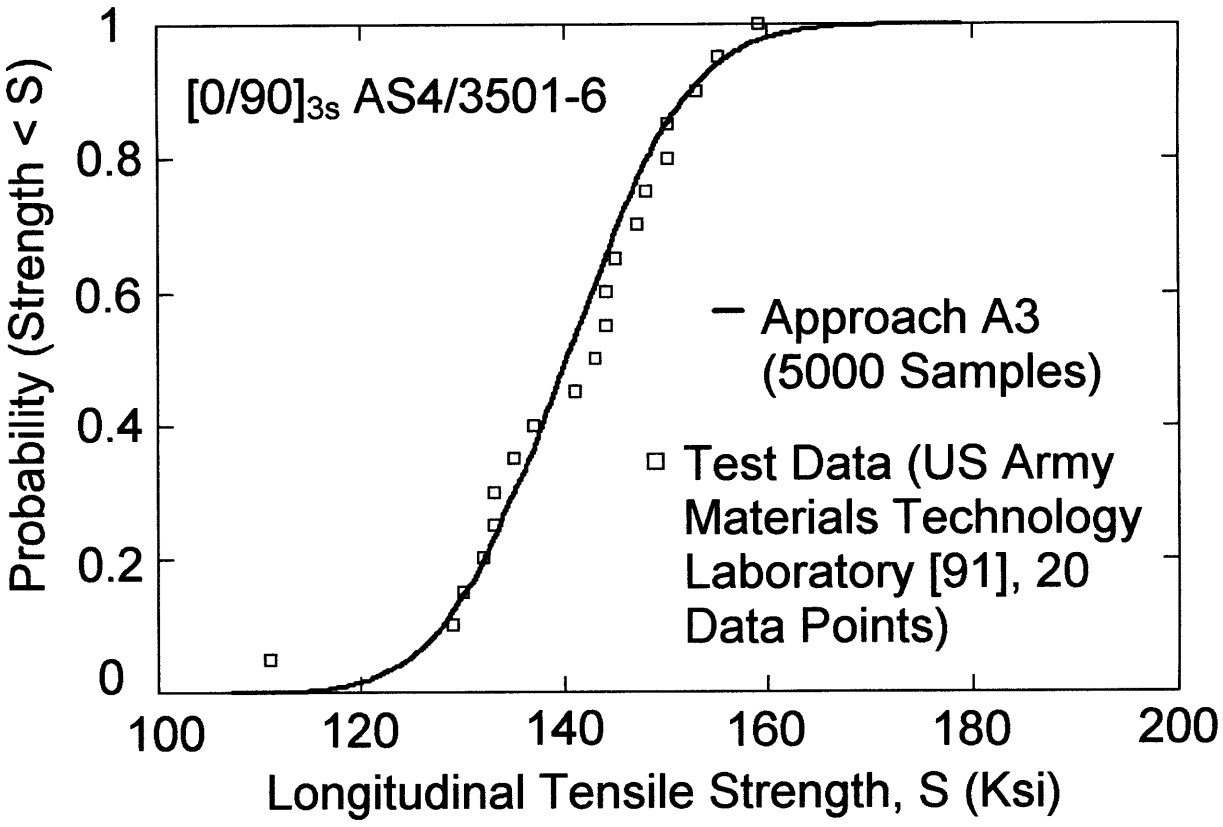

Figure 5.2 Experimental and predicted CDFs for longitudinal tensile strength

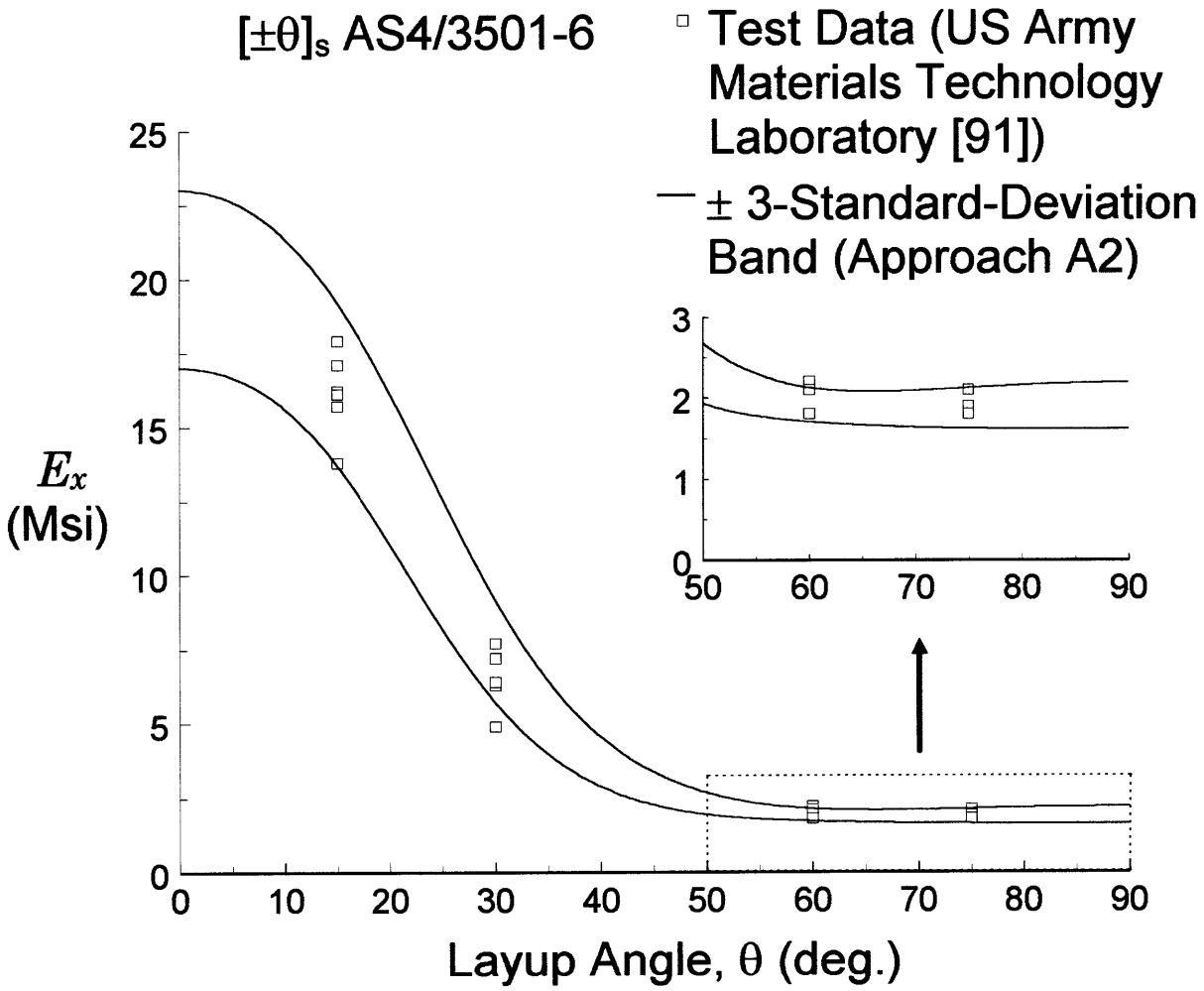

Figure 5.3 Plot of experimental data and predicted 3-standard-deviation band for longitudinal stiffness of $[\pm\theta]_s$ laminate family

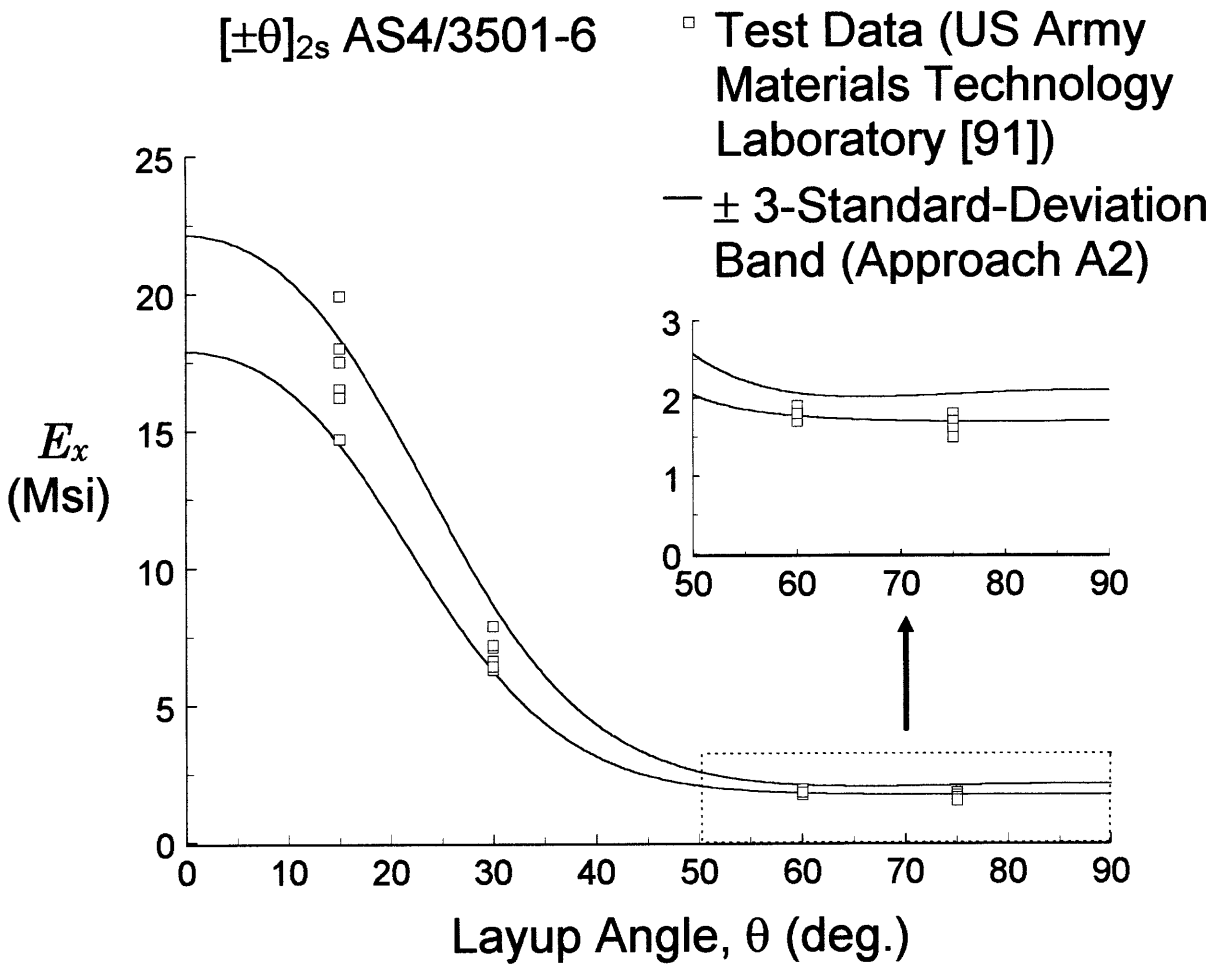

Figure 5.4 Plot of experimental data and predicted 3-standard-deviation band for longitudinal stiffness of $[\pm\theta]_{2s}$ laminate family

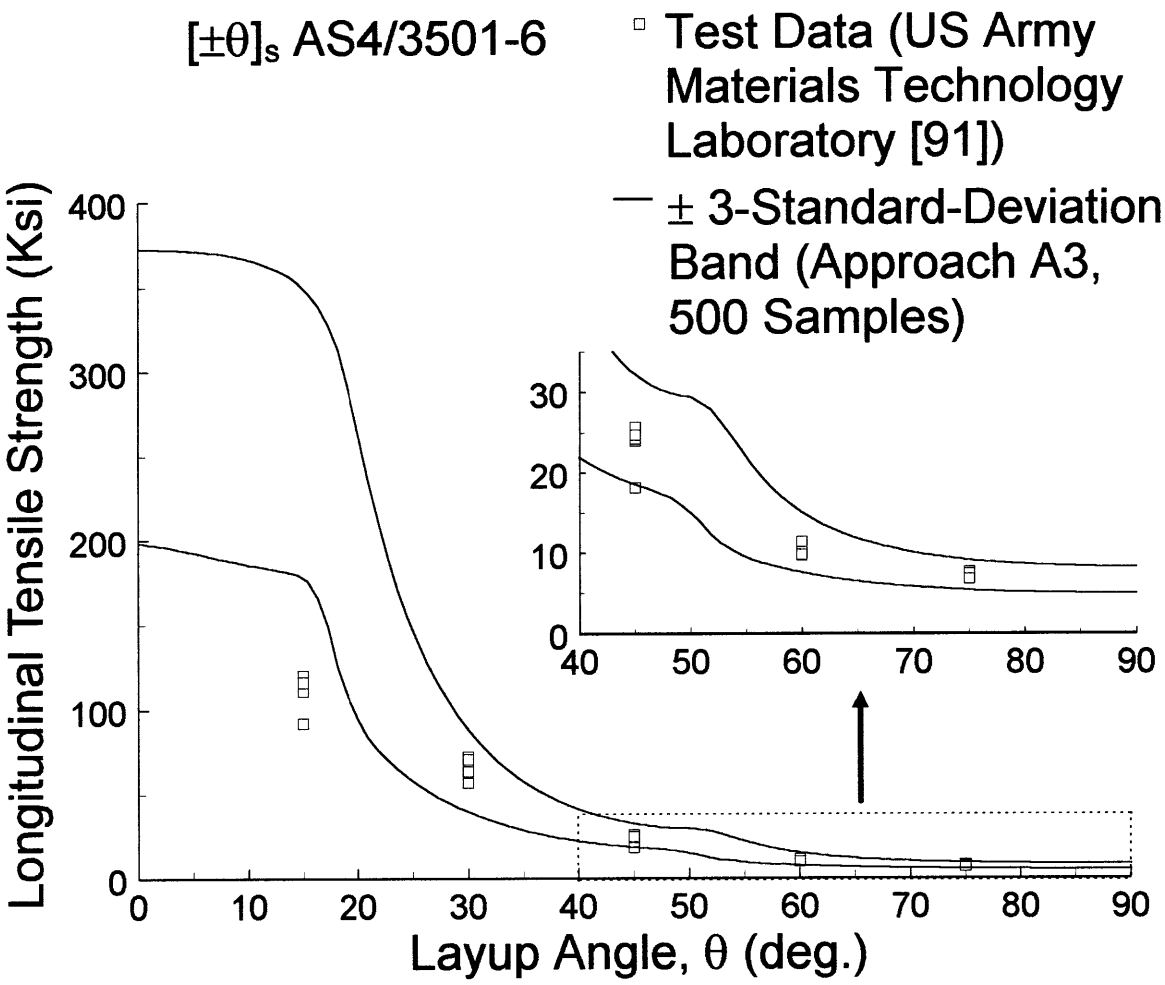

Figure 5.5 Plot of experimental data and predicted 3-standard-deviation band for longitudinal tensile strength of $[\pm\theta]_s$ laminate family

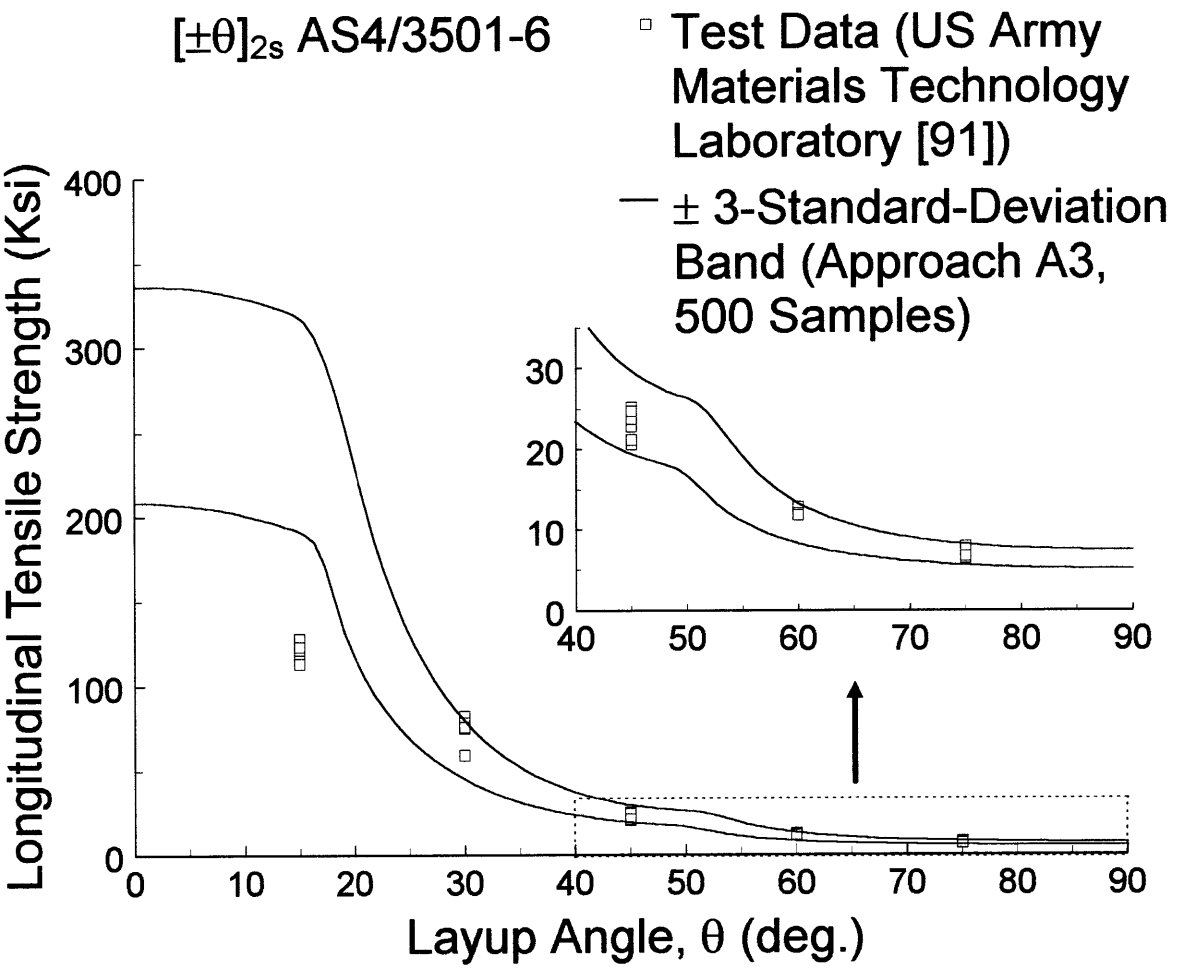

Figure 5.6 Plot of experimental data and predicted 3-standard-deviation band for longitudinal tensile strength of $[\pm\theta]_{2s}$ laminate family

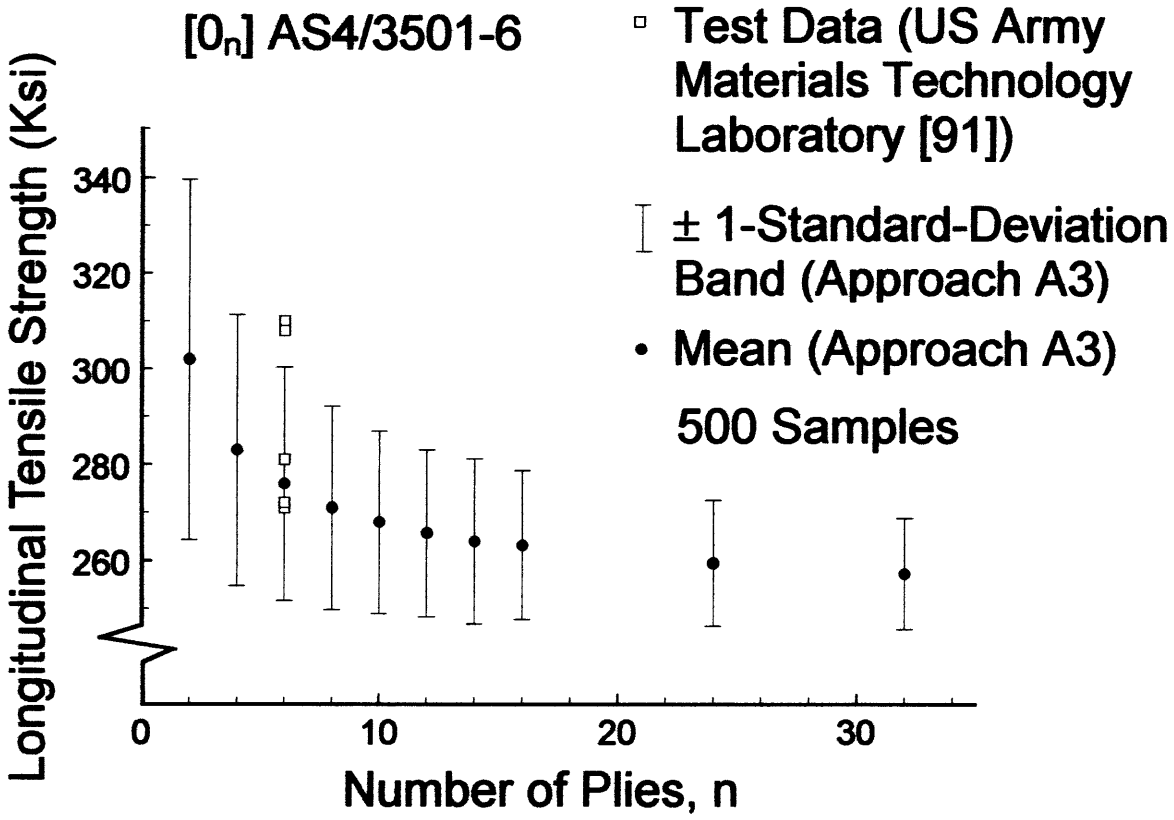

Figure 5.7 Plot of experimental data and predicted 1-standard-deviation band for longitudinal strength of $[0_n]$ laminate for various n

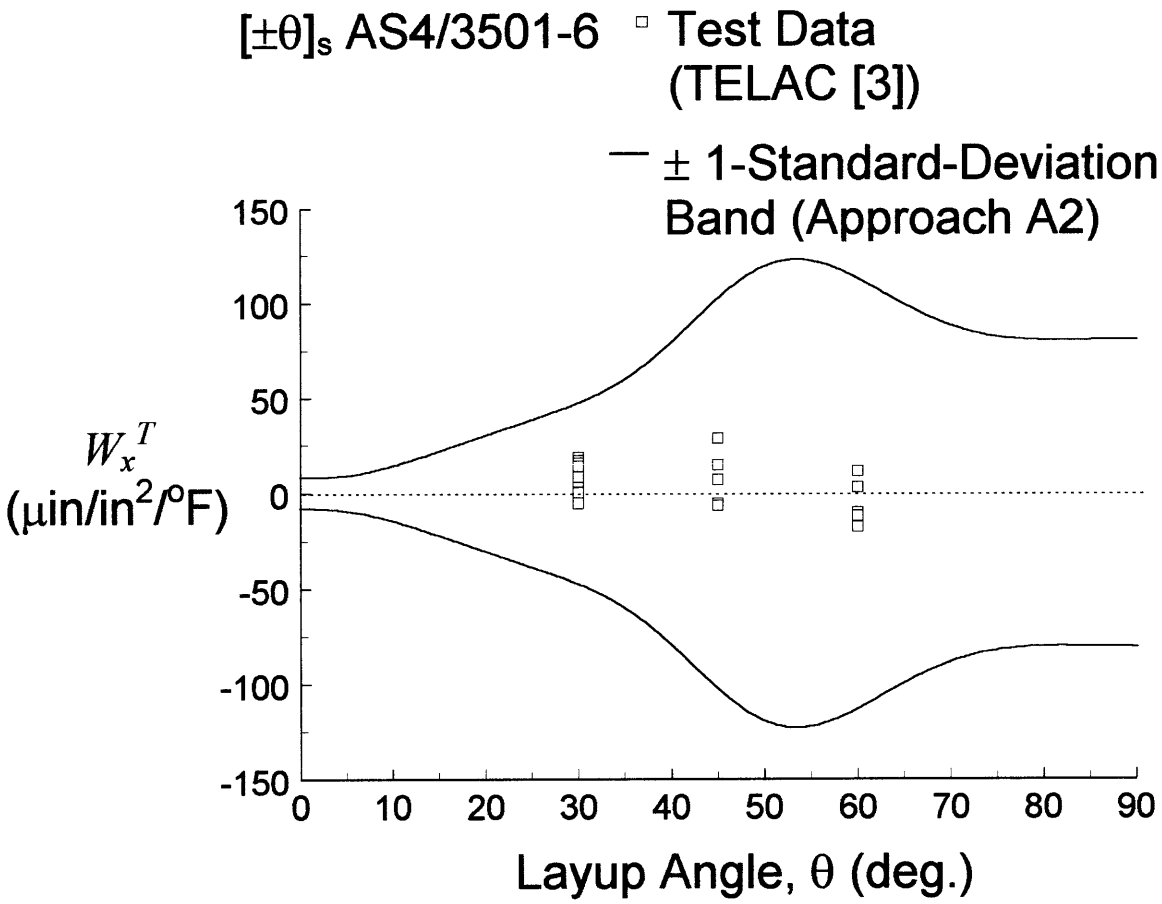

Figure 5.8 Plot of experimental data and predicted 1-standard-deviation band for longitudinal CTB of $[\pm\theta]_s$ laminate family

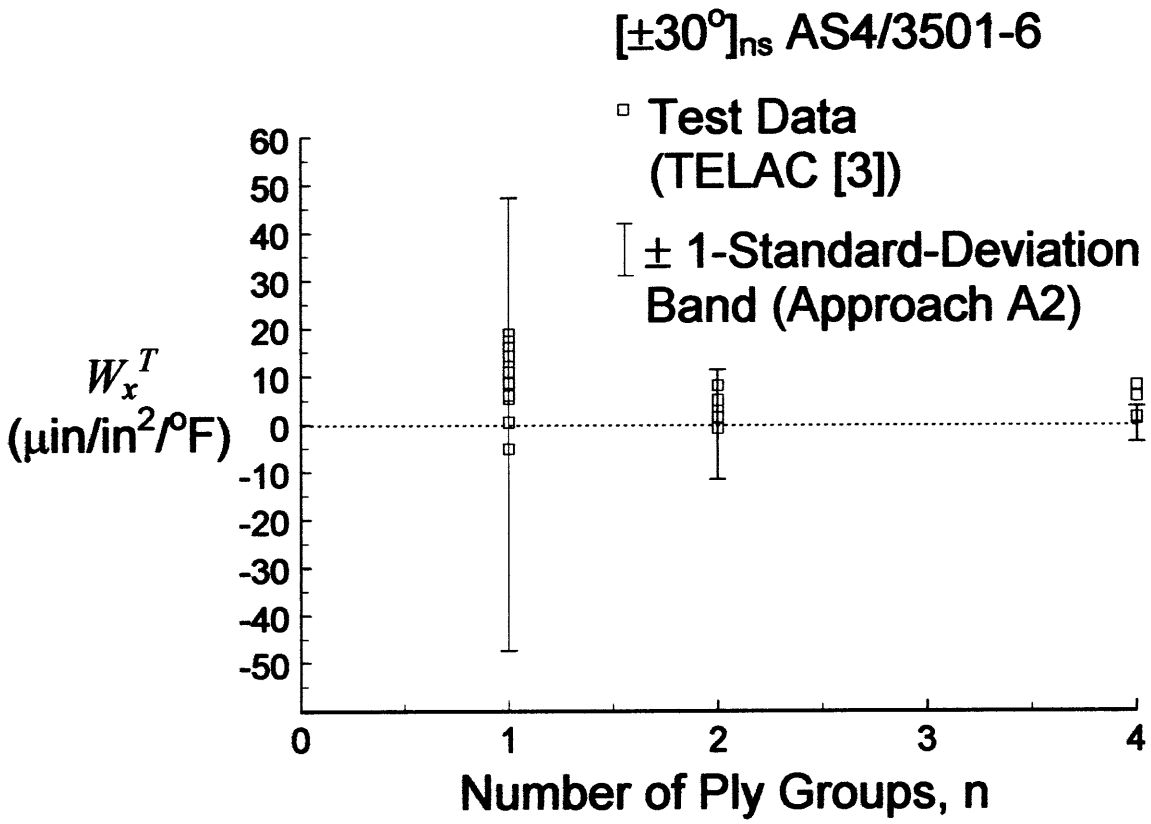

Figure 5.9 Plot of experimental data and predicted 1-standard-deviation band for longitudinal CTB for $[\pm 30^{\circ}]_{ns}$ laminates with n=1,2,4

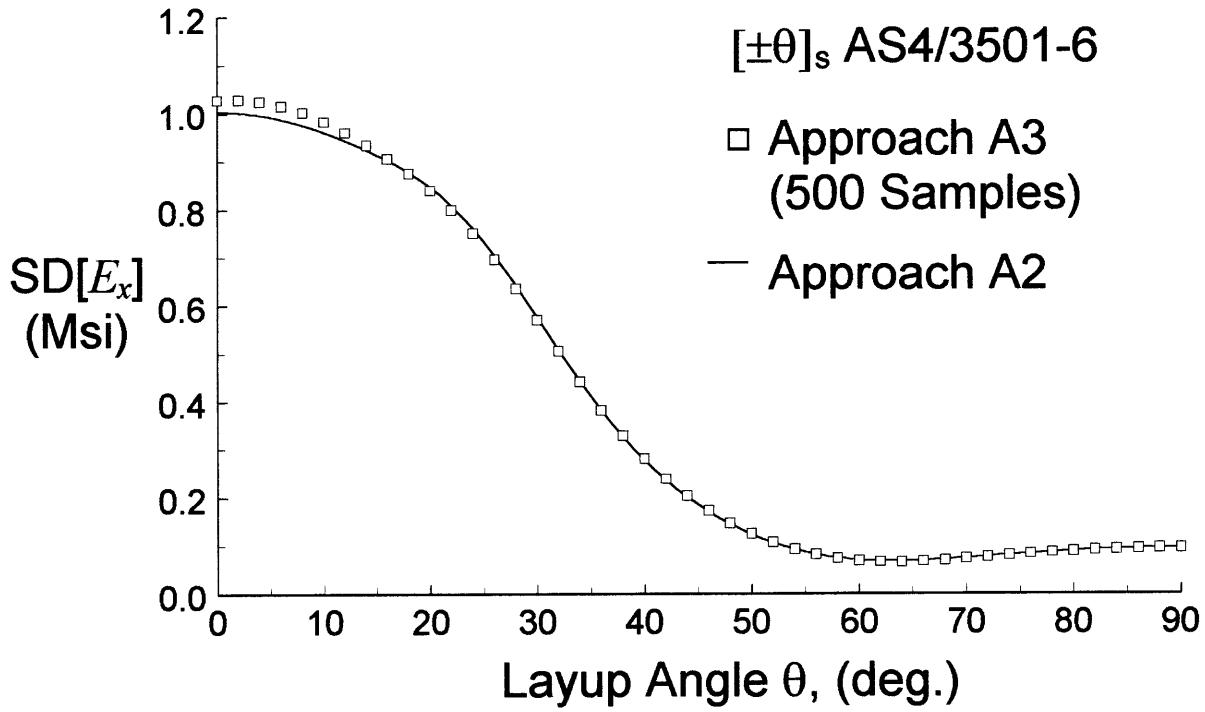

Figure 5.10 Comparison of predicted standard deviation of laminate longitudinal stiffness from approaches A2 and A3 for the $[\pm\theta]_s$ laminate family

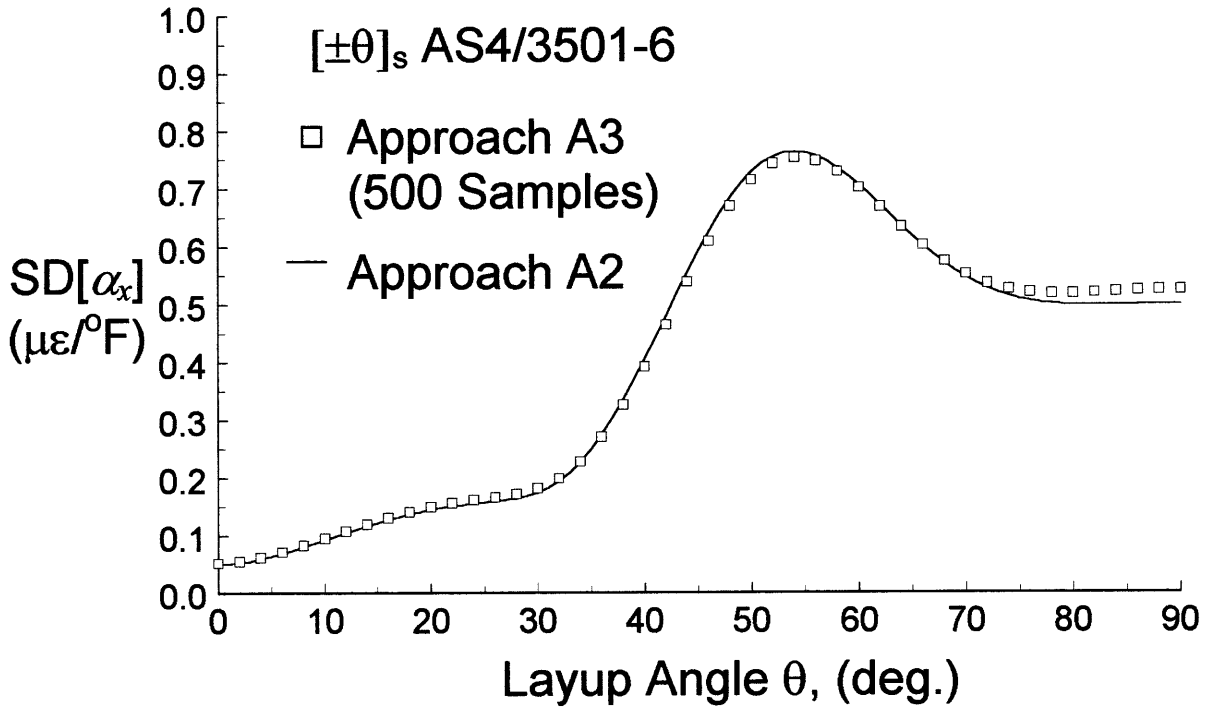

Figure 5.11 Comparison of predicted standard deviation of laminate longitudinal CTE from approaches A2 and A3 for the $[\pm\theta]_s$ laminate family

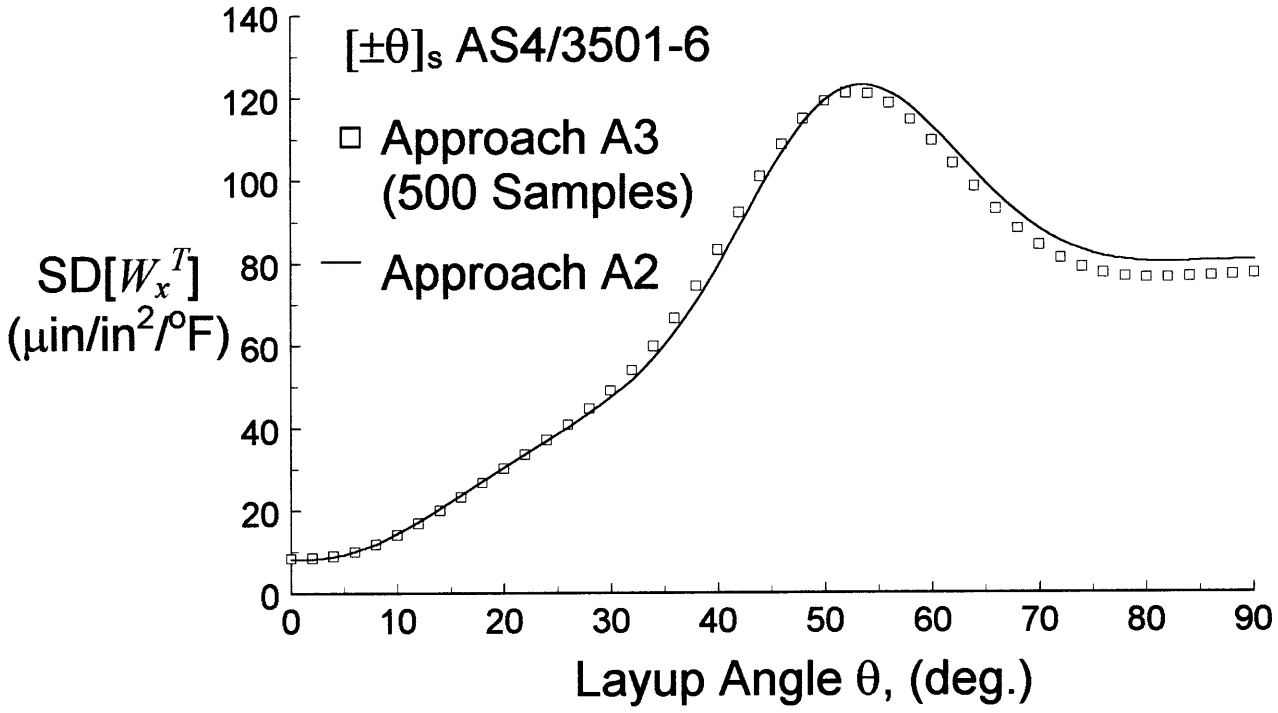

Figure 5.12 Comparison of predicted standard deviation of laminate longitudinal CTB from approaches A2 and A3 for the $[\pm\theta]_s$ laminate family

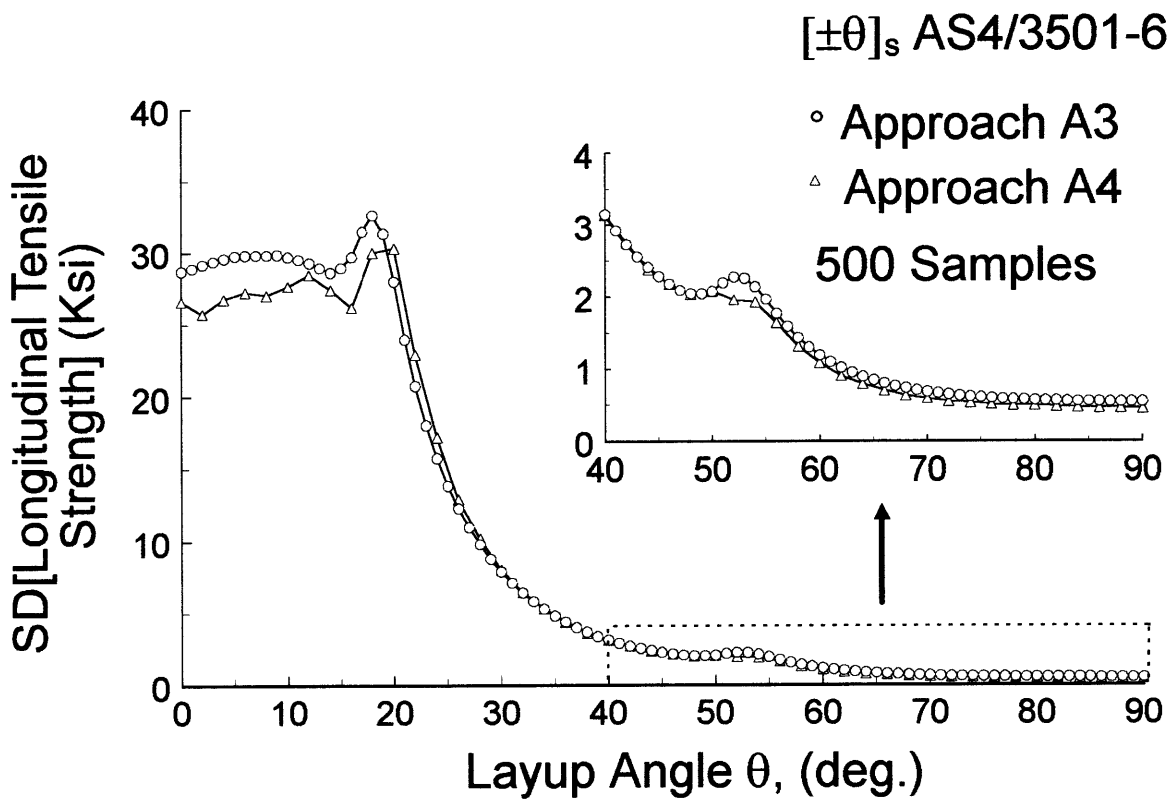

Figure 5.13 Comparison of predicted standard deviation of laminate longitudinal tensile strength from approaches A3 and A4 for the $[\pm\theta]_s$ laminate family

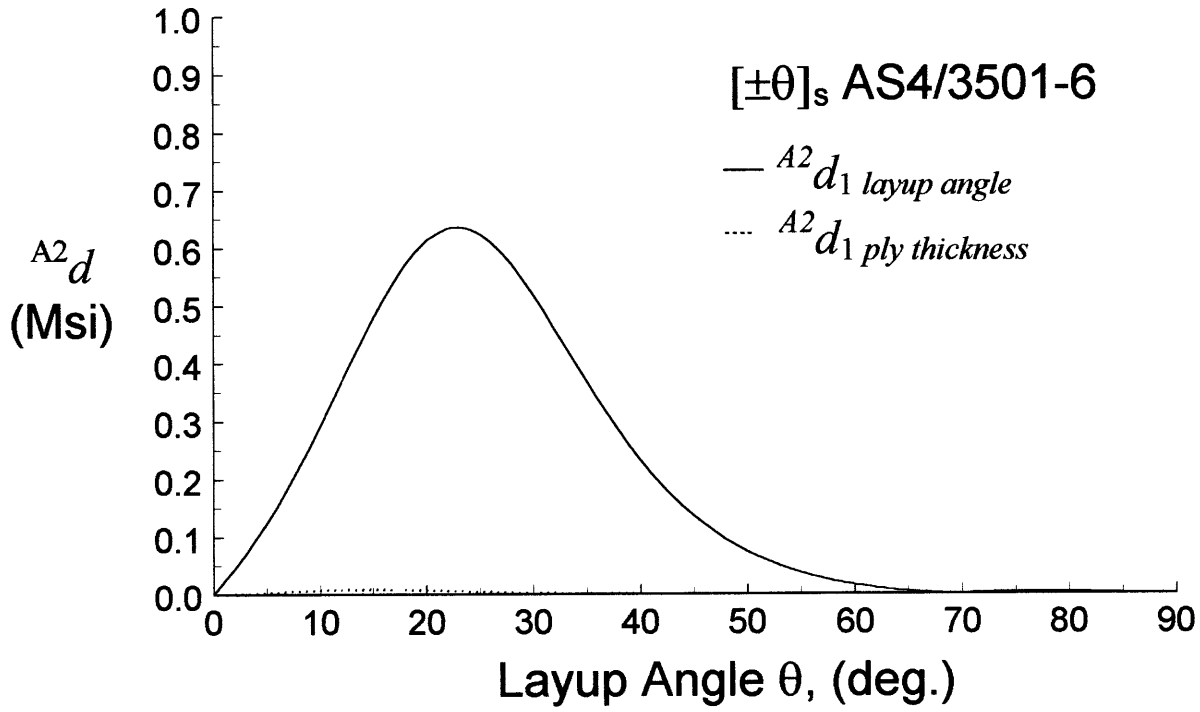

Figure 5.14 Plot of the sensitivity of the laminate longitudinal stiffness to layup angle and ply thickness variations for the $[\pm\theta]_s$ laminate family

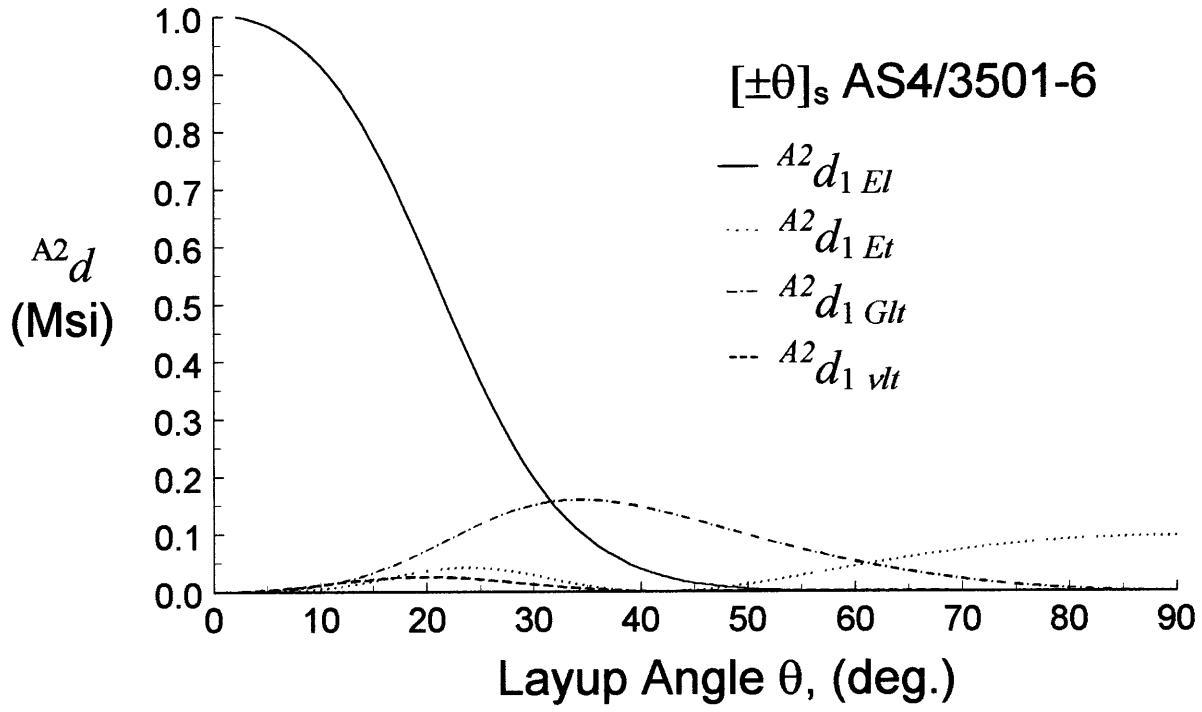

Figure 5.15 Plot of the sensitivity of the laminate longitudinal stiffness to ply stiffness (E_l, E_t, G_{lt}) and Poisson's ratio (ν_{lt}) variations for the $[\pm\theta]_s$ laminate family

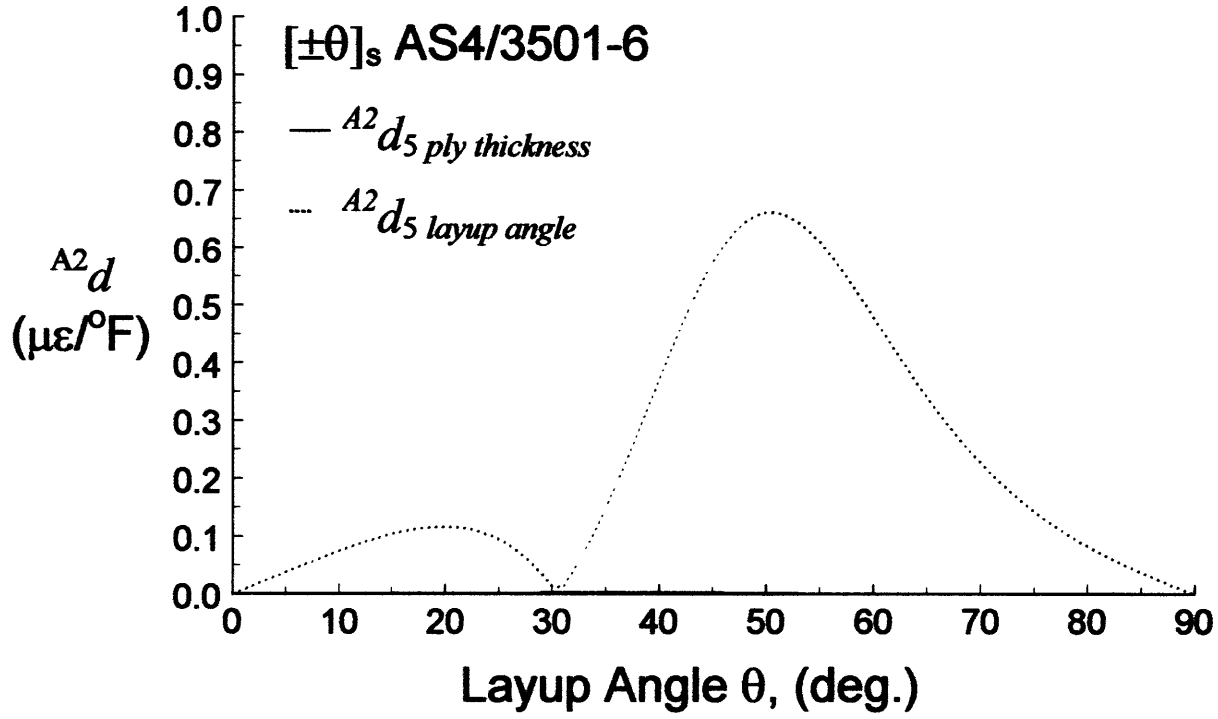

Figure 5.16 Plot of the sensitivity of the laminate longitudinal CTE to layup angle and ply thickness variations for the $[\pm\theta]_s$ laminate family; note $^{A2}d_{5\ ply\ thickness} << {}^{A2}d_{5\ layup\ angle}$

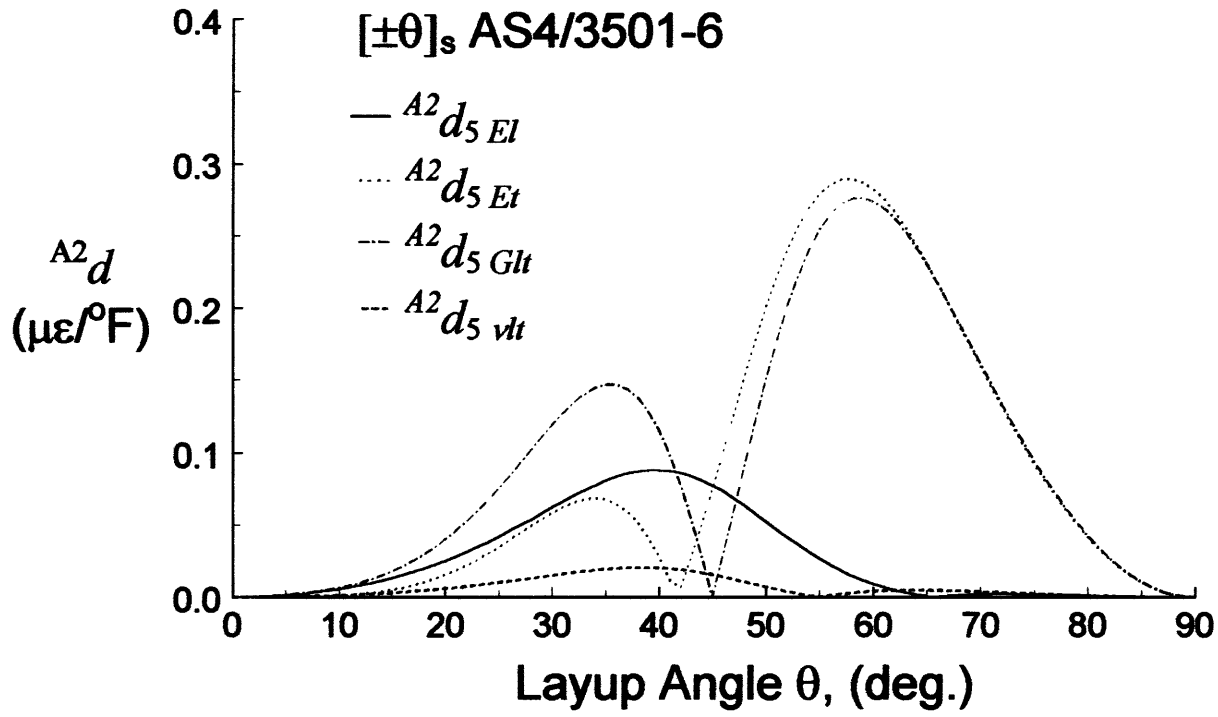

Figure 5.17 Plot of the sensitivity of the laminate longitudinal CTE to ply stiffness (E_l, E_t, G_{lt}) and Poisson's ratio (ν_{lt}) variations for the $[\pm\theta]_s$ laminate family

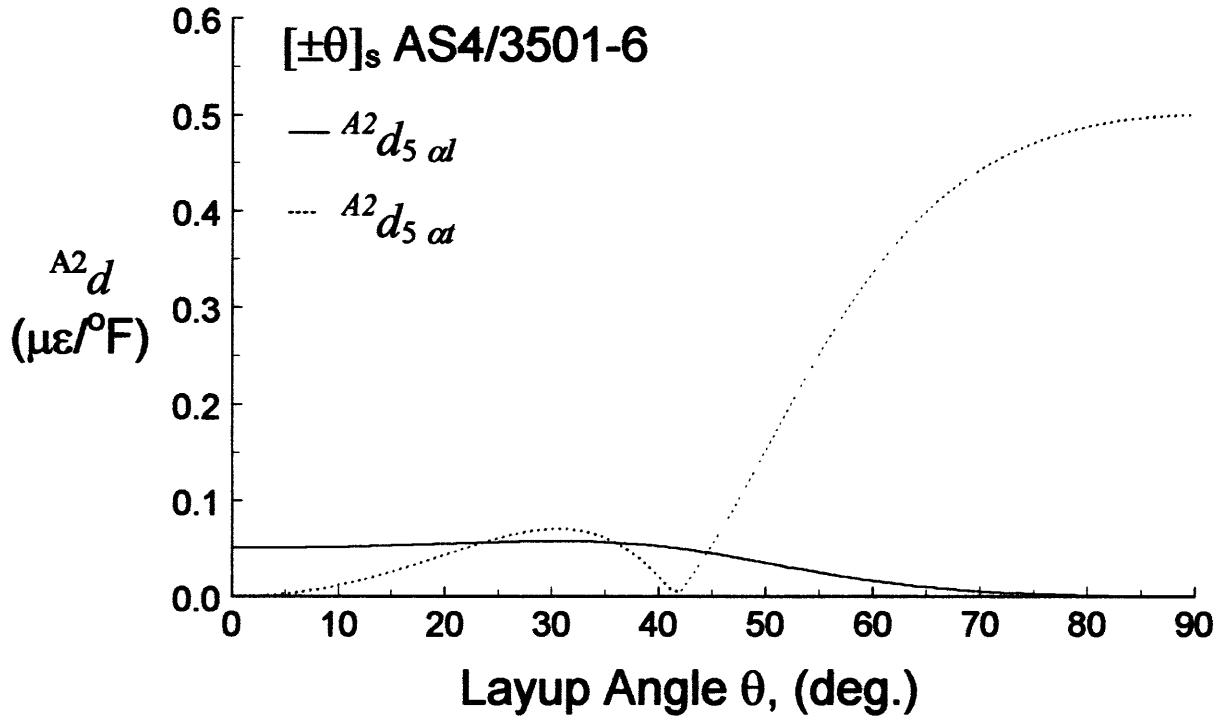

Figure 5.18 Plot of the sensitivity of the laminate longitudinal CTE to ply thermoelastic property variations, α_l and α_t, for the $[\pm\theta]_s$ laminate family

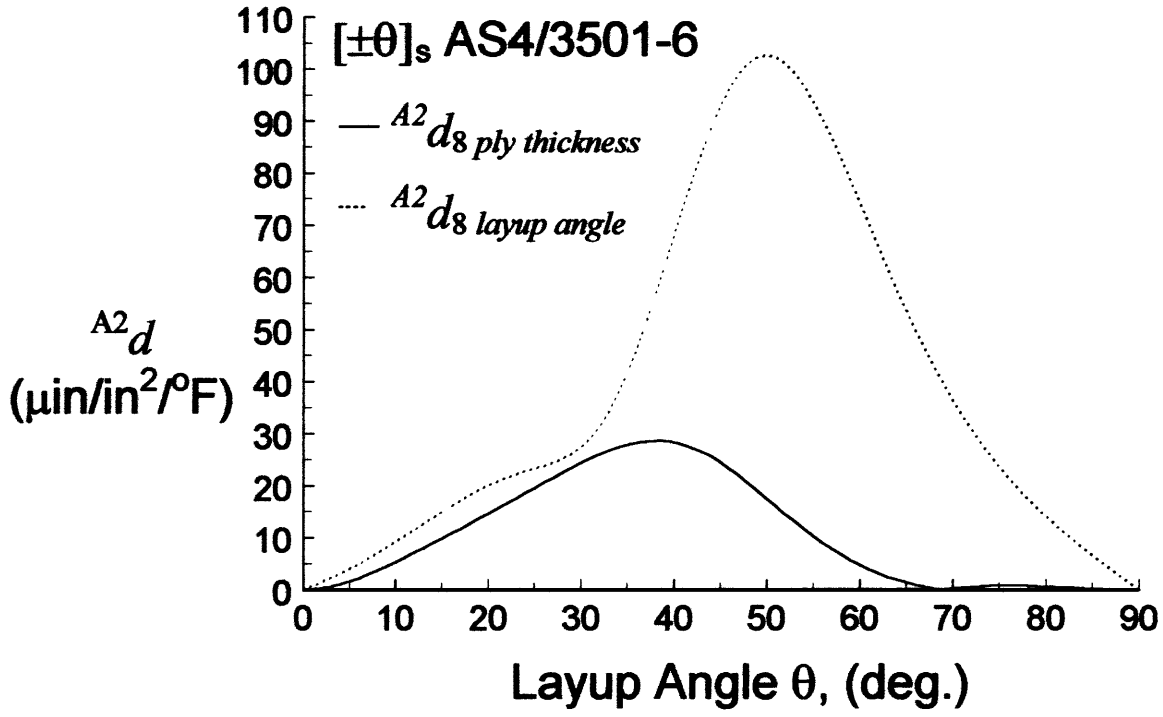

Figure 5.19 Plot of the sensitivity of the laminate longitudinal CTB to layup angle and ply thickness variations for the $[\pm\theta]_s$ laminate family

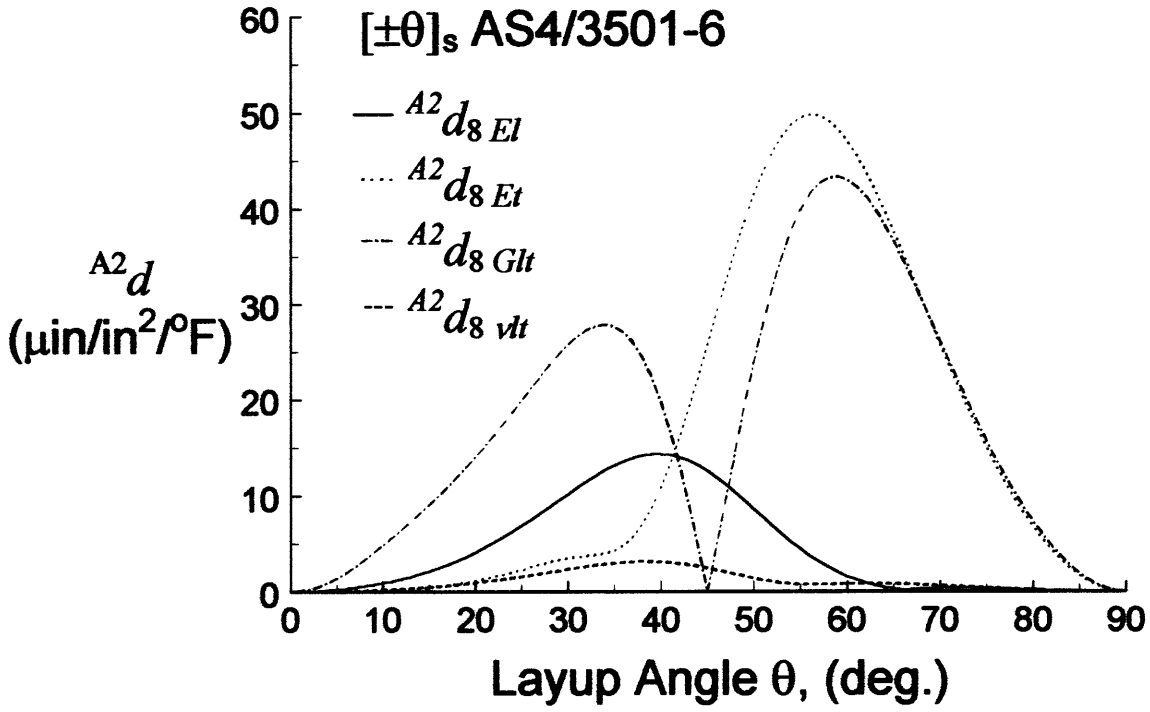

Figure 5.20 Plot of the sensitivity of the laminate longitudinal CTB to ply stiffness (E_l, E_t, G_{lt}) and Poisson's ratio (ν_{lt}) variations for the $[\pm\theta]_s$ laminate family

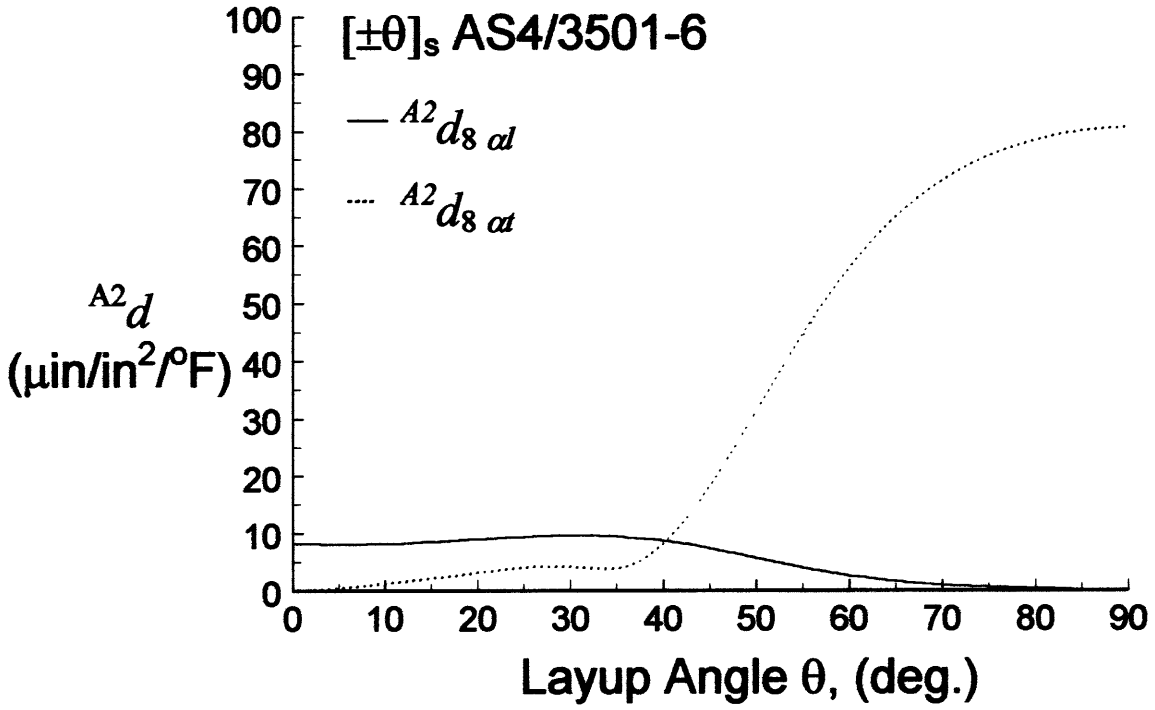

Figure 5.21 Plot of the sensitivity of the laminate longitudinal CTB to ply thermoelastic property variations, α_l and α_t, for the $[\pm\theta]_s$ laminate family

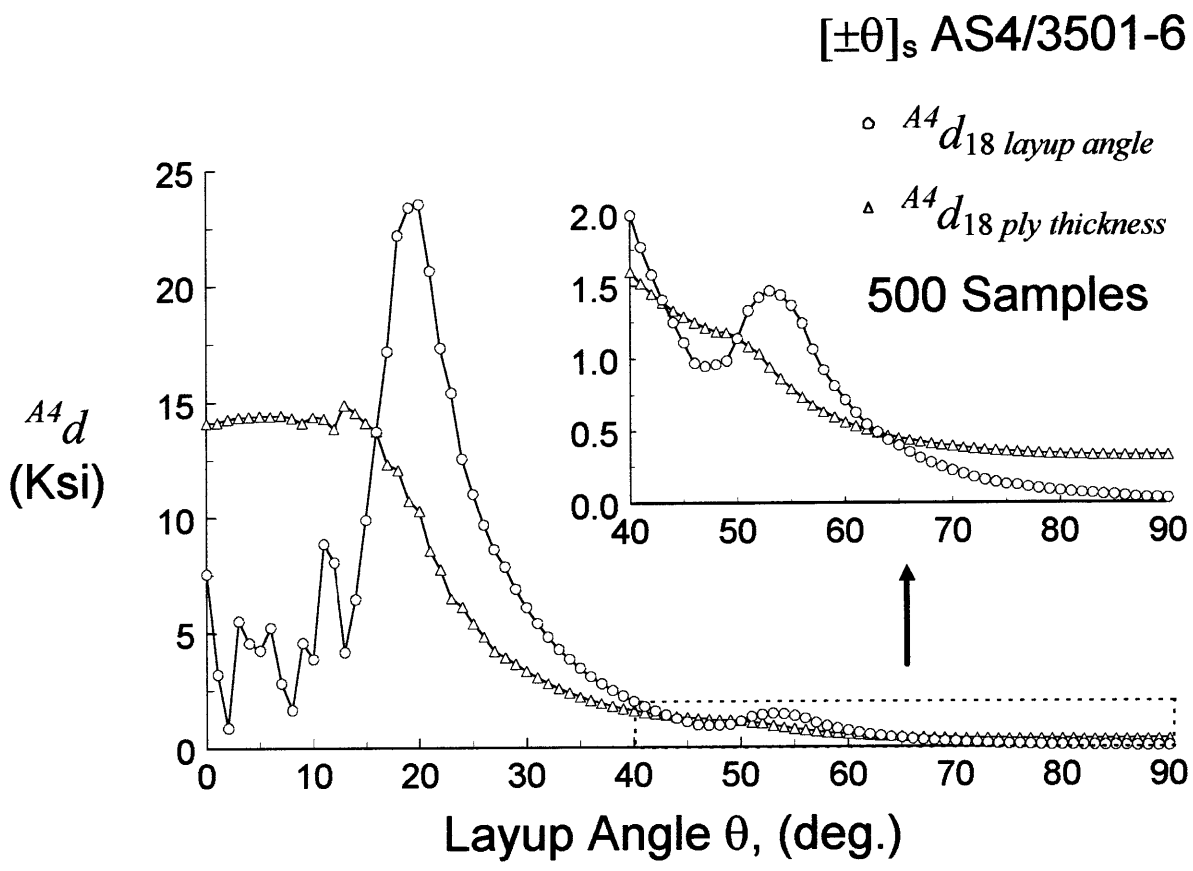

Figure 5.22 Plot of the sensitivity of the laminate longitudinal tensile strength to layup angle and ply thickness variations for the $[\pm\theta]_s$ laminate family

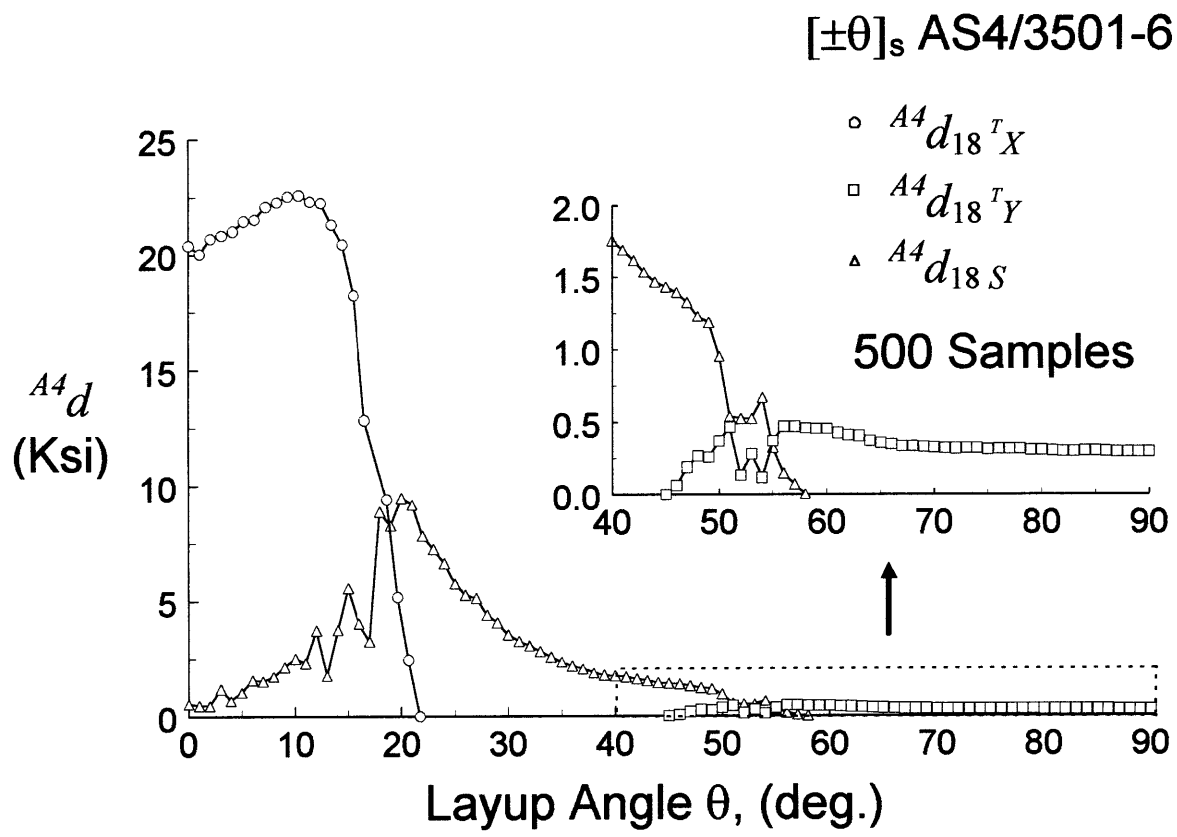

Figure 5.23 Plot of the sensitivity of the laminate longitudinal tensile strength to ply strength (${}^{T}X$, ${}^{T}Y$, S) variations for the $[\pm\theta]_s$ laminate family

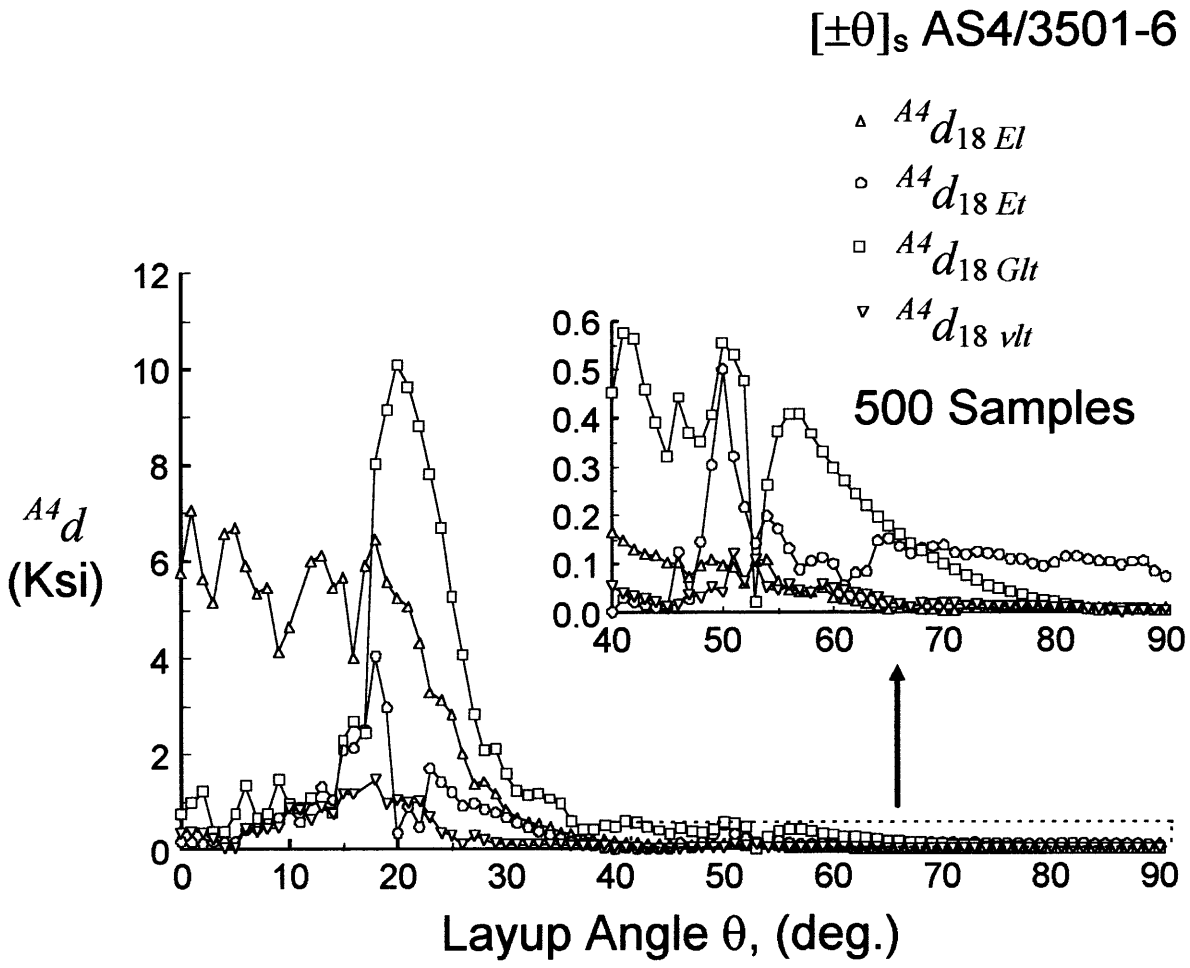

Figure 5.24 Plot of the sensitivity of the laminate longitudinal tensile strength to ply stiffness (E_l, E_t, G_{lt}) and Poisson's ratio (ν_{lt}) variations for the $[\pm\theta]_s$ laminate family

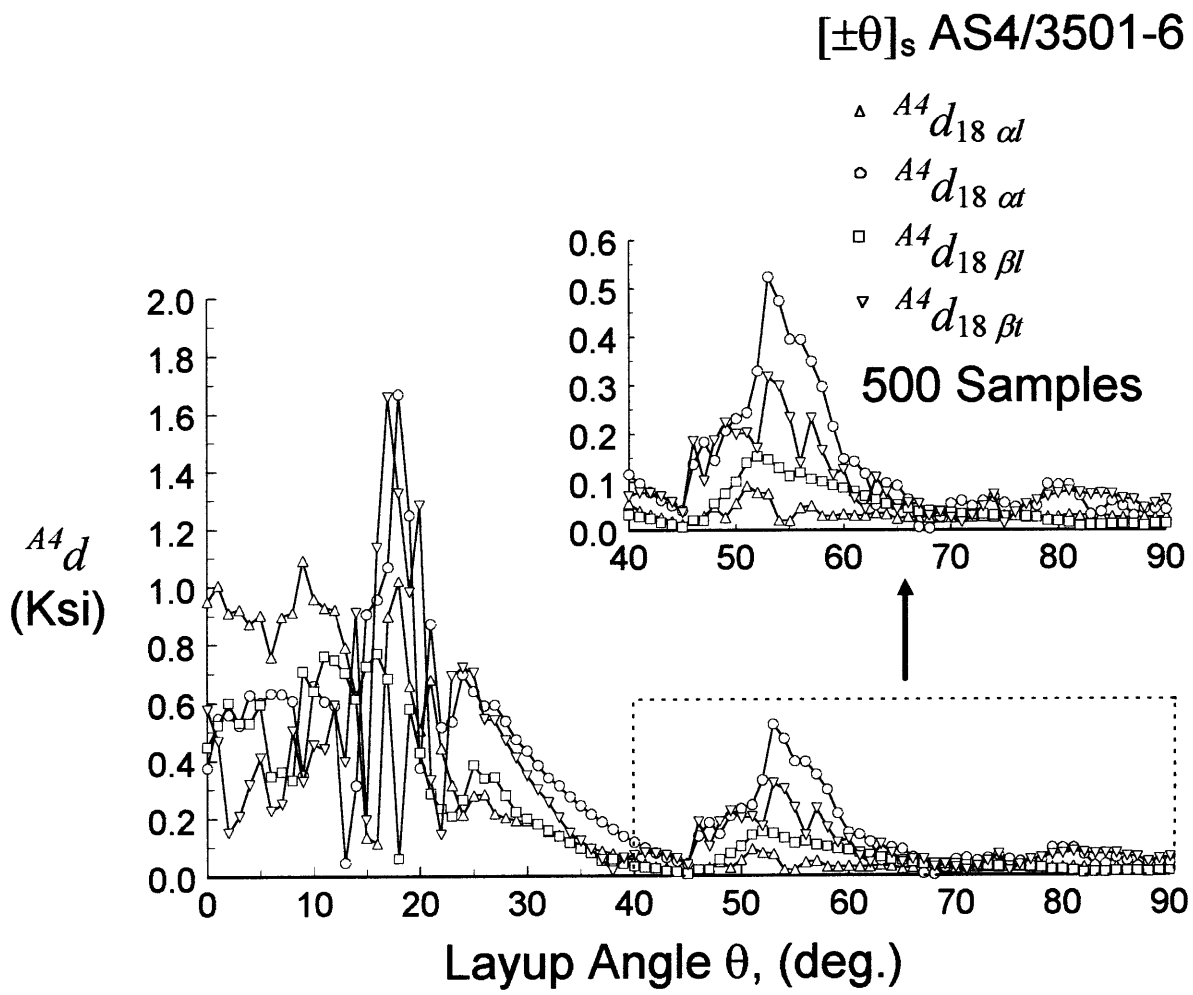

Figure 5.25 Plot of the sensitivity of the laminate longitudinal tensile strength to ply thermo and hygro elastic property (α_l, α_t, β_l, β_t) variations for the $[\pm\theta]_s$ laminate family

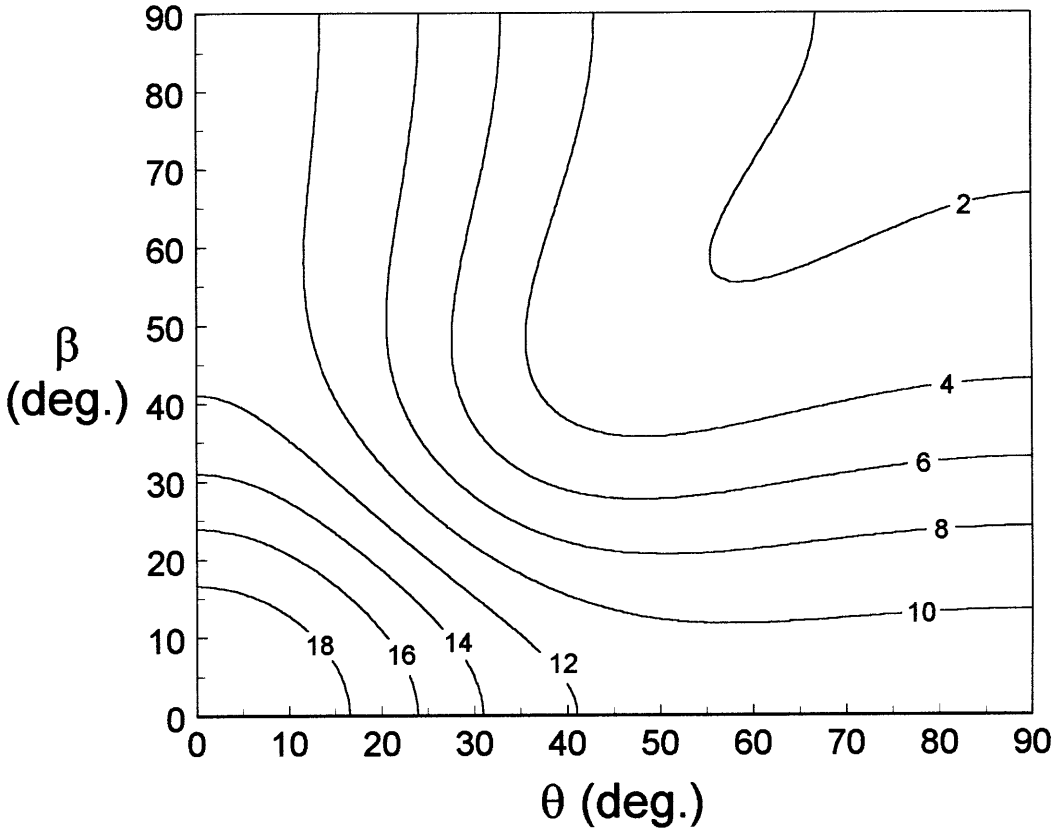

Figure 5.26 Contour plot of the mean longitudinal stiffness (Msi) for the $[\pm\theta/\pm\beta]_s$ AS4/3501-6 laminate family (approach A2)

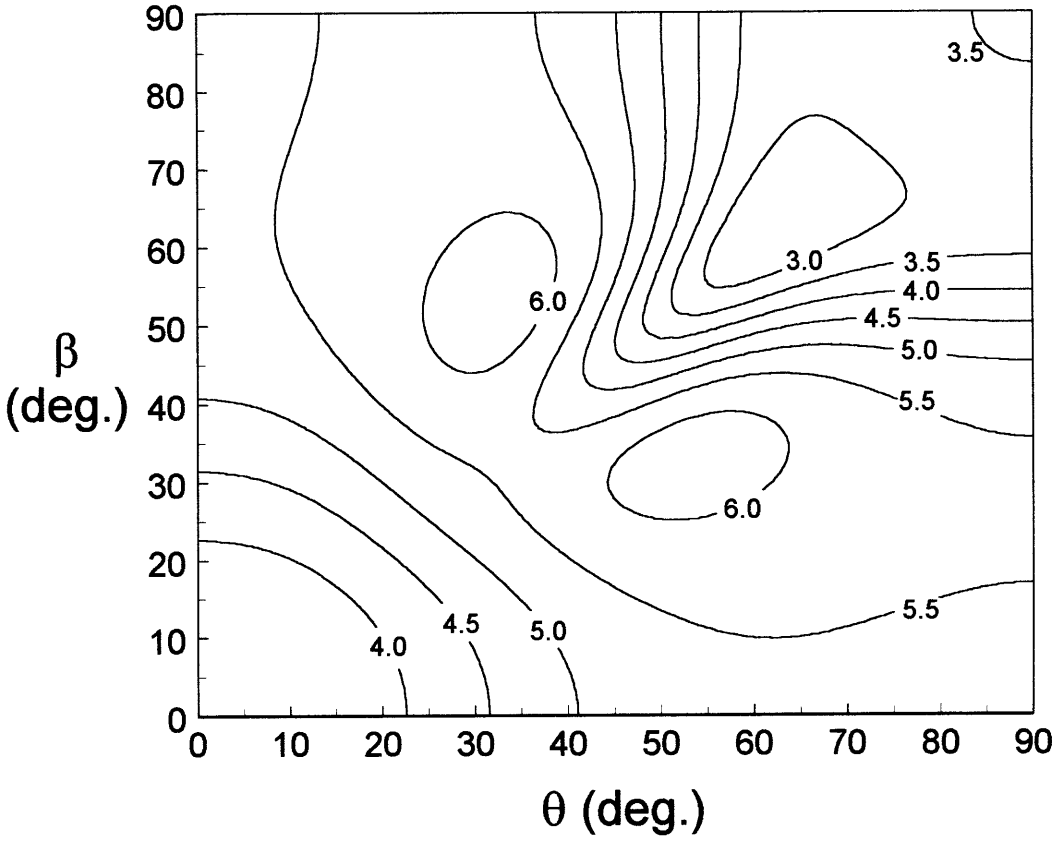

Figure 5.27 Contour plot of the coefficient of variation (%) of the longitudinal stiffness (Msi) for the $[\pm\theta/\pm\beta]_s$ AS4/3501-6 laminate family (approach A2)

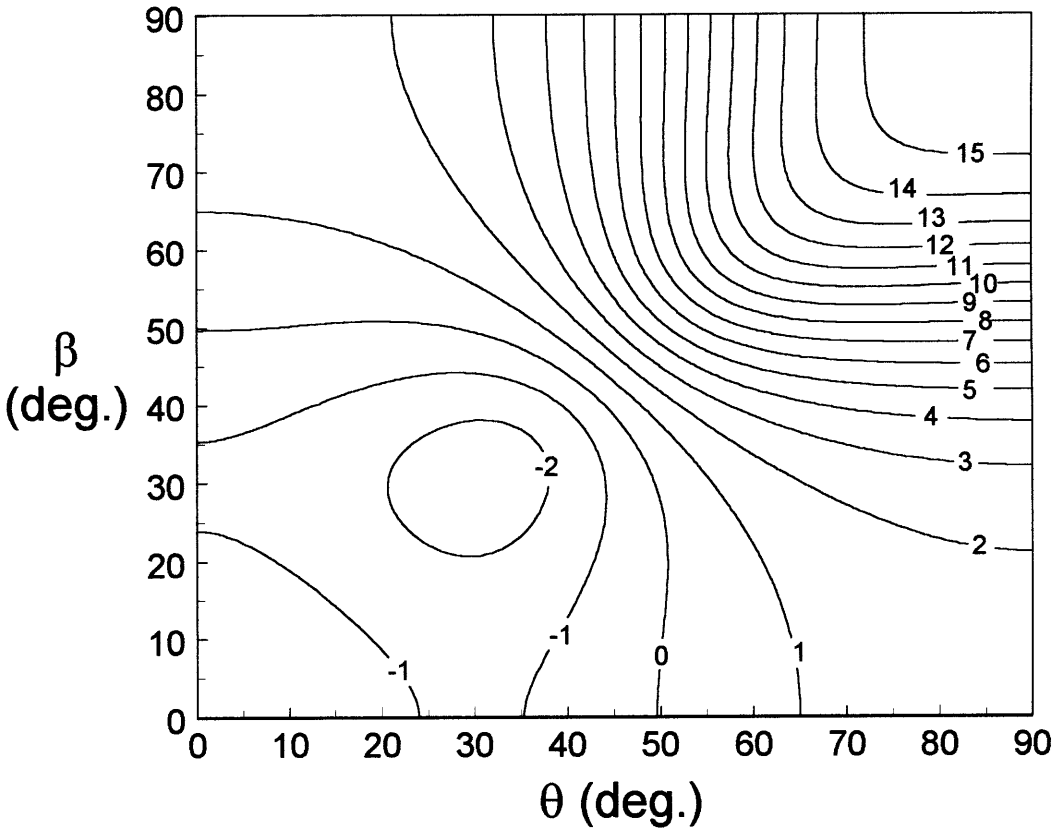

Figure 5.28 Contour plot of the mean longitudinal CTE (με/°F) for the $[\pm\theta/\pm\beta]_s$ AS4/3501-6 laminate family (approach A2)

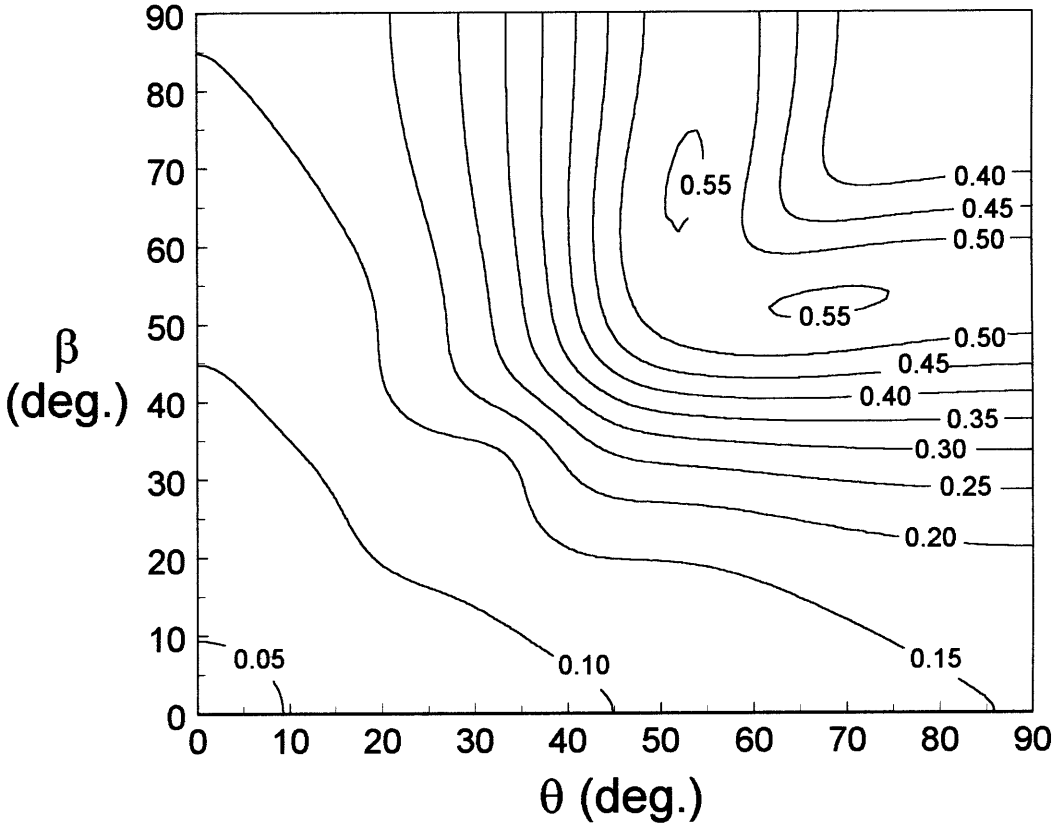

Figure 5.29 Contour plot of the standard deviation of the longitudinal CTE (με/°F) for the $[\pm\theta/\pm\beta]_s$ AS4/3501-6 laminate family (approach A2)

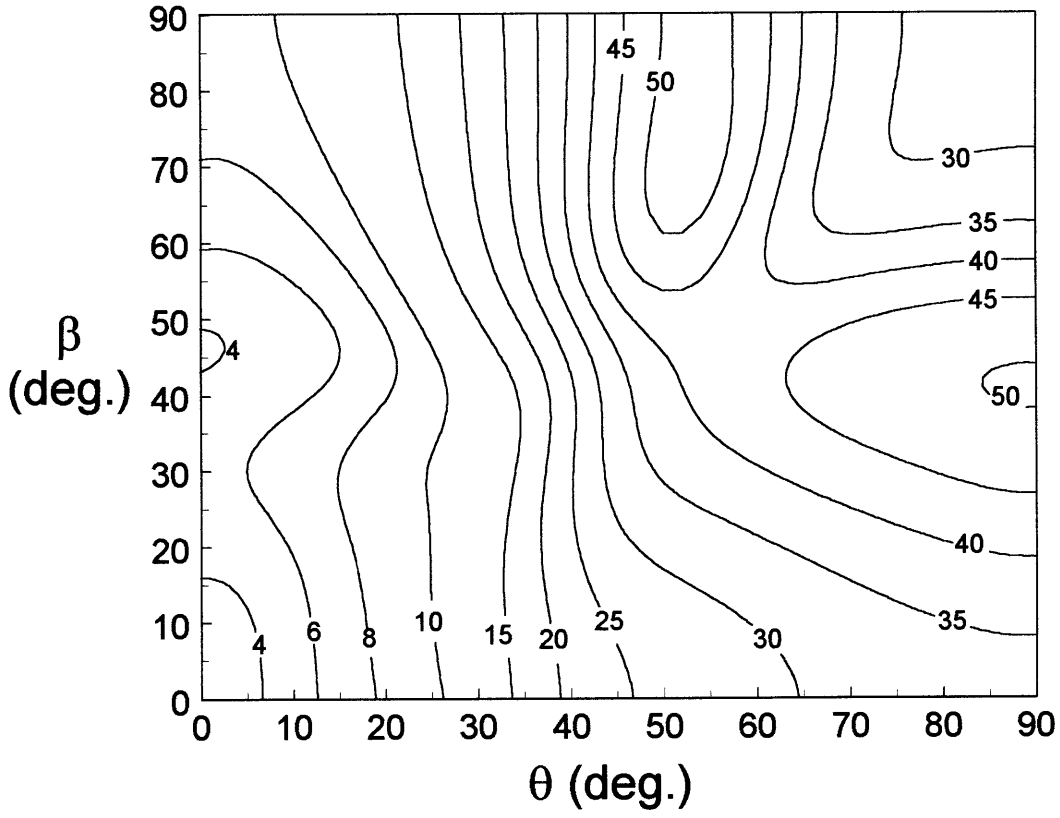

Figure 5.30 Contour plot of the standard deviation of the longitudinal CTB ($\mu in/in^2/^oF$) for the $[\pm\theta/\pm\beta]_s$ AS4/3501-6 laminate family (approach A2)

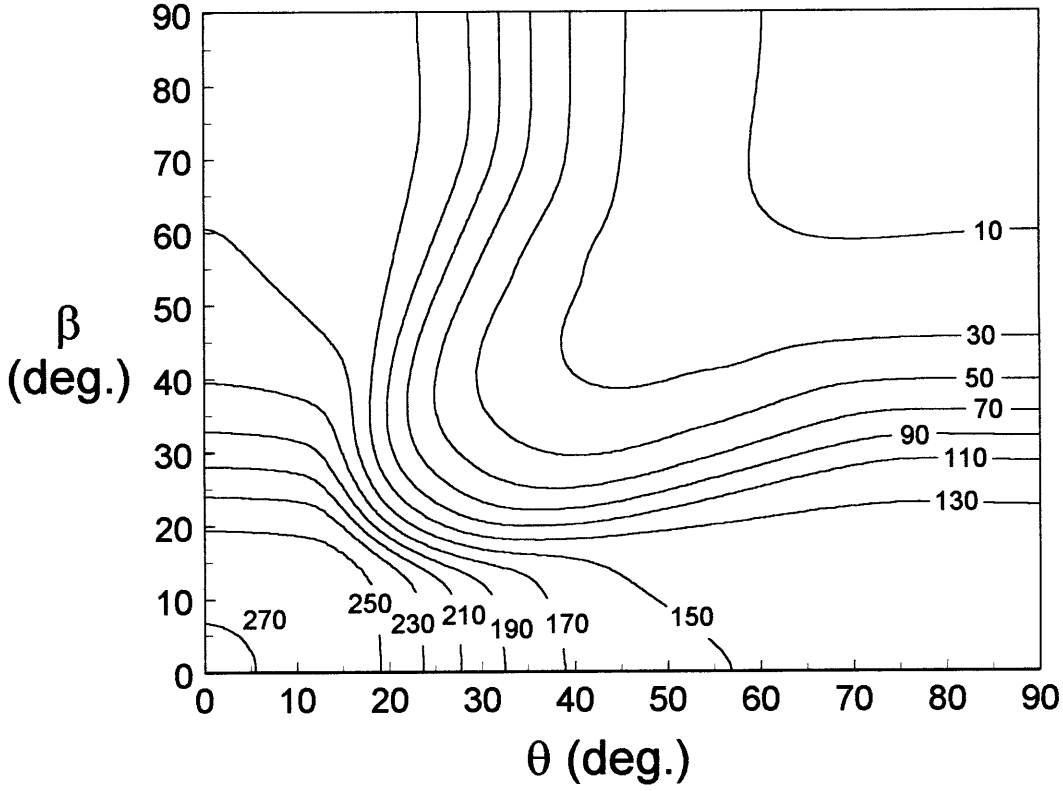

Figure 5.31 Contour plot of the mean longitudinal tensile strength (Ksi) for the $[\pm\theta/\pm\beta]_s$ AS4/3501-6 laminate family (approach A3, 500 samples)

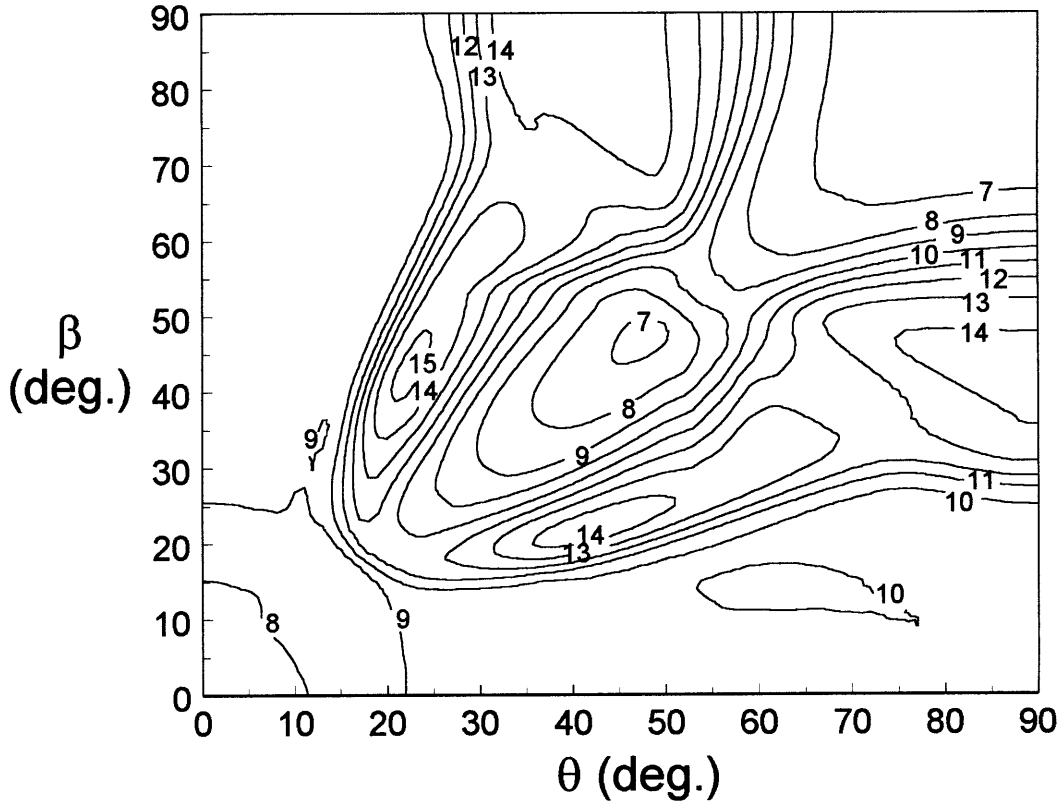

Figure 5.32 Contour plot of the coefficient of variation (%) of the longitudinal tensile strength for the $[\pm\theta/\pm\beta]_s$ AS4/3501-6 laminate family (approach A3, 1000 samples)

5.4 OPTIMIZATION RESULTS

In this section two different optimization problems are considered. The first problem is that of matching the stiffness properties of a composite laminate to that of a typical aircraft aluminum. The second problem is to minimize the longitudinal CTEs, CMEs, CTBs, and CMBs of a laminate, while also maximizing the stiffness properties. Several cases are considered where the weights on the thermal, hygral, and stiffness portions of the cost function are different (e.g., cases are considered where thermal deformation is more important to minimize than hygral, etc.).

The material system considered is T300/934. The means and standard deviations of the properties for T300/934 are summarized in Table 5.3. The material properties of the T300/934 material are nearly identical to the AS4/3501-6 material; however, an important difference between the two materials is the longitudinal CTE, which is significantly higher for the T300/934 material. This results in a greater flexibility when designing for dimensional stability since more zero mean CTE designs exist, as can be seen by comparing Figures 5.33 and 5.28 (there are two zero mean CTE contours for T300/934 and only one for AS4/3501-6).

5.4.1 Optimization For Matching Properties Of A Composite Laminate To Another Material

The specific problem considered is to match the mean stiffness and Poisson's ratio of a composite laminate with that of a typical aircraft

aluminum (2000 series). The material properties for the aluminum are summarized in Table 5.2.

The cost function to be minimized follows:

$$f_c(\theta) = A_1\left|E_x - \tilde{E}_x\right| + A_2\left|E_y - \tilde{E}_y\right| + A_3\left|G_{xy} - \tilde{G}_{xy}\right| + A_4\left|\nu_{xy} - \tilde{\nu}_{xy}\right|$$

$$f_c(\theta^*) = \min_{\theta}\{f_c(\theta)\} \qquad \text{(5.3,a,b)}$$

$$\text{subject to: } 0 \le \theta \le \frac{\pi}{2}$$

The ~ is to signify the mean laminate property goals, i.e. the mean stiffnesses of aluminum. This cost function does not attempt to minimize the standard deviations of the laminate properties (i.e. the B_i are set to zero). The objective is to only match the mean laminate stiffnesses with those of aluminum. The $[\pm\theta_1/\pm\theta_2/.../\pm\theta_D]_s$ laminate families are considered with D=1, 2, 3, 4, and 5. Here, $\theta=\{\theta_1,\theta_2,...,\theta_D\}$ and θ^* is a vector of the optimal layup angles. The weight factors, A_i, are used to nondimensionalize and bring each of the terms in Eq. 5.3a to order one. Other weight factors can be chosen that favor the matching of a particular property more than the others (e.g. one term is weighted to be of order two and the others to be of order one). Here it is assumed that an equal weighting is desired, so the weight factors are chosen as the inverse of the laminate property goals (i.e. the inverse of the properties of aluminum):

$$A_1 = \frac{1}{\tilde{E}_x}$$
$$A_2 = \frac{1}{\tilde{E}_y}$$
$$A_3 = \frac{1}{\tilde{G}_{xy}} \qquad (5.4)$$
$$A_4 = \frac{1}{\tilde{\nu}_{xy}}$$

This choice of weight factors results in the cost function being a sum of the percent differences (divided by 100) between the properties of the aluminum and the laminate.

Table 5.4 summarizes the optimal layups for the various values of D. Table 5.5 is a summary of the properties of the laminates for the various D values (which ideally would be identical to the properties of the aluminum, however these results show that this is an unobtainable goal with the T300/934 material system and laminate families considered).

5.4.2 Optimization For Minimal Thermal And Hygral Deformation And Maximal Stiffness

In this section an optimization for minimal thermal and hygral deformation and maximal stiffness is considered. This is a significantly more complicated problem than the one considered in Section 5.4.1, and hence requires significantly more explanation. This section is divided into four parts. First the cost function is defined in Section 5.4.2.1. The goals for the mean laminate properties are defined in Section 5.4.2.2. Sensible weight factors that represent the relative importance of the thermal, hygral, and

Table 5.2 Typical Material Properties of 2000 Series Aluminum

Symbol	Material Property	Mean
$\widetilde{E}_x$	longitudinal stiffness	10.5 Msi
$\widetilde{E}_y$	transverse stiffness	10.5 Msi
$\widetilde{G}_{xy}$	shear stiffness	4.0 Msi
$\widetilde{\nu}_{xy}$	Poisson's ratio	0.3

Table 5.3 Mean and Standard Deviations of Ply Properties And Parameters For T300/934

Symbol	Ply Property/Parameter	Mean	Standard Deviation
$t_1,.., t_n$	thickness of ply 1,..,n	$5.2(10)^{-3}$ in.	$2.6(10)^{-4}$ in.
$\theta_1,.., \theta_n$	layup angle of ply 1,.., n	-	2°
$E_{l1},..,E_{ln}$	longitudinal stiffness of ply 1,.., n	20 Msi	1 Msi
$E_{t1},.., E_{tn}$	transverse stiffness of ply 1,.., n	1.4 Msi	0.07 Msi
$G_{lt1},.., G_{ltn}$	shear stiffness of ply 1,.., n	0.7 Msi	0.035 Msi
$\nu_{lt1},.., \nu_{ltn}$	major Poisson's ratio of ply 1,.., n	0.3	0.015
$\alpha_{l1},.., \alpha_{ln}$	longitudinal CTE of ply 1,.., n	0.05 με/°F	0.1 με/°F
$\alpha_{t1},.., \alpha_{tn}$	transverse CTE of ply 1,.., n	16 με/°F	1 με/°F
$\beta_{l1},.., \beta_{ln}$	longitudinal CME of ply 1,.., n	45 με/%	30 με/%
$\beta_{t1},.., \beta_{tn}$	transverse CME of ply 1,.., n	5500 με/%	300 με/%

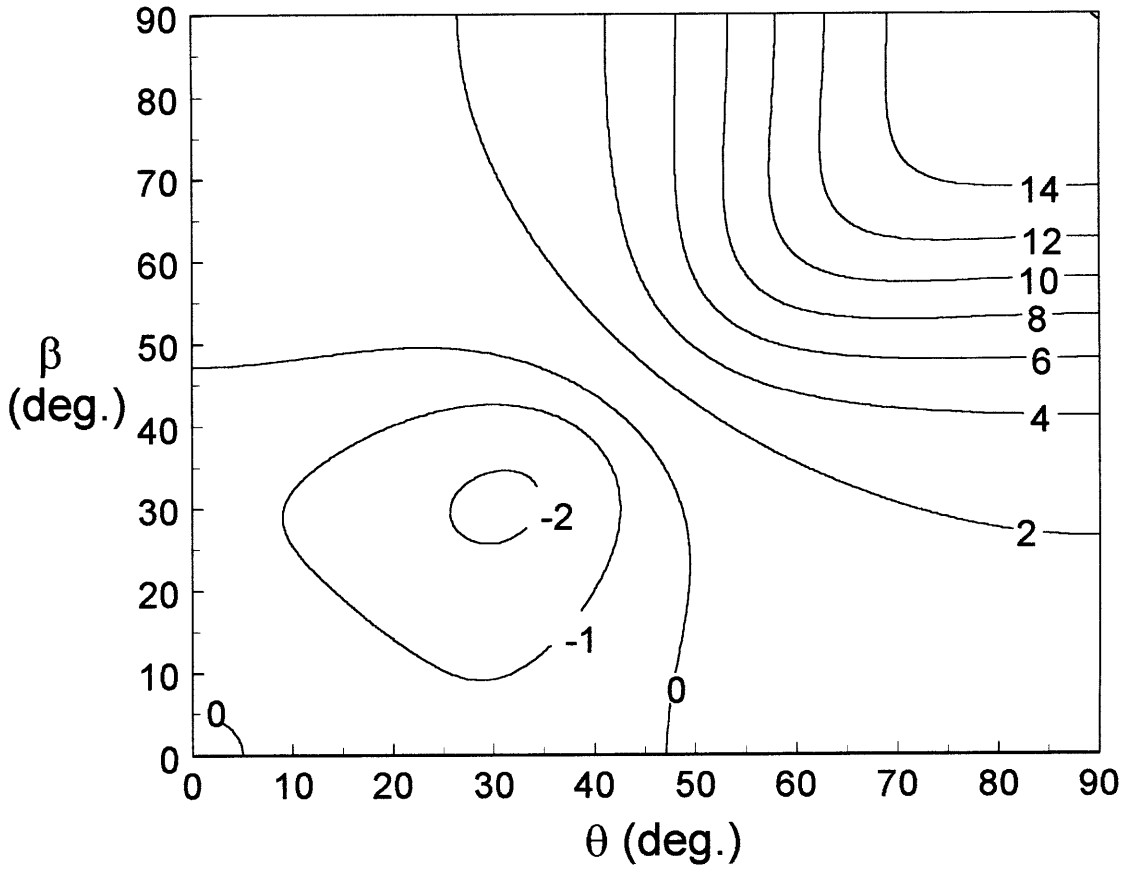

Figure 5.33 Contour plot of the mean longitudinal CTE (με/°F) for the $[\pm\theta/\pm\beta]_s$ T300/934 laminate family (approach A2)

Table 5.4 Optimal Layup Angles

D	Optimal Layup
1	$[\pm 60.7]_s$
2	$[\pm 62.6/\pm 10.5]_s$
3	$[\pm 28.4/\pm 10.0/\pm 72.9]_s$
4	$[\pm 0.0/\pm 23.5/\pm 39.6/\pm 87.5]_s$
5	$[\pm 12.8/\pm 57.7/\pm 26.9/\pm 80.6/\pm 12.0]_s$

Table 5.5 Mean Stiffnesses of Optimal Laminates and Aluminum

D	E_x (Msi)	E_y (Msi)	G_{xy} (Msi)	ν_{xy}
1	1.54	7.17	3.98	0.30
2	9.99	6.86	2.48	0.30
3	10.5	6.61	2.39	0.30
4	10.5	6.62	2.40	0.30
5	10.3	6.69	2.42	0.30
Aluminum	10.5	10.5	4.0	0.30

stiffness portions of the cost function are systematically derived in Section 5.4.2.3. Last, the optimization results are presented in Section 5.4.2.4.

5.4.2.1 The cost function

The goal is to minimize the longitudinal CTEs, CMEs, CTBs, and CMBs of a laminate, and their standard deviations, while also maximizing the stiffness properties. The cost function to be minimized follows:

$$f_c(\theta) = \xi_1\left\{\begin{matrix}\left(A_1\left|\alpha_x - \tilde{\alpha}_x\right| + B_1\,\mathrm{SD}\left[\alpha_x\right]\right) + \\ \left(B_2\,\mathrm{SD}\left[W_x^T\right]\right)\end{matrix}\right\} + \xi_2\left\{\begin{matrix}\left(A_2\left|\beta_x - \tilde{\beta}_x\right| + B_3\,\mathrm{SD}\left[\beta_x\right]\right) + \\ \left(B_4\,\mathrm{SD}\left[W_x^H\right]\right)\end{matrix}\right\} + \xi_3\left\{\begin{matrix}\left(A_3\left|E_x - \tilde{E}_x\right| + B_5\,\mathrm{SD}\left[E_x\right]\right) + \\ \left(A_4\left|E_y - \tilde{E}_y\right| + B_6\,\mathrm{SD}\left[E_y\right]\right) + \\ \left(A_5\left|G_{xy} - \tilde{G}_{xy}\right| + B_7\,\mathrm{SD}\left[G_{xy}\right]\right)\end{matrix}\right\}$$

$$f_c(\theta^*) = \min_{\theta}\left\{f_c(\theta)\right\} \qquad (5.5,\text{a,b})$$

$$\text{subject to: } 0 \le \theta \le \frac{\pi}{2}$$

The $[\pm\theta_1/\pm\theta_2]_s$ laminate families are considered. Here, $\theta=\{\theta_1,\theta_2\}$ and θ^* is a vector of the optimal layup angles. The ξ_i are *primary* weight factors that are used to weight the thermal, hygral, and stiffness portions of the cost function. The A_i and B_i are *secondary* weight factors that are used to nondimensionalize and bring each of their respective terms to order one so

that the thermal, hygral, and stiffness portions of the cost function are comparable on equal grounds.

The thermal portion of the cost function is weighted by ξ_1, the hygral part by ξ_2, and the stiffness part by ξ_3. The thermal and hygral portions of the cost function are constructed to minimize the longitudinal CTE, CTB, CME, and CMB; the stiffness portion of the cost function is constructed to maximize the longitudinal, transverse, and shear stiffnesses.

5.4.2.2 The goals for the mean laminate properties

The goals for the mean thermal, hygral, and stiffness properties are signified by the ~ (except for the longitudinal CTB and CMB because their means are zero since only symmetric laminates are considered). The goals for the laminate properties are defined as follows:

$$\begin{aligned}
\tilde{\alpha}_x &= \min_{\theta}\left\{|\alpha_x| + \mathrm{SD}[\alpha_x]\right\} \\
\tilde{W}_x^T &= \min_{\theta}\left\{\mathrm{SD}\left[W_x^T\right]\right\} \\
\tilde{\beta}_x &= \min_{\theta}\left\{|\beta_x| + \mathrm{SD}[\beta_x]\right\} \\
\tilde{W}_x^H &= \min_{\theta}\left\{\mathrm{SD}\left[W_x^H\right]\right\} \\
\tilde{E}_x &= \max_{\theta}\left\{E_x\right\} \\
\tilde{E}_y &= \max_{\theta}\left\{E_y\right\} \\
\tilde{G}_{xy} &= \max_{\theta}\left\{G_{xy}\right\}
\end{aligned} \qquad \text{(5.6a-g)}$$

These goals represent the ideal (although not simultaneously obtainable) mean properties of the laminate. The numerical values for the goals, defined in Eqs. 5.6a-g, and their corresponding optimal layup angles, are

summarized in Table 5.6 for the T300/934 material system. Optimization runs to solve Eqs. 5.6e-g were not necessary since the layups for maximum stiffness are well known. Optimization runs were necessary to solve Eqs. 5.6a-d to determine the thermal and hygral laminate property goals.

Figures 5.34 and 5.35 illustrate the results from the optimization run for determining the longitudinal CTE goal. Figure 5.34 is a convergence plot showing how "fast" the SSM converges to the minimum. Figure 5.35 is a plot of the points sampled by the SSM during the optimization run and zero mean CTE contours. Each cross in the plot represents a point that has either passed the Boltzmann test or is a result of a downhill simplex method step (see Sections 4.4.1 and 4.4.2). Figure 5.35 shows how the SSM tends to sample around the zero CTE contours, and eventually (as the parameter temperatures become small) samples only in the vicinity of the global optima (which is on the zero CTE contour in the lower left hand corner of the plot).

5.4.2.3 The weight factors

To determine sensible secondary weight factors for the thermal and hygral portions of the cost function the temperature and moisture environment must be considered. The amount of deformation induced by temperature changes is in general different then the amount induced by changes in moisture content. This difference should be considered when determining the secondary weights for the thermal and hygral parts of the cost function. For example, if the environment is such that there is a very

large temperature change and only a small change in moisture content it is reasonable to weight the CTE more than the CME to account for the larger thermally induced deformation. The secondary weights for the thermal and hygral portions of the cost function are determined by considering the amount of strain due to a given temperature and moisture content change. The secondary thermal and hygral weight factors are defined as follows:

$$
\begin{aligned}
A_1 = B_1 &= \left(\frac{1}{\tilde{\alpha}_x}\right)\left(\frac{2\tilde{\alpha}_x \Delta T}{\tilde{\alpha}_x \Delta T + \tilde{\beta}_x \Delta H}\right) \\
A_2 = B_3 &= \left(\frac{1}{\tilde{\beta}_x}\right)\left(\frac{2\tilde{\beta}_x \Delta H}{\tilde{\alpha}_x \Delta T + \tilde{\beta}_x \Delta H}\right) \\
B_2 &= \left(\frac{1}{\tilde{W}_x^T}\right)\left(\frac{2\tilde{W}_x^T \Delta T}{\tilde{W}_x^T \Delta T + \tilde{W}_x^H \Delta H}\right) \\
B_4 &= \left(\frac{1}{\tilde{W}_x^H}\right)\left(\frac{2\tilde{W}_x^H \Delta H}{\tilde{W}_x^T \Delta T + \tilde{W}_x^H \Delta H}\right)
\end{aligned}
\qquad (5.7,\text{a-d})
$$

The first term in parenthesis in these expressions is the inverse of the goal for the respective laminate property. The first term is used for nondimensionalization and to bring the terms in the cost function to order one. The second term in parenthesis in these expressions is of order one and has the purpose of taking into account the relative magnitude of thermal and hygral induced deformations. If the ΔT and ΔH values result in equal strain (using the ideal laminate properties) then the second term in parenthesis in Eqs. 5.7a-d are equal to one. As $\tilde{\alpha}_x \Delta T$ becomes large the secondary weight factors for the hygral properties approach zero and the second term in parenthesis in Eqs. 5.7a,c approach two (i.e. only thermal deformation is

considered important to minimize). As $\tilde{\beta}_z \Delta H$ becomes large the secondary weight factors for the thermal properties approach zero and the second term in parenthesis in Eqs. 5.7b,d approach two (i.e. only hygral deformation is considered important to minimize).

Exposed objects in low earth orbit experience approximately ±150 °F temperature swings. Hence, it is reasonable to consider a 300 °F temperature range, that is ΔT=300 °F. The typical moisture content of a graphite/epoxy material, on earth, is 1%; in space the moisture content of a laminate is, eventually, 0%. Hence, it is reasonable to consider a 1% change in moisture content, that is ΔH=1%.

The secondary weight factors for the stiffness portion of the cost function are chosen to nondimensionalize and bring their respective terms to order one. Each stiffness property is weighted equally (i.e. it is assumed that it is just as important to maximize shear stiffness as longitudinal stiffness, etc.). The secondary weight factors are chosen as:

$$A_3 = B_5 = \frac{1}{\tilde{E}_x}$$
$$A_4 = B_6 = \frac{1}{\tilde{E}_y} \qquad \text{(5.8a-c)}$$
$$A_5 = B_7 = \frac{1}{\tilde{G}_{xy}}$$

Six cases with different primary weight factors on the thermal, hygral, and stiffness portions of the cost function were considered (e.g., cases are considered where thermal deformation is more important to minimize than

hygral, etc.). Each set of primary weight factors corresponds to an optimization run. Each optimization run is referred to as run O1, O2, ..., O6 for convenience. Table 5.7 summarizes the primary weight factors that correspond to each of the optimization runs.

The primary weight factors for the first three optimization runs, O1, O2, and O3, respectively, were chosen to optimize for maximum stiffness, minimum longitudinal thermal deformation, and minimum longitudinal hygral deformation, respectively. The primary weight factors for O4 were chosen to optimize for minimum thermal and hygral deformation simultaneously. The primary weight factors for O5 were chosen to optimize for minimum thermal and hygral deformation, and maximum stiffness, simultaneously. The primary weight factors for O6 are similar to O5 except that a much larger weight is placed on stiffness relative to the thermal and hygral portions of the cost function (i.e. stiffness is considered more important to maximize than it is to minimize the thermal and hygral deformation).

5.4.2.4 Results

Table 5.8 lists the optimal layups for each of the optimization runs (O1-O6). Note that the optimal layups for O2-O5 are very similar, however the optimal layups for O1 and O6 differ considerably from O2-O5, and each other. Table 5.9 summarizes the means and standard deviations of the longitudinal thermal and hygral properties for the optimal layups. Table

5.10 summarizes the means and standard deviations of the stiffness properties of the optimal layups. Note that even though the primary weight factors for O6 favor the maximization of stiffness, the optimal layup still results in excellent thermal and hygral laminate properties (i.e. very low means and standard deviations of the longitudinal CTE, CME, CTB, and CMB).

5.5 DESIGN OF A SATELLITE STRUCTURE FOR MAXIMAL DIMENSIONAL STABILITY WITH FREQUENCY CONSTRAINT

In this section an example problem is considered to demonstrate how the present probabilistic and optimization methods may be used as a tool for the design of a structure. The problem considered is that of designing a composite laminate for an optical support structure for a recently proposed space based optical telescope [1]. The structure is cylindrical in shape with a diameter of 0.4 meters (16 inches) and a length of one meter (40 inches) and a mass of 50kg (which includes the optics and all supporting equipment).

The design requirements (greatly abridged to simplify the discussion, see [1] for details) are to have very little (ideally no) longitudinal thermal deformation and a high fundamental frequency of the structure. The structure is exposed to temperature swings as it moves in and out of the earth's shadow and therefore must be built with a material that has a very low longitudinal CTE to prevent defocusing of the optics due to thermal deformation. The structure must have a fundamental frequency that is high

Table 5.6 Optimization Results Used For Secondary Weight Factors

Symbol	Value	Optimal Layup
$\widetilde{\alpha}_x$	0.04 (με/°F)	$[\pm 1.57/\pm 4.78]_s$
$\widetilde{W}_x^T$	2.92 (μin/in²/°F)	$[\pm 0.02/\pm 0.00]_s$
$\widetilde{\beta}_x$	15.0 (με/%)	$[\pm 2.28/\pm 7.90]_s$
$\widetilde{W}_x^H$	876 (μin/in²/%)	$[\pm 0.00/\pm 0.17]_s$
$\widetilde{E}_x$	20.0 (Msi)	$[\pm 0.00/\pm 0.00]_s$
$\widetilde{E}_y$	20.0 (Msi)	$[\pm 90.0/\pm 90.0]_s$
$\widetilde{G}_{xy}$	5.18 (Msi)	$[\pm 45.0/\pm 45.0]_s$

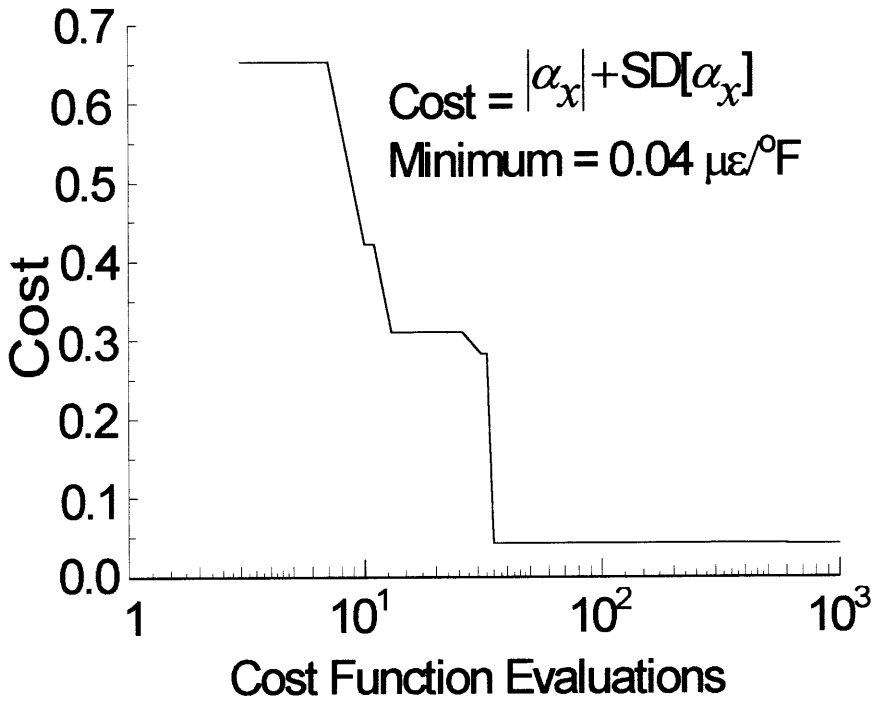

Figure 5.34 Convergence plot for optimization for minimal longitudinal thermal expansion

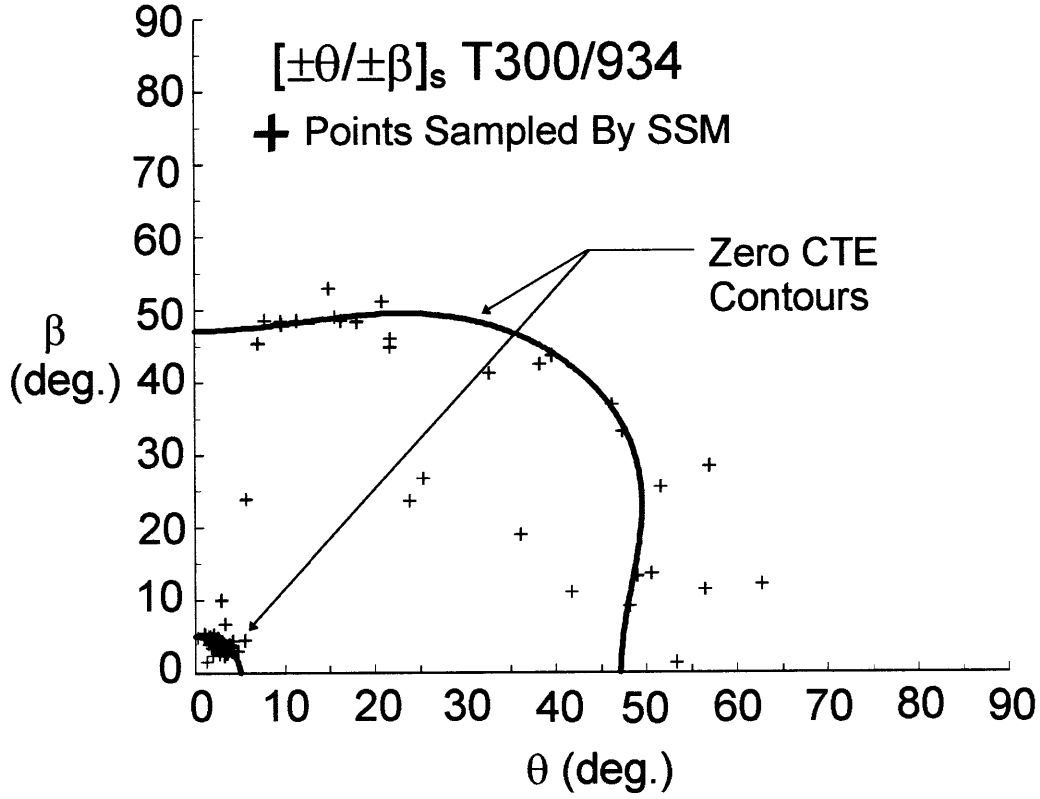

Figure 5.35 Plot of zero mean longitudinal CTE (με/°F) contours for the $[\pm\theta/\pm\beta]_s$ T300/934 laminate family, and points sampled by SSM during optimization for minimal longitudinal thermal expansion (corresponds to Figure 5.34)

Table 5.7 Primary Weight Factors

Optimization Run Name	ξ_1	ξ_2	ξ_3
O1	0	0	1
O2	1	0	0
O3	0	1	0
O4	1	1	0
O5	1	1	1
O6	1	1	100

Table 5.8 Optimal Layup Angles

Optimization Run Name	Optimal Layup
O1	$[\pm 25.9/\pm 64.1]_s$
O2	$[\pm 0.3/\pm 5.0]_s$
O3	$[\pm 0.5/\pm 8.2]_s$
O4	$[\pm 0.3/\pm 5.0]_s$
O5	$[\pm 0.4/\pm 5.0]_s$
O6	$[\pm 0.0/\pm 46.8]_s$

Table 5.9 Longitudinal Hygral And Thermal Properties For Optimal Layups

Optimization Run Name	α_x {SD[α_x]} (με/°F)	W_x^T {SD[W_x^T]} (μin/in²/°F)	β_x {SD[β_x]} (με/%)	W_x^H {SD[W_x^H]} (μin/in²/%)
O1	1.35 {0.12}	0.00 {9.1}	488 {40.5}	0.00 {3035}
O2	0.00 {0.04}	0.00 {3.0}	27.9 {12.5}	0.00 {911}
O3	-0.08 {0.05}	0.00 {3.1}	0.00 {15.0}	0.00 {961}
O4	0.00 {0.04}	0.00 {3.0}	27.9 {12.5}	0.00 {911}
O5	0.00 {0.04}	0.00 {3.0}	27.9 {12.5}	0.00 {911}
O6	-0.02 {0.08}	0.00 {3.4}	20.6 {27.1}	0.00 {1060}

Table 5.10 Stiffness Properties For Optimal Layups

Optimization Run Name	E_x {SD[E_x]} (Msi)	E_y {SD[E_y]} (Msi)	G_{xy} {SD[G_{xy}]} (Msi)
O1	6.75 {0.30}	6.75 {0.30}	3.46 {0.12}
O2	19.8 {0.36}	1.40 {0.025}	0.77 {0.029}
O3	19.5 {0.36}	1.40 {0.024}	0.88 {0.044}
O4	19.8 {0.36}	1.40 {0.025}	0.77 {0.029}
O5	19.8 {0.36}	1.40 {0.025}	0.77 {0.029}
O6	11.2 {0.30}	3.62 {0.18}	2.93 {0.075}

enough to prevent a resonant vibration resulting from a forcing due to the reaction wheels (which would cause jittering of the optics resulting in degraded image resolution).

The design requirements considered here are as follows: the structure must have a fundamental frequency greater than 75 Hz, and the longitudinal CTE must be as close to zero as is practically possible. The optimization problem statement follows:

$$\begin{aligned} & f_c(\theta) = |\alpha_x| + \mathrm{SD}[\alpha_x] \\ & f_c(\theta^*) = \min_{\theta}\{f_c(\theta)\} \\ & \text{subject to: } 0 \le \theta \le \frac{\pi}{2} \\ & \qquad\qquad \omega_f > 75 \text{ Hz} \end{aligned} \tag{5.9}$$

The $[\pm\theta_1/\pm\theta_2]_s$ laminate families are considered. Here, $\theta=\{\theta_1,\theta_2\}$ and θ^* is a vector of the optimal layup angles.

There are two ways to incorporate the frequency (or any other) constraint using the SSM. The first is to keep generating new points if the frequency constraint is not satisfied, as explained in Section 4.4.2. This would require that the fundamental frequency of the structure be calculate for every iteration during optimization to check that the constraint is satisfied. This is a good approach, but it is difficult to implement in a computer code in a general way such that the code is applicable to other problems. In the present implementation hyper-rectangles may be specified inside of which the layup angles are excluded from optimization (other

shapes also may be used). This is a general way to take into account various constraints that may arise for different problems. For the present problem, rectangles are specified that enclose the layup angles that correspond to fundamental frequencies below 75 Hz (as well as can be done with rectangles).

Figure 5.36 is contour plot of the fundamental frequency (calculated using methods developed in [1]) that also shows the three specified rectangles inside of which the layup angles are excluded from consideration during optimization. Figures 5.37 and 5.38 illustrate the results from the optimization run for minimizing the longitudinal CTE. Figure 5.37 is a convergence plot showing how "fast" the SSM converges to the minimum. Note that the minimum cost value is significantly higher than the case with no frequency constraint shown in Figure 5.34. Figure 5.38 is a plot of the points sampled by the SSM during the optimization run and zero mean CTE contours. Each cross in the plot represents a point that has either passed the Boltzmann test or is a result of a downhill simplex method step (see Sections 4.4.1 and 4.4.2). Note that the zero mean CTE contour in the lower left hand corner is excluded from optimization; this is why the minimum cost value is higher than the case with no frequency constraint (the global optima, without any constraints, is on the zero CTE contour in the lower left hand corner of Figure 5.33). The optimal layup for this problem is $[\pm 47^{o}/\pm 0^{o}]_{s}$.

It is interesting that this layup is very similar to the layup that corresponds to the maximum fundamental frequency, as can be seen in Figure 5.36. Even more interesting is that this layup is also very similar to the layup for minimal longitudinal thermal and hygral deformation and maximal stiffness (recall optimization run O6 in Section 5.4.2). Indeed, given the superb qualities of this layup, it is the one that was chosen for the structure.

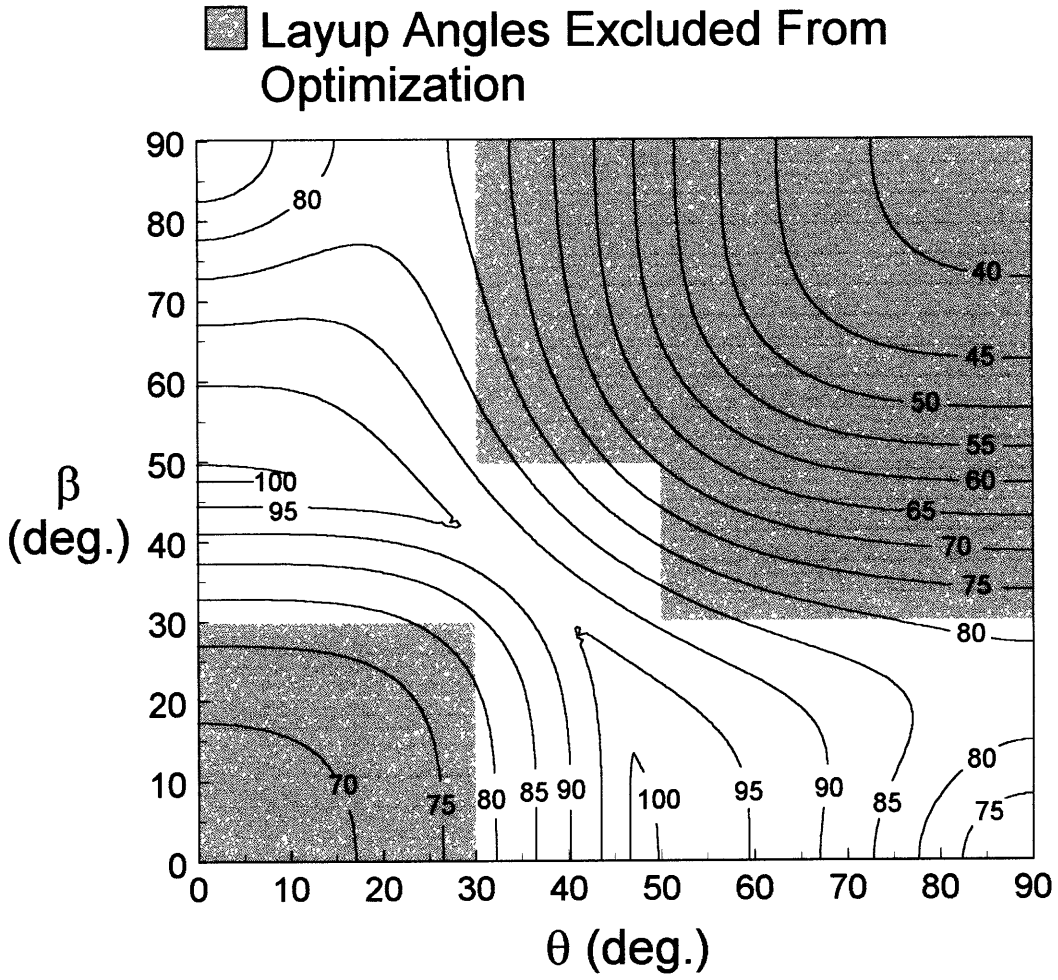

Figure 5.36 Contour plot of fundamental frequency (Hz) of optical support structure for the $[\pm\theta/\pm\beta]_s$ T300/934 laminate family, and regions of non-admissible layup angles

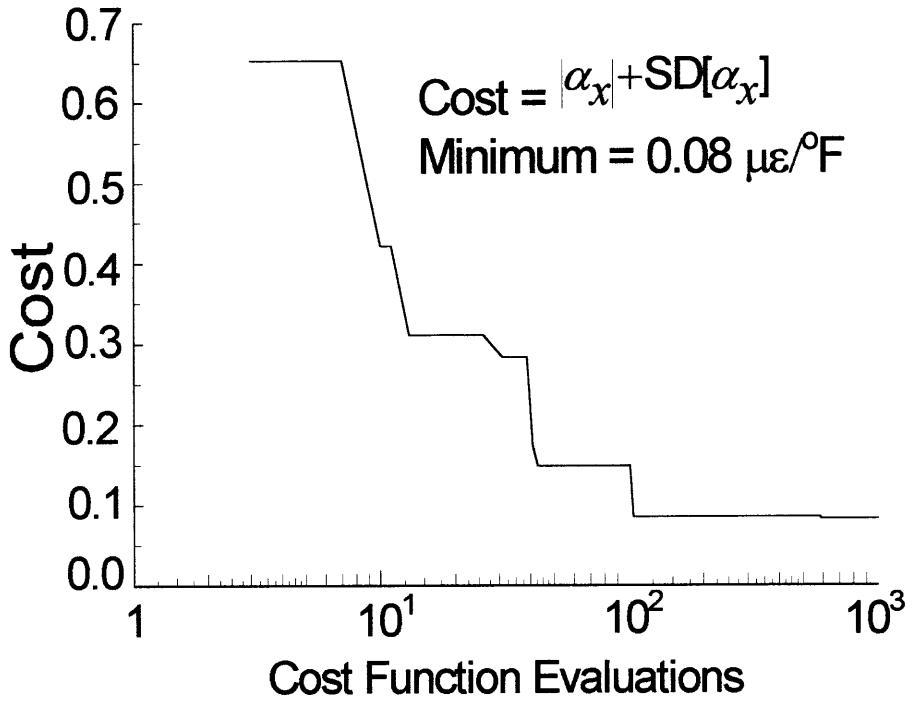

Figure 5.37 Convergence plot for optimization for minimal longitudinal thermal expansion with constraints on layup angles

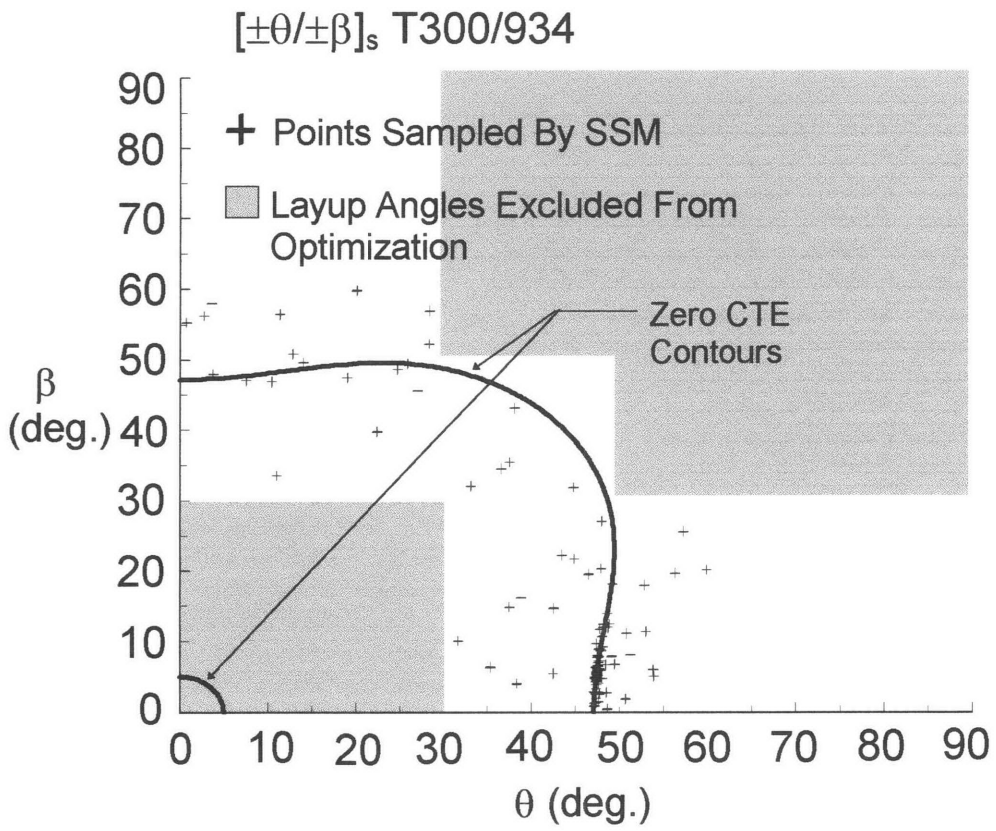

Figure 5.38 Plot of zero mean longitudinal CTE (με/°F) contours for the $[\pm\theta/\pm\beta]_s$ T300/934 laminate family, and points sampled by SSM during optimization for minimal longitudinal thermal expansion with constraints on layup angles (corresponds to Figure 5.37)

CHAPTER 6

DISCUSSION

The purpose of this chapter is to interpret, and discuss the implications of, the experimental, predicted, and optimization results presented in Chapter 5. The experimental and predicted results are discussed in Section 6.1. The optimization results are discussed in Section 6.2. Section 6.3 is a general discussion including important lessons learned, modeling and lengthscale issues, and an alternate interpretation of the probabilistic/optimization methodology.

6.1 DISCUSSION OF EXPERIMENTAL AND PREDICTED RESULTS

6.1.1 Comparison With Experimental Data

Overall, the predictions are in good agreement with the experimental data. The experimental and predicted CDFs for the longitudinal stiffness and tensile strength, shown in Section 5.1.2, are in very good agreement. Also, the predicted standard deviation bands seem to capture the trends in the (limited amount of) data for the different layups, as shown in Section 5.1.3. Two noteworthy exceptions are the longitudinal tensile strength for the $[\pm 15^{\circ}]_{s}$ and $[\pm 15^{\circ}]_{2s}$ laminates.

The tensile strength of the $[\pm 15^{\circ}]_s$ and $[\pm 15^{\circ}]_{2s}$ laminates is significantly over-predicted (see Figures 5.5 and 5.6). The reason for this is believed to be due to edge delamination resulting in a lower tensile strength. These laminates are known to be prone to delamination which significantly reduces their tensile strength in comparison to that if only in-plane failure modes occur [85]. Since delamination was not modeled this over-prediction was expected.

The data for the CTBs shown in Figure 5.8 seems to exhibit less scatter than indicated by the 1-standard-deviation band. This is believed to be a result of the $[\pm 45^{\circ}]_s$ and $[\pm 60^{\circ}]_s$ test specimens being cut from the same panel; the data does not capture ply material and geometric variations that occur from panel to panel. Hence, the predicted variability is expected to be greater than that of the data, as is the case.

The predicted standard deviation bands show a significant decrease of the laminate property standard deviations as the number of plies increases (see Figures 5.3-5.7, 5.9). This was expected based on arguments using linear probabilistic methods. If a laminate property is modeled using a simple linear rule of mixtures of the ply properties, it is straight forward to derive (using approach A1, Section 4.3.1) that the standard deviation of the laminate property is inversely proportional to the square root of the number of plies. This result is consistent with the observed decrease of the standard deviations.

An important point regarding the predictions for the mean tensile strength of unidirectional, $[0^o]_n$, laminates is that the mean decreases as the number of plies, n, increases (see Figure 5.7). This behavior is due to the fact that as the number of plies increases so does the probability of there being a ply with, for example, a low strength (due to a flaw), which results in a lower strength of the laminate. This *size effect* (which is not limited to unidirectional laminates) has an important implication: mean unidirectional laminate in-plane strengths are a function of the number of plies and are different from the mean in-plane ply strengths. This is an important point since often unidirectional laminate strengths are reported as ply strengths. As can be seen in Figure 5.7, this study predicts that the unidirectional tensile strength of a laminate may differ by as much as 25% from the ply strength.

6.1.2 Comparison Of Approaches A2 And A4 With A3

The correlation of approaches A2 and A4 with A3 is excellent, as shown in Section 5.2. Figures 5.10-5.12 show that predictions using approach A2 are nearly identical to those of A3. This indicates that the assumptions made in A2 (within the context of the mathematical modeling) are applicable since A3 operates on the full nonlinear problem. This is an important result since A2 is more efficient than A3, making A2 more

attractive when the standard deviation need be calculated many times, e.g. for optimization for minimal variability.

In Figure 5.13 standard deviations calculated from A4 by taking the Euclidean norm of the sensitivity metrics, are compared with direct predictions from A3 to infer if the sensitivity metrics are accurate. Correlation is very good between A3 and A4 indicating that the assumptions made in, and sensitivity metrics from, A4 are in an aggregate sense accurate.

The roughness of the plot from A4 is a result of the low number of samples used. More samples could be used to achieve a smoother (and probably more accurate) plot, however the computation time required would be excessive. Approach A4 was not designed for, nor is computationally efficient at, calculating standard deviations. A3 is a more efficient approach, however it does not allow for the definition of sensitivity metrics. A4 was designed for the calculation of sensitivity metrics for problems that violate the assumptions of A2 (i.e. when the sensitivity metrics from A2 are not applicable, as is the case for the failure models).

6.1.3 Sensitivity Study

An important advantage of approaches A2 and A4 over A3 is that they allow for the definition of sensitivity metrics. Sensitivity metrics allow for the identification of critical ply material properties and geometric parameters that most contribute to the variability in the laminate properties. In

practice, sensitivity metrics are useful for determining what aspects of a manufacturing process must be controlled to assure laminate performance.

In Section 5.3.1 sensitivity studies are presented showing the sources of variability in the laminate longitudinal stiffness, CTE, CTB, and tensile strength. No generalizations for arbitrary laminate designs can be drawn from these studies. For example, the sensitivity metrics are a function of the standard deviations of the ply properties and geometric parameters, which depend on manufacturing processes, the material system, etc. The primary purpose of these studies is to drive home the important point that the sensitivity of a laminate property to variations in a ply material property or geometric parameter is a strong function of the laminate design (e.g. layup angles, material system, etc.).

Figure 5.14 is a plot of the sensitivity of the laminate longitudinal stiffness, E_x, to layup angle and ply thickness variations. This plot shows that the sensitivity of E_x to variations in layup angle is far greater than that of ply thickness. However, the longitudinal CTB, for example, is sensitive to both ply thickness and layup angle variations, as shown in Figure 5.19.

The sensitivity of E_x to ply stiffness (E_l, E_t, G_{lt}) and Poisson's ratio (n_{lt}) variations is shown in Figure 5.15. This plot indicates that variations in E_l are the dominant source of variations in E_x for low angle layups, and that variations in E_t are the dominant source of variations in E_x for high angle layups. For intermediate angle layups E_x is sensitive to all the ply material

properties, especially G_{lt}. The thermoelastic properties exhibit a similar behavior (see Figures 5.17 and 5.20); variations in α_l are the dominant source of variations in α_x and W_x^T for low angle layups, and variations in α_t are the dominant source of variations in α_x and W_x^T for high angle layups. Again, for intermediate layup angles α_x and W_x^T are sensitive to all the ply material properties. The sharp drop of the sensitivity to G_{lt} and other properties at a layup angle near 45° shown in Figures 5.17 and 5.20 is interesting. The author can offer no simple physical explanation for this behavior.

Figures 5.22-5.25 are plots of the sensitivity metrics for laminate longitudinal tensile strength. Figure 5.22 shows that the impact of both ply angle and thickness variations on laminate strength can be significant, however there are wide variations in the sensitivities for different layups. Figure 5.23 shows the sensitivity of laminate strengths to different ply strengths. Low angle layups are sensitive to primarily longitudinal ply strength. As the layup angle increases the sensitivity to longitudinal strength eventually disappears while the sensitivity to ply shear strength grows; as the layup angle is further increased there is a small region where there is a sensitivity to both shear and transverse ply strengths; then finally only a sensitivity to transverse ply strength for the higher angle layups. The changes in sensitivites correspond to changes in the probable failure modes of the laminate. If there is no chance that the laminate will fail in a mode involving a particular ply strength, the laminate will show no sensitivity to

that strength. The fact that the sensitivity of some laminates is non-zero for more than one ply strength indicates that some nominally identical laminates can fail in different modes. In general, the results (Figures 5.22-5.24) show that the variability of the tensile strength of a laminate can be a strong function of the variability of several different ply properties and geometric parameters. In particular, variations in ply thickness, layup angle, and longitudinal stiffness and strength all significantly contribute to the variability of the tensile strength of laminates, including (interestingly enough) unidirectional ones.

The scatter in the sensitivity plots for the laminate tensile strength is an artifact, caused by the low number of samples used in A4. A sample size of 500 was used for the plots, which is sufficient to accurately predict most of the sensitivities, however there are two exceptions.

The first exception is when the sensitivity to a ply property or geometric parameter contributes little to the variation of tensile strength. The reason for this exception is that more samples are required to accurately predict the difference between ${}^{\varepsilon}\hat{\sigma}_{Yij}$ and $\hat{\sigma}_{Yij}$ (defined in Section 4.3.5) since A3 is used to predict ${}^{\varepsilon}\hat{\sigma}_{Yij}$ and $\hat{\sigma}_{Yij}$. This is, in part, the reason for the large amount of scatter in the sensitivities of the tensile strength to hygro/thermo elastic ply properties (Figure 5.25); the sensitivity of the tensile strength to the hygro/thermal elastic properties is non zero (due to thermal/hygral

residual stresses), but it is small relative to other sensitivities (for this particular laminate family).

The second exception is due to the possibility that the number of samples to get an accurate prediction of the ${}^{\varepsilon}\hat{\sigma}_{Yij}$ and $\hat{\sigma}_{Yij}$ is also a function of, laminate behavior. For example, the failure modes of some laminates can change due to slight changes in ply strengths, while the failure modes of other laminates are insensitive to changes in ply strengths. The more failure modes the more samples it takes to characterize each of them. Hence, it is conceivable that it takes more samples to calculate the standard deviation of a laminate that may fail in several different failure modes. This is the likely reason that the sensitivity to ply shear strength exhibits a lot of scatter in the vicinity of the 20° layup, since two failure modes are possible here (see Figure 5.23).

In general, these exceptions are not drawbacks of A4 for two reasons: (i) the scatter is not unavoidable, it may be decreased by increasing the number of samples, and more importantly (ii) the larger sensitivities are usually what one is interested in.

6.1.4 Parametric Study

The parametric study consists of contour plots of the mean, standard deviation, and coefficient of variation (when applicable) of all of the laminate properties for the $[\pm\theta/\pm\beta]_s$ laminate family. The entire parametric study is

presented in Appendix D. Figures 5.26-5.32 in Chapter 5 are a representative collection, and are discussed here.

The most important point drawn from this study is that the magnitude of variability of all of the laminate properties is a strong function of laminate design. For example, the Coefficient Of Variation (COV) varies from three to six percent, and seven to 15 percent, for the longitudinal stiffness and tensile strength respectively (see Figures 5.27 and 5.32, respectively). These results indicate that not only is it difficult, but restrictive to define a safety factor that blankets the infinite possible laminate designs.

The contour plot of the COV of longitudinal tensile strength in Figure 5.31, together with Figure 5.23 (which shows the various failure modes that are operating), indicate that in regions where multiple failure modes are possible the COV tends to be high. This makes sense since the initial failure mode can influence following failure modes (i.e. influence the path to failure). The last ply failure load is dependent on the path to failure. Hence, laminates that have unpredictable failure modes tend to have high COVs of tensile strength.

It should be noted that the contour plots of the means, standard deviations, and COVs of the longitudinal tensile strengths and FPF loads (Figures 5.31 and 5.32, and Appendix D respectively) are weakly nonsymmetric. Theoretically these plots should be symmetric as the number of samples approaches infinity (in practical terms about 5000 samples is sufficient); only 500 to 1000 samples (depending on the plot) were used to

generate the plots, hence the weak nonsymmetry. The computation time to generate the contour plots was long even for the low sample sizes (~24 hours for each plot on a Pentium® 166 MHz). The use of a larger sample size is primarily of aesthetic value, and was deemed unnecessary given the computational requirements.

The contour plots of the CTBs and CMBs are strongly nonsymmetric. The nonsymmetric behavior is a result of a dependence on stacking sequence. Figure 5.30 shows that stacking sequence can have a large effect on the magnitude of variability of the longitudinal CTB. The standard deviation of the longitudinal CTB for a $[\pm 0^{\circ}/\pm 90^{\circ}]_s$ laminate is 9.0 $\mu in/in^2/^{\circ}F$ and the standard deviation for a $[\pm 90^{\circ}/\pm 0^{\circ}]_s$ is 34 $\mu in/in^2/^{\circ}F$, nearly a 400% increase!

A very important point regarding predicted means, standard deviations, and COVs of the laminate properties must be noted. Even though the predicted statistics of the laminate properties are in good agreement with experimental data for many laminates, it is dangerous to assume that this implies that the predictions are accurate in general. For example, a very simple failure model was used for the strength predictions which is known to result in unconservative estimates in certain cases. It is well known [98] that *in situ* transverse ply strengths are not constants, they are a function of the ply thickness and the layup angles of adjacent plies. Also, edge delaminateion [85], effects of structural details, etc., which can all significantly reduce failure loads, are not modeled. The contour plots of the

statistics of all the laminate properties presented in Chapter 5 and Appendix D are intended to illustrate points such as the strong dependence of COVs on laminate design. The results presented in this thesis, in general, are not intended for, and should not be used for, design purposes.

6.2 DISCUSSION OF OPTIMIZATION RESULTS

Three optimization problems were considered in Chapter 5: optimization for matching the mean properties of a composite laminate to those of another material (Section 5.4.1), optimization for minimal thermal and hygral deformation and maximal stiffness (Section 5.4.2), and optimal design of a satellite structure for minimal thermal deformation (Section 5.5). The first two problems are discussed in Sections 6.2.1 and 6.2.2 respectively. The third problem is not discussed in this chapter since the discussion given in Section 5.5 is sufficient. In Section 6.2.3 the effect of the functional form of the cost function on the optimization results is discussed.

6.2.1 Discussion Of Optimization Results For Matching Properties Of A Composite Laminate To Another Material

The problem was to match the mean stiffnesses and Poisson's ratio of a composite laminate with that of a typical aircraft aluminum. The composite material system considered was T300/934, with the ply properties listed in Table 5.3. The aluminum properties are listed in Table 5.2.

Tables 5.4 and 5.5 summarize the optimization results. The results indicate that a laminate cannot be designed, using the T300/934 material system, to have the same mean properties as aluminum. However, the five optimal designs, shown in Table 5.4, do approach some of the mean properties of the aluminum very closely, as shown in Tables 5.5. All of the laminates have the same mean Poisson's ratio as the aluminum. The four ply laminate has nearly the same mean shear stiffness as the aluminum, although the mean longitudinal and transverse stiffnesses are significantly different. The eight ply laminate has nearly the same mean longitudinal stiffness as the aluminum, although the mean transverse and shear stiffnesses are significantly different. However, the mean properties of the eight ply laminate more closely resemble those of aluminum than the four ply laminate. The mean properties of the 12, 16, and 20 ply laminates are similar to the eight ply laminate. These results show that increasing the number of plies, which increases the size (dimension) of the design space, does not always result in the existence of a "better" laminate design for a problem.

It is interesting to note that all the optimal laminates have two mean properties that are very similar to those of aluminum, while the other mean properties differ significantly. This *locking* behavior is a result of the functional form of the cost function. When the cost function cannot meet all of the property goals it favors designs that meet a few of the property goals

very closely at the price of other properties differing significantly from the goals. This behavior is discussed in more detail in Section 6.2.3.

6.2.2 Discussion Of Optimization Results For Minimal Thermal And Hygral Deformation And Maximal Stiffness

The problem was to minimize the longitudinal CTEs, CMEs, CTBs, and CMBs of a laminate, and their standard deviations, while also maximizing, and minimizing the standard deviation of, the stiffness properties. Several cases are considered where the weights on the thermal, hygral, and stiffness portions of the cost function are different (e.g. cases were considered where thermal deformation is more important to minimize than hygral, etc.). The material system considered was T300/934, with the ply properties listed in Table 5.3.

Table 5.8 lists the optimal layups for each of the optimization runs, referred to as O1-O6. The layups corresponding to the O2-O5 optimization runs are very similar. This was expected for the O2-O4 runs, which were for minimal thermal and/or hygral deformation, for two reasons: (i) For the temperature and moisture content changes considered the second term in parenthesis in Eqs. 5.7a-d are close to unity; hence, the thermal and hygral parts of the cost function are nearly equally weighted. (ii) The ply longitudinal and transverse CTEs and CMEs for T300/934 are such that the layups corresponding to zero mean laminate CTEs and CMEs are very similar.

The O5 run was for minimal thermal and hygral deformation and maximal stiffness. The layup from the O5 run is similar to the layups from the O2-O4 runs since it happens that the layup for minimal thermal and hygral deformation also corresponds to a laminate with a high longitudinal stiffness. The cost function for the O6 run was similar to that for the O5 run, with the exception that the stiffness part of the cost function was weighted much more heavily than the thermal and hygral parts. This is why the layup from O6 corresponds to an overall stiffer laminate than the layup from O5 (as shown in Table 5.10). The O1 run was for maximization of stiffness only. Hence, the layup from O1 corresponds to the overall stiffest laminate.

In practice, laminate manufacturing procedures are often limited to integer layup angles. None of the optimal layups presented in Chapter 5 have integer layup angles. However, optimization results presented in Section 5.4.2.4 take into account the variability of layup angles, which is on the order of two degrees. Hence, rounding the optimal layup angles to integer values, as would be done in practice, will not significantly change the performance of the laminate.

6.2.3 The Effect Of The Functional Form Of The Cost Function

In this section the effect of the functional form of the cost function on the optimization results is discussed. In particular, the locking behavior pointed out in Section 6.2.1 is explained. For cases where the locking

behavior is not desired, a slightly different form of the cost function, that discourages the locking behavior, is presented.

The original form of the is:

$$f_c(\theta) = \sum_i \left[A_i \left| P_i - P_{gi} \right| + B_i \hat{\sigma}_{P_i} \right] \tag{6.1}$$

For this cost function, the penalty for laminate properties, P_i, deviating from their respective goals, P_{gi}, increases linearly with the magnitude of deviation. This is a relatively weak penalization and is why this cost function exhibits the locking behavior. This cost function favors locking on to a few property goals at the price of other properties differing significantly from the goals. A cost function which penalizes the deviation of properties from their respective property goals more would discourage this locking behavior. An example of such a cost function is:

$$f_c(\theta) = \left\{ \sum_i \left[A_i \left| P_i - P_{gi} \right| + B_i \hat{\sigma}_{P_i} \right]^\rho \right\}^{\frac{1}{\rho}} \tag{6.2}$$

The original cost function (Eq. 6.1) may be recovered by setting ρ to one. As ρ increases so does the penalty for the deviation of properties from their respective goals. For large values of ρ (e.g. 4 or 6) the deviation of the laminate properties from their respective goals becomes relatively uniform (if equally weighted). No one property deviates much, with respect to the others, since the penalty grows as the ρ^{th} power of the amount of deviation from the property goal. The payoff of locking on to a few properties is not worth the cost of other properties deviating significantly from their goals.

In the computer code that accompanies this thesis ρ is a user input. The default value of ρ in the code is one. No quantitative investigation of the effects of different ρ values has yet been carried out.

6.3 DISCUSSION

6.3.1 Important Lessons Learned

The problem addressed in this thesis had three parts: (i) to develop a methodology for determining the mean and standard deviation of laminate properties, (ii) to develop an optimization method for tailoring mean laminate properties to specified goals, while also minimizing the standard deviation of the laminate properties, and (iii) define a sensitivity metric. Many lessons were learned while addressing this problem (as explained throughout this thesis), most related entirely to either the probabilistic or optimization methods. However, the two most important lessons learned from this work are closely related to all three aspects of the problem and to each other:

I. The magnitude of variability of laminate properties is strongly dependent on laminate design.

II. Multiple optimal laminate designs exist for minimal variability about specified laminate property goals.

The first lesson has an important implication: not only is it difficult, but restrictive to define a safety factor (e.g. for strength, thermal deformation, etc.) that blankets the infinitely possible laminate designs. It is

difficult to define such a safety factor since the worst case design must be identified. It is restrictive to use such a safety factor since a worst case design must be assumed when the actual design may be far superior.

The second lesson has two important implications. The first implication is related to the multimodal nature of the cost function(s), the second to the choice of the functional form of the cost function. The first implication is this: since multiple optima exist, a global optimization method must be used to determine the globally optimal laminate design. This is an important implication since it is very difficult to find the global optima among many (relative to the case if only one optima existed).

The second implication is that optimization (in the present context) cannot be used to determine a single "best" laminate design for a particular application. Rather, the user has control over the functional form of the cost function by changing the laminate property goals, ρ in Eq. 6.2, or choosing different weight factors, all of which affects the "optimal" laminate design. In practice, there is no one absolutely optimal laminate design; the user has the freedom to choose one among many based on practical considerations which are not incorporated in the cost function.

6.3.2 Some Modeling and Lengthscale Issues

The models used in the present work, particularly the failure models, are admittedly simplistic. Regardless, in many cases predicted results are in

very good agreement with experiment. This raises an important question: are more complex models necessary?

The fact that predicted and experimental results are in good agreement does imply that some of the relevant physics are captured by the simple models. However, it is foolish to assume that all of the relevant physics are captured. For example, other failure modes can occur that are not modeled here, such as edge delamination [85]. It is also well known that the transverse and/or shear stress at which microcracking initiates in a ply (if it occurs) is a function of both ply thickness and the layup angles of adjacent plies [93, 98-100]. The present model does not capture this dependence.

Lengthscale issues regarding the models for the laminate properties are also important considerations. In this work, there is an implicit assumption that material properties and geometric parameters are uniform throughout each ply, and only vary from ply to ply. However, modeling variations at this scale may not be sufficient to capture some relevant phenomena. For example, material properties and geometric parameters vary as a function of position within each ply. Here, it is assumed that these complex spatial variations can be modeled, in an average sense, as a uniform variability of ply properties and geometric parameters within each ply.

The favorable comparisons of experimental and predicted results is encouraging and indicates that the simple models used in the present work do a reasonable job in some cases. However, modeling is a function of

intended purpose. The intended purpose of the models used in the present work was to aid in the development of a methodology, not necessarily a design tool. The designer must, in the specific case they are dealing with, understand the limits and suitability of the models that they use in this methodology.

6.3.3 An Alternate And Useful Interpretation Of The Probabilistic/Optimization Methodology

Previously the predicted standard deviations were used to infer the variability of the laminate properties that one would see in practice. There is an alternate view of the standard deviation that can be useful. The standard deviation can also be viewed as a metric of knowability, which is different from actual variability.

In this interpretation the standard deviations of the constituent properties are a measure of their knowability. This is what makes this interpretation useful; the standard deviations of the constituent properties can be chosen such that they encompass some range of values which may be based on experience, accuracy of models, known upper and lower bounds, etc. This results in the predicted standard deviations of the laminate properties being a metric of their knowability (based on experience, modeling accuracy, etc.) rather than a metric of variability.

The sensitivity metrics also have an alternate interpretation. The sensitivity metrics indicate what constituent properties need to be better

known (or understood) to most increase the knowability of a laminate property.

Previously optimization was done to tailor mean laminate properties to specified goals, while also minimizing the variability of the laminate properties. For the alternate interpretation, optimization is done to tailor laminate properties to specified goals, while also minimizing the impact of the ignorance of the constituent properties, the lack of accurate models, etc.

CHAPTER 7

CONCLUSIONS AND RECOMMENDATIONS FOR FUTURE WORK

7.1 CONCLUSIONS

A method for predicting the values, variations and sensitivities of laminate properties, given ply properties and geometric parameters, has been developed. The method was coupled with a new optimization technique to yield a very useful analysis and design tool. The tool is capable of predicting mean laminate properties and their standard deviations; predicting the sensitivities of laminate properties to the various ply properties and geometric parameters; and finding laminates that are optimal in the sense of both meeting property goals and minimizing variations of the properties about those goals.

The accuracy and utility of the method has been verified in a number of ways. Experimental results obtained from the literature are in good agreement with the predicted trends in both the means and the standard deviations of the laminate properties. Four different methods for calculating property variations and sensitivities were developed. The methods trade accuracy and generality for computational speed, and provide the user with a menu to choose from for different applications. These methods were checked against one

another, with good results. A new optimization technique, suitable for the complex problems encountered in this work, was developed. It was checked on a set of standard benchmarking problems, and found to converge very fast.

The method was used to perform a variety of parametric and design studies. The studies illustrated the ways the method can be used to solve practical problems. They also reveled some interesting things about the behavior of composite laminates, and difficulties encountered in their optimization. In fact, the method appears to be a promising way of achieving a deeper understanding of this very rich field. Here, some of the obvious lessons that fell out of the studies done are reviewed; they represent only a fraction of the possible insights that can be gained from the method, or indeed even from the studies presented in this work.

The variations in laminate properties are a very strong function of the laminate design itself, most notably the ply angles (the layup). Coefficients of variations of properties of interest varied by large factors from one laminate to the next. These results indicate that it is not only difficult, but restrictive to define a safety factor (for strength, thermal deformation, etc.) that blankets the infinite possible laminate designs.

Laminate properties were found to be sensitive to (and hence their variablities dependent on) all the ply properties and geometric parameters. Which ply properties and geometric parameters were critical depended on both the laminate design and the laminate property of interest. Even for a given

laminate design and selected laminate property, it was observed that no one ply property or geometric parameter generally dominated.

A "size effect" which causes laminates with greater numbers of plies to have lower mean strengths (due to a greater chance of one "weak" ply) but also less scatter in properties (due to averaging out of ply property variances), was noted. This is consistent with the size effects well known and documented for fiber bundles, etc. This effect falls out of the analysis; it has not (to the author's knowledge), been experimentally verified at this level.

Finally, the design space even for simple problems was found to be very complex. The consideration of minimization of variations among the cost function parameters only exacerbates this known problem. Multiple local minima, often of very similar depths, typically exist. These observations had some clear implications. A global optimization method must be used to determine the globally optimal laminate design. Cost functions should be chosen carefully. Finally, judgment must be used to choose between a number of "optimum" designs for a given problem.

It must be repeated that the methodology developed here uses simple models of composite behavior, and that its usefulness is restricted to cases in which the behavior of the actual material conforms to the models! In the hands of a user with an understanding of the models and their limitations, these tools should prove to be very useful for design and analysis.

7.2 RECOMMENDATIONS FOR FUTURE WORK

Recommendations for short term opportunities to improve the method and its use are presented here.

The simple progressive failure model should be extended to include more advanced failure theories, such as the dependence of ply strengths on ply thickness and layup angles of adjacent plies [100, 101], the effects of progressive microcracking in plies [93], and edge delamination [85].

The laminate property calculations should be extended to handle nonsymmetric laminates; that is, to specify a stiffness matrix as a goal as opposed to effective (engineering) laminate properties which only apply to symmetric laminates. The optimization methods should be extended to allow for the specification of arbitrary upper and lower bounds (constraints) on the mean plus a specified multiple of the standard deviation of a laminate property; this would require a check to see if a laminate design exists that meets the constraints. The parameters for the SSM for a particular (class of) cost function(s) should be recursively optimized (using the SSM) .

Finally, among the many possible additional parametric studies, investigations of the effects of different cost functions; in particular, the effects of different ρ values in Eq. 6.2, are called for.

REFERENCES

1. Dunn, C., "Multifunctional Design of a Satellite Structure" (title subject to change), Massachusetts Institute of Technology, S.M. Thesis, 1997.

2. "Pegasus Payload User's Guide (Release COML-3.00)", pp. 4-2,4-3, Orbital Sciences Corp., 1993.

3. Abernathy, E., "Probabilistic Analysis and Design of Dimensionally Stable Composite Structures", Massachusetts Institute of Technology, S.M. Thesis, 1995.

4. Tompkins, S. S., Funk, J. G., Bowles, D. E., Towell, T. W., and Connell, J. W., "Composite Materials for Precision Space Reflector Panels", *SPIE International Symposium and Exhibition on Optical Engineering and Photonics*, Orlando, Florida, 1992.

5. Tompkins, S. S., Bowles, D. E., Slemp, W. S., and Teichman, L. A., "Response of Composite Materials to the Space Station Orbit Environment", *AIAA/NASA Space Station Symposium*, Williamsburg VA, 1988.

6. Thompson, D. F. and Babel, H. W., "Material Applications on the Space Station: Key Issues and the Approach to their Solution", *SAMPE Quarterly*, Vol. 21, No. 1, 1989, pp. 27-33.

7. Brent, D. N. and Lou, M. C., "Thermal and Mechanical Stability of the WF/PC II Optical Alignment", *AIAA-94-1738-CP*, 1993.

8. Telcamp, A. R. and Derby, E. A., "Design Considerations for Composite Materials Used in the Mars Observer Camera", *SPIE*, Orlando, Florida, 1990.

9. Krumweide, G. C., "Attacking Dimensional Instability Problems in Graphite/Epoxy Structures", Composite Optics, Inc., March 24, 1992.

10. Madsen, H. O., Krenk, S., and Lind, N. C., *Methods of Structural Saftey*, Prentice-Hall, Inc., Englewood Cliffs, NJ, 1986.

11. Boyce, L., "Probabilistic Structural Analysis Methods for Improving Space Shuttle Engine Design", *Journal of Propulsion*, Vol. 5, 1988, pp. 426-430.

12. Millwater, H., Wu, Y. T., Torng, T., Thacker, B., Riha, R., and Leung, C. P., "Recent Develpments of the NESSUS Probabilistic Structural Analysis Computer Program", *AIAA/ASME/ASCE/AHS/ASC 33rd Structures, Structural Dynamics, and Materials Conference*, Dallas TX, 1992, pp. 614-624.

13. Shiao, M. C. and Chamis, C. C., "Reliability of Composite Structures With Multi-Design Criteria", *AIAA/ASME/ASCE/AHS/ASC 35th Structures, Structural Dynamics, and Materials Conference*, 1994, pp. 606-615.

14. Tani, S., Nakagiri, S., and Higashino, T., "Assessment of the Reliability Indices of CFRP Laminated Plate", *Computational Probabilistic Methods, ASME-AMD-93*, Berkeley CA, 1988, pp. 27-36.

15. Chamis, C. C., "Computer Codes Developed and Under Development at Lewis", *Computational Structure Technology for Airframes and Propulsion Systems, NASA CP-3142*, Hampton VA, 1991, pp. 43-57.

16. Liaw, D. G., Singhal, S. N., Murthy, P. L. N., and Chamis, C. C., "Quantification of Uncertainties in Composites", *AIAA-93-1440-CP*, 1993, pp. 1163-1173.

17. Singhal, S. N., Abumeri, G. H., and Shiao, M. C., "Probabilistic Assessment of Tailored Composite Structures", *AIAA-94-1418-CP*, 1994, pp. 871-876.

18. Greene, W. H., "Effects of Random Member Length Errors on the Accuracy and Internal Loads of Truss Antennas", *Journal of Spacecraft*, Vol. 22, 1984, pp. 554-559.

19. Hedgepeth, J. M., "Influence of Fabrication Tolerances on the Surface Accuracy of Large Antenna Structures", *AIAA Journal*, Vol. 20, 1981, pp. 680-686.

20. Bowles, D. E. and Tompkins, S. S., "Prediction of Coefficients of Thermal Expansion for Unidirectional Composites", *Journal of Composite Materials*, Vol. 23, 1989, pp. 370-387.

21. Shapery, R. A., "Thermal Expansion Coefficients of Composite Materials Based on Energy Principles", *Journal of Composite Materials*, Vol. 2, No. 3, 1968, pp. 380-404.

22. Ishiwaka, T., Fukunaga, H., and Ono, K., "Thermal Expansion Coefficient of Unidirectional Composites", *Journal of Composite Materials*, Vol. 12, 1978, pp. 153-168.

23. Ishiwaka, T., Fukunaga, H., and Ono, K., "Graphite-Epoxy Laminates with Almost Null Coefficient of Thermal Expansion Under a Wide Temperature Range", *Journal of Materials Science*, Vol. 24, 1989, pp. 2011-2017.

24. Strife, J. R. and Prewo, K. M., "The Thermal Expansion Behavior of Unidirectional and Bidirectional Kevlar/Epoxy Composites", *Journal of Composite Materials*, Vol. 13, 1979, pp. 264-277.

25. Chamis, C. C., "Simplified Composite Micromechanics Equations for Hygral, Thermal, and Mechanical Properties", *SAMPE Quarterly*, Vol. 15, 1984, pp. 14-23.

26. Rosen, B. W. and Hashin, Z., "Effective Thermal Expansion Coefficients and Specific Heats of Composite Materials", *International Journal of Engineering Science*, Vol. 8, 1970, pp. 157-173.

27. Hashin, Z., "Analysis of Properties of Fiber Composites with Anisotropic Constituents", *Journal of Applied Mechanics*, Vol. 46, 1979, pp. 543-550.

28. Rogers, K. F., Phillips, L. N., Kingston-Lee, D. M., Yates, B., Overy, M. J., Sargent, J. P., and McCalla, B. A., "The Thermal Expansion of Carbon-Fibre Reinforced Plastics Part 1, The Influence of Fibre Type and Orientation", *Journal of Materials Science*, Vol. 12, 1977, pp. 718-734.

29. Rogers, K. F., Phillips, L. N., Kingston-Lee, D. M., Yates, B., Overy, M. J., Sargent, J. P., and McCalla, B. A., "The Thermal Expansion of Carbon-Fibre Reinforced Plastics Part 2, The Influence of Fibre Volume Fraction", *Journal of Materials Science*, Vol. 13, 1978, pp. 433-440.

30. Jones, R., Lukez, R., Peterson, B., Batty, J. C., and Redd, F. J., "Extended Thermal Cycle Testing of Graphite/Epoxy Composite Struts for Space Station Applications," *SAMPE Quarterly*, Vol. 21, No. 1, October, 1989, pp. 34-38.

31. Romeo, G. and Frulla, G., "Analytical and Experimental Results of the Coefficient of Thermal Expansion of High-Modulus Graphite-Epoxy Materials", *Journal of Composite Materials*, Vol. 29, No. 6, 1995, pp. 751-765.

32. Wolf, E. G., "Moisture and Viscoelastic Effects on Dimensional Stability", *Dimensional Stability, in Proceedings of SPIE,* 1990, pp. 70-79.

33. Romeo, G., Miraldi, E., Ruscica, G., Bertoglio, F., Frulla, G., and G., R., "A New Test Facility for Measuring the Coefficient of Moisture Expansion of Advanced Composite Materials", *Journal of Composites Technology & Research*, Vol. 14, No. 4, 1992, pp. 225-230.

34. Wanthal, S. P. and Petter, E. H., "Probabilistic Assessment of Composite Constituent, Lamina and Laminate Properties", *AIAA-93-1445-CP,* 1993, pp. 1218-1227.

35. Kessler, J. A. and Adams, D. F., "Composite Specimen Design Analysis - Volume II: Experimental Efforts", Report MTL TR 91-5, U.S. Army Materials Technology Laboratory, January, 1991.

36. Tompkins, S. S. and Funk, J. G., "Sensitivity of the Coefficient of Thermal Expansion of Selected Graphite Reinforced Composite Laminates to Lamina Thermoelastic Properties", *SAMPE Quarterly*, No. April, 1992, pp. 55-61.

37. Chamis, C. C., "Simplified Composite Micromechanics Equations For Strength, Fracture Toughness and Environmental Effects", *SAMPE Quarterly*, 1984, pp. 41-55.

38. Yamada, S. E. and Sun, C. T., "Analysis of Laminate Strength and Its Distribution", *Journal of Composite Materials*, Vol. 12, 1978, pp. 275-284.

39. McManus, H. L., "Probabilistic Methods for the Calculation of Laminate Properties", *Journal of Reinforced Plastics and Composites*, 1993, Vol. 12, pp. 712-722.

40. Sable, W. W., "A Probabilistic Model of the Thermal Dimensional Stability of Composite Structural Components", *SPIE International Symposium and Exhibition on Optical Engineering and Photonics*, Orlando, Florida, 1992.

41. Abernathy, E. and McManus, H. L., "Effects of Material and Manufacturing Variations on Dimensionally Stable Composite Structure", *Journal of Reinforced Plastics and Composites*, (in press).

42. Fang, C. and Springer, G. S., "Design of Composite Laminates by a Monte Carlo Method", *Journal of Composite Materials*, Vol. 27, No. 7, 1993, pp. 721-753.

43. Mitsunori, M. and Sugiyama, Y., "Optimum Design of Laminated Composite Plates Using Lamination Parameters", *AIAA Journal*, Vol. 31, No. 5, 1993, pp. 921-922.

44. Fukunaga, H. and Chou, T. W., "Simplified Design Techniques for Laminated Cylindrical Pressure Vessels under Stiffness and Strength Constraints", *Journal of Composite Materials*, Vol. 22, 1988, pp. 1156-1169.

45. Landriani, G. S. and Rovati, M., "An Optimal Design for Two-Dimensional Structures Made of Composite Materials", *ASME Journal of Engineering Materials and Technology*, Vol. 113, 1991, pp. 341-354.

46. Obraztsov, I. F. and Vasilev, V. V., "Optimum Design and Strength of Layered Thin Composites", *Proceedings of the First USA-USSR Symposium on Fracture of Composite Materials*, Rockville, Maryland, 1977, pp. 225-265.

47. Qian, B., Reiss, R., and Aung, W., "The Maximum Stiffness Design of Rectangular Symmetric Angle-Ply Laminates", ed. de Wilde, W. P., and Blain, R., Springer Verlag, New York, 1990, pp. 451-464.

48. McKeown, J. J., "A Quasi-Linear Programming Algorithm for Optimising Fibre-Reinforced Structures of Fixed Stiffness", *Computer Methods in Applied Mechanics and Engineering*, Vol. 6, 1977, pp. 123-154.

49. Pedersen, P., "Concurrent Engineering Design of and With Advanced Composite Materials", S56, Danish Center for Applied Mathematics and Mechanics, The Technical University of Denmark, 1991.

50. Pederson, P., "On Thickness and Orientation Design with Orthotropic Materials", 412, Danish Center for Applied Mathematics and Mechanics, The Technical University of Denmark, 1990.

51. Kam, T. Y. and Snyman, J. A., "Optimal Design of Laminated Composite Plates Using a Global Optimization Technique", *Composite Structures*, Vol. 19, 1991, pp. 351-370.

52. Tauchert, T. R. and Adibhatla, S., "Design of Laminated Plates for Maximum Bending Strength", *Engineering Optimization*, Vol. 8, 1985, pp. 253-263.

53. Li, B. and Sun, B., "Multilevel Optimization Procedure of Composite Structures", *Composite Structures, Proceedings of the 4th International Conference on Composite Structures*, 1987, pp. 351-367.

54. Rao, L. P. and Singh, K., "Optimum Design of Laminates with Natural Frequency Constraints", *Journal of Sound and Vibration*, Vol. 67, 1979, pp. 101-112.

55. Murotsu, Y., Miki, M., and Shao, S., "Optimal Configuration for Fiber Reinforced Composites Under Uncertainties of Material Properties and Loadings", *Probabilistic Mechanics and Structural and Geotechnical Reliability, Proceedings of the Specialty Conference*, 1992, pp. 547-550.

56. Holland, J., *Adaption in Natural and Artificial Systems*, University of Michigan Press, Ann Arbor, MI, 1975.

57. Goldberg, D. E., *Genetic Algorithms is Search, Optimization and Machine Learning*, Addison-Wesley, Reading, MA, 1989.

58. Bethke, A. D., "Genetic Algorithms as Function Optimizers", University of Michigan, Ann Arbor, MI, Ph.D. Thesis, 1981.

59. De Jong, K. A., "An Analysis of the Behavior of a Class of Genetic Adaptive System", University of Michigan, Ann Arbor, MI, Ph.D. Thesis, 1981.

60. Gurdal, Z., Haftka, R. T., and Hajela, P., *Design and Optimization of Laminated Composite Materials*, (Manuscript in Preperation), 1996.

61. Callahan, J. K. and Weeks, G. E., "Optimum Design of Composite Laminates Using Genetic Algorithms", *Composites Engineering*, Vol. 2, No. 3, 1992, pp. 149-160.

62. Kogiso, N., Watson, L. T., Gurdal, Z., Haftka, R. T., and Nagendra, S., "Design of Composite Laminates by a Genetic Algorithm with Memory", *Mechanics of Composite Materials and Structures*, Vol. 1, No. 1, 1994, pp. 95-117.

63. Kodiyalam, S. and Nagendra, S., "Composite Sandwich Structure Optimization with Application to Satellite Components", *AIAA Journal*, Vol. 34, No. 3, 1996, pp. 614-621.

64. Harrison, P. N., Le Riche, R., and Haftka, R. T., "Design of Stiffened Composite Panels by Genetic Algorithm and Response Surface Approximations", *AIAA-95-1163-CP*, 1995, pp. 58-68.

65. Le Riche, R., "Optimization of Composite Structures by Genetic Algorithms", Virgina Polytechnic Institute and State University, Ph.D. thesis Thesis, 1994.

66. Bushnell, D., "Truss-Core Sandwich Design Via PANDA2", *Computers and Structures*, Vol. 44, No. 2, 1990, pp. 1091-1119.

67. Ingber, I. and Rosen, B., "Genetic Algorithms and Very Fast Simulated Reannealing: A Comparison", *Mathl. Comput. Modelling*, Vol. 16, No. 11, 1992, pp. 87-100.

68. Southard, B. M. and McManus, H. L., "Paths to Failure and Variability of Failure Loads of Composite Laminates", *AIAA/ASME/ASCE/AHS/ASC 37th Structures, Structural Dynamics and Materials Conference*, Salt Lake City, UT, 1996.

69. Spendley, W., Hext, G. R., and Himsworth, F. R., "Sequential Application of Simplex Designs in Optimization and Evolutionary Operation", *Technometrics*, Vol. 4, 1962, pp. 441-461.

70. Nelder, J. A. and Mead, R., "A Simplex Method for Function Optimization", *Comput. J.*, Vol. 7, 1965, pp. 308-313.

71. Metropolis, N., Rosenbluth, A. W., Rosenbluth, M. N., Teller, A. H., and Teller, E., "Equation of State Calculations by Fast Computing Machines", *J. Chem. Phys.*, Vol. 21, No. 6, 1953, pp. 1087-1092.

72. Aarts, E. H. L. and Korst, J. H. M., *Simulated Annealing and Boltzmann Machines*, Chichester: Wiley, 1988.

73. Romeijn, H. E. and Smith, R. L., "Simulated Annealing and Adaptive Search in Global Optimization", *Probability in the Engineering and Informational Sciences*, Vol. 8, 1994, pp. 571-590.

74. Kirkpatrick, S., Gelatt, C. D., and Vecchi, M. P., "Optimization by Simulated Annealing", *Science*, Vol. 220, No. 4598, 1983, pp. 671-680.

75. Ingber, L., "Very Fast Simulated Re-Annealing", *Mathl Comput. Modelling*, Vol. 12, No. 8, 1989, pp. 967-973.

76. Ingber, L., "Simulated Annealing: Practice versus Theory", *Mathl. Comput. Modelling*, Vol. 18, No. 11, 1993, pp. 29-57.

77. Ingber, L. and Sworder, D. D., "Statistical Mechanics of Combat with Human Factors", *Mathl. Comput. Modelling*, Vol. 15, No. 11, 1991, pp. 99-127.

78. Ingber, L., Fujio, H., and Wehner, M. F., "Mathematical comparison of combat computer models to exercise data", *Mathl. Comput. Modelling*, Vol. 15, No. 1, 1991, pp. 65-90.

79. Ingber, L., "Statistical Mechanical Aids to Calculating Term Structure Models", *Phys. Rev. A*, Vol. 42, No. 12, 1990, pp. 7057-7064.

80. Ingber, L., Wehner, M. F., Jabbour, G. M., and Barnhill, T. M., "Application of Statistical Mechanics Methodology to Term-Structure Bond-Pricing Models", *Mathl. Comput. Modelling*, Vol. 15, No. 11, 1991, pp. 77-98.

81. Ingber, L., "Statistical Mechanics of Neocortical Interactions: A Scaling Paradigm Applied to Electroencephalography", *Phys. Rev. A*, Vol. 44, No. 6, 1991, pp. 4017-4060.

82. Ingber, L., "Generic Mesoscopic Neural Networks Based on Statistical Mechanics of Neocortical Interactions", *Phys. Rev. A*, Vol. 45, No. 4, 1992, pp. 2183-2186.

83. Wofsey, M., *Technology: Shortcut Tests Validity of Complicated Formulas,* in *The Wall Street Journal, CCXXII.* September 24, 1993, New York. pp. B1.

84. Jones, R. M., *Mechanics of Composite Materials,* Hemisphere Publishing, 1975.

85. Brewer, J. C., and Lagace, P. A., "Quadratic Stress Criterion for Initiation of Delamination", *Journal of Composite Materials,* Vol. 22, 1988, pp. 1141-1155.

86. Sveshnikov, A. A., *Problems in Probability Theory, Mathematical Statistics and Theory of Random Functions,* Dover Publications, New York, 1978, pp. 136-137.

87. Devroye, L., *Non-Uniform Random Variate Generation,* Springer-Verlag, New York, 1986.

88. Press, W. H., Teukolsky, S. A., Vetterling, W. T., and Flannery, B. P., *Numerical Recipes in C: the Art of Scientific Computing,* second edition, Cambridge University Press, 1992.

89. Knuth, D. E., *Seminumerical Algorithms,* second edition, Vol. 2 of *The Art of Computer Programming*, Addison-Wesley, Reading, MA, 1981, chapter 3.

90. Freund, J. E., *Mathematical Statistics*, Prentic-Hall Inc., Englewood Cliffs, NJ, 1962.

91. Kessler, J. A., and Adams, D. F., "Composite Specimen Design Analysis - Volume II: Experimental Efforts," U.S. Army Materials Technology Laboratory, Report MTS TR 91-5, January, 1991.

92. Spearing, M. S., Lagace, P. A., and McManus, H. L., "On The Role of Lengthscale In The Prediction of Failure of Composite Structures: Assessment And Needs," 10th International Conference on Composite Materials, Whistler, Canada, August, 1995.

93. Maddocks, J. R., "Microcracking in Composite Laminates Under Thermal and Mechanical Loading," S.M. Thesis, TELAC Report 95-2, MIT, 1995.

94. Szu, H., and Hartley, R., "Fast Simulated Annealing," *Phys. Lett. A*, Vol. 122, 1987, pp. 157-162.

95. Schraudolph, N. N. and Belew, R. K., "Dynamic Parameter Encoding For Genetic Algorithms," Technical Report LAUR 90-2795, Los Alamos National Laboratory, Los Alamos, NM, 1990.

96. Corana, A., Marchesi, M., Martini, C., and Ridella, S., "Minimizing Multimodal Functions of Continuous Variables With The Simulated Annealing Algorithm," *ACM Trans. on Mathematical Software*, Vol. 13, No. 3, 1987, pp. 272-280.

97. Schraudolph, N. N. and Grefenstette, J. J., "A Users Guide to GAUCSD 1.2," San Diego Technical Report, Computer Science and Engineering Department, University of California, La Jolla, CA, 1991.

98. Flaggs, D. L. and Kural, M. H., "Experimental Determination of the In Situ Transverse Strength in Graphite/Epoxy Laminates," *Journal of Composite Materials*, Vol. 16, March, 1982, pp. 103-116.

99. Chang, F. K. and Lessard, L. B., "Damage Tolerance of Laminated Composites Containing an Open Hole and Subject to Compressive Loadings: Part I - Analysis," *Journal of Composite Materials*, Vol. 25, January, 1991, pp. 2-43.

100. Wang, J. and Karihaloo, B. L., "Fracture Mechanics and Optimization - A Useful Tool For Fibre-Reinforced Composite Design," *Composite Structures*, Vol. 32, 1995, pp. 453-466.

101. Schraudolph, N. N. and Belew, R. K., "Dynamic Parameter Encoding for Genetic Algorithms," Technical Report LAUR 90-2795, Los Alamos National Laboratory, Los Alamos, NM, 1990.

APPENDIX A

WHY DOES $\lambda = 2$ WORK WELL?

Originally trial and error was used to determine λ in approach A2 (Section 4.3.2) by comparing with the Monte Carlo approach A3 (Section 4.3.4). The purpose of this appendix is to give insight as to why $\lambda = 2$ works well.

To accomplish this a simple one parameter family of nonlinear functions is constructed that exhibits the types of nonlinearities typical of CLPT. Basic probability theory is used to determine the "exact" standard deviation which is compared with the predicted standard deviation using approach A2 with various values of λ. An optimal λ is determined by minimizing and error norm between the "exact" and predicted values for the class of nonlinear functions considered. This optimal λ is approximately 1.86, which is very close to the value of 2 determined by trial and error.

Consider the one parameter family of nonlinear functions:

$$f(x)=\begin{cases}\dfrac{1}{\pi}\tan^{-1}\left(\dfrac{\pi x}{10\alpha}\right)+\dfrac{1}{2} & x\le x^*\\ \dfrac{(x-x^*)}{10}+\delta & x\ge x^*\end{cases}$$

$$\text{where: } x^*=\sqrt{\frac{\alpha}{\pi^2}(1-\alpha)} \qquad \text{(A.1)}$$

$$\delta=\frac{1}{\pi}\tan^{-1}\left(\frac{\pi x^*}{10\alpha}\right)+\frac{1}{2}$$

$$0<\alpha<1$$

As $\alpha\to 1$ $f(x)$ becomes a straight line of slope 0.1. As $\alpha\to 0$ and $x<0$, $f(x)$ goes to zero; when $\alpha\to 0$ and $x>0$, $f(x)$ becomes a straight line of slope 0.1 with $x^*=0$ and $\delta=1$; there is a discontinuity at $x=0$. Figure A.1 is a plot of $f(x)$ with various values of α. The level of nonlinearity increases as α is decreased.

Here, x is considered to be a normally distributed random variable with mean μ and variance σ^2, and y a dependent random variable:

$$y=f(x) \qquad \text{(A.2)}$$

The probability density function of y, $P(y)$, can be found from Eq. A.1 using the fundamental transformation law of probabilities (e.g. [90]):

$$P(y)=\begin{cases}\dfrac{\alpha\pi}{10\sigma}\sqrt{\dfrac{\pi}{2}}\sec^2\left(\pi\left(y-\dfrac{1}{2}\right)\right)e^{-\frac{1}{2}\left(\frac{\frac{\alpha\pi}{10}\cot(\pi y)+\mu}{\sigma}\right)^2} & y\le\delta\\ \dfrac{10}{\sigma\sqrt{2\pi}}e^{-\frac{1}{2}\left(\frac{10y-(\mu+10\delta)}{\sigma}\right)^2} & y\ge\delta\end{cases} \qquad \text{(A.3)}$$

As $\alpha\to 1$ $P(y)$ becomes the normal distribution with mean μ and standard deviation 0.1σ. Figure A.2 is a plot of $P(y)$ with various values of α and

μ=σ=1. $P(y)$ is far from the normal distribution for most α; for lower values of α, $P(y)$ has two peaks due to the jump in $f(x)$ near x=0.

The standard deviation of y is (see, e.g., Freund [90]):

$$\sigma_y = \sqrt{\int_0^\infty y^2 P(y)dy - \left(\int_0^\infty yP(y)dy\right)^2} \tag{A.4}$$

The percent error is defined as:

$$E = \frac{{}^{A2}\sigma_y - \sigma_y}{\sigma_y} \times 100 \tag{A.5}$$

where ${}^{A2}\sigma_y$ is the standard deviation calculated using the approach A2 (which depends only λ) as described in Section 4.3.2. Eq. A.4 is integrated numerically to determine σ_y.

Figure A.3 is a plot of the percent error verse μ with λ=0.001, σ=1 and various values of α. For this small value of λ approach A2 is essentially equivalent to approach A1, which is a linear method. Approach A1 is not applicable near μ=0 since this region is highly nonlinear; the derivatives in the tailor expansion become large, and so does the error, in the vicinity of the cliff (at x=0) shown in Figure A.1. The error is low away from the cliff since in this region $f(x)$ is linear, as can be seen in Figure A.1.

To determine an optimal λ the maximum absolute value of the error is minimized with α = 0.95, 0.3, 0.08, and 0.015, σ=1, and 0<μ<4. The optimal λ is nearly constant (±0.1) for the different α values. The average of the optimal λ values is 1.86.

Figure A.4 is a plot of the error verse μ with λ=1.86, σ=1, and various values of α. The error is far less than the case with λ=0.001. The "bumps" in the error near $\mu=\lambda\sigma$ are a result of the method suddenly "seeing" the cliff (see figure A.1) since the method gathers information over a range of $\pm\lambda\sigma$ about μ. Again, the error is low far away from the cliff.

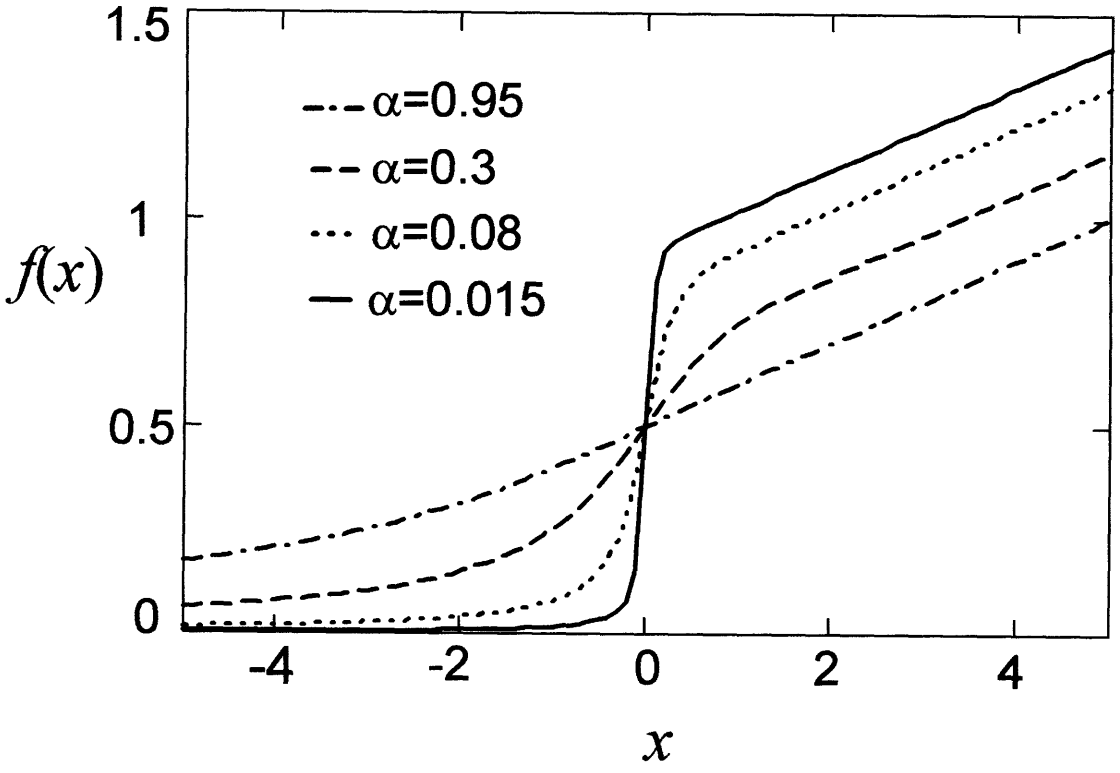

Figure A.1 Plot of constructed nonlinear function for various α

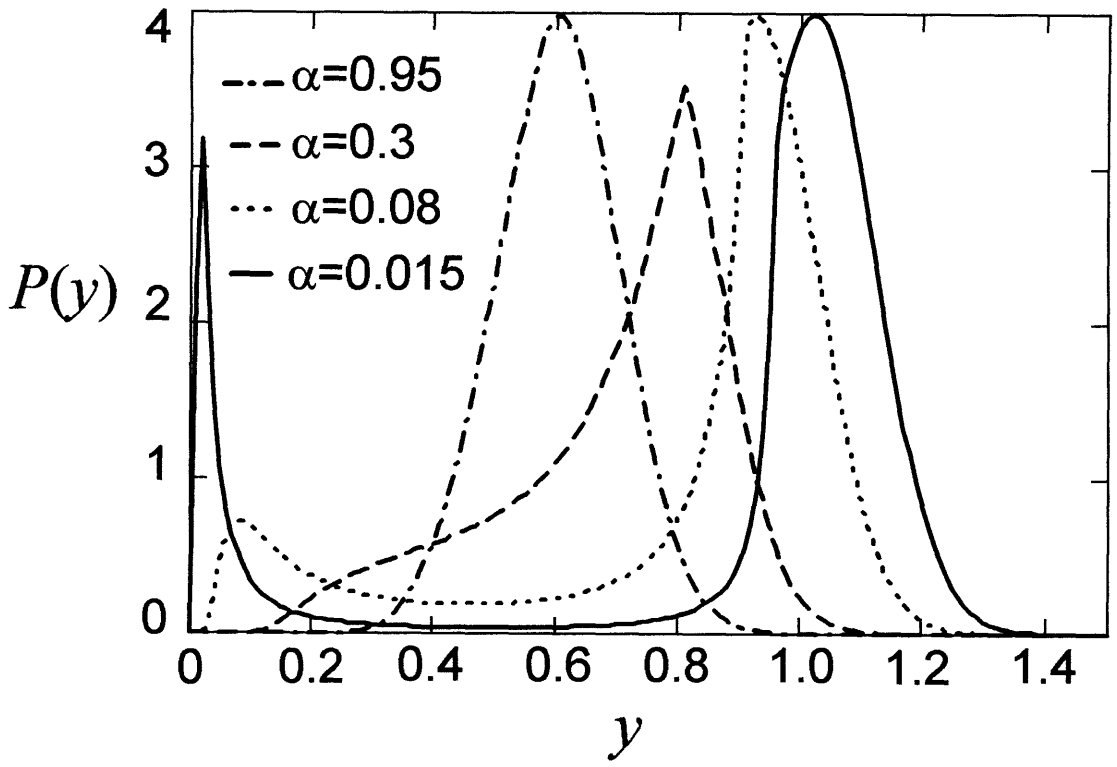

Figure A.2 Probability density functions of y for various α with $\mu=\sigma=1$

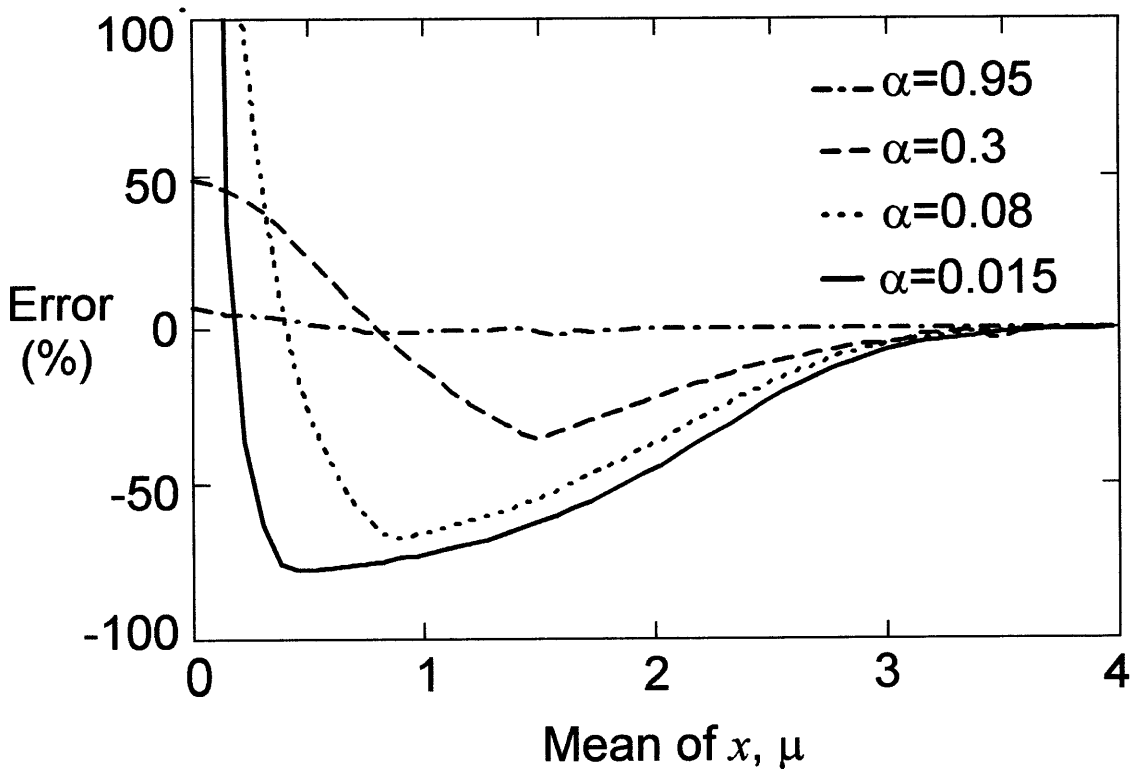

Figure A.3 Plot of percent error verse the mean of x, μ, with λ=0.001 and σ=1

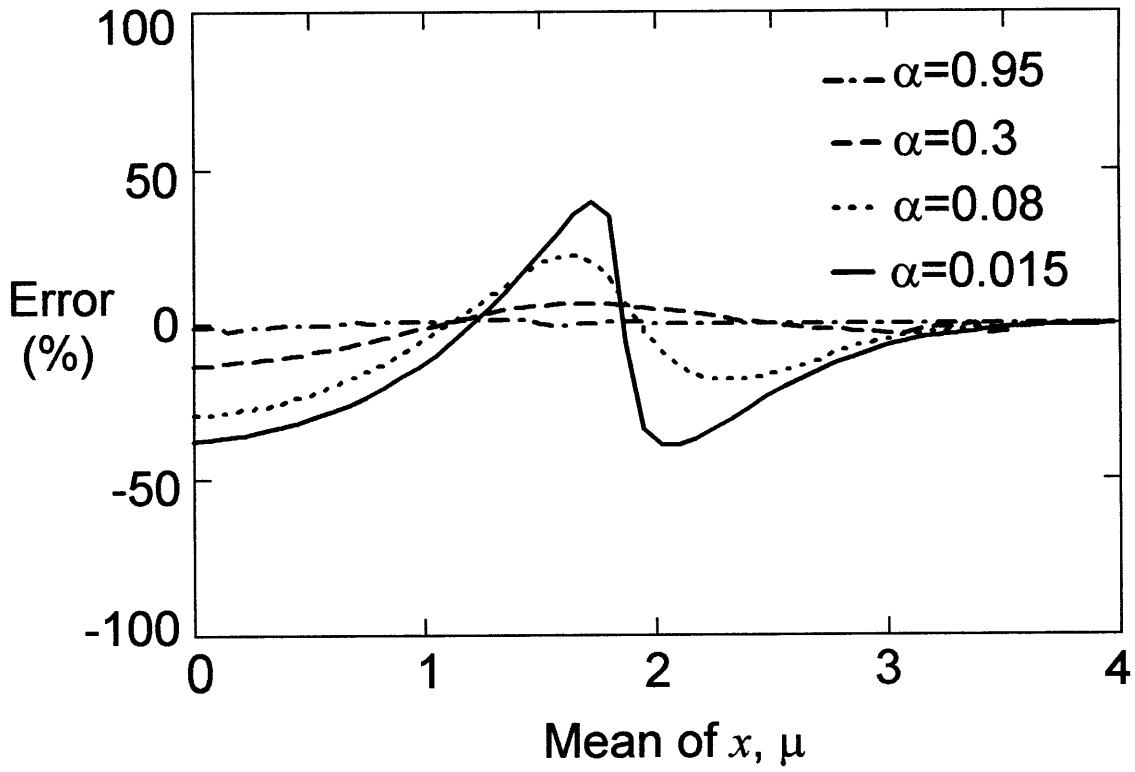

Figure A.4 Plot of percent error verse the mean of x, μ, with λ=1.86 and σ=1

APPENDIX B

THE DEPENDENCE OF γ_{ij} ON THE $\hat{\sigma}_{Xj}$

The purpose of this appendix is to demonstrate the dependence of γ_{ij} on the $\hat{\sigma}_{Xj}$.

In Section 4.3.1 A1 is described and the following equation for the standard deviation of the laminate properties is derived:

$$\hat{\sigma}_{Yi}^2 \approx \sum_{J=1}^{15n} \left(\left. \frac{\partial f_{Yi}}{\partial X_J} \right|_{\bar{X}_1, \bar{X}_2, \ldots, \bar{X}_M} \hat{\sigma}_{Xj} \right)^2 \tag{B.1}$$

In Section 4.3.2 A2 is described and Eq. B.1 is modified as follows:

$$\hat{\sigma}_{Yi}^2 \approx \sum_{J=1}^{15n} {}^{A2}d_{ij}^2 \tag{B.2}$$

Where:

$${}^{A2}d_{ij} = \left| \frac{\left[\begin{array}{r} f_{Yi}\left(\bar{X}_1, \bar{X}_2, \ldots, \bar{X}_J + \lambda\hat{\sigma}_{Xj}, \ldots, \bar{X}_M\right) - \\ f_{Yi}\left(\bar{X}_1, \bar{X}_2, \ldots, \bar{X}_J - \lambda\hat{\sigma}_{Xj}, \ldots, \bar{X}_M\right) \end{array} \right]}{2\lambda} \right| \tag{B.3}$$

In Section 4.3.5 A4 is described and Eqs. B.1 and B.2 are generalized as:

$$\hat{\sigma}_{Y_i}^2 = \sum_{j=1}^{15n} \left(\gamma_{ij} \hat{\sigma}_{Xj}\right)^2 \tag{B.4}$$

Where the γ_{ij} are constants to be determined. For A1, γ_{ij} is

$$\gamma_{ij} = \left.\frac{\partial f_{Y_i}}{\partial X_j}\right|_{\bar{X}_1, \bar{X}_2, \ldots, \bar{X}_M} \tag{B.5}$$

For A2, γ_{ij} is

$$\gamma_{ij} = \frac{{}^{A2}d_{ij}}{\hat{\sigma}_{Xj}} \tag{B.6}$$

In A1 it is assumed that the γ_{ij} are independent of the $\hat{\sigma}_{Xj}$. In A2 it is assumed a γ_{ij} is dependent on only the j^{th} $\hat{\sigma}_{Xj}$ (in a simple way), and is independent of all the other $\hat{\sigma}_{Xj}$. Both of these assumptions are now numerically shown to be poor for the FPF and LPF loads. Specifically, a numerical example is used to show that the γ_{ij} for the FPF and LPF loads depend on the magnitude of not only the j^{th} $\hat{\sigma}_{Xj}$, but others as well. Approach A1 and A2 do not account for this *interaction* behavior.

If the γ_{ij} are not dependent on the $\hat{\sigma}_{Xk}$ ($k \neq j$) then the γ_{ij} should not change if all of the $\hat{\sigma}_{Xk}$ ($k \neq j$) are varied and $\hat{\sigma}_{Xj}$ is kept constant. This is not the case. To demonstrate this the γ_{ij} with i=17,18 and j=$2n$+1,..,$3n$ are considered; the i's correspond to the FPF and LPF loads respectively, the j's correspond to the terms in Eq. B.4 that are multiplied by the standard

deviation of the ply longitudinal modulus. In analogy with the combined sensitivity metrics defined in Section 4.3.3, a combined γ_{ij} is defined as

$$\gamma_{FPF}^{EI} = \sqrt{\sum_{J=2n+1}^{3n} \left(\gamma_{17_J}\right)^2} \tag{B.7}$$

Similarly, for the LPF load

$$\gamma_{LPF}^{EI} = \sqrt{\sum_{J=2n+1}^{3n} \left(\gamma_{18_J}\right)^2} \tag{B.8}$$

The assumptions in A1 and A2 are violated if γ_{FPF}^{EI} or γ_{LPF}^{EI} change when the standard deviations not corresponding to the ply longitudinal modulus are varied. Figure B.1 is a plot of γ_{FPF}^{EI} for a one parameter family of laminates; there are two curves, one corresponds to the standard deviations of the ply material properties and geometric parameters in Table 5.1, and the other to one tenth of the standard deviations in Table 5.1 (except for the ply longitudinal modulus standard deviations which are not reduced). Figure B.1 shows that γ_{FPF}^{EI} is quite different for the two cases, hence the assumptions made in both A1 and A2 are not applicable. The same holds true for γ_{LPF}^{EI} as shown in Figure B.2. It should be noted that if other terms in Eq. B.4 where considered, as opposed to the ply longitudinal modulus terms, similar behavior is observed.

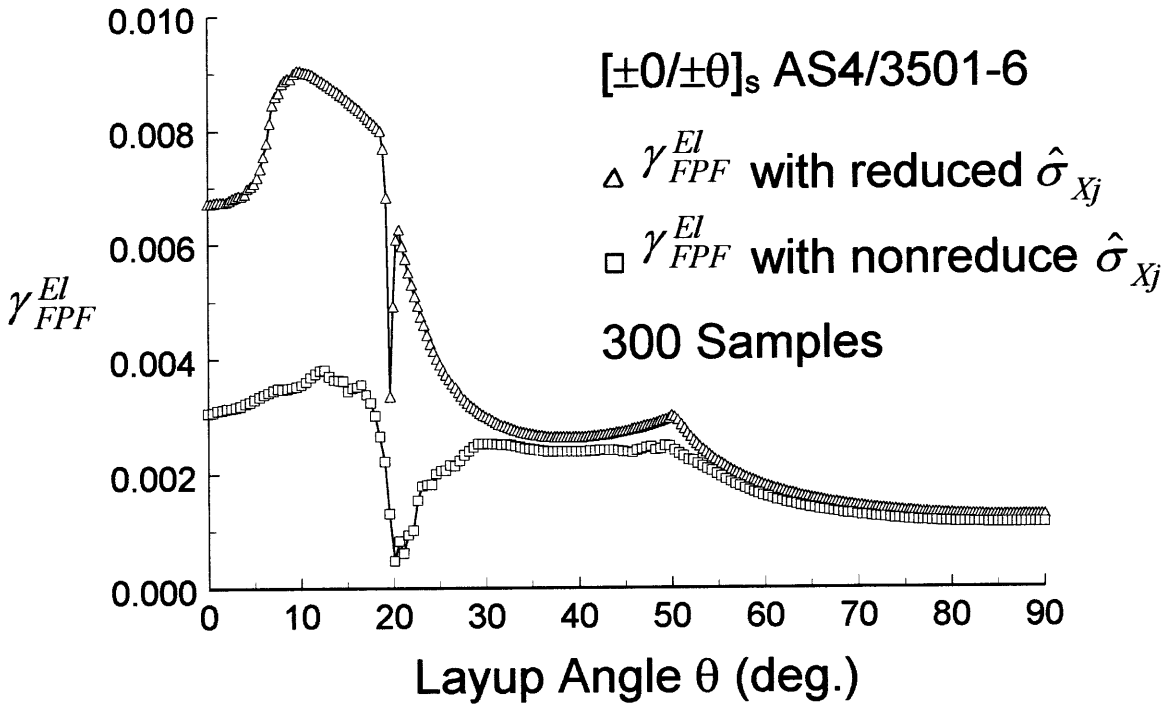

Figure B.1 γ_{FPF}^{El} for two different sets of ply material property geometric parameter standard deviations

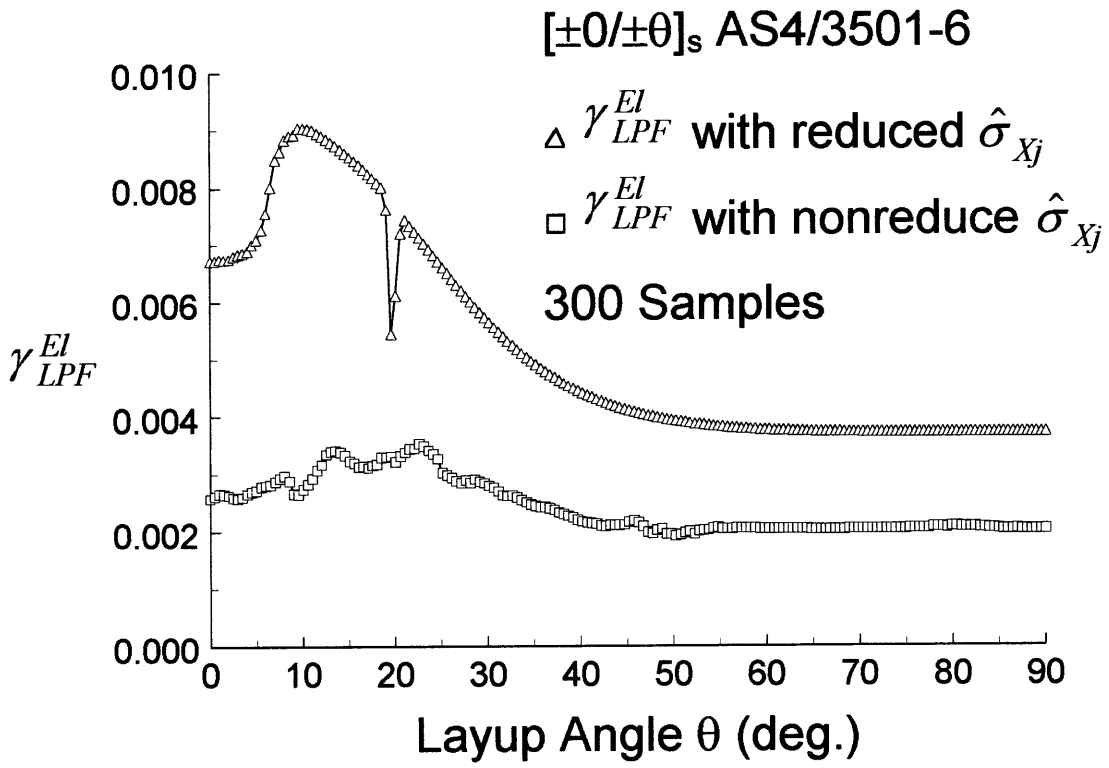

Figure B.2 γ_{LPF}^{El} for two different sets of ply material property and geometric parameter standard deviations

APPENDIX C

DETAILS CONCERNING THE CHOICE OF N

When creating data for plots using A3 and A4 a large N is required so that the calculated means and standard deviations do not exhibit a lot of scatter. The reason is that as the number of samples N is increased the probability that the calculated means and standard deviations are far from their respective exact values is reduced. However, as the number of points in a plot is increased the chance of getting a *bad* set of random numbers (i.e. a set of $r^{(k)}$ that by chance happens to cluster in one area in the interval (0,1)), for a particular N, increases. Hence, N must increase as the number of points in a plot does (otherwise there are always a few points on the plot that are far from their respective exact values). The requirement of a large N for "smooth" plots results in a very high computation time, particularly for plots with many points (since as the number of points increases so must N).

The goal is to avoid bad sets of random numbers, the solution is simple. When generating random numbers using a computer, a seed to initiate the sequence of random numbers is required. A computer is not capable of generating a true random number, it needs a random seed

(number) to initiate the sequence of calculated pseudo random numbers (see Knuth [89] for a deep discussion and references). The relation of the sequence of generated numbers to the seed is constructed to be so complex that it is assumed random. For a particular seed there is a particular sequence of random numbers that the computer will generate. Some of these sequences are bad, some good. The simple idea is to find a good seed for the random number generator, by trial and error, and stick with it throughout the computer run to generate the points for the plot. As a result the number of samples N needed to produce a plot without a point far from its respective exact value is independent of the number of points in the plot (since the same sequence of random numbers, $r^{(k)}$, is used for each point). Also, if f_{Y_i} is continuous so is the computed mean and standard deviation (since the sequence of random numbers used does not change). This is a particularly nice feature for plots, since plots of the means and standard deviations using A3 are smooth. Without using the same seed this property of continuity only occurs as $N \to \infty$. In the computer code used to generate the plots for this thesis a particular seed is hard written into the code and is not changed.

APPENDIX D

CONTOUR PLOTS OF LAMINATE PROPERTIES FOR THE $[\pm\theta/\pm\beta]_s$ LAMINATE FAMILY

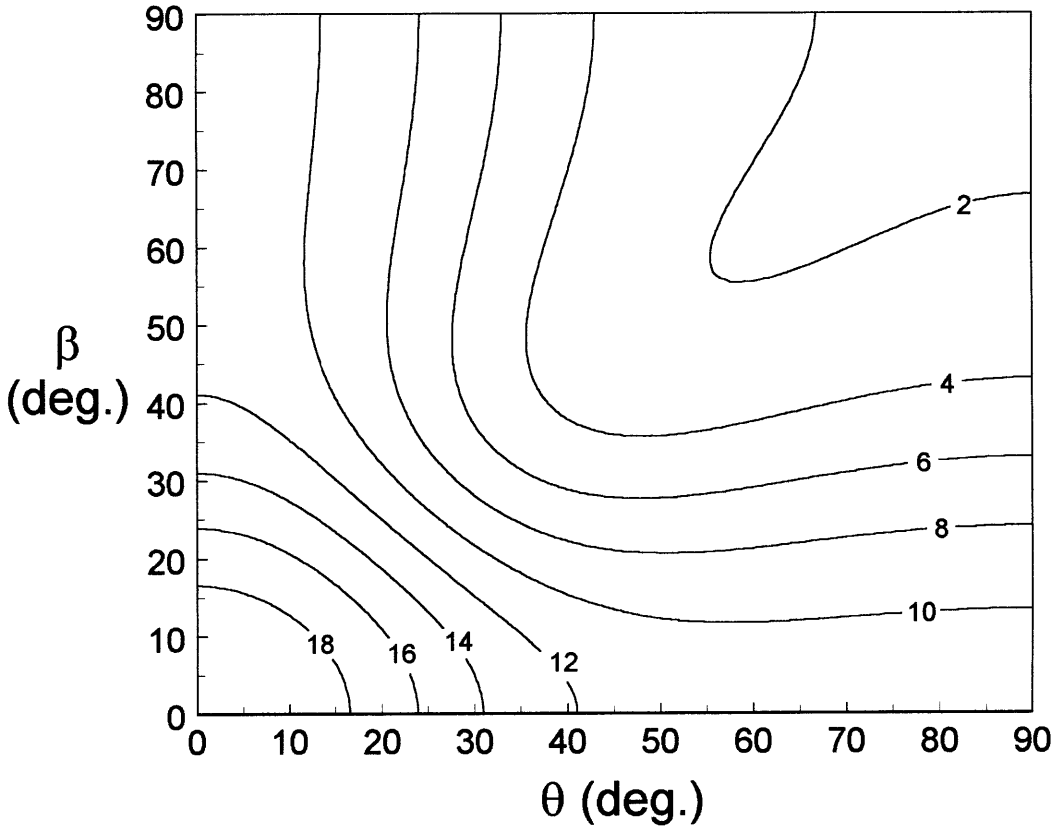

Figure D.1 Contour plot of the mean longitudinal stiffness (Msi) for the $[\pm\theta/\pm\beta]_s$ AS4/3501-6 laminate family (approach A2)

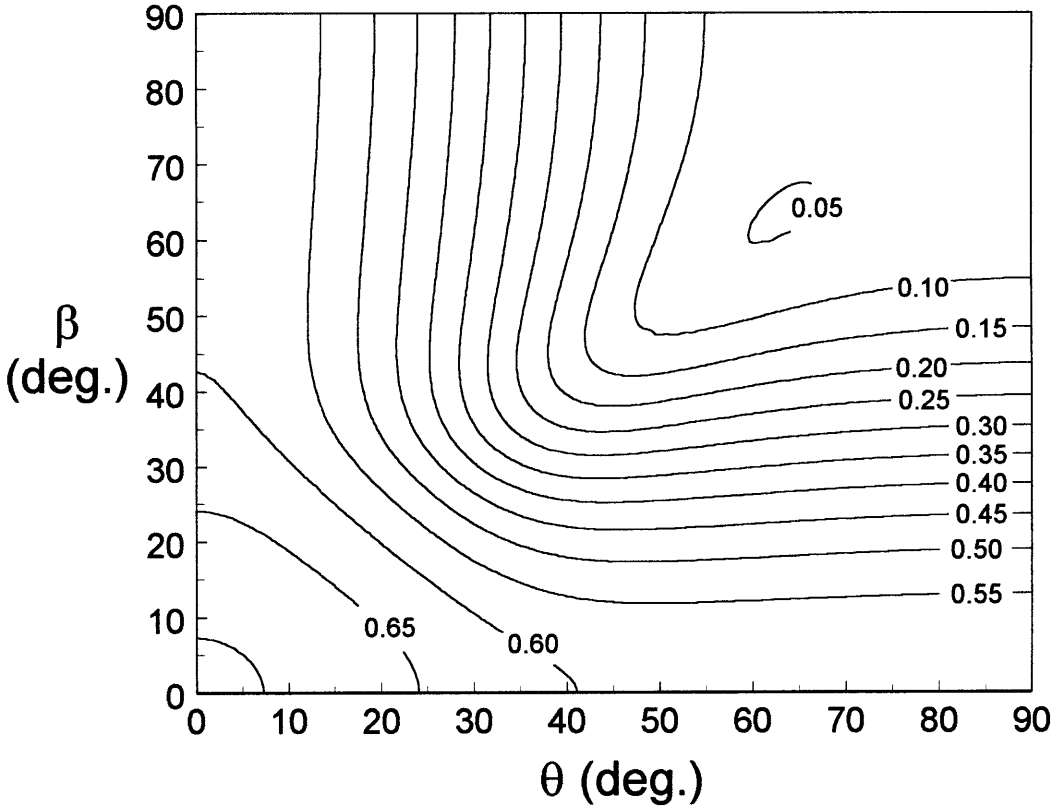

Figure D.2 Contour plot of the standard deviation of the longitudinal stiffness (Msi) for the $[\pm\theta/\pm\beta]_s$ AS4/3501-6 laminate family (approach A2)

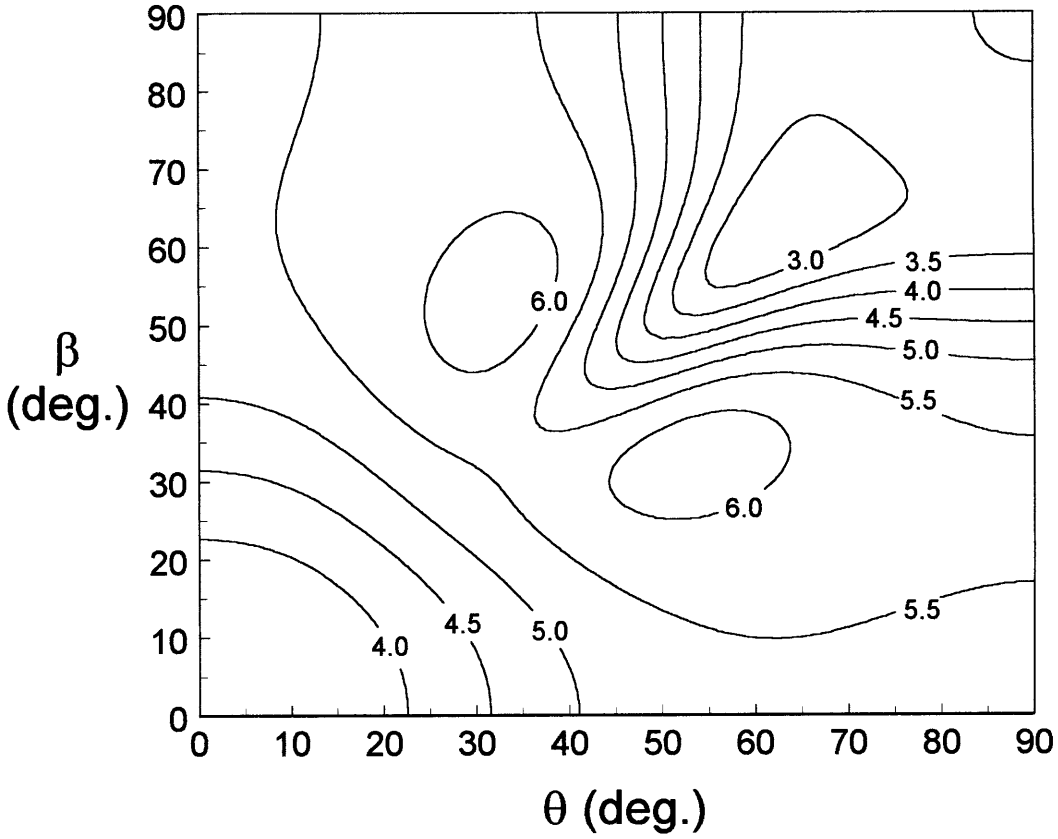

Figure D.3 Contour plot of the coefficient of variation (%) of the longitudinal stiffness (Msi) for the $[\pm\theta/\pm\beta]_s$ AS4/3501-6 laminate family (approach A2)

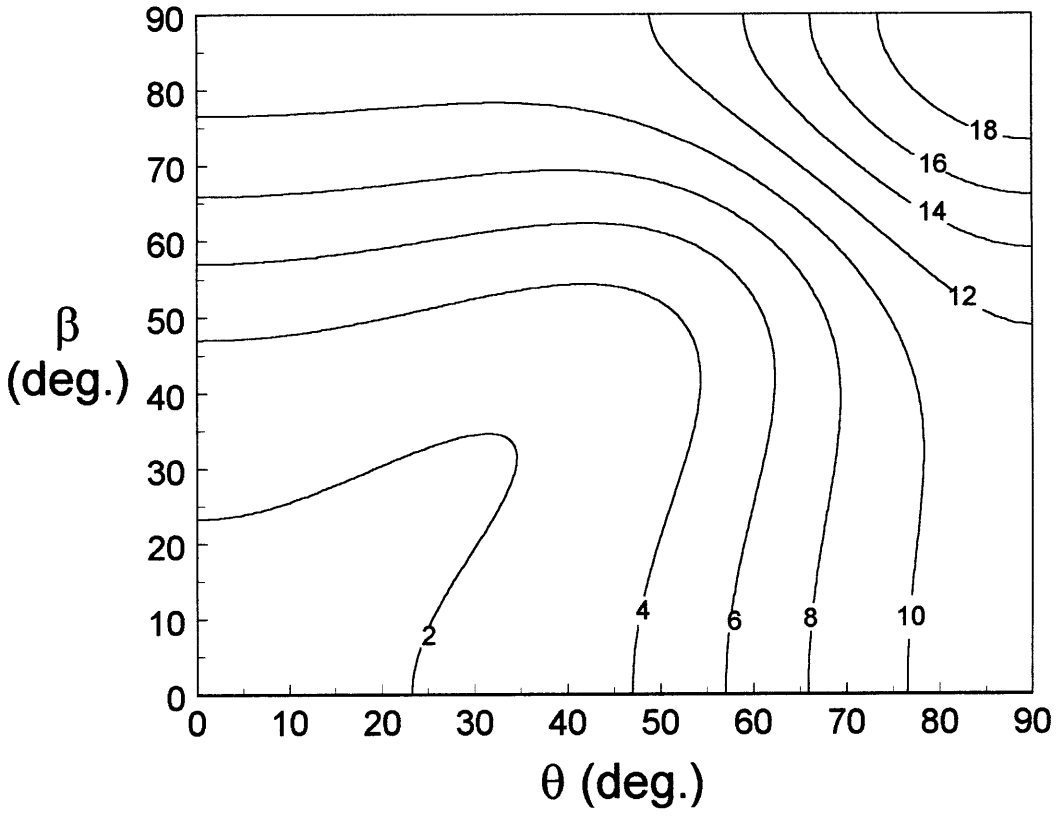

Figure D.4 Contour plot of the mean transverse stiffness (Msi) for the $[\pm\theta/\pm\beta]_s$ AS4/3501-6 laminate family (approach A2)

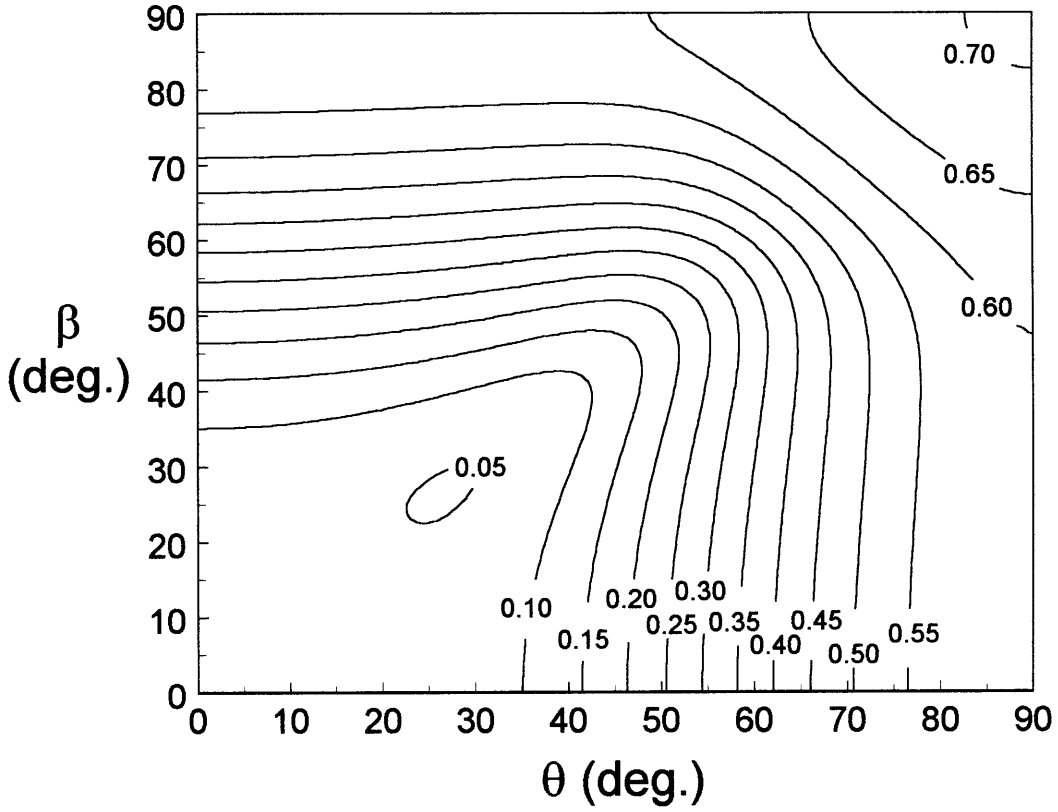

Figure D.5 Contour plot of the standard deviation of the transverse stiffness (Msi) for the $[\pm\theta/\pm\beta]_s$ AS4/3501-6 laminate family (approach A2)

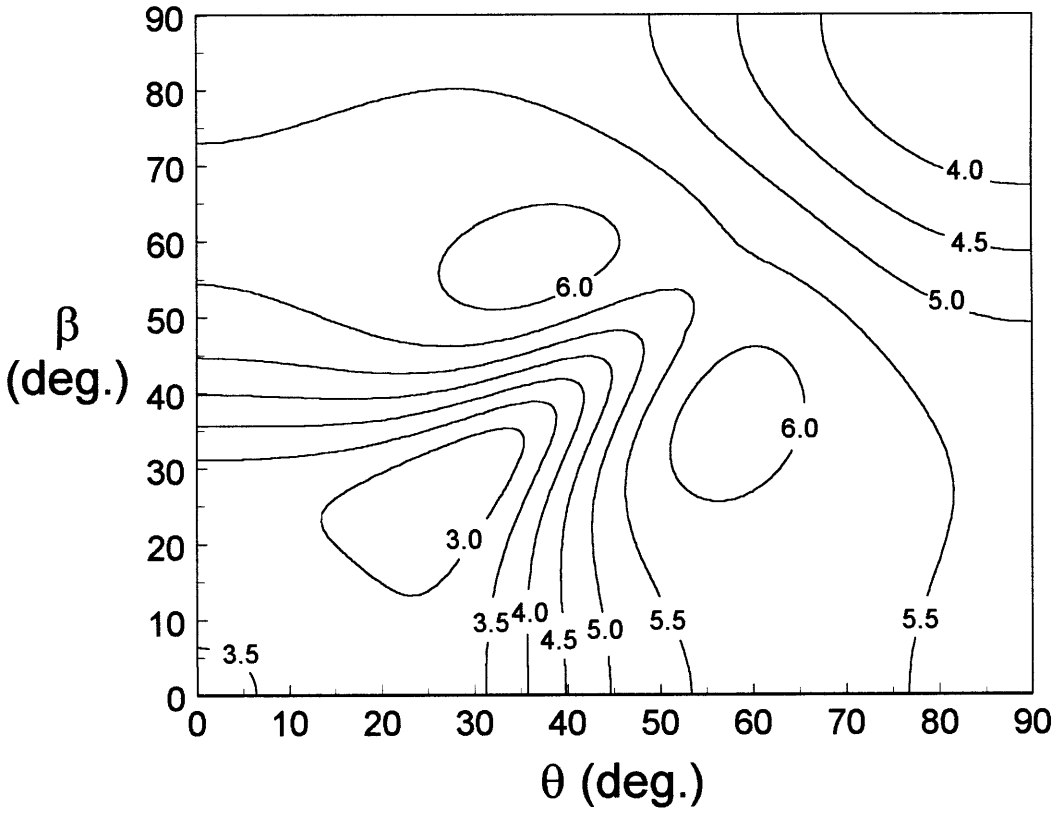

Figure D.6 Contour plot of the coefficient of variation (%) of the transverse stiffness (Msi) for the $[\pm\theta/\pm\beta]_s$ AS4/3501-6 laminate family (approach A2)

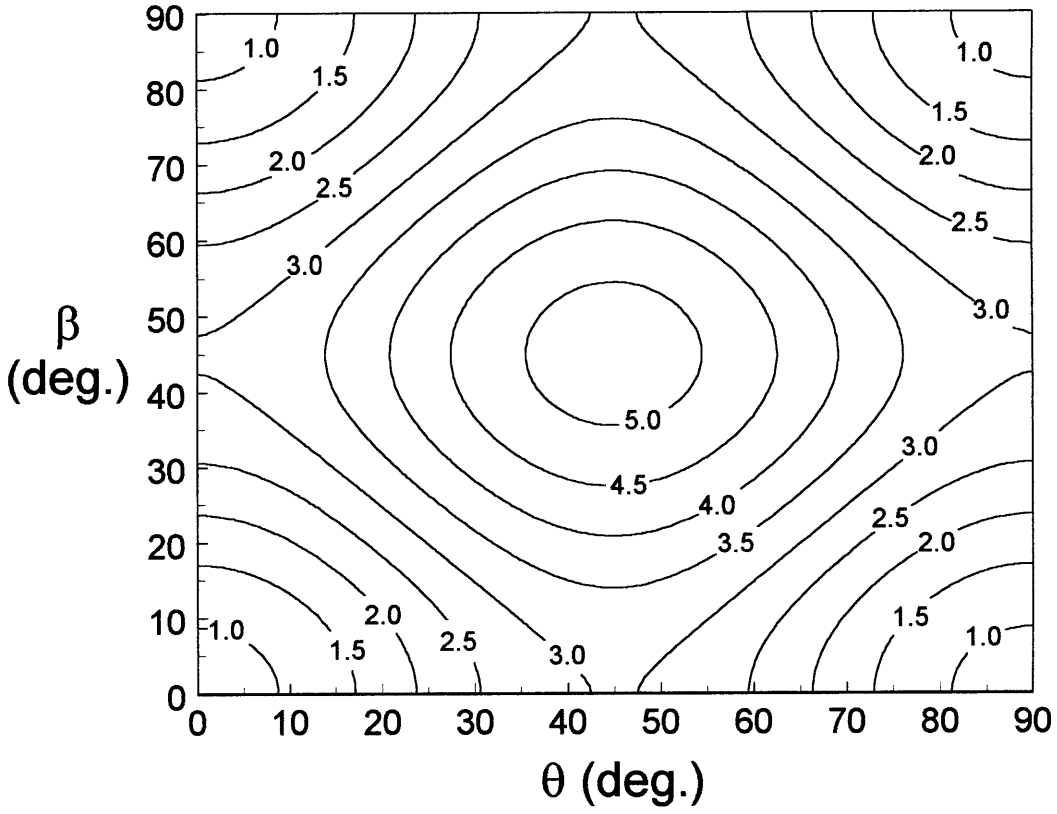

Figure D.7 Contour plot of the mean shear stiffness (Msi) for the $[\pm\theta/\pm\beta]_s$ AS4/3501-6 laminate family (approach A2)

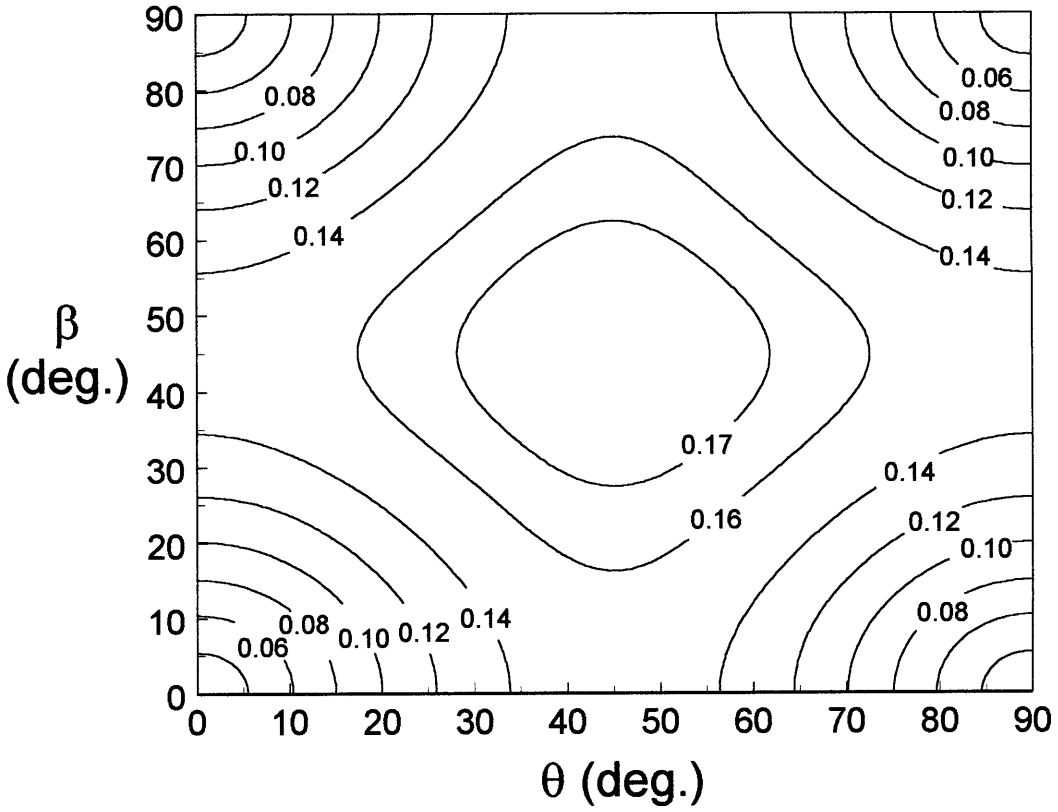

Figure D.8 Contour plot of the standard deviation of the shear stiffness (Msi) for the $[\pm\theta/\pm\beta]_s$ AS4/3501-6 laminate family (approach A2)

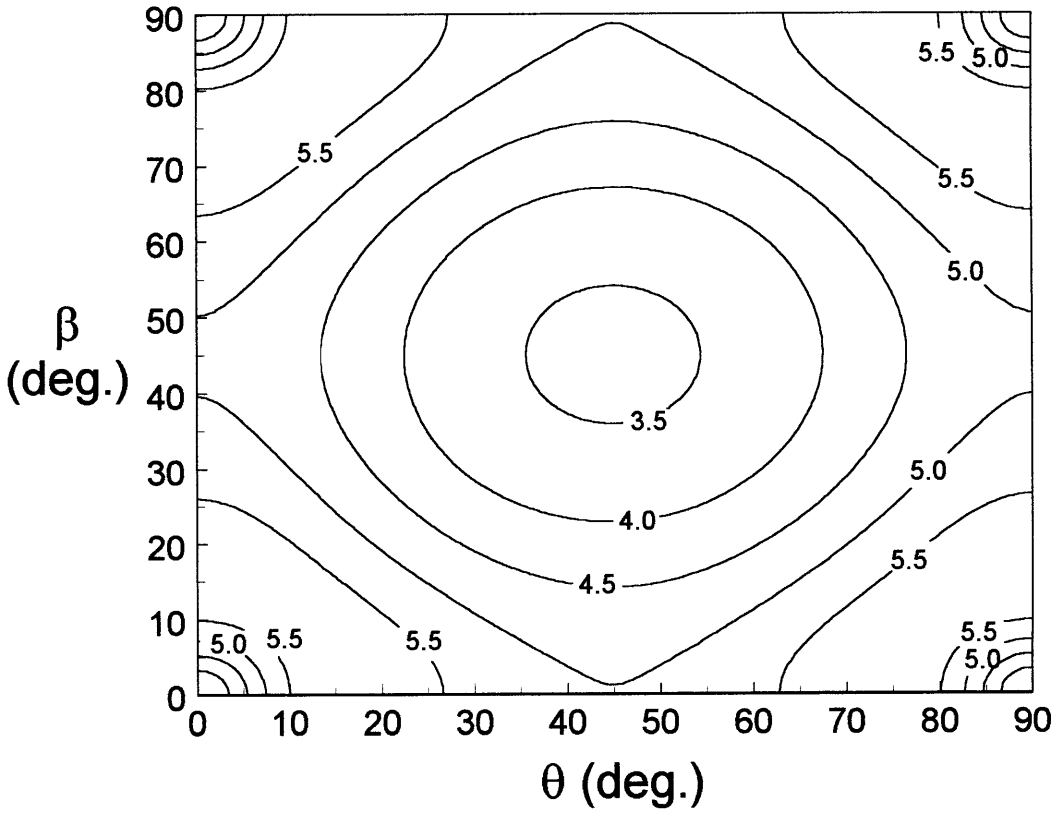

Figure D.9 Contour plot of the coefficient of variation (%) of the shear stiffness (Msi) for the $[\pm\theta/\pm\beta]_s$ AS4/3501-6 laminate family (approach A2)

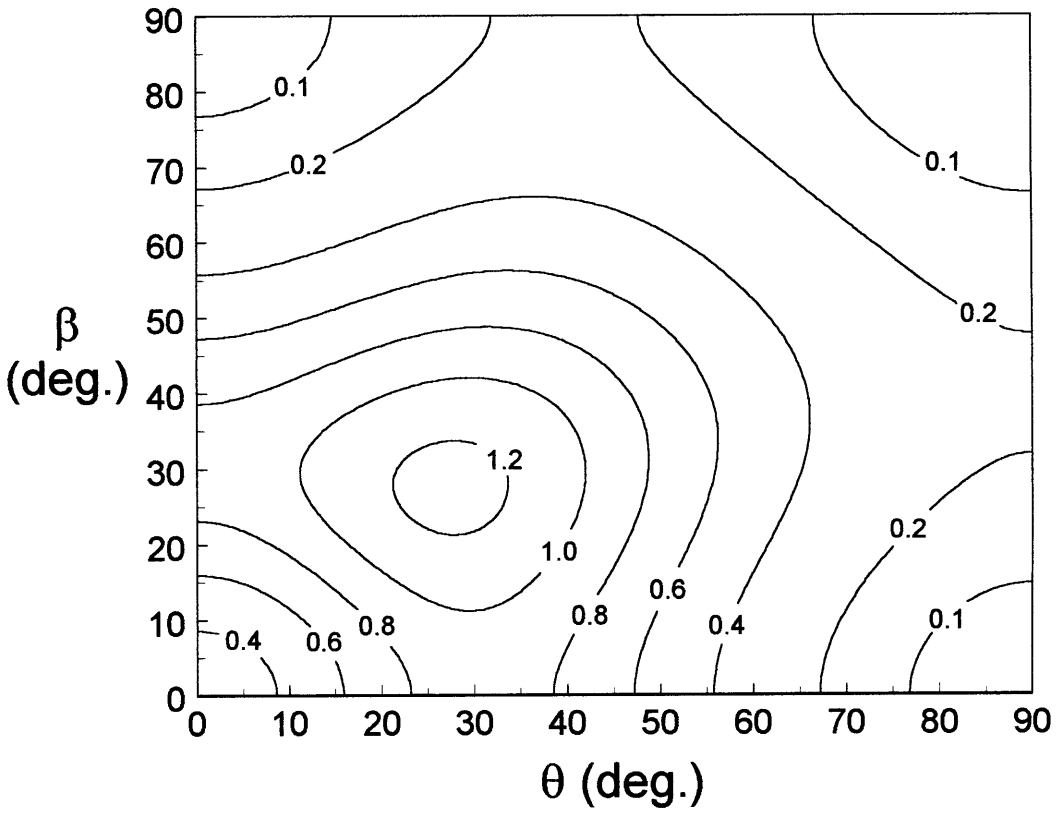

Figure D.10 Contour plot of the mean Poisson's ratio for the $[\pm\theta/\pm\beta]_s$ AS4/3501-6 laminate family (approach A2)

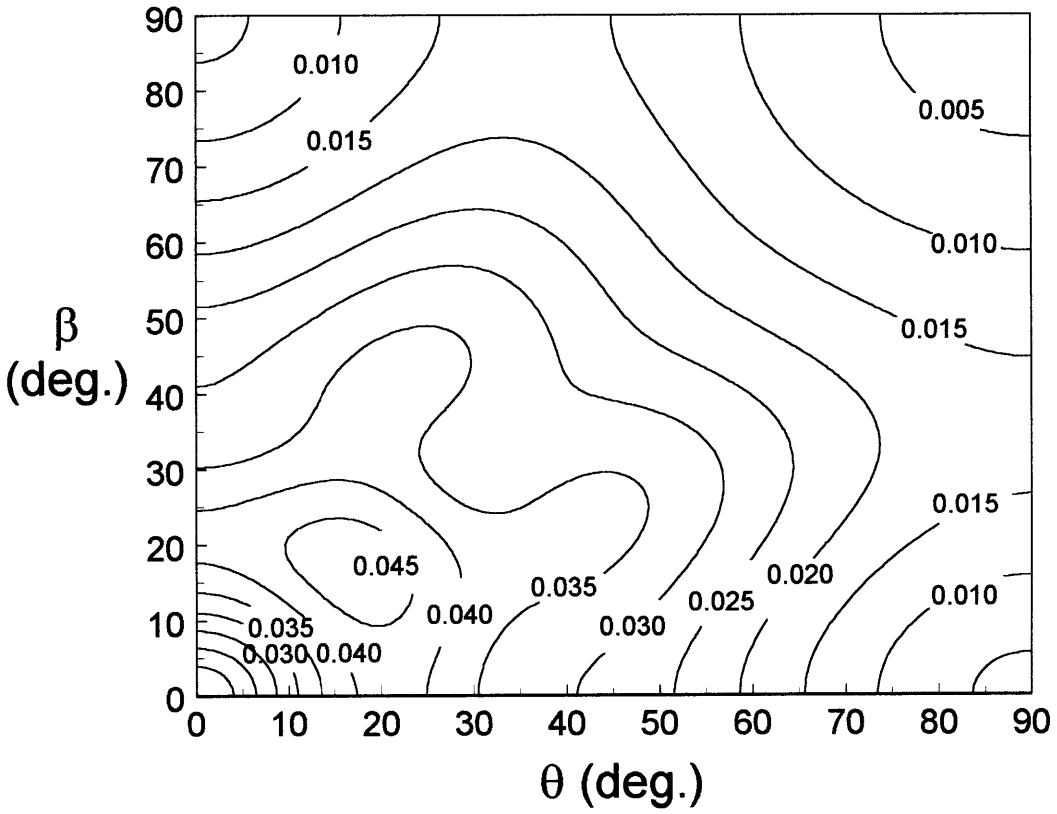

Figure D.11 Contour plot of the standard deviation of the Poisson's ratio for the $[\pm\theta/\pm\beta]_s$ AS4/3501-6 laminate family (approach A2)

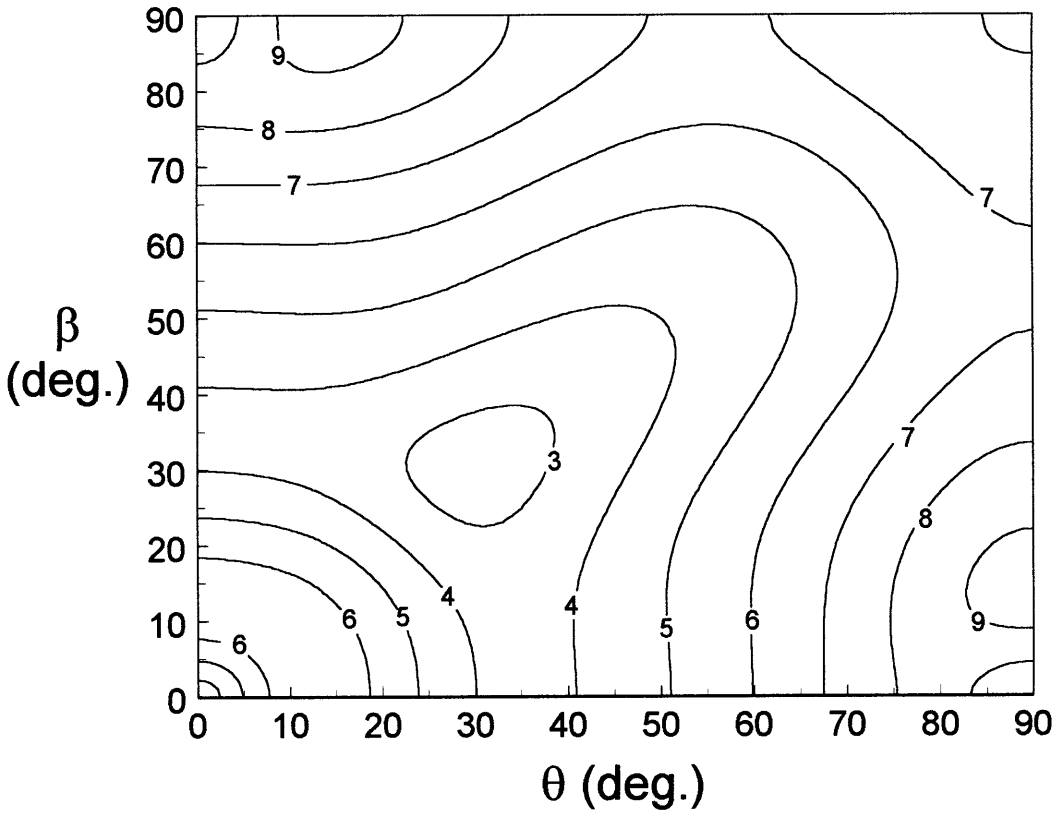

Figure D.12 Contour plot of the coefficient of variation (%) of the Poisson's ratio for the $[\pm\theta/\pm\beta]_s$ AS4/3501-6 laminate family (approach A2)

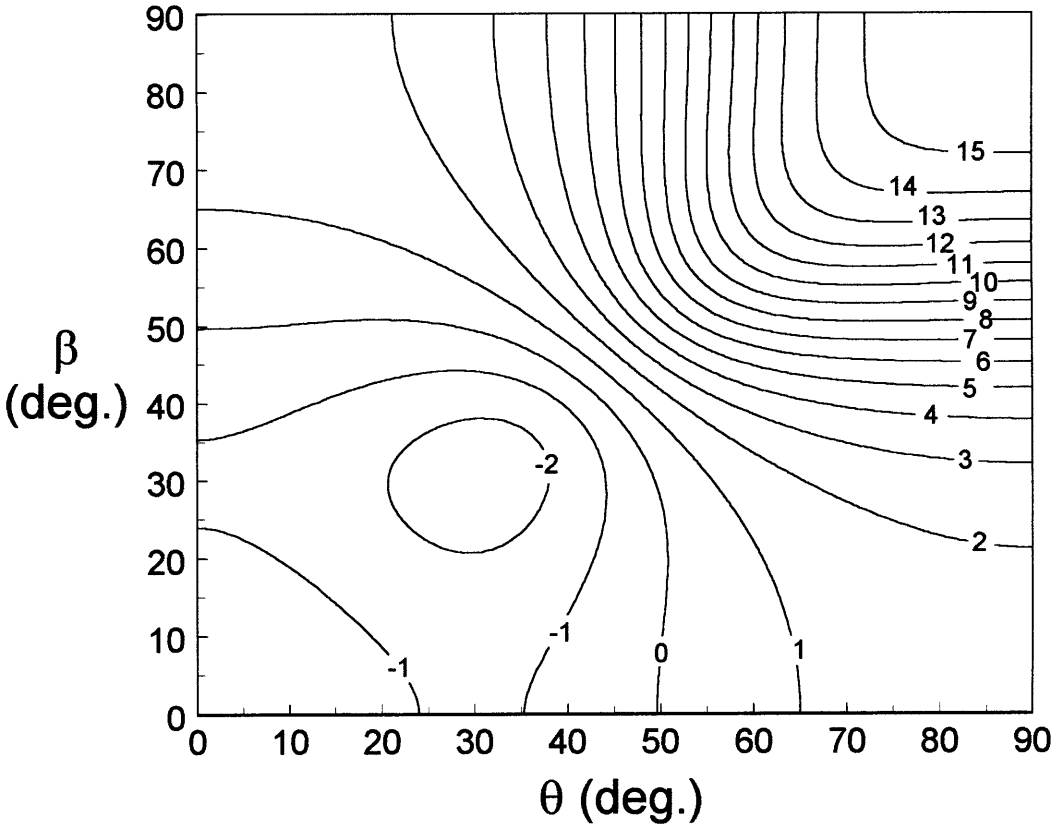

Figure D.13 Contour plot of the mean longitudinal CTE (με/°F) for the $[\pm\theta/\pm\beta]_s$ AS4/3501-6 laminate family (approach A2)

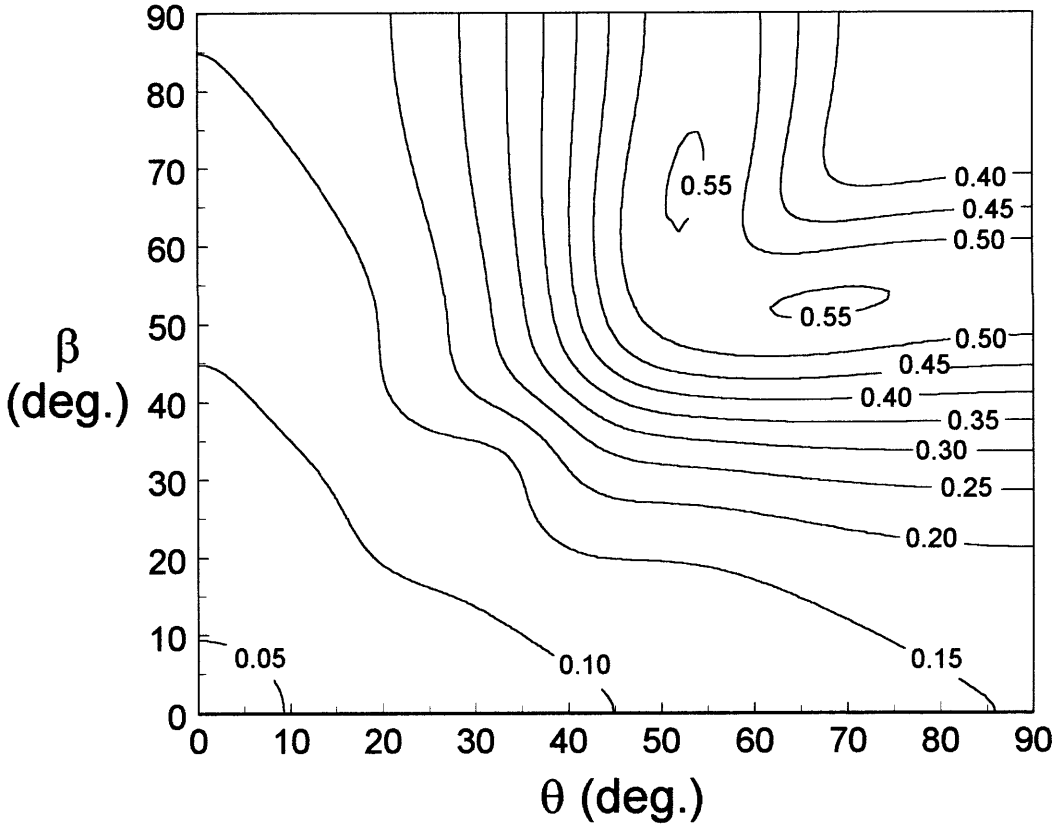

Figure D.14 Contour plot of the standard deviation of the longitudinal CTE ($\mu\varepsilon/^{o}F$) for the $[\pm\theta/\pm\beta]_s$ AS4/3501-6 laminate family (approach A2)

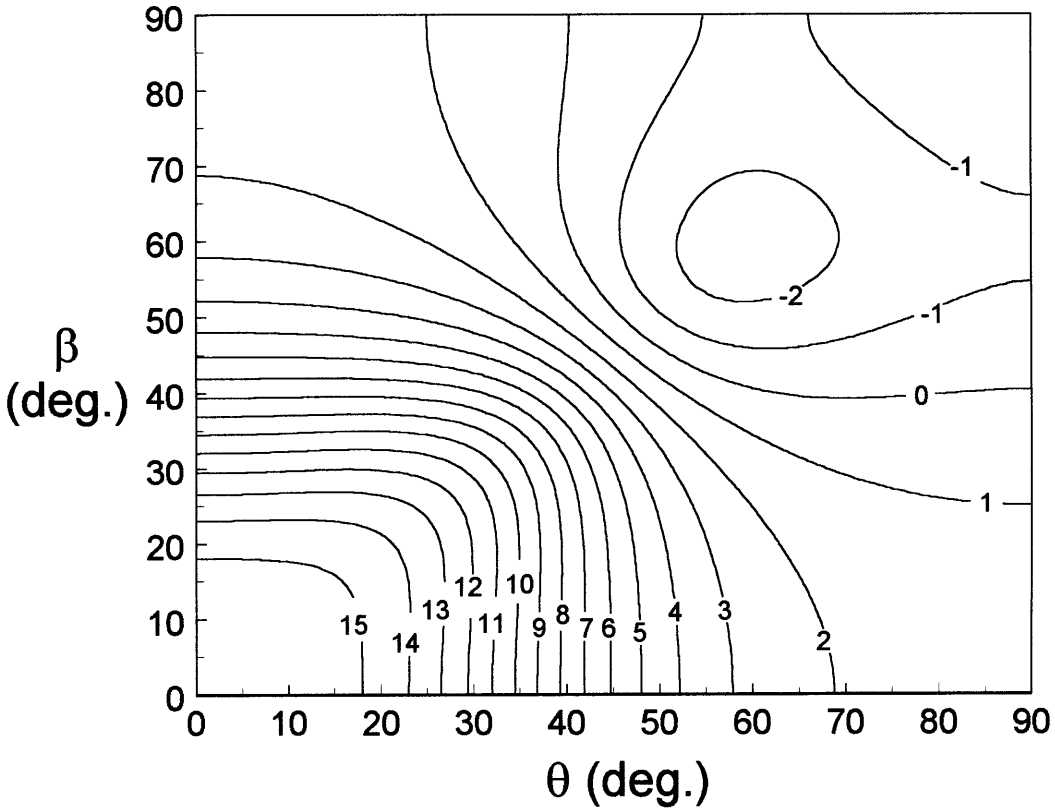

Figure D.15 Contour plot of the mean transverse CTE (με/°F) for the $[\pm\theta/\pm\beta]_s$ AS4/3501-6 laminate family (approach A2)

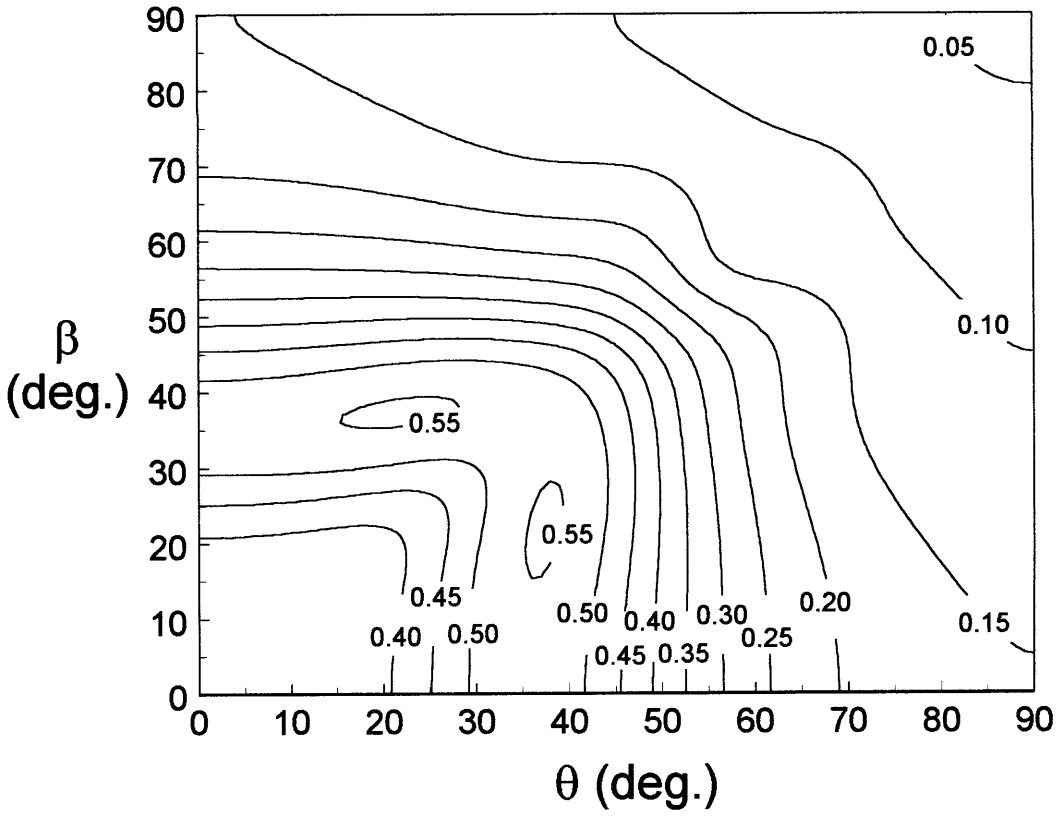

Figure D.16 Contour plot of the standard deviation of the transverse CTE ($\mu\varepsilon/^{o}F$) for the $[\pm\theta/\pm\beta]_s$ AS4/3501-6 laminate family (approach A2)

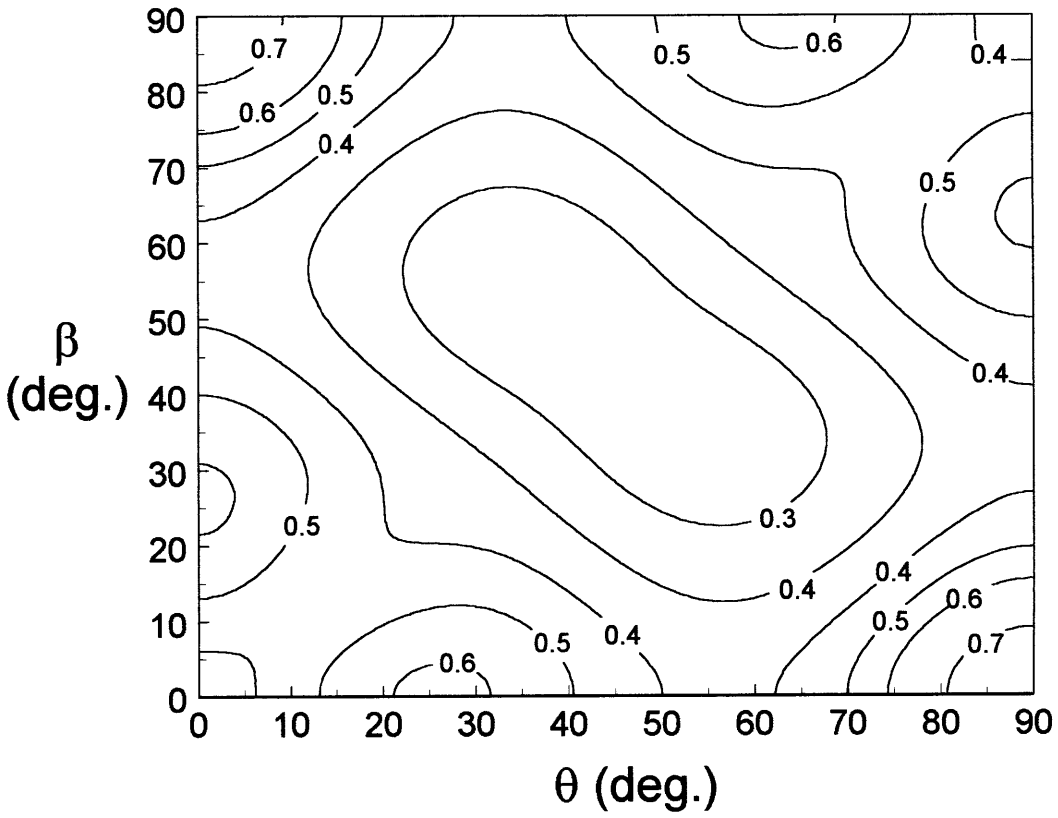

Figure D.17 Contour plot of the standard deviation of the shear CTE ($\mu\varepsilon/^{o}F$) for the $[\pm\theta/\pm\beta]_s$ AS4/3501-6 laminate family (approach A2)

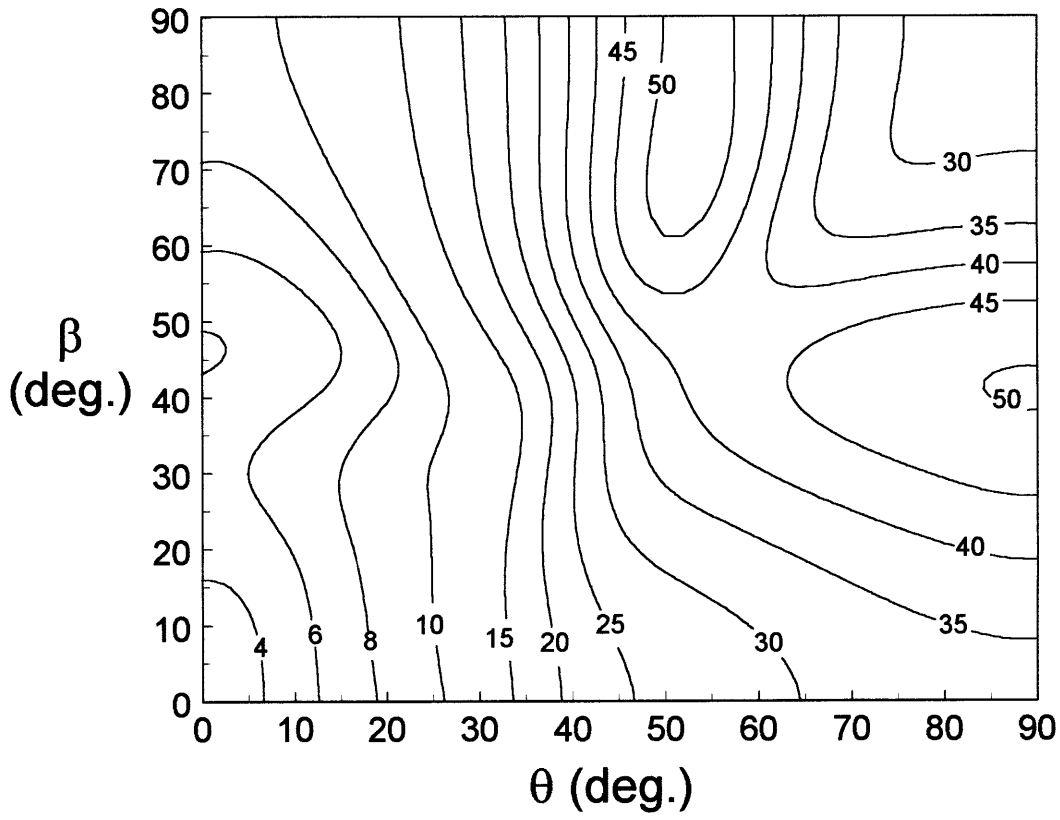

Figure D.18 Contour plot of the standard deviation of the longitudinal CTB ($\mu in/in^2/^oF$) for the $[\pm\theta/\pm\beta]_s$ AS4/3501-6 laminate family (approach A2)

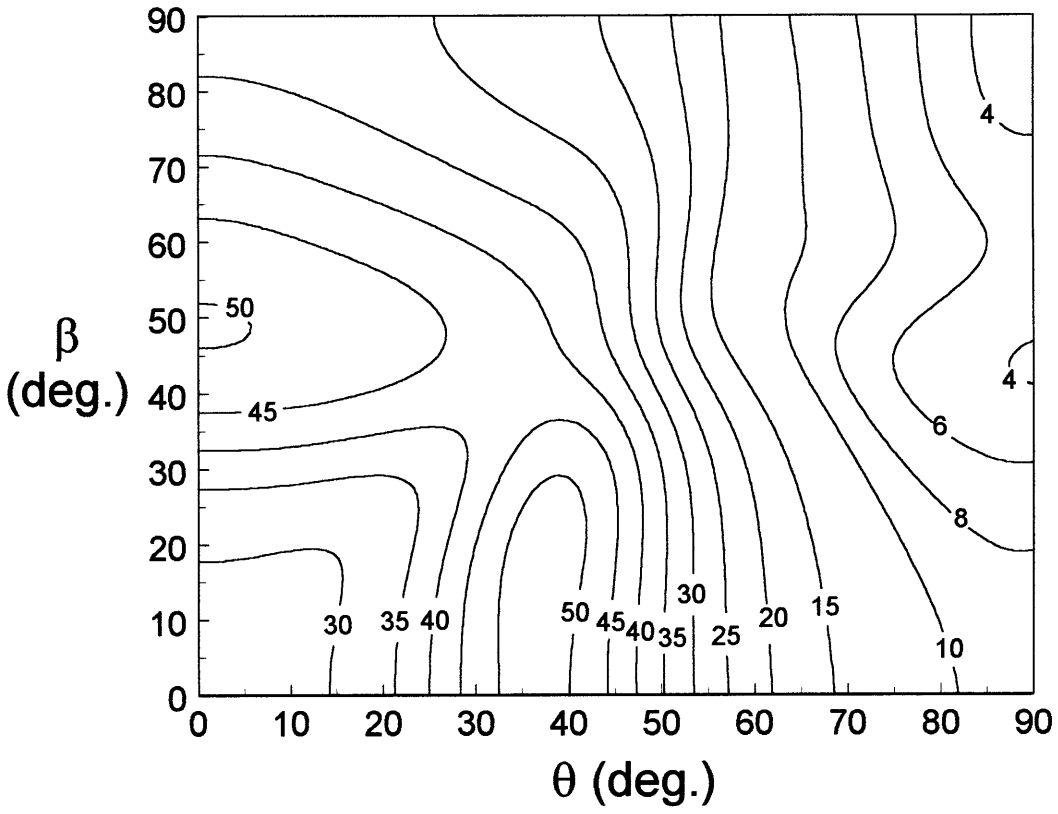

Figure D.19 Contour plot of the standard deviation of the transverse CTB ($\mu in/in^2/^oF$) for the $[\pm\theta/\pm\beta]_s$ AS4/3501-6 laminate family (approach A2)

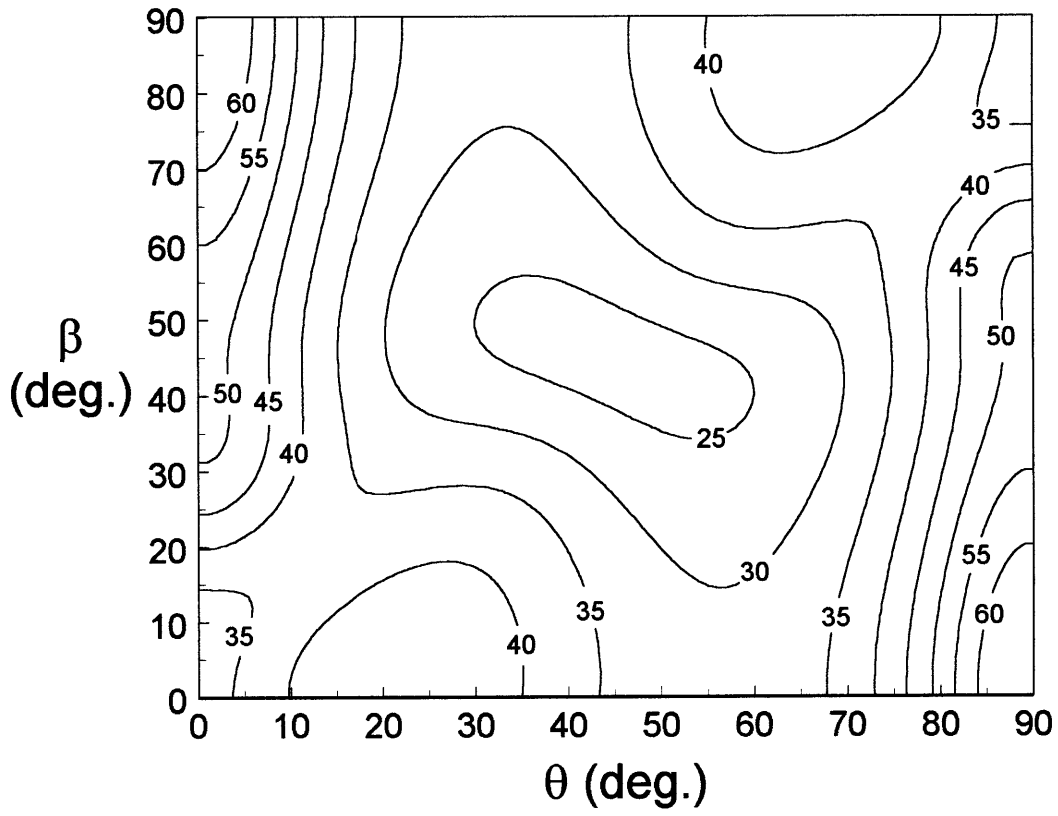

Figure D.20 Contour plot of the standard deviation of the twist CTB ($\mu in/in^2/^oF$) for the $[\pm\theta/\pm\beta]_s$ AS4/3501-6 laminate family (approach A2)

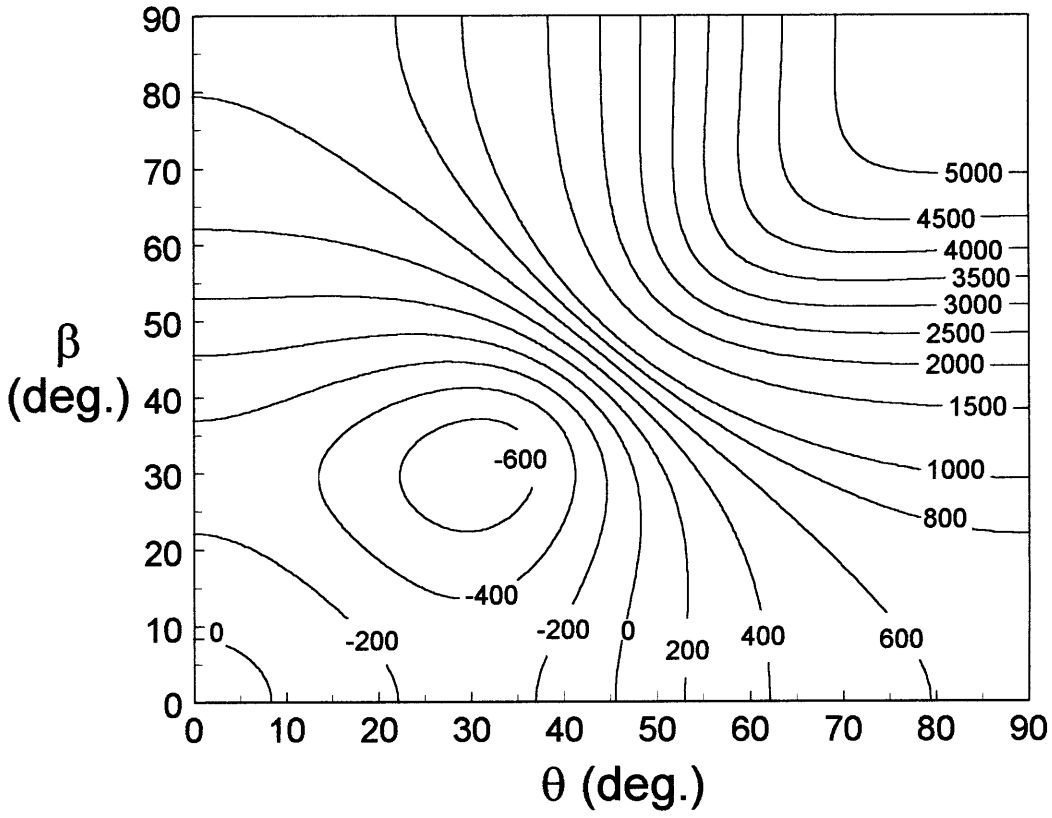

Figure D.21 Contour plot of the mean longitudinal CME (με/%) for the $[\pm\theta/\pm\beta]_s$ AS4/3501-6 laminate family (approach A2)

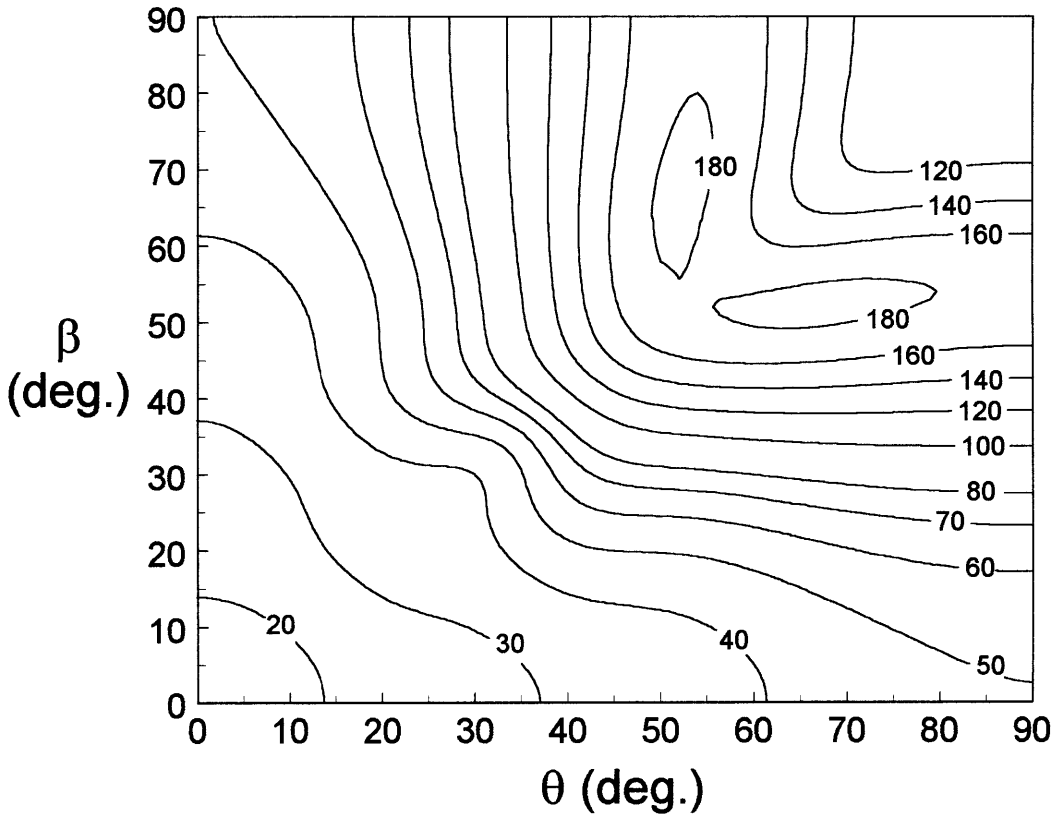

Figure D.22 Contour plot of the standard deviation of the longitudinal CME ($\mu\varepsilon/\%$) for the $[\pm\theta/\pm\beta]_s$ AS4/3501-6 laminate family (approach A2)

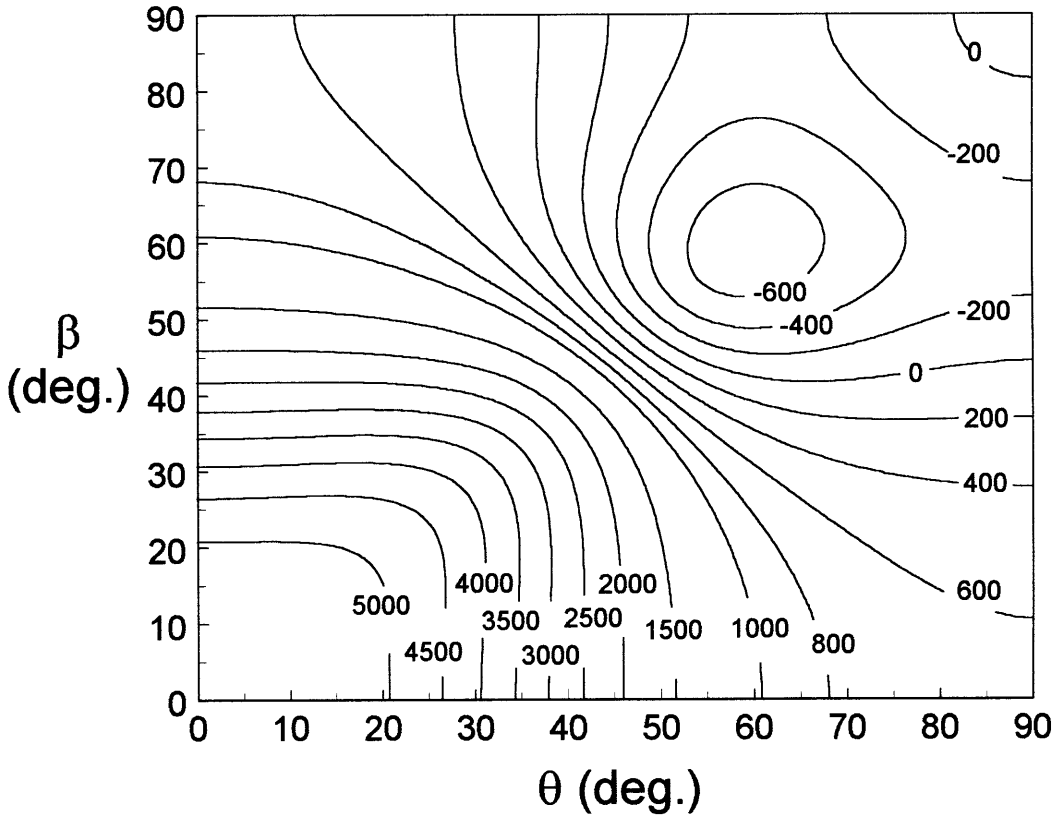

Figure D.23 Contour plot of the mean transverse CME (με/%) for the $[\pm\theta/\pm\beta]_s$ AS4/3501-6 laminate family (approach A2)

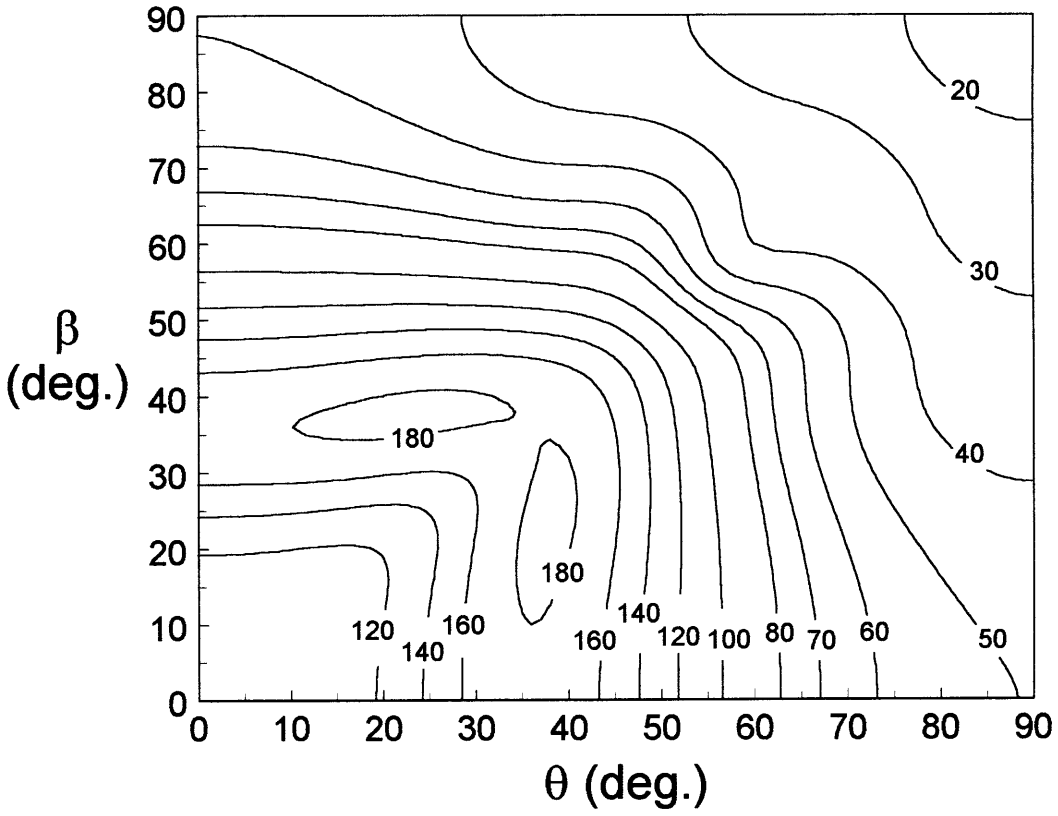

Figure D.24 Contour plot of the standard deviation of the transverse CME (με/%) for the $[\pm\theta/\pm\beta]_s$ AS4/3501-6 laminate family (approach A2)

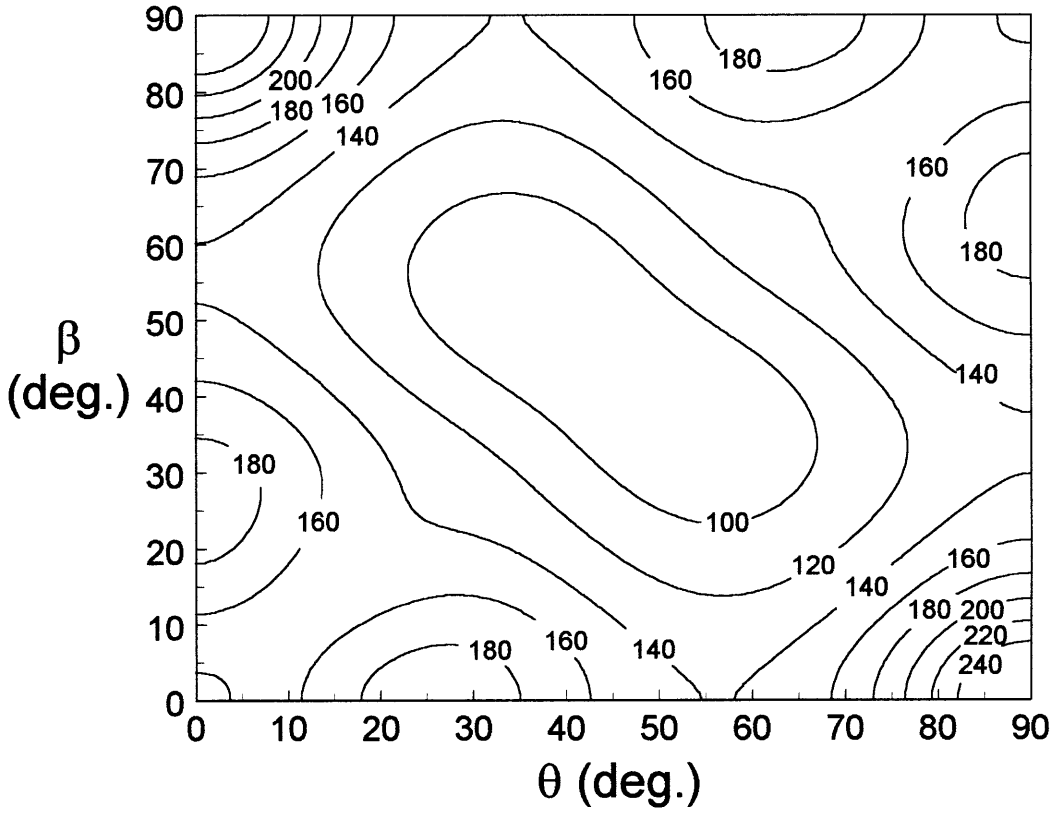

Figure D.25 Contour plot of the standard deviation of the shear CME ($\mu\varepsilon/\%$) for the $[\pm\theta/\pm\beta]_s$ AS4/3501-6 laminate family (approach A2)

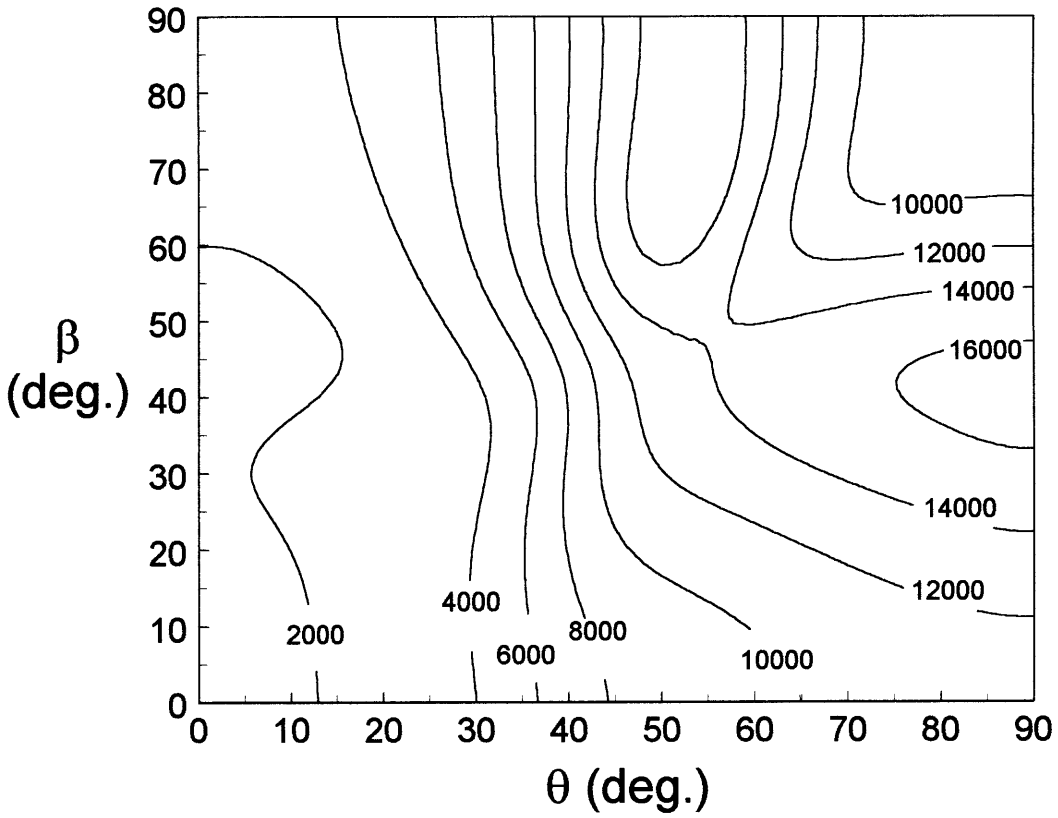

Figure D.26 Contour plot of the standard deviation of the longitudinal CMB ($\mu in/in^2/\%$) for the $[\pm\theta/\pm\beta]_s$ AS4/3501-6 laminate family (approach A2)

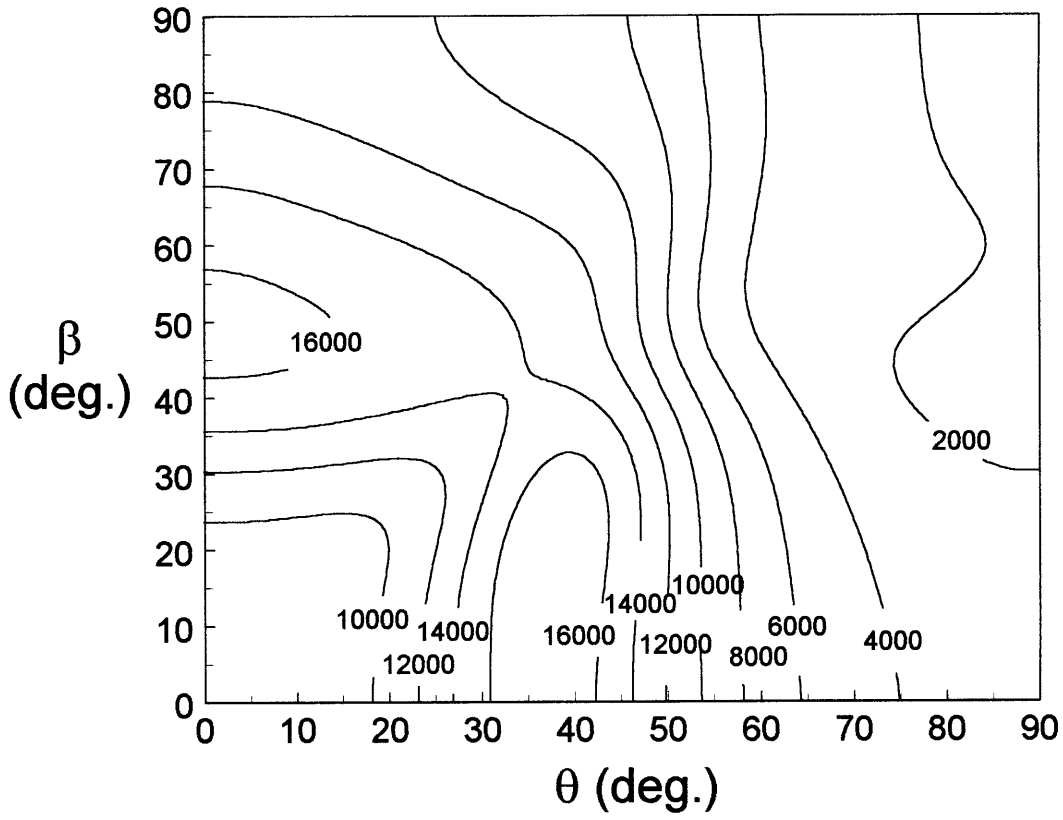

Figure D.27 Contour plot of the standard deviation of the transverse CMB ($\mu in/in^2/\%$) for the $[\pm\theta/\pm\beta]_s$ AS4/3501-6 laminate family (approach A2)

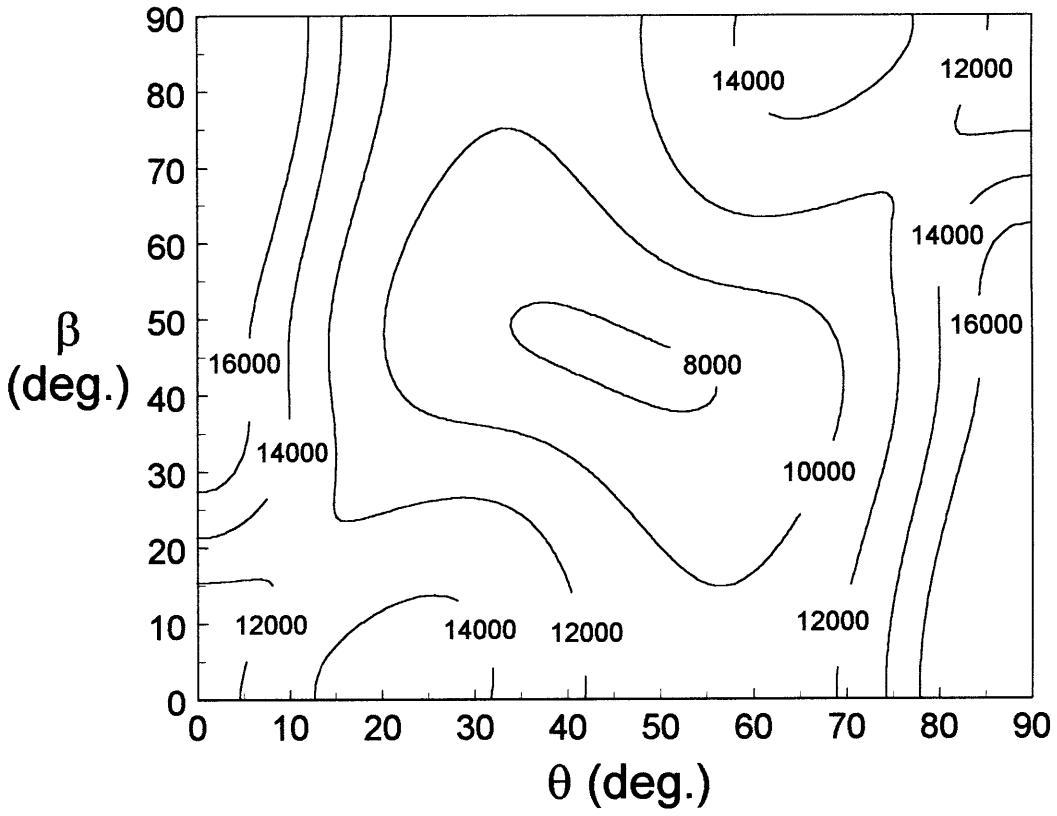

Figure D.28 Contour plot of the standard deviation of the twist CMB ($\mu in/in^2/\%$) for the $[\pm\theta/\pm\beta]_s$ AS4/3501-6 laminate family (approach A2)

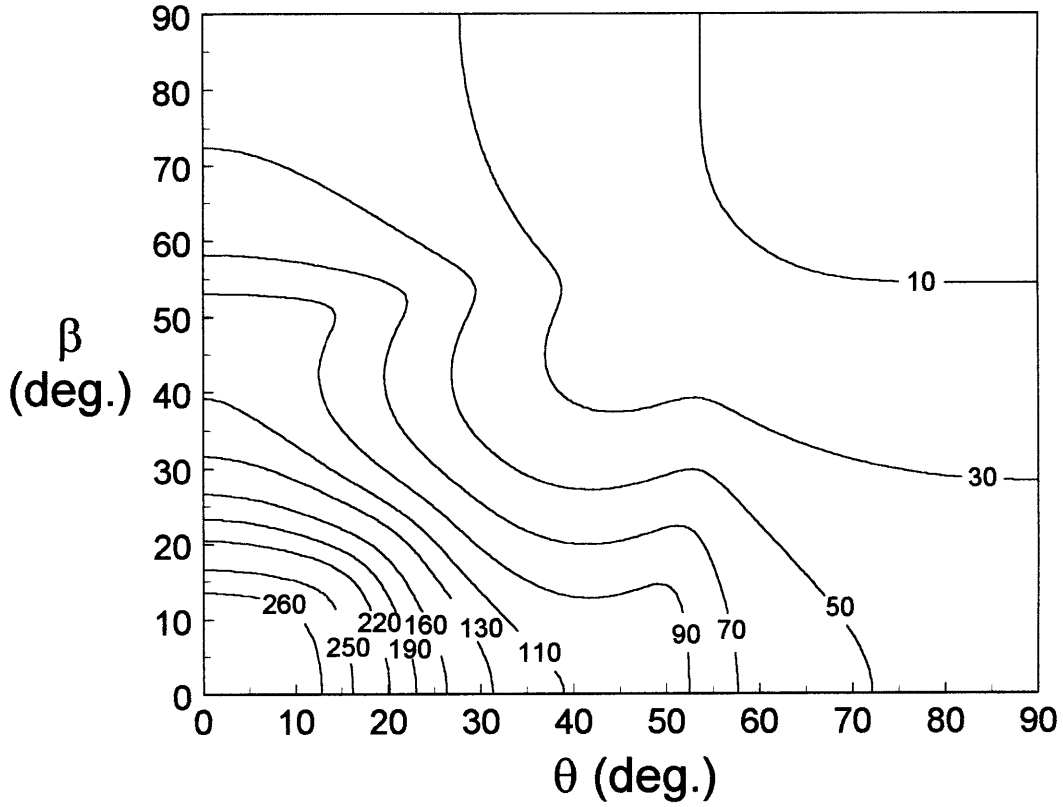

Figure D.29 Contour plot of the mean longitudinal tensile FPF load (Ksi) for the $[\pm\theta/\pm\beta]_s$ AS4/3501-6 laminate family (approach A3, 500 samples)

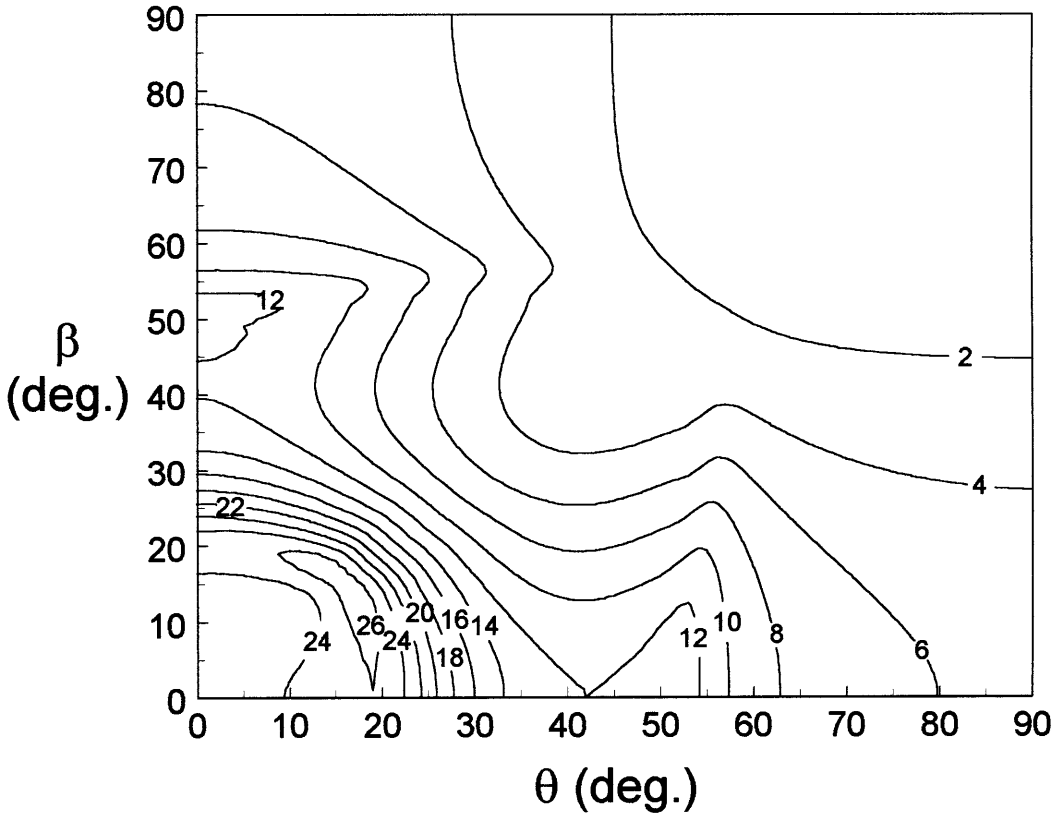

Figure D.30 Contour plot of the standard deviation of the longitudinal tensile FPF load (Ksi) for the $[\pm\theta/\pm\beta]_s$ AS4/3501-6 laminate family (approach A3, 1000 samples)

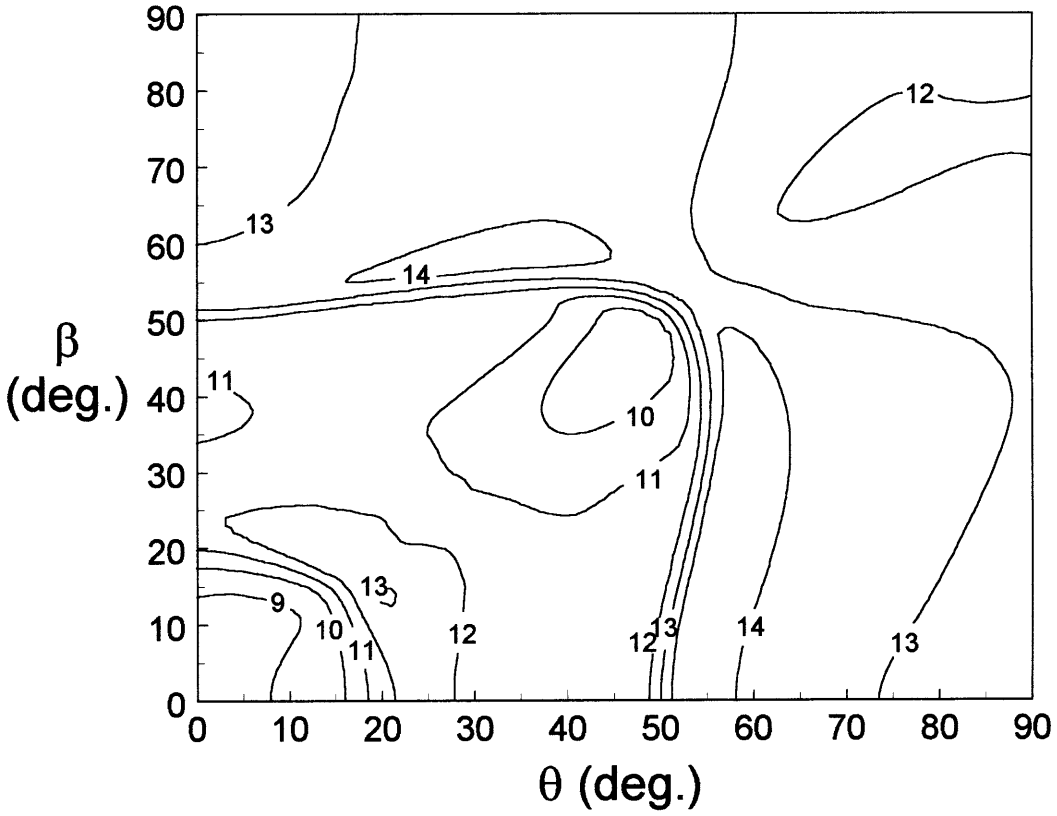

Figure D.31 Contour plot of the coefficient of variation (%) of the longitudinal tensile FPF load for the $[\pm\theta/\pm\beta]_s$ AS4/3501-6 laminate family (approach A3, 1000 samples)

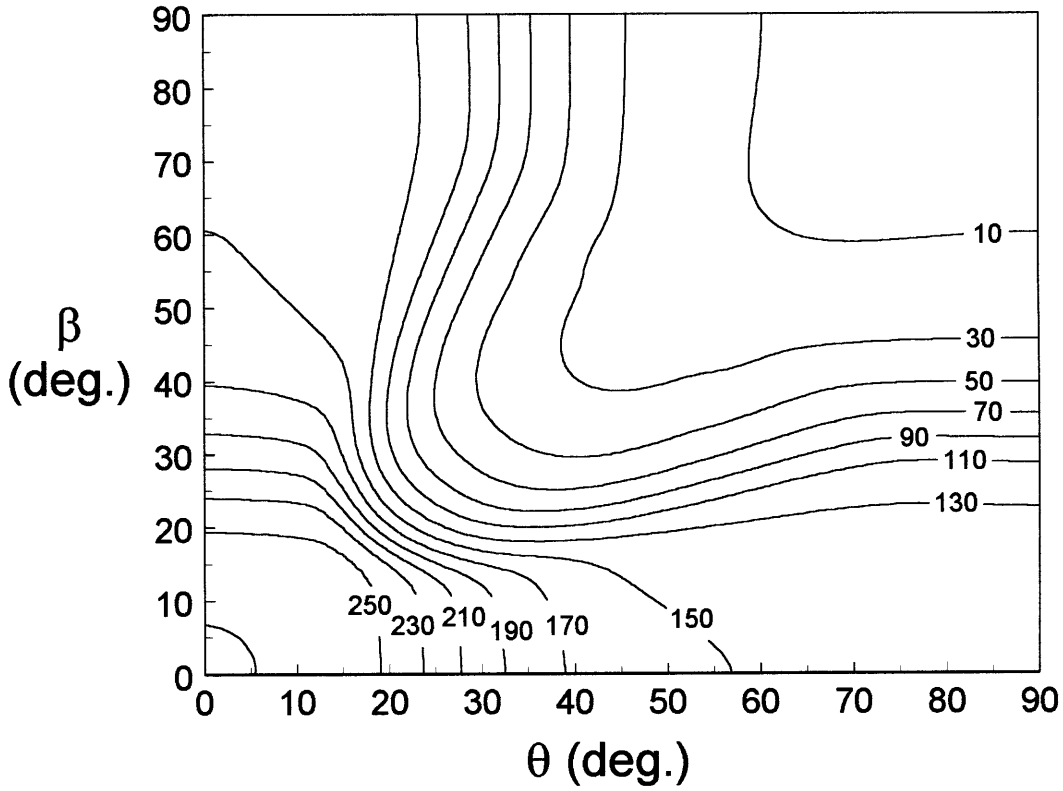

Figure D.32 Contour plot of the mean longitudinal tensile strength (Ksi) for the $[\pm\theta/\pm\beta]_s$ AS4/3501-6 laminate family (approach A3, 500 samples)

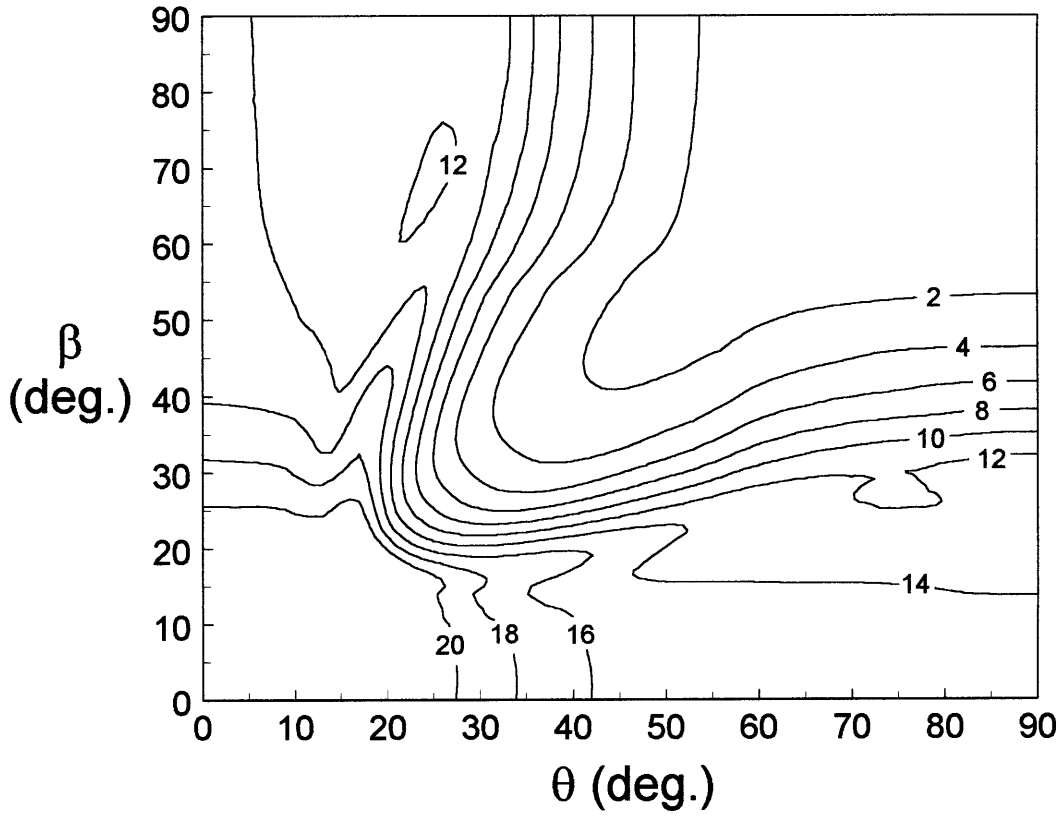

Figure D.33 Contour plot of the standard deviation of the longitudinal tensile strength (Ksi) for the $[\pm\theta/\pm\beta]_s$ AS4/3501-6 laminate family (approach A3, 1000 samples)

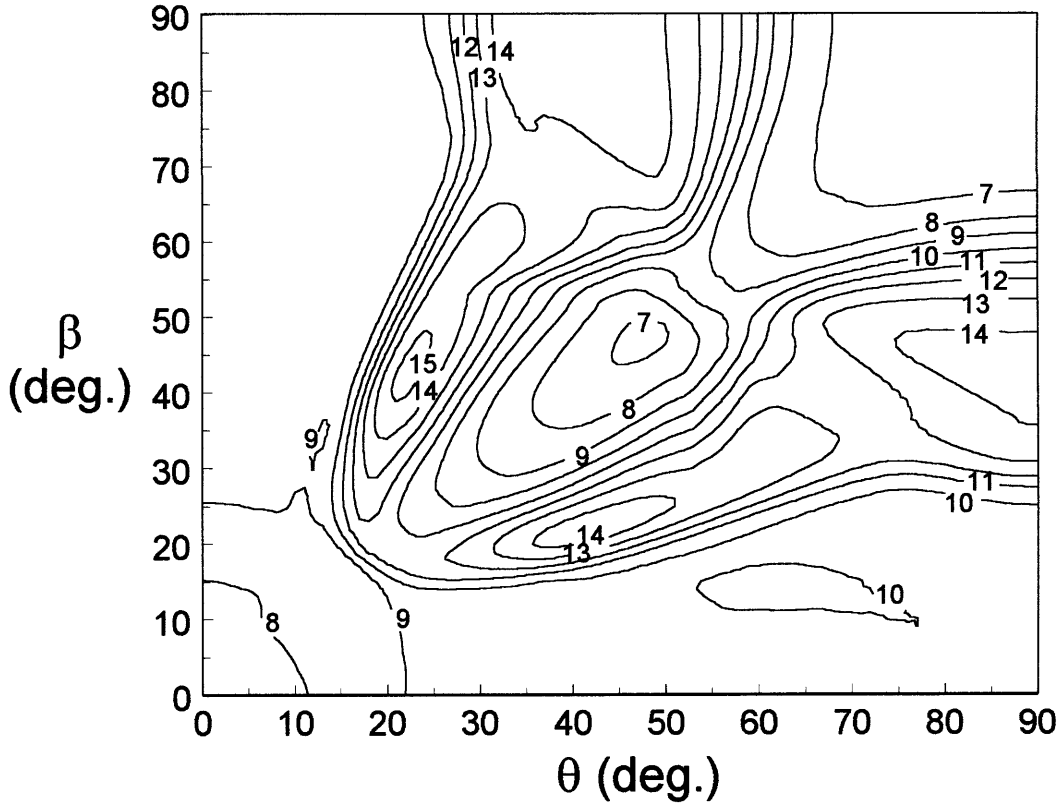

Figure D.34 Contour plot of the coefficient of variation (%) of the longitudinal tensile strength for the $[\pm\theta/\pm\beta]_s$ AS4/3501-6 laminate family (approach A3, 1000 samples)

APPENDIX E

GA, ASA, AND SSM SIMULATION COMPARISONS

E.1 TEST FUNCTIONS

ASA, a Genetic Algorithm (GA), and the SSM were evaluated on a set of six robust test cost functions $\{f_n : n=0,...,5\}$. The test suite was designed to test algorithms on functions that are:

- Continuous or Discontinuous
- Convex or Concave
- Unimodal or Multimodal
- Linear or Nonlinear
- Low Dimensional or High Dimensional
- Deterministic or Stochastic

The functions 1-5 are De Jong's five function test bed and are typically used for GA benchmarking [59, 67]. The performance of GAs on these functions is well documented [95]. Also included is the function f_0, the objective function of Corana *et al.* [96]. The GA runs were adopted from [67] and were simulated on the University of California at San Diego Genesis 1.2

Genetic Algorithms Simulator [97]. There are two sets of ASA runs for each function, one set from [67] (using an unknown machine) and one set using an ASA code written by the author and run on a Pentium® 166Mhz personal computer. Two sets of ASA runs were used to ensure that ASA and the SSM were compared on equal grounds, since the SSM was only run on a Pentium®, and to verify the results of [67]. It is important to note that the two ASA codes were independently written, compiled, and run on different machines.

The test functions follow:

$$f_0(x_1,\ldots,x_4) = \sum_{i=1}^{4} \begin{cases} \left(t_i\, sgn(z_i) + z_i\right)^2 c d_i & if\ |x_i - z_i| < |t_i| \\ d_i x_i^2 & otherwise \end{cases}$$

$$z_i = \left\lfloor \left| \frac{x_i}{s_i} \right| + 0.49999 \right\rfloor sgn(x_i) s_i \quad s_i = 0.2 \quad t_i = 0.05 \quad i = 1,\ldots,4$$

$$d_i = \{1.0, 1000.0, 10.0, 100.0\}$$

$$c = 0.15$$

$$-1000.0 \le x_i \le 1000.0 \quad i = 1,\ldots,4$$

Where s_i, t_i, d_i, and c are coefficients defined such that f_0 defines a paraboloid with axis parallel to the coordinates, and a set of holes that increase in depth near the origin.

$$f_1(x_1,x_2,x_3) = \sum_{j=1}^{3} x_j^2$$

$$-5.12 \le x_i \le 5.12 \quad i = 1,..,3$$

$$f_2(x_1,x_2) = 100\left(x_1^2 - x_2\right)^2 + \left(1 - x_1\right)^2$$

$$-2.048 \le x_i \le 2.048 \quad i = 1,2$$

$$f_3(x_1,\ldots,x_5) = 30.0 + \sum_{j=1}^{5} \lfloor x_j \rfloor$$
$$-5.12 \le x_i \le 5.12 \quad i = 1,\ldots,5$$

$$f_4(x_1,\ldots,x_{30}) = \sum_{j=1}^{30} x_j^4 + \eta$$
$$-1.28 \le x_i \le 1.28 \quad i = 1,\ldots,30$$

Where η is a random variable with uniform distribution and bounded by [0,1).

$$f_5(x_1,x_2) = \frac{1}{\frac{1}{500} + \sum_{j=1}^{25} \left(\frac{1}{\left[j + \sum_{i=1}^{2} \left(x_i - a_{ji} \right)^6 \right]} \right)}$$

$$a_{j1} = \{-32,-16,0,16,32,-32,-16,0,16,32,-32,-16,0,16,32,-32,-16,0,16,32,-32,-16,0,16,32\}$$
$$a_{j2} = \{-32,-32,-32,-32,-32,-16,-16,-16,-16,-16,0,0,0,0,0,16,16,16,16,16,32,32,32,32,32\}$$

$$-65.536 \le x_i \le 65.536 \quad i = 1,2$$

The following description of the functions and initial parameters for the GA was adopted from [67]: "Function f_0 is somewhat like function f_2. It is very difficult to minimize correctly in four dimensions, with over 10^{20} local minima to be trapped in. Optimization methods based on gradient descent are quite likely to be caught in one of the many local minima. Function f_1 tests simple sum of squares with one minimum at x_i=0. The function f_2 is the classical function of Rosenbrock and Chebyquad in two dimensions that is

unimodal, yet difficult to minimize [96]. The next function, f_3, is the plateau function, generated as the sum of integer threshold values. The five dimensional space has one minimum and is discontinuous. Function f_4 is a noisy quartic function of 30 variables originally defined as $f_4(x_1,\ldots,x_{30}) = \sum_{j=1}^{4} x_j^4 + \eta$ where η is produced by Gaussian noise with distribution (0,1) [59]. While the intent of this function is to determine an optimizer's performance in the presence of noise, this function is perhaps flawed, as no definite global minimum exists. Once the algorithm minimizes $\sum_{j=1}^{4} x_j^4$, it could continue executing, waiting for smaller values of η to be produced. By performing more function evaluations, an inefficient optimization technique might find better solutions than an efficient one (that terminates with fewer function calls). In response to this problem η is chosen to be a random variable with uniform distribution, and bounded by [0,1). Lastly, f_5 spans a 2-dimensional space, with global minima~0.998004. It is similar to f_0 but has only 25 local minima.

For all GA simulation runs, the fitness functions to maximize were $-f_n$. Real values were encoded as binary strings of various lengths. f_0 used 32 bits. For the others, the defaults given in the GA simulator were used: f_1 used 10 bits, f_2 used 12 bits, f_3 used 10 bits, f_4 used 8 bits, and f_5 used 17 bits. (Although this entailed some prior tuning for these specific systems, no such tuning was done for the ASA runs reported here.) Bit string lengths depend on the function being optimized; when states are encoded as short bit strings,

they converge more quickly than those encoded as long strings. However, the decoded precision of the shorter string is less than those encoded as long strings. Factors such as the string length, population sizes, mutation rates, number of generations, and percent of population culled were heuristically determined, and were dependent on the function being optimized. These relatively minor procedures are considered to be part of the algorithm defining GA."

The only clue to the parameters used in the ASA code that generated the data adopted from [67] is the comment that "Both the GA and ASA algorithms were taken from existing libraries previously prepared for other problems." The ASA code written by the author used default parameters that were obtained from an ASA code written by the algorithms inventor, Lester Ingber. The code was obtained via anonymous ftp from ftp.alumni.caltech.edu [131.215.139.234] in the /pub/ingber directory. The parameters used for the SSM are summarized in Table E.1. The parameters for the SSM were not altered for any of the runs reported here. It should be noted that this choice of parameters for the SSM is almost certainly not optimal. The parameter settings for ASA are supported by an extensive experience base which does not yet exist for the SSM. It is expected that the speed of the SSM will increase significantly as more experience is gained in setting the algorithms parameters. Regardless, the SSM is still much faster than ASA, and orders of magnitude faster than the GA.

E.2 RESULTS

Figures E.1-E.12 illustrate the performances of the three algorithms on the corresponding functions f_0 through f_5. The odd numbered figures (i.e. E.1, E.3, ..., E.11) are from [67]; solid and short dashed lines each represent one ASA run each, and dashed and long dashed lines represent one GA run each. The even numbered figures (i.e. E.2, E.4, ..., E.12) are from runs completed by the author; solid lines represent one ASA run each, and dotted lines represent one SSM run each. The runs are log-log plotted to show the relative convergence rates. The abscissa indicates the number of function calls, and the ordinate shows the best function evaluation found so far (cost). Convergence to 0 is indicated with a downward pointing arrow.

The ASA runs completed by the author are very similar to those from [67]. For all intents and purposes the results of the ASA runs from [67] are identical to the ASA runs carried out by the author. As a result, the SSM and ASA are compared on equal grounds.

Overall ASA is orders of magnitude faster than the GA, and the SSM is an order of magnitude faster than ASA (even with the non-optimal parameter settings). SSM is approximately an order of magnitude faster than ASA for functions f_0, f_1, and f_5, and two orders of magnitude faster for f_2. The performances of SSM and ASA are close for the function f_4. This was expected due to the random nature of the function. The variances of ASA

and the SSM for the function f_3 were substantial, making a rigid comparison difficult.

Table E.1 Optimization Parameters Used In The SSM

Symbol	Value
T_{oi}	1
${}^{o}T_{\text{acceptance}}$	100
T_{fi}	10^{-5}
k_{fi}	100
q	1
η	1
k_{rescale}	100
k_{restart}	100

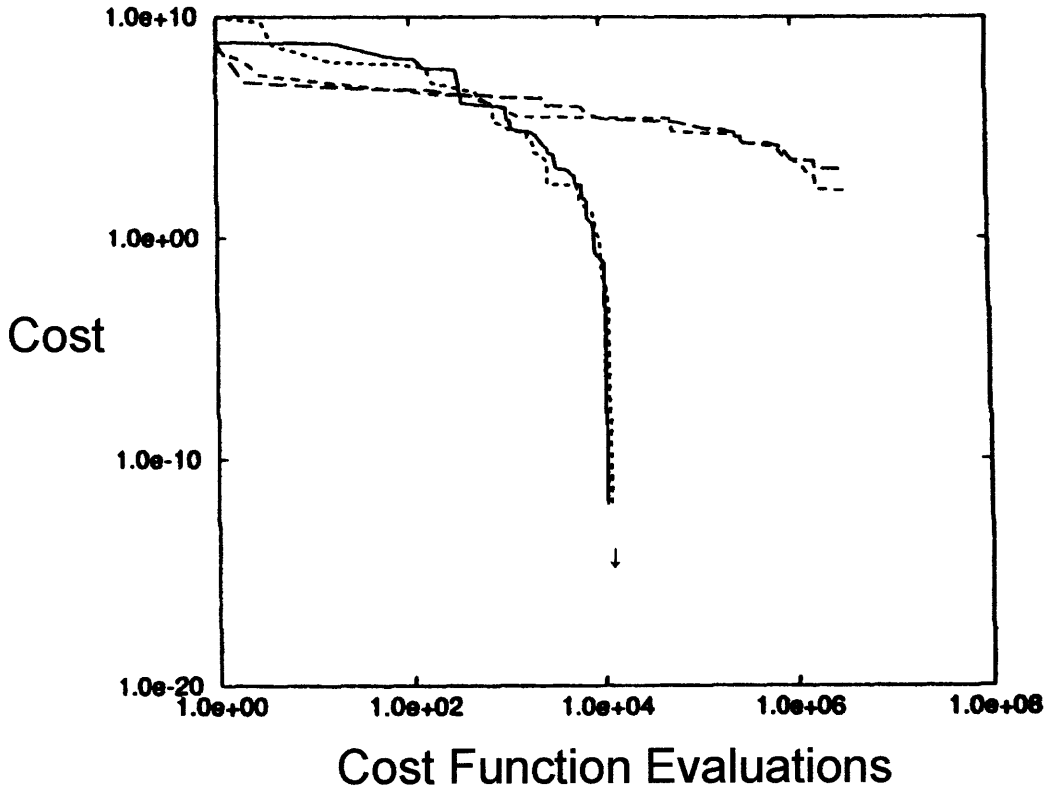

Figure E.1 Comparison of GA and ASA for f_0 (from [67]); solid and short dashed lines each represent one ASA run; dashed and long dashed lines each represent one GA run

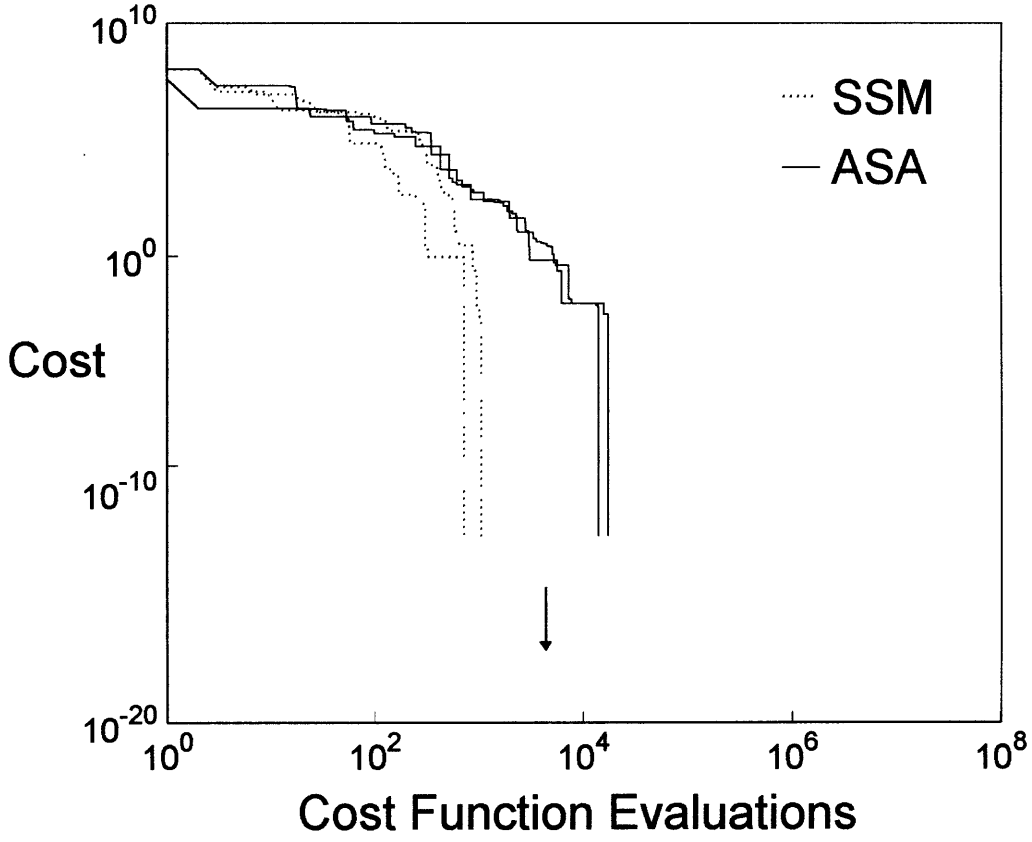

Figure E.2 Comparison of ASA and the SSM for f_0

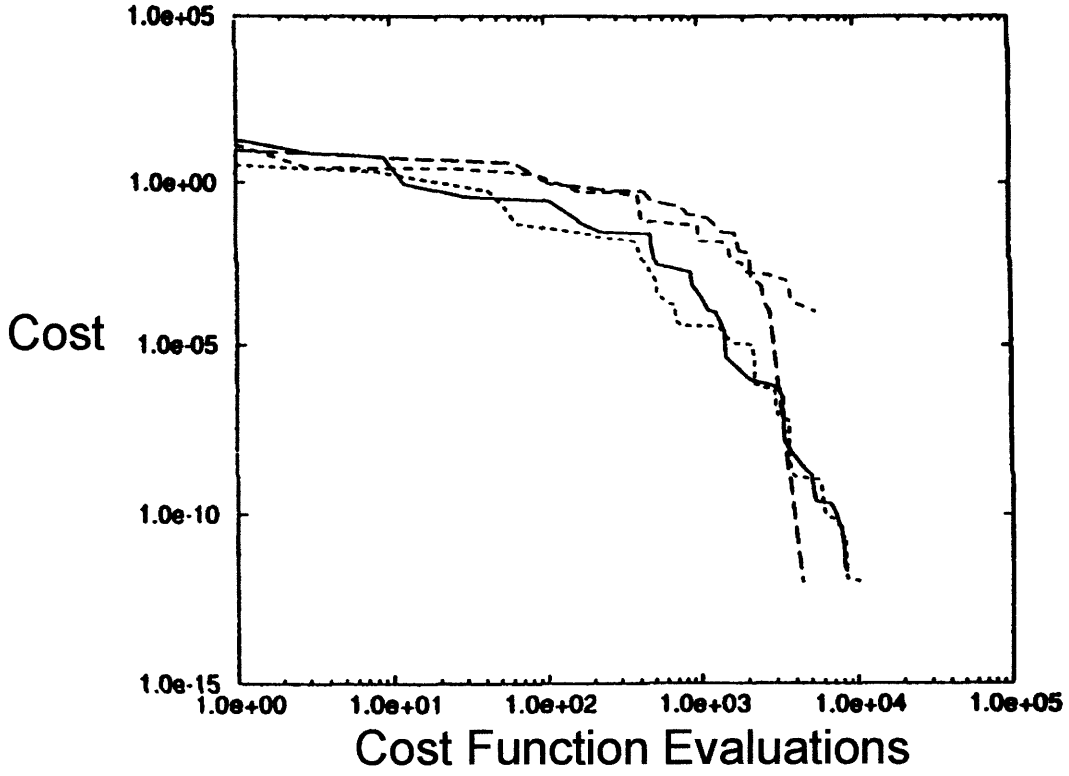

Figure E.3 Comparison of GA and ASA for f_1 (from [67]); solid and short dashed lines each represent one ASA run; dashed and long dashed lines each represent one GA run

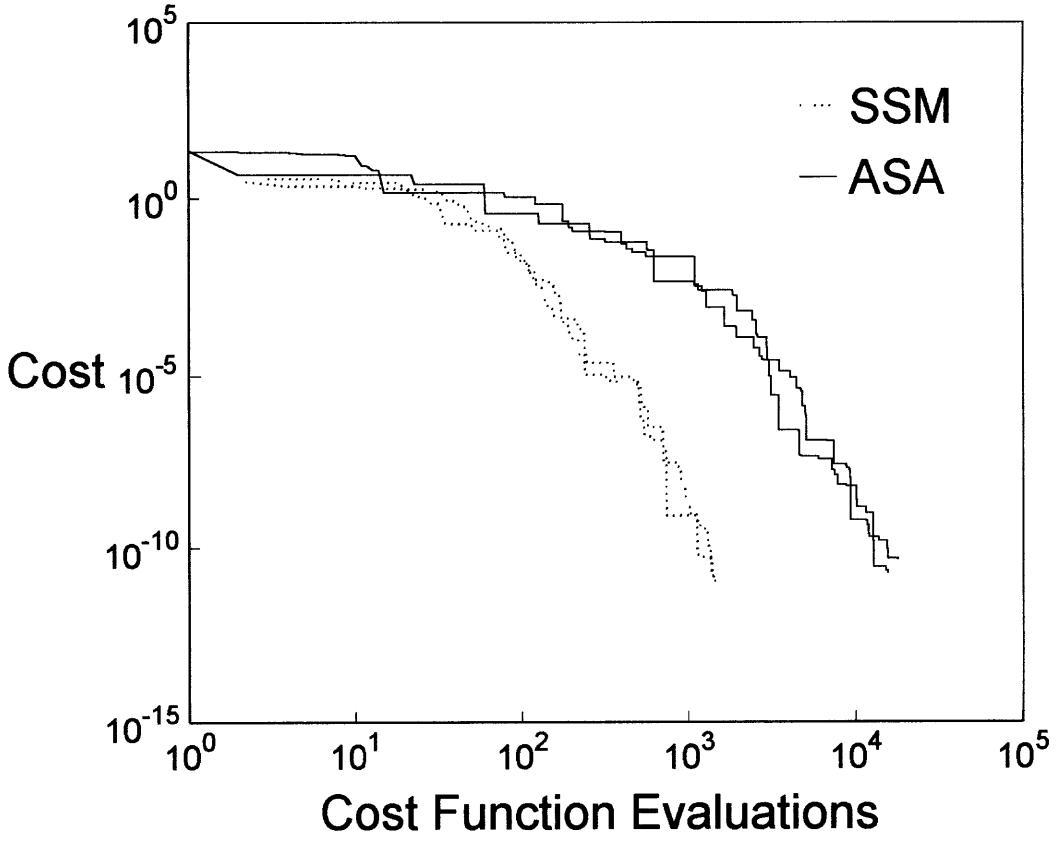

Figure E.4 Comparison of ASA and the SSM for f_1

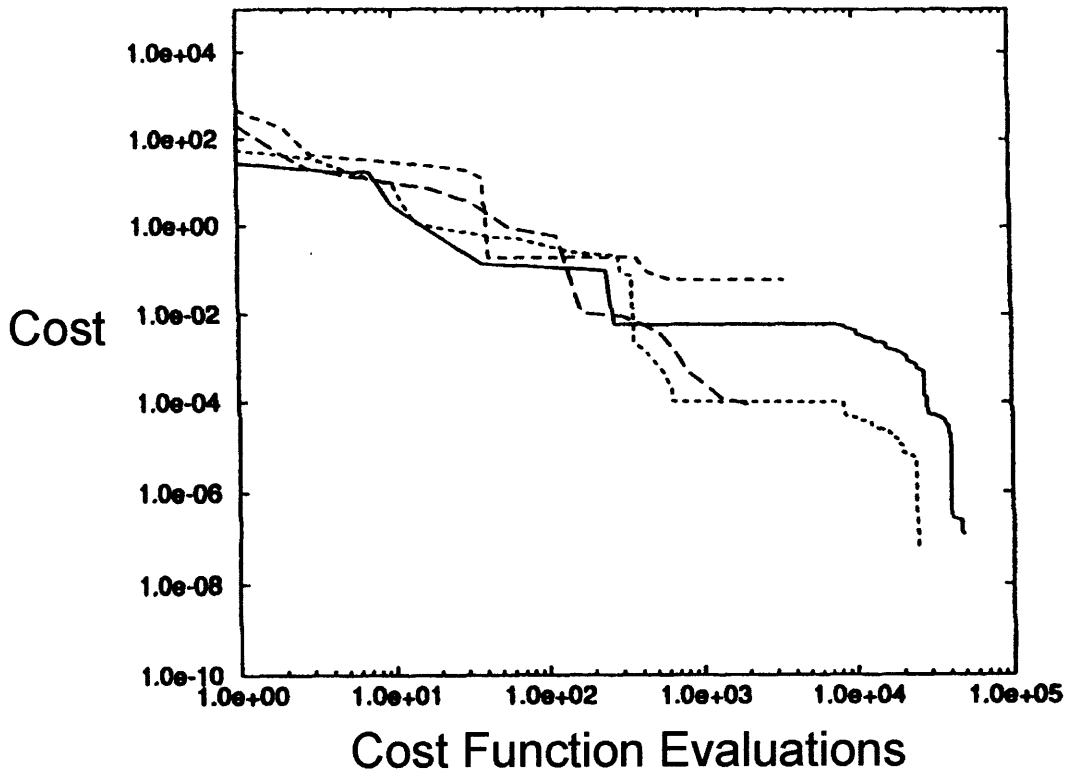

Figure E.5 Comparison of GA and ASA for f_2 (from [67]); solid and short dashed lines each represent one ASA run; dashed and long dashed lines each represent one GA run

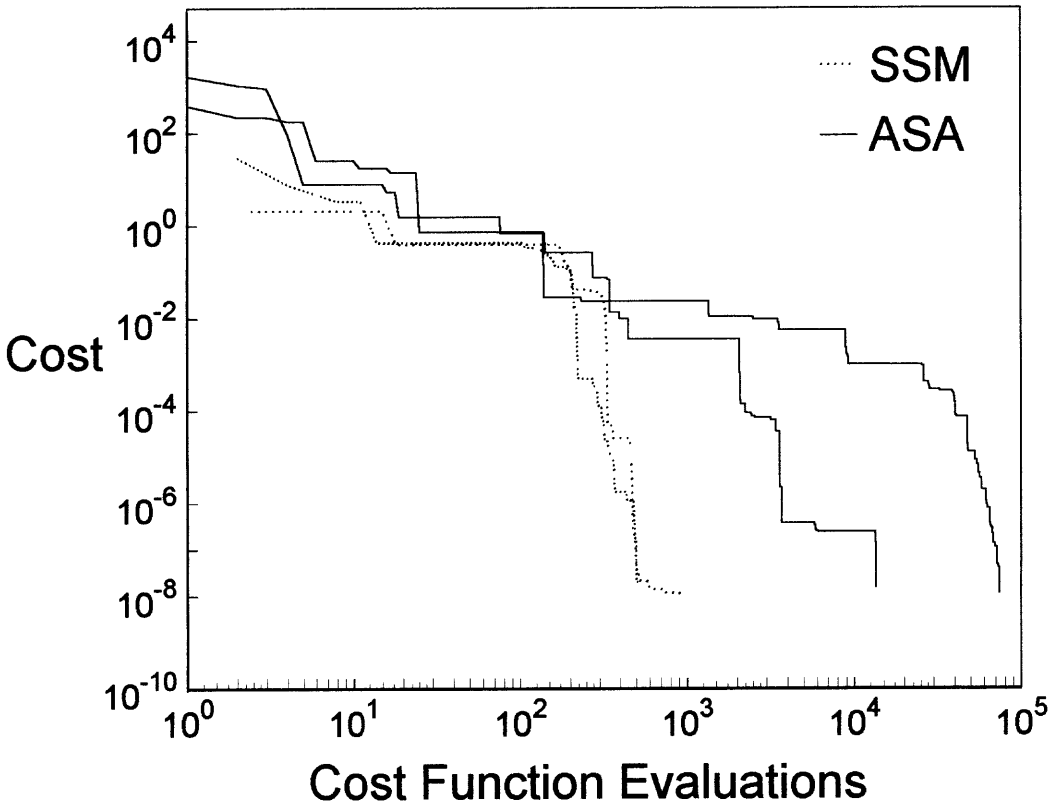

Figure E.6 Comparison of ASA and the SSM for f_2

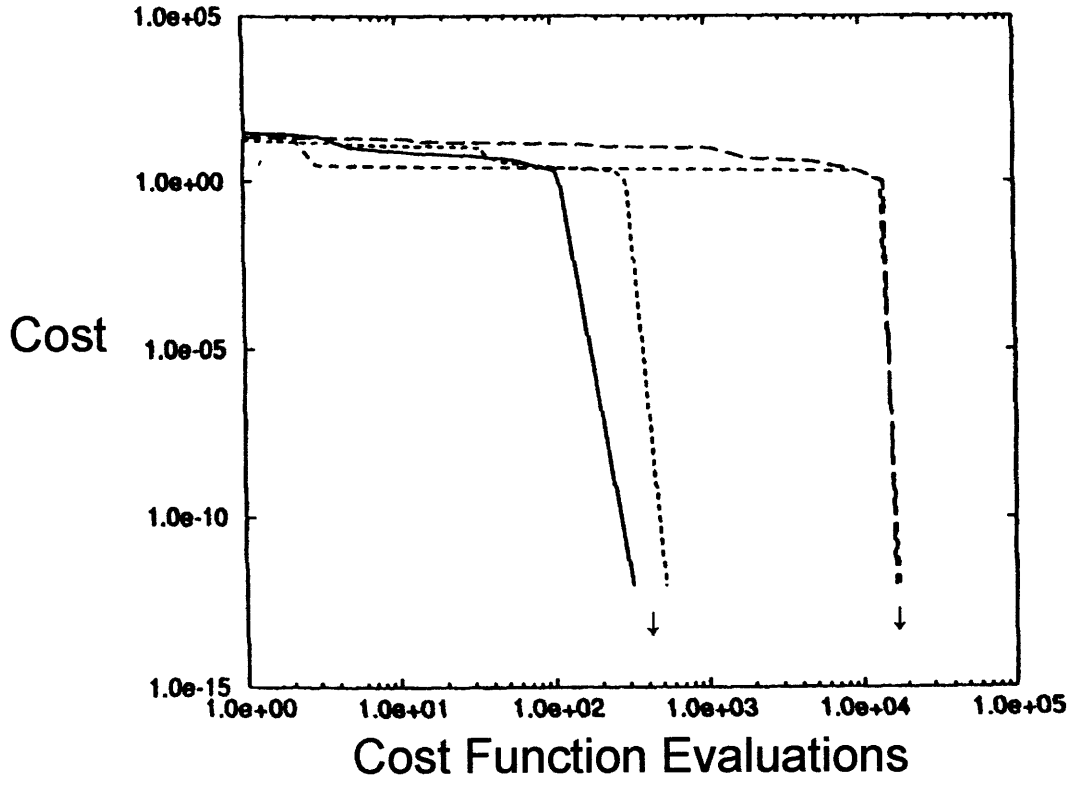

Figure E.7 Comparison of GA and ASA for f_3 (from [67]); solid and short dashed lines each represent one ASA run; dashed and long dashed lines each represent one GA run

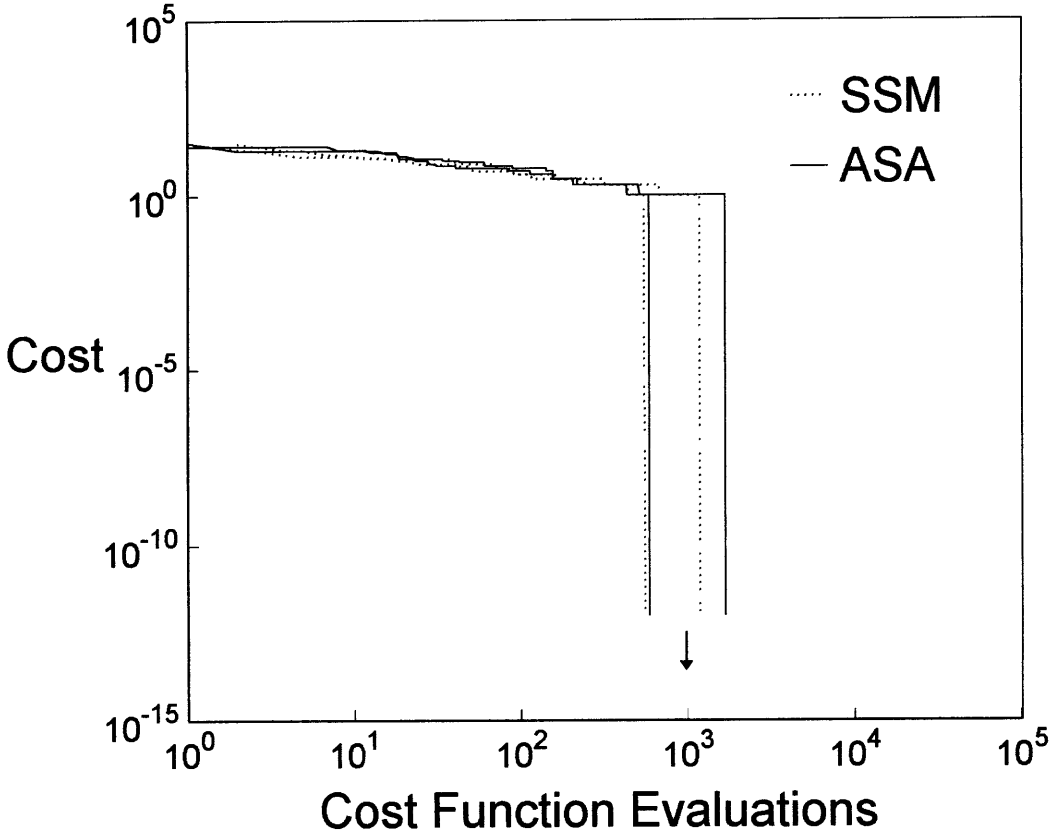

Figure E.8 Comparison of ASA and the SSM for f_3

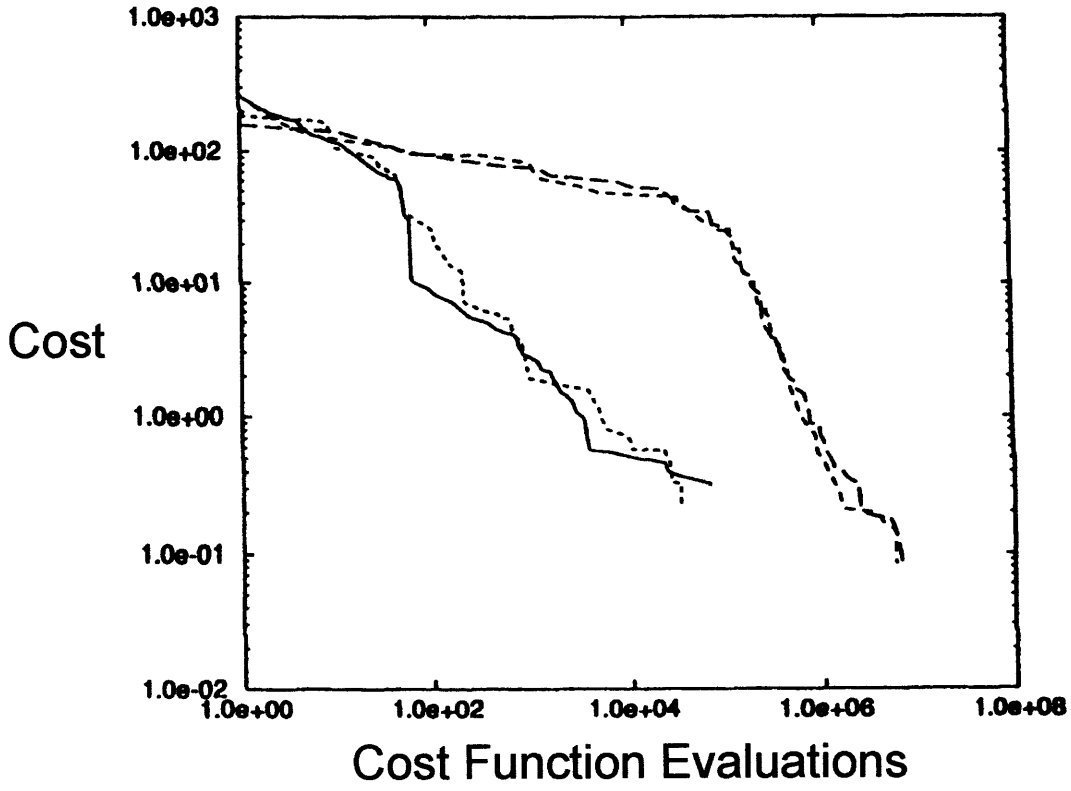

Figure E.9 Comparison of GA and ASA for f_4 (from [67]); solid and short dashed lines each represent one ASA run; dashed and long dashed lines each represent one GA run

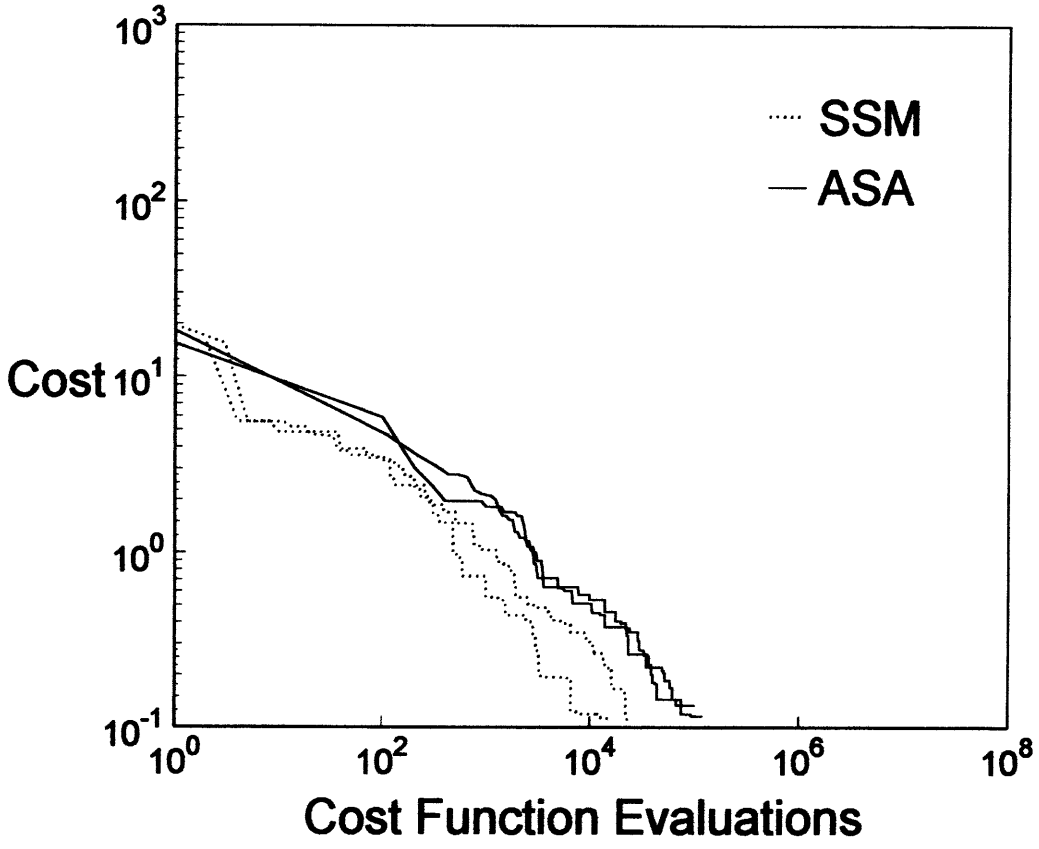

Figure E.10 Comparison of ASA, and the SSM for f_4

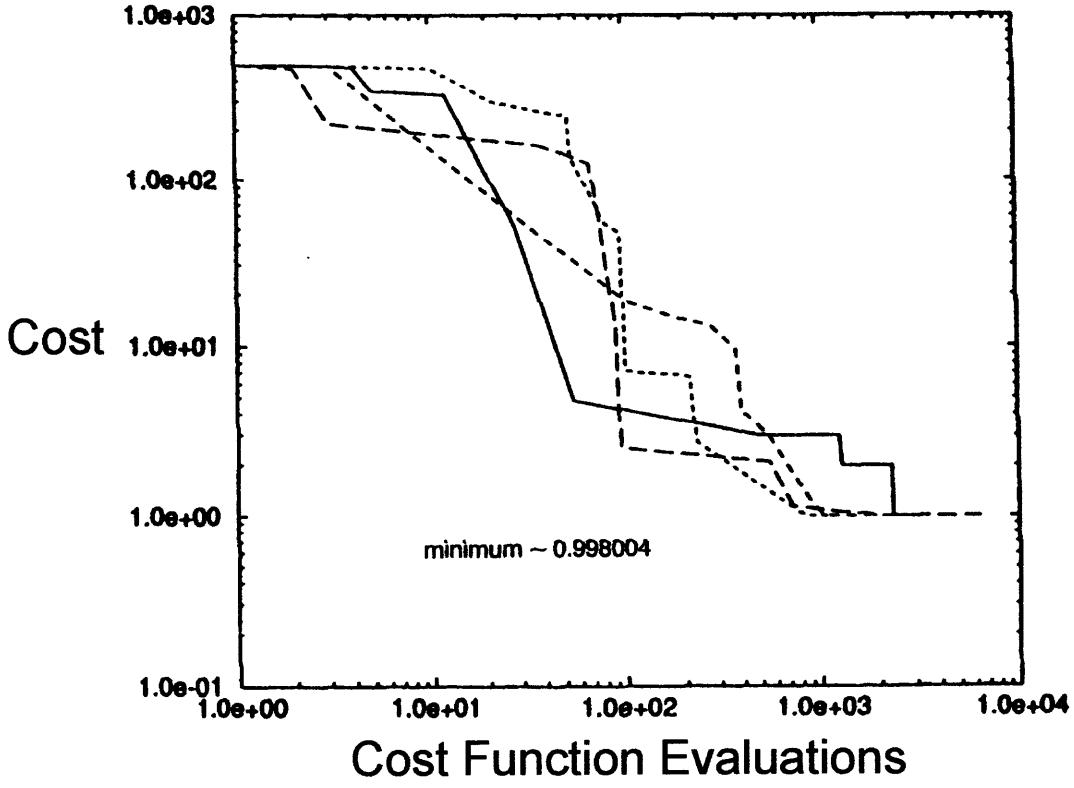

Figure E.11 Comparison of GA and ASA for f_5 (from [67]); solid and short dashed lines each represent one ASA run; dashed and long dashed lines each represent one GA run

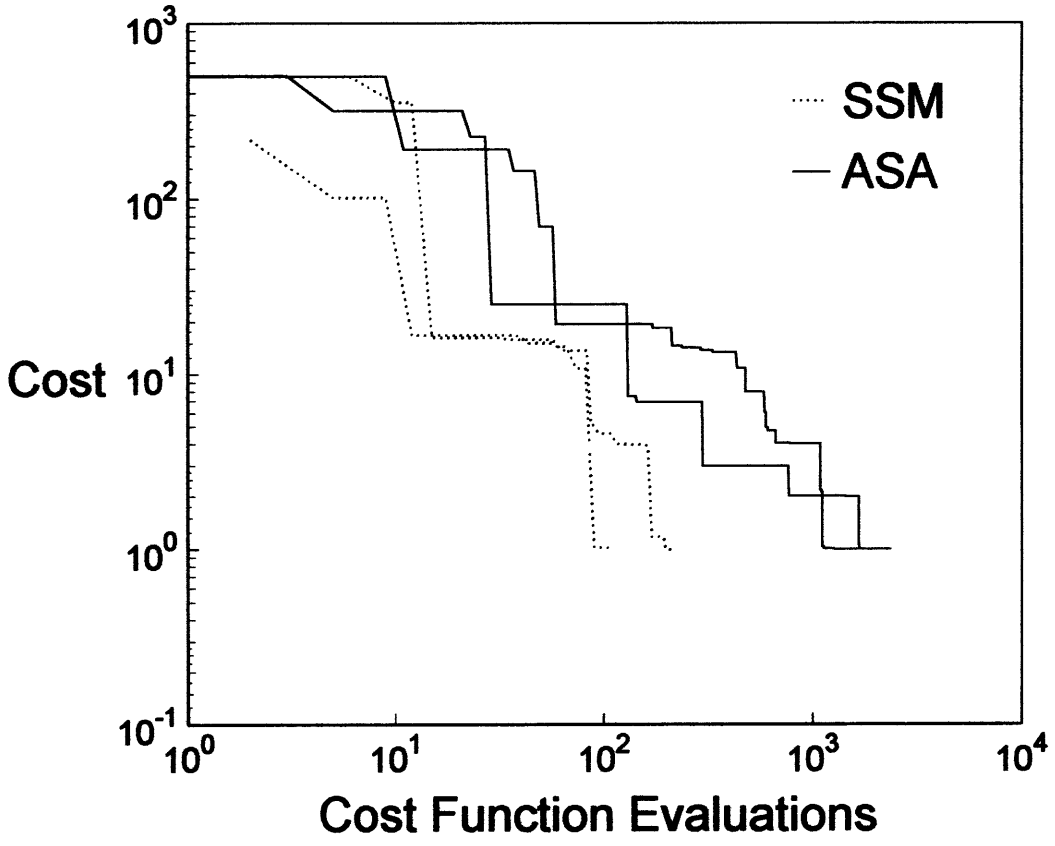

Figure E.12 Comparison of ASA and the SSM for f_5